Supplementary Materials
Molecular Biology of the Cell
Gunkel *et al*.

An evolutionary conserved bimodular domain anchors ZC3HC1 and its yeast homologue Pml39p to the nuclear basket

Philip Gunkel, Haruki Iino, Sandra Krull, and Volker C. Cordes

Max Planck Institute for Multidisciplinary Sciences, Am Fassberg 11, 37077 Göttingen, Germany

Contact: Volker.Cordes@mpinat.mpg.de

Running title: The bimodular homologues ZC3HC1 and Pml39p

Supplemental Information, Figures, Discussion, Materials and Methods, Tables, Sequences, and References

Supplemental Information

Supplemental Information 1. Origins of the Pfam motifs zf-C3HC and Rsm1.

Supplemental Information 2. BLD signatures in the course of time.

Supplemental Information 3. Approaches of sequence database mining for ZC3HC1 homologues.

Supplemental Information 4. Distribution of ZC3HC1 and its homologues among eukaryotes.

Supplemental Information 5. Low overall sequence similarity and a lack of shared, database-deposited sequence motifs as one reason for a kinship so far gone unrecognized between distinct ZC3HC1 homologues.

Supplemental Information 6. Assessment of the input datasets' respective contributions to user-initiated BLD structure predictions by AlphaFold2.

Supplemental Information 7. BLD structure predictions unveiling evolutionarily conserved α-helices, with some common to both BLDs and others either BLD1- or BLD2-specific.

Supplemental Information 8. A relationship between *Sc*Pml39p/*Hs*ZC3HC1 and *Sc*Nup157p/*Hs*NUP155?

Supplemental Information 9. Instability of the Mlp-dependent association of *Sc*Pml39p with NPCs under common cell fractionation conditions?

Supplemental Information 1. Origins of the Pfam motifs zf-C3HC and Rsm1.

The so-called zf-C3HC motif (http://pfam.xfam.org/family/PF07967) was initially based on sequences representing nine different proteins, of which three were of vertebrate origin and one corresponding to *Sp*Rsm1p. Already back then, the zf-C3HC motif had been described as representing a domain often occurring as a repeat, which might be the reason why this motif's initial version had been deduced from sequence segments representing both BLDs (http://ftp.ebi.ac.uk/pub/databases/Pfam/releases/Pfam16.0/; Finn *et al*, 2006; further below, see also Supplemental Figure S2D1).

On the other hand, part of the second BLD of *Hs*ZC3HC1 was assigned only later (http://ftp.ebi.ac.uk/pub/databases/Pfam/releases/Pfam24.0/; e.g., Finn *et al*, 2010) the by then so-called Rsm1 motif (Finn *et al*, 2008; http://pfam.xfam.org/family/PF08600). The latter had initially been defined by ten non-redundant sequence segments only corresponding to the second BLD, with seven of these segments of fungal origin, again including *Sp*Rsm1p but no mammalian sequences (http://ftp.ebi.ac.uk/pub/databases/Pfam/releases/Pfam20.0/; Supplemental Figure S2D1).

Supplemental Information 2. BLD signatures in the course of time.

For creating collections of ZC3HC1 amino acid substitution mutants, we initially focused on the minimal sequence signature that is identical for the central part of both BLDs in vertebrates, where it reads C-$X_{(3,5)}$-G-W-$X_{(9,15)}$-C-$X_{(2)}$-C-$X_{(31,153)}$-H-$X_{(3)}$-C-X-W (Figure 2A2). This signature for a single BLD, here numbered (1), resembled the ILP family's minimal sequence signature already described earlier (Higashi *et al*, 2005), except for the first cysteine, characteristic for vertebrates, that preceded the signature's G-W dipeptide. Apart from a few differences, this early signature also resembled the WebLogos (Crooks *et al*, 2004) that we built (Supplemental Figure S2D1) from those sequences that had been used for the first versions of the Pfam motifs zf-C3HC (http://ftp.ebi.ac.uk/pub/databases/Pfam/releases/Pfam16.0/) and Rsm1 (http://ftp.ebi.ac.uk/pub/databases/Pfam/releases/Pfam20.0/).

For sequence database mining (see further below, e.g., Supplemental Information 3), we then generated collections of signatures composed of either two identical or two different BLD signatures arranged in tandem once we had found the integrity of both of BLDs essential for the protein's interaction with the NB and TPR. One of the earliest tandem BLD signature motifs used for some initial mining trials based on the minimalist BLD sequence signature G-W-$X_{(9,15)}$-C-$X_{(2)}$-C-$X_{(31,153)}$-H-$X_{(3)}$-C-X-W, that stemmed from signature (1) but lacked the first "C", the latter removed after having found C102 and C249 of *Hs*ZC3HC1 dispensable (Supplemental

Figures S2B and S2D), and since other potential homologues lacked such a cysteine at corresponding positions anyhow. With two of these signatures in tandem and with the spacer length between them reflecting the lengths in the vertebrate ZC3HC1 homologues, the resulting signature, here numbered (2), was then reading G-W-$X_{(9,15)}$-C-$X_{(2)}$-C-$X_{(31,153)}$-H-$X_{(3)}$-C-X-W-$X_{(94,97)}$-G-W-$X_{(9,15)}$-C-$X_{(2)}$-C-$X_{(31,153)}$-H-$X_{(3)}$-C-X-W. While representing the two BLDs of the vertebrate ZC3HC1 homologues with their corequisite zinc fingers, it turned out immediately evident that this signature hardly allowed for detecting, beyond the Chordata, possible homologues in other phyla, with the only exceptions later found being three species of the clade Stramenopiles (accession numbers XP_012195780, OQR86123, and OQS04627). These proteins appeared to be ZC3HC1 homologues but to match the abovementioned signature only coincidentally. Other likely ZC3HC1 homologues, for example, the fission yeast protein Rsm1p (Yoon, 2004), whose sequence similarity with *Hs*ILP1/ZC3HC1 had already been noted earlier (Higashi *et al*, 2005; Finn *et al*, 2006; http://pfam.xfam.org/family/PF07967) could not be identified with this signature.

For creating further versions of such tandem BLD signatures, we then took the results of our other *Hs*ZC3HC1 deletion and aa substitution mutations into account. Namely that the large insertion within the second BLD of *Hs*ZC3HC1 was dispensable for NB association and that some positions of the tandem BLD signature (2) tolerated certain substitutions, as had been demonstrated for *Hs*ZC3HC1 by W107Y, W107F, W256Y, and W256F, which all had no notable effect on the NB association of the respective mutant versions of *Hs*ZC3HC1 (Supplemental Figure S2C). Furthermore, attentively having also considered the published information available until then (Higashi *et al*, 2005; Kokoszynska *et al*, 2008; Finn *et al*, 2006, 2008, 2010), pointing at very variable spacings between the two BLDs and between the second BLD's two pairs of suspected zinc-coordinating residues, i.e., between the C-$X_{(2)}$-C and H-$X_{(3)}$-C sequences, we compiled yet another minimal single BLD sequence signature. Holding for the central part of both BLDs of several potential ZC3HC1 homologues in different phyla, this signature read G-[WYF]-$X_{(8,72)}$-C-$X_{(2)}$-C-$X_{(15,524)}$-H-$X_{(3)}$-C. With two copies of this once again low stringency signature arranged in tandem (Supplemental Figure S2D2) and with the linker's length between the two copies initially deduced from published information (Higashi *et al*, 2005; Kokoszynska *et al*, 2008), this would, in the sequel, allow for already specifically identifying only one ZC3HC1 homologue per species in various organisms of different phyla. Here numbered (3), this tandem BLD signature read G-[WYF]-$X_{(8,72)}$-C-$X_{(2)}$-C-$X_{(15,524)}$-H-$X_{(3)}$-C-$X_{(62,117)}$-G-[WYF]-$X_{(8,72)}$-C-$X_{(2)}$-C-$X_{(15,524)}$-H-$X_{(3)}$-C, and with this signature we could readily identify not only *Sp*Rsm1p but already also *Sc*Pml39p as a putative homologue in

budding yeast, in which a ZC3HC1 homologue had remained undetectable until then (see further below).

This signature (3) and yet further subsequent versions of tandem BLD signatures were used for progressively searching sequence databases for ZC3HC1 homologues (see Supplemental Information 3). With the early and next-generation tandem BLD signatures notably differing in complexity in the course of our study, we nonetheless collectively designated all the full-length versions of them as simplifying signatures of the NuBaID.

Some further exemplary ones of these NuBaID signatures, one of which represented an intermediate one summarizing the signature features of potential ZC3HC1 homologues identified at some point, and the other representing yet another version used for further rounds of data mining, read as follows: G-[WYF]-$X_{(6,24)}$-C-$X_{(2)}$-C-$X_{(17,82)}$-H-$X_{(3)}$-C-X-[WY]-$X_{(48,232)}$-G-[WYF]-$X_{(8,140)}$-C-$X_{(2)}$-C-$X_{(14,994)}$-H-$X_{(3)}$-C-X-[WY], with this signature here numbered (4), and G-[WYF]-$X_{(5,25)}$-C-$X_{(2,3)}$-C-$X_{(10,100)}$-H-$X_{(3)}$-C-X-[WYFML]-$X_{(40,250)}$-G-[WYF]-$X_{(5,150)}$-C-$X_{(2)}$-C-$X_{(10,1500)}$-H-$X_{(3)}$-C-X-[WYFRCV], here referred to as signature (5).

For signature (5), for example, (i) we had expanded, based on educated guesses, the spacings between some of the residues beyond those spacer lengths we had detected so far. Furthermore, (ii) we had considered that the spacing between the first two cysteines of the first BLD's zinc finger signature could be variable too. In fact, we had noted by then that some fungal homologues appeared to have come up during evolution with different spacing between the first two cysteines of the first BLD's zinc finger signature, reading C-$X_{(3)}$-C instead of C-$X_{(2)}$-C (Figure 3C), and we had found a C-$X_{(2)}$-C to C-$X_{(3)}$-C exchange tolerated within the BLD1 of *Hs*ZC3HC1, as the corresponding mutant was still capable of binding to the NB even in the wild-type (WT) version of ZC3HC1 (Supplemental Figure S3). Moreover, (iii) we also had considered conspicuous residue diversity between alleged homologues at positions corresponding to the tryptophan residues W158 and W431 of *Hs*ZC3HC1. Representing the ones that follow two residues after each BLD's H-$X_{(3)}$-C pentapeptide, we had found these tryptophans not essential for NE-association in a human ZC3HC1 knock-out (KO) cell (e.g., Supplemental Figure S2B1), and in some groups of organisms, we noted a whole range of residues occurring at a potential homologue's corresponding positions. Later, studying other facets of the ZC3HC1 protein's structure and function, we found at least some of these residues allowing for NB and TPR association, as will be presented in another context elsewhere, and some of them we also found functionally adequate in the context of the human protein.

Currently, a NuBaID signature describing the majority and illustrating the diversity of those putative ZC3HC1 homologues that we have detected so far (July 2022) and can imagine being

NB-binding-competent in most phyla reads G-[WYF]-$X_{(6,24)}$-C-$X_{(2,3)}$-C-$X_{(17,82)}$-H-$X_{(3)}$-C-X-[WYFML]-$X_{(48,232)}$-G-[WYF]-$X_{(8,140)}$-C-$X_{(2)}$-C-$X_{(14,994)}$-H-$X_{(3)}$-C-X-[WYFRCV], with this signature here numbered (6). However, we do not exclude that the potential ZC3HC1 homologues of yet some other species might reflect even more diversity.

Supplemental Information 3. Approaches of sequence database mining for ZC3HC1 homologues.

To search for potential ZC3HC1 homologues, i.e., for proteins possessing a NuBaID signature, we used complementary approaches, including signature-based and primary sequence end-to-end alignment searches that made it possible to progressively comb the eukaryotic realm's available sequence data interactively, allowing for iterative refinement of the mining process. Our data mining for potential ZC3HC1 homologues added to former studies relating to this issue (e.g., Higashi *et al*, 2005; Kokoszynska *et al*, 2008).

In particular, we wanted to know whether possessing only one type of NuBaID signature-encoding gene per species, which we early on knew for sure was the case in vertebrates, might also be common to species beyond the chordates. Along this line, we wondered whether possessing one or another version of a NuBaID signature might mark proteins from also different phyla as NB- and TPR-interaction partners, even if such proteins do not appear to have other immediately apparent primary sequence features in common. Or whether some organisms in other phyla and clades might make wider use of the NuBaID signature - and the type of construction it represents - by featuring it as part of very different proteins with possibly different functions.

While we used a broader range of search tools (see also Supplemental Materials and Methods and, e.g., Supplemental Information 5) in the later course of recurrently mining the sequence databases over the years, we essentially made use of only two tools at the very beginning of our searches for ZC3HC1 homologues across the eukaryotic realm. On the one hand, this was the ScanProsite tool (de Castro *et al*, 2006; https://prosite.expasy.org/scanprosite) which we used most commonly for repeatedly scanning over time both the reviewed, manually annotated Swiss-Prot and the unreviewed, computationally annotated TrEMBL protein databases (Bairoch & Apweiler, 1997). As the query signatures, we used various versions of the initially so-called tandem BLD signatures, also including those examples outlined in Supplemental Information 2, which we eventually then all referred to as simplifying signatures of the NuBaID. On the other hand, these signature-based searches were constantly complemented by primary sequence alignment searches within the freely accessible nucleotide and protein sequence

databases, particularly those of the National Center for Biotechnology Information (NCBI; https://www.ncbi.nlm.nih.gov/). For this purpose, we used the omnipresent Basic Local Alignment Search Tool BLAST (Altschul *et al*, 1990; https://blast.ncbi.nlm.nih.gov/Blast.cgi). As the query sequences, we used selections from the steadily increasing collection of putative ZC3HC1 homologues (see also Supplemental List of Sequences) that we identified in different taxa. Furthermore, we used BLASTP for regularly conducting reverse BLAST searches to sort out those sequences falsely assigned to a given species (see also Supplemental Materials and Methods).

We also used the BLAST tools with collections of query sequences for screening expressed sequence tag (EST) and whole-genome shotgun (WGS) databases via TBLASTN. Thereby, we occasionally also ventured to re-interpret genomic information, particularly by newly predicting and assembling exon sequences and by re-defining open reading frame (ORF) boundaries in those cases in which we felt sure that computational ORF predictions and automatic annotations had not deciphered the corresponding gene correctly. In addition, to further validate or supplement sequences already deposited in the databases, we isolated mRNAs for cDNA synthesis and sequencing from some organisms of interest. Beyond that, when TBLASTN-searching the nucleotide sequence databases of protist phyla, we considered that some protists exhibit exceptions to the standard nuclear genetic code in eukaryotes (https://www.ncbi.nlm.nih.gov/Taxonomy/Utils/wprintgc.cgi).

Later, we complemented the ScanProsite-based approach and sometimes replaced it by searching NCBI-based sequences with the pattern-hit initiated BLAST (PHI-BLAST) program (Zhang *et al*, 1998). The latter uses as input not only a signature to search for pattern-conforming subject sequences but also a query sequence, in our case first only the one for *Hs*ZC3HC1 and later also the ones of clearly identified ZC3HC1 homologues, to subsequently construct local alignments next to the pattern's residues, between the query and the identified sequences. This hybrid strategy of PHI-BLAST allowed for sorting out more easily than with ScanProsite those sequences whose possession of relaxed NuBaID signatures of very low sequence stringency was regarded as random, namely when no additional traces of sequence similarity in the signature's vicinity indicated kinship.

Furthermore, the abovementioned approaches were later also complemented by checking the identified sequences for additional signature elements conforming to either complete or partial versions of the Pfam motifs zf-C3HC and Rsm1. The latter was done even though the Rsm1 motif, in particular, often did not allow for identifying proteins we had been able to define by then as prototypic NuBaID-containing ones like, for example, *Sc*Pml39p and the *D. discoideum*

protein DDB0349234. Both of these ZC3HC1 homologues still have not been assigned an Rsm1 motif, as defined by Pfam, to date (July 2022; (http://ftp.ebi.ac.uk/pub/databases/Pfam/releases/Pfam35.0/; https://pfam.xfam.org/family/PF08600). Furthermore, while the *Dictyostelium* homologue had a zf-C3HC motif assigned to it (http://ftp.ebi.ac.uk/pub/databases/Pfam/releases/Pfam18.0/; e.g., Finn *et al*, 2008) when we conducted such searches, this was not so for *Sc*Pml39p, with the latter only listed as a zf-C3HC motif-possessing protein later (http://ftp.ebi.ac.uk/pub/databases/Pfam/releases/Pfam30.0/). Even so, the zf-C3HC motif has not yet (July 2022) been assigned to *Sc*Pml39p in some databases, such as NCBI's Conserved Domain Database (CDD; https://www.ncbi.nlm.nih.gov/Structure/cdd/cdd.shtml; see also Supplemental Information 5). By contrast, already when having used the tandem arrangement (Supplemental Figure S2D2) of the abovementioned minimalist signature (3) for database searches via ScanProsite, we had found *Sc*Pml39p to be the only protein in the budding yeast complying with this motif (see also Supplemental Information 2), and this then also held for all further derivatives of this signature, including (4) and (5) mentioned above. While the *Dictyostelium* homologue had not been identifiable with the tandem arrangement of signature (3), it too was then readily detectable with (4) and (5).

Nonetheless, despite not all putative ZC3HC1 homologues appearing to have been assigned a Pfam motif to date, we further inspected those Pfam database-deposited sequences and species that were listed there as possessing a zf-C3HC or an Rsm1 motif. We thereby searched for potential candidates that might have remained undetected by the other abovementioned local sequence alignment searches and the pattern-based ones using a NuBaID signature, yet eventually found all of the reliably intact and full-length sequences in the Pfam database also identifiable via the one or other NuBaID signature.

However, while we had also realized that certain organisms appear to lack a functional ZC3HC1 homologue, we considered it possible that some species may possess a ZC3HC1 that simply had neither been detectable by the current NuBaID signatures nor the primary sequence alignment searches conducted till then. Therefore, for re-scanning the database-deposited sequences of those species for which we had not been able to detect a ZC3HC1 homologue, we eventually also assembled low stringency NuBaID signatures that incorporated characteristic sequence features of the BIR domains, described further below (e.g., Supplemental Figure S12F). However, these approaches did not allow for detecting a likely ZC3HC1 homologue in certain species either, for example, not in *Drosophila*.

Nonetheless, we momentarily cannot exclude for sure that there might exist either (i) ZC3HC1-homologous proteins evolutionarily altered beyond recognition from those

homologues currently regarded as prototypic or (ii) analogous proteins of equivalent function at the NBs of such species.

Supplemental Information 4. Distribution of ZC3HC1 and its homologues among eukaryotes.

Altogether, our combination of complementary approaches, including signature-based and primary sequence end-to-end alignment searches (see Supplemental Information 3), had allowed us to progressively comb through the sequence databases of the eukaryotic realm in a reiterative and interactive manner. Such mining eventually resulted in identifying numerous potential ZC3HC1 homologues in all eukaryotic supergroups, namely in the Opisthokonta, Amoebozoa, and Viridiplantae (Figure 3A, see also Supplemental List of Sequences for ZC3HC1 Homologues), in other divisions of the Archaeplastida, in the Excavata, and in several lineages within the SAR supergroup. In addition, we could identify likely homologues in many other protist groups and genera whose affiliation was still uncertain (e.g., Adl *et al*, 2012; Pawlowski, 2013; Burki, 2014) at times when we intermittently conducted rounds of such signature-based data mining for ZC3HC1 homologues also in lower eukaryotes.

Also remarkable, in species with a non-duplicated genome, we found only one gene coding for a protein with a NuBaID signature, together with a few complementing features that we eventually defined as characterizing a prototypic ZC3HC1 homologue. Only in some groups of organisms in which one or more rounds of whole-genome duplications appear to have occurred (e.g., Sinha *et al*, 2017; Li *et al*, 2018; Qiao *et al*, 2019) could one identify two or more of such NuBaID-encoding genes per species. The latter was the case, listing only some examples, in plants (Figure 3D), in some fungi, here exemplified by *Hortaea werneckii* (see Supplemental List of Sequences) as a member of the class Dothideomycetes, and in some hexapods, like in springtails, here represented by *Allacma fusca* (Figure 3B2; Supplemental List of Sequences). In such organisms, the similarities between the respective proteins' sequences were evident also beyond their NuBaID signatures, again in line with early findings of two closely related ILPs in *Arabidopsis thaliana* (Higashi *et al*, 2005), here now referred to as ZC3HC1 homologues.

Only within some few phyla and classes, like, for example, in Porifera and Cephalochordata (Figure 3A and 3B1), a genuine ZC3HC1 homologue remained undetectable even to date (July 2022), which was also the case for most insect orders (Figure 3B2), the latter in line with ILPs having been reported not detectable in *Drosophila* (Higashi *et al*, 2005). In a class like the Insecta, the loss of recognizable ZC3HC1 homologues apparently had occurred at different time points during insect evolution and the splitting of its lineages that led to its different orders.

Here, we found this exemplified by ZC3HC1 homologues not detected in the Paleoptera and most orders of the Neoptera while still present in other Neoptera orders (Figure 3B2). Furthermore, we regard it as of note that in some groups of organisms, like, for example, in the chordates' subphylum Tunicata (Figure 3B1), the existing ZC3HC1 homologues appear to be subject to various mutations of which most, at the corresponding positions of the human homologue, would entirely abolish the latter's ability of binding to the NB and TPR.

While a more detailed description of the data mining's findings and outcome went beyond the scope of the current study, we here chose two of the proteins we had newly identified as potential ZC3HC1 homologues, namely *Dd*ZC3HC1 and *Sc*Pml39p, for addressing two questions. Namely, first, whether possessing a NuBaID signature would also mark a different phyla's protein as one that would be positioned next to its species' NPC and interact with its TPR homologue, irrespective of how little sequence similarity such a putative ZC3HC1 homologue might share with *Hs*ZC3HC1. And second, whether residues we had found essential for allowing *Hs*ZC3HC1 to bind to *Hs*TPR might also be similarly essential for a distant, NuBaID-containing relative and its binding to a TPR homologue.

Supplemental Information 5. Low overall sequence similarity and a lack of shared, database-deposited sequence motifs as one reason for a kinship so far gone unrecognized between distinct ZC3HC1 homologues.

Unlike when scanning fungal sequences via ScanProsite with the NuBaID signatures, we could not detect *Sc*Pml39p when conducting local alignment searches via standard protein-protein BLASTP (Altschul *et al*, 1990) when starting with *Hs*ZC3HC1 as the query sequence, and neither was this possible vice versa. Furthermore, finding the other species' homologue was also not possible with tools using position-specific score matrices (PSSMs), like position-specific iterated (PSI)-BLAST (Altschul *et al*, 1997), when we had been searching the genus *Saccharomyces* with *Hs*ZC3HC1 as the query, and neither was this possible, again, vice versa when searching for the vertebrate homologues with *Sc*Pml39p. Similarly, the homology search tool MMseqs2 (Steinegger & Söding, 2017), used for ColabFold-based protein structure predictions (Mirdita *et al*, 2021, 2022), did not detect the human or yeast homologue with the respective other homologue's sequence either. Furthermore, even when using as the input either the human or the yeast sequence together with one of the abovementioned NuBaID signatures for then conducting searches via pattern hit-initiated (PHI)-BLAST (Zhang *et al*, 1998; https://blast.ncbi.nlm.nih.gov/Blast.cgi?PAGE=Proteins), the other homologue was not detected. In addition, other profile-based approaches, including tools like JackHMMER (Johnson *et al*,

2010) or pHMMER (Finn *et al*, 2011; Potter *et al*, 2018; https://www.ebi.ac.uk/Tools/hmmer/) that make use of Hidden Markov Models (HMM) built from multiple sequence alignments (MSA), did not allow for the identification of *Sc*Pml39p when searching the genus *Saccharomyces* with default settings and *Hs*ZC3HC1 as the query. Again, neither were the mammalian homologues identified using *Sc*Pml39p for searches via the HMMER tools. Furthermore, one also did not detect the human homologue when using the tool domain enhanced lookup time accelerated (DELTA)-BLAST (Boratyn *et al*, 2012) for a search starting with *Sc*Pml39p. However, DELTA-BLAST allowed for detecting *Sc*Pml39p when starting the search with *Hs*ZC3HC1.

These latter results can be briefly explained as follows. DELTA-BLAST makes use of the signatures and HMMs present in the Conserved Domain Database (CDD; https://www.ncbi.nlm.nih.gov/Structure/cdd/cdd.shtml) for constructing an MSA for those proteins to which such motifs have been attributed. Such MSAs are then the prerequisite for computing PSSMs that eventually are used for searching the sequence databases. In other words, DELTA-BLAST searches the CDD with a query sequence and then uses the domains the query gets aligned with to create a PSSM. This approach thus differs from other search tools commonly used for detecting distantly related homologues, with some among the latter using, for example, an MSA for constructing an HMM then used for database searching or, as another example, with some creating a PSSM based on an MSA that derives from a regular BLASTP search.

Regarding *Hs*ZC3HC1, the Pfam zf-C3HC and Rsm1 motifs were assigned to it long ago, with this information then also deposited in the CDD. The latter thus allowed for its alignment with sequences possessing the same motifs, for next deriving a PSSM from such an MSA, and for then using the latter for sequence database searches.

However, concerning *Sc*Pml39p, the Pfam database has not attributed an Rsm1 motif to it to date (July 2022; http://ftp.ebi.ac.uk/pub/databases/Pfam/releases/Pfam35.0/; https://pfam.xfam.org/family/PF08600). Moreover, while a zf-C3HC motif has been assigned to *Sc*Pml39p recently (http://ftp.ebi.ac.uk/pub/databases/Pfam/releases/Pfam30.0/), this information has not yet been incorporated (July 2022) into the CDD. The latter, in turn, means that there is no CDD-deposited profile for *Sc*Pml39p that would allow its alignment with its homologues possessing such Pfam motifs, which means that with *Sc*Pml39p as the query sequence, DELTA-BLAST will not be able to use a PSSM for its sequent search. In other words, since DELTA-BLAST *"owes its generally very good performance regarding search sensitivity and quality of alignment to the information available in the CDD"* (Boratyn *et al*, 2012), any situation in which it is not possible to attribute such information to a query sequence of interest,

results in DELTA-BLAST conducting merely a BLASTP search with this sequence. The latter thus happens to be the case for *Sc*Pml39p, for which we already knew that a BLASTP search does not allow for detecting the human homologue.

Supplemental Information 6. Assessment of the input datasets' respective contributions to user-initiated BLD structure predictions by AlphaFold2.

While we, at some point, had regarded X-ray crystallographic analyses of the ZC3HC1 structures as the next natural step, this turned out more challenging than anticipated for the human homologue. Therefore, until crystallographic data becomes available, we turned towards inspecting the ZC3HC1 structures that some of the recent neural network-based deep-learning programs allowed for predicting computationally, with us eventually using DeepMind's deep-learning program AlphaFold2 (Jumper *et al*, 2021; Tunyasuvunakool *et al*, 2021) and the ColabFold platform (Mirdita *et al*, 2021). Beforehand, though, we had scrutinized how the composition and variation of the information packages representing the input materials used for such predictions would affect any subsequently predicted BLD structures. Eventually, the outcome of several trial predictions dissipated some of our initial concerns regarding certain aspects of a BLD's structure prediction and the predicted ZC3HC1 structures' comparability, as outlined in the following.

After having inspected the predicted structures of *Hs*ZC3HC1 and *Sc*Pml39p available in the AlphaFold database for the first time and also having compared the human homologue's BLDs with both the crystal and AlphaFold2-predicted structures of the BIR domains (see, e.g., Supplemental Figure S11), we had considered it justified to look at these domains' predicted similarities with some caution, both despite and because of the human and yeast ZC3HC1 homologues' overall sequence dissimilarities on the one hand and the BLDs' and BIR domains' profile HMM similarities on the other.

In brief, we were aware that AlphaFold2 uses the primary amino acid sequence, i.e., the query sequence, for first searching both protein sequence and protein structure databases, then converts these search results into distinct input datasets, and then uses the latter for its further computations (Jumper *et al*, 2021). On the one hand, the searching of the sequence databases would result in the construction of an MSA composed of sequences from evolutionarily related proteins, with this process involving tools like Jackhmmer (Johnson *et al*, 2010; Eddy, 2011; https://www.ebi.ac.uk/Tools/hmmer/search/jackhmmer) and HHblits (Remmert *et al*, 2011; https://toolkit.tuebingen.mpg.de/tools/hhpred). On the other hand, AlphaFold2 would search the Protein Data Bank (PDB)-deposited crystal structures for structures it regards as potentially

similar to the one the query sequence would adopt. In fact, the second of AlphaFold2's input datasets are constructions that it calls the "pair representations", with these the outcome of having aligned PDB structure templates and query sequence for computing some initial representations of the query's structure (Jumper *et al*, 2021). In the subsequent computation steps, AlphaFold2 would then refine the MSA and the pair interactions, thereby exchanging information between the MSA and the structure templates iteratively. Finally, AlphaFold2 would use the exhaustively refined MSA and pair representation to construct a three-dimensional structure model (Jumper *et al*, 2021; see also https://www.blopig.com/blog/2021/07/alphafold-2-is-here-whats-behind-the-structure-prediction-miracle/).

Having then noted that for constructing the abovementioned pair representations, a ZC3HC1 query sequence would be assigned to the PDB-deposited BIR domain crystal structures as templates for AlphaFold2's computations for a BLD structure, we had wondered to which extent an alignment of a BLD with a given BIR structure, channeling the prediction into one direction, might introduce a discussible level of bias into the prediction. In fact, since AlphaFold2 was known to have been trained to produce a prediction that would be the one "*most likely to appear as part of a PDB structure*" (Jumper *et al*, 2021), we wondered how informative it would be when a structure predicted for a query sequence would look very similar to already available crystal structures considered related. In other words, with the profile HMMs of query sequences being used for database searches via HMM comparisons (Jumper *et al*, 2021), using tools like, e.g., HHSearch and HHblits (Söding, 2005; Remmert *et al*, 2011; Zimmermann *et al*, 2018) and Jackhmmer (Johnson *et al*, 2010), we wondered how such a correlation of similar but not identical HMMs with one type of crystal structure would affect the outcome of a structure prediction. In particular, since HHSearch was apparently identifying Pfam's BIR profile with a *Hs*ZC3HC1 query sequence via the HMM of its zf-C3HC motif, this would result in assigning ZC3HC1 homologues with such a profile HMM to the numerous BIR crystal structures already deposited in the PDB.

Beyond that, we had noticed that AlphaFold2 had been mentioned to take ligands and ions into account when these *"are predictable from the sequence alone"*, with AlphaFold2 *"likely to produce a structure that respects those constraints implicitly"* (Jumper *et al*, 2021), yet then found this not appear to be so for the BLDs' likely zinc ion coordination spheres (see further below, and Supplemental Figure S9D). Such latter findings, though, were in line with statements elsewhere, according to which AlphaFold2 does not make predictions about any non-protein components that might be part of a protein of interest (https://www.embl.org/news/science/alphafold-potential-impacts/). The latter, in turn, meant that AlphaFold2 would also not

take into account any potential role that the ZC3HC1 homologues' zinc ions could execute in the protein's folding process. Since it is known, though, that zinc ions can play a crucial role in the proper folding of zinc proteins, in addition to stabilizing a resulting fold (Maret & Li, 2009; Gomes & Wittung-Stafshede, 2010; Padjasek *et al*, 2020), with this also imaginable for ZC3HC1, we wondered whether non-consideration of the zinc ions' contributions by AlphaFold2 would demand caution when interpreting the predicted structures.

Further along this line, we had realized in an initial series of trial predictions that AlphaFold2 does not appear to predict the structural impact that substitutions of NuBaID's signature residues should have, which both held for mutations naturally occurring *in vivo* and others experimentally created in the current study. On the one hand, the AlphaFold2-predicted structures of such BLD single aa substitution mutants appeared essentially indistinguishable from the WT protein's predicted structure. On the other hand, we had already found such mutations abolishing the protein's ability to bind specifically to the NB and TPR. Moreover, additional experimental evidence indicated that at least some of the aa-substituted versions were no longer correctly folded *in vivo*. In contrast to the WT protein, such mutants were often more rapidly degraded and more readily sedimented by centrifugation and tended to interact with other proteins non-specifically (e.g., Gunkel & Cordes, 2022, and our unpublished data), indicating that such mutations had indeed disrupted the BLDs' natural structure. At some point then, we found it mentioned that *"AlphaFold has not been trained or validated for predicting the effect of mutations"* and was "*not expected to capture the effect of point mutations that destabilise a protein"* (https://www.embl.org/news/science/alphafold-potential-impacts/). It was also inferable why this might be so since AlphaFold2 had been trained to correlate sequence information with only the end products of protein folding processes (Jumper *et al*, 2021) and with such end products having been primarily the proteins' WT versions or parts thereof. Nonetheless, such realization meant that we had to be cautious also in this context and to avoid pitfalls when interpreting the predicted structures of, for example, distinct ZC3HC1 homologues that represent some particular, naturally existing mutant versions.

Given such preliminary insight, yet lacking the expertise to comment on the program's algorithms and codes, while at the same time wanting to assess better the range of AlphaFold2's opportunities and restraints in order to define how far we could go in interpreting predicted BLD structures, we conducted, in a semi-systematic manner, some additional series of simple trial predictions. With some, we wanted to assess the degree of interdependency between the MSA-based and the template-based part of AlphaFold2's prediction process and how the PDB-deposited structures would contribute to a user-initiated structure prediction. In other words, we

wanted to know how the exclusion of PDB information, i.e., not permitting the program to use the PDB-deposited BIR domain crystal structures as reference templates, might affect the predicted BLD structures' appearance (e.g., Supplemental Figure S9A and S9B). Furthermore, we also intended to use the ColabFold platform (https://colab.research.google.com/github/sokrypton/ColabFold/blob/main/AlphaFold2.ipynb) for conducting such trial predictions to benefit from its accelerated predictions made possible by combining the fast homology search of the MMseqs2 program with AlphaFold2 (Mirdita *et al*, 2021), instead of conducting all structure predictions directly via AlphaFold2. We thus considered it also necessary to compare the AlphaFold2 predictions with those obtained via the ColabFold-accelerated approach (Supplemental Figure S9A and S9B).

Then, with other trials, we tested the outcome of using MSAs only composed of sequences lacking Pfam Rsm1 motifs while representing ZC3HC1 homologues nonetheless, according to our criteria. In other words, we wanted to know how far sequences lacking such a profile HMM, which might also not have been part of the MSAs used for the PDB template alignments during AlphaFold2's initial training sessions, would allow for user-initiated BLD structure predictions resembling those that one obtains with the programs' default settings (e.g., Supplemental Figure S9C). In again other words, with approaches of this kind, we aimed to assess how the MSA's composition and how selectively changing it would affect the outcome of a prediction process.

Finally, we wanted to learn more about AlphaFold2's inability to predict the effects caused by mutations. So far, we knew that the sequence of an individual aa substitution mutant, used as the query, would lead to an MSA primarily composed of WT sequences. Since this WT-sequence-dominated MSA would then be the input dataset guiding the subsequent structure prediction process, we wondered whether it might be the dominance of WT sequences, "assimilating" the mutant sequence, that would prevent appreciating a single mutation's structural consequences. Now, we wanted to know whether the outcome would be different if such an MSA were composed exclusively of sequences similarly mutated. In other words, using the approach via ColabFold, we wanted to feed AlphaFold2's "evoformer" (Jumper *et al*, 2021) with an MSA that we would force into being composed merely of mutant sequences all harboring the same mutations (Supplemental Figure S9D). With this approach, we aimed to assess whether or not AlphaFold2's neural network training might have already educated it so that even compilations of mutations within an MSA might no longer be recognizable as such.

In brief, the outcome of these trial experiments can be summarized as follows. First, using ColabFold's default settings, we noted that the BLD and BIR domain structures predicted via

ColabFold were essentially indistinguishable from those derived directly from AlphaFold2's database of predicted structures (e.g., Supplemental Figures S9A, S9B, and S11A2).

Second, we noted that user-initiated predictions of BLD and BIR domain structures, when not accessing PDB template information, resulted, nonetheless, in structures that, too, were essentially indistinguishable from those derived directly from AlphaFold2's database, as long as sufficiently informative MSAs were provided (e.g., Supplemental Figures S9A, S9B, and S11A2). In other words, once AlphaFold2's initial neural network training had been completed, crystal structures like, e.g., those of the BIR domains were apparently dispensable as templates for a then user-initiated prediction of structures like, e.g., those of the BLDs. For such template-free modeling, we sometimes used also the AlphaFold-Colab notebook (https://colab.research.google.com/github/deepmind/alphafold/blob/main/notebooks/AlphaFold.ipynb), the latter a simplified version of AlphaFold2 omitting in its predefined settings an alignment with PDB templates. However, for systematically conducting trials of this kind, we used ColabFold instead. For example, having noted that those MSAs compiled by ColabFold's default settings, e.g., for *Hs*ZC3HC1 and *Sc*Pml39p, would be linked, e.g., via the HHsearch tool, to the PDB-deposited metazoan BIR structures, we made use of ColabFold's options for barring or including such PDB information. Nonetheless, the template-free approach also led to predicting essentially the same BLD structures as with AlphaFold2's default settings (e.g., Supplemental Figure S9A and S9B).

Third, we found that a BLD2 structure prediction that had started with an MSA only composed of sequences without a pre-existing Rsm1 profile, while representing ZC3HC1 homologues nonetheless, could result in structures closely resembling those obtained with the template-based and template-barring settings of ColabFold and the default settings of AlphaFold2. For example, even without any template information and no profile HMM appertaining to the input sequences representing the homologues' BLD2 (the latter at least so at the time when we initially conducted such trials before, e.g., the HHpred web server updates in 2022; https://toolkit.tuebingen.mpg.de/tools/hhpred; Zimmermann *et al*, 2018), the predicted structure of the *Sc*Pml39p BLD2 still closely resembled the initial predictions based on MSAs composed of sequences with Rsm1 motifs already assigned to them (Supplemental Figure S9C).

Fourth, we found that AlphaFold2 did not predict the effect of amino acid substitution mutations even when several of such mutations had been introduced into all sequences of an MSA then to be the input dataset for a structure prediction. For example, having introduced several mutations into all of the MSA's sequences used for predicting the BLD structures of *Sc*Pml39p, even a high-sensitivity HMM comparison tool like HHpred, again at the time prior

to its 2022 web server updates, could no longer correlate an HMM deduced from such an MSA with any BLD-reminiscent structure. Nonetheless, the structure predicted for such a manifoldly mutated BLD2 was still essentially the same as obtained with ColabFold's default settings (Supplemental Figure S9D).

As a whole, these trial experiments provided some guiding principles for us as to how far we could go in carefully interpreting the predicted structures presented in the current study, with these trials' findings having outlined the confines within which we considered it justified to deduce conclusions cautiously from the data provided by AlphaFold2. Aware that the predictions, even for the BLDs' core parts, are likely not perfect, not expecting them to provide already the definite positions of the BLDs' structural elements, we regard further efforts that aim at still gaining crystal structure information for the ZC3HC1 BLDs as reasonable. On the other hand, though, we regard the information provided by these predictions as already highly valuable within the range of resolution and presumed accuracy we considered sufficient for the current study's objectives. One of the latter was to provide a first overall impression of the ZC3HC1 homologues' molecular features, including the approximate positions of their BLDs' different structural elements relative to each other. Furthermore, such predictions provided hints as to where to expect the ZC3HC1 homologues' potential binding sites for their respective TPR homologues, allowing us to conjecture which additional structural parts of ZC3HC1 might be promising for further molecular manipulations. Moreover, by illustrating the similarity and equivalence of their structural elements, these predictions markedly underscored the kinship of *Hs*ZC3HC1 and *Sc*Pml39p. Apart from that, the predictions allowed us to argue against some other models, which we initially did not deem justified to categorically exclude, of what the zinc ion-coordination topology of ZC3HC1 might look like (Supplemental Figure S14), thereby supporting a model already proposed by others (Higashi *et al*, 2005).

However, our trial experiments also provided some information that we regarded as unsettling to some extent. Having realized that AlphaFold2 would predict an essentially intact, i.e., non-mutated protein from a query sequence and an MSA composed only of *in-silico* mutated sequences, with mutations that, in reality, would most likely render the protein conspicuously unfolded, we regarded this as a warning to keep in mind. In particular, when considering using this program for predicting the structures of naturally-occurring mutated versions of ZC3HC1.

Supplemental Information 7. BLD structure predictions unveiling evolutionarily conserved α-helices, with some common to both BLDs and others either BLD1- or BLD2-specific.

The structure predictions of the BLDs of *Hs*ZC3HC1, *Dd*ZC3HC1, and *Sc*Pml39p had revealed several α-helices at equivalent positions in all three homologues, with some of these α-helices occurring equivalently within each homologue's two BLDs while others are specific for either only BLD1 or BLD2. Some of these α-helices belong to those BLD parts that we referred to as the central ones (e.g., Figure 6A and 6B). The other α-helices are located beyond these central parts and are now assigned to the BLDs' so-called extended versions (e.g., Figure 6C and 6D). Our realization that some of these additional α-helices should actually be regarded as part of a BLD has actually led us to newly define the BLDs' expanse and the BLDs' novel boundaries, as will be outlined further below. Altogether, seven α-helices can now be regarded as being part of the NuBaID in all three homologues, with the newly defined BLD1 and BLD2 harboring three and four α-helices, respectively. All of these α-helices will be addressed in the following.

First, though, regarding only the central parts of each homologue's BLDs, a total of three α-helices could be assigned to them. For the predictions presented in Figure 6A, we introduced only some minor adjustments to these BLD boundaries, with such adjustments based on an initial superimposition and alignment of the three homologues' AlphaFold2-predicted structures.

Of these three α-helices, two could be regarded as being equivalent ones occurring in both BLD1 and BLD2. These α-helices, being the grey-colored ones, e.g., in Figure 6–C, and Supplemental Figures S10B1, S10B2, S11C1, and S11F, appear to play roles in intra- and inter-BLD contacts (e.g., Supplemental Figures S10B1 and S11F). An equivalent α-helix is also part of the BIR domain (e.g., Supplemental Figure S11C1 and S11E). In *Hs*ZC3HC1, these grey-colored α-helices range from P99 to K104 in BLD1 and from E211 to E231 in BLD2. The third α-helix of the BLDs' central parts is, by contrast, specific for BLD1 and is shown and referred to as the light-pink-colored one in the following. This rather extended, evolutionarily conserved BLD1 α-helix (e.g., Figure 6A–C, Supplemental Figures S10B1 and S11C1) ranges from F134 to T150 in *Hs*ZC3HC1. Such a BLD1-specific α-helix is not only absent from BLD2; an equivalent α-helix is not part of the BIR domains either (Supplemental Figure S11C1, S11D, and S11E).

Among the four α-helices that one can then additionally assign to the BLDs' extended versions are two that are BLD2-specific. One of these conspicuous α-helices ranges from E211 to E231 in *Hs*ZC3HC1, representing the light-blue-colored one in, e.g., Figure 6C and

Supplemental Figure S10B1 and S11E2. This α-helix is positioned outside of the initially defined BLD2 region (Kokoszynska *et al*, 2008, and Figure 1). While present in many ZC3HC1 homologues, including the three homologues presented here, this α-helix appears to be absent, though, in some organisms, for example, in some but not other families of the nematodes.

The other BLD2-specific α-helix, evolutionarily widely conserved and also located beyond the initial BLD2 boundaries, ranges from G457 to S471 in *Hs*ZC3HC1. It represents the light-yellow-colored α-helix in, e.g., Figure 6C and Supplemental Figure S10B1 and S11E2.

However, even these two α-helices, the light-blue-colored one in its entirety and the light-yellow-colored one with almost all of its residues, were part of the minimalist *Hs*ZC3HC1 deletion mutant we had found still capable of NE-association (Figure 1; for further details, see main Results and Supplemental Figure S12). We also consider it noteworthy that at least the light-blue-colored α-helix was found absent from not only the BLD1 but also the BIR domains (Supplemental Figure S11E).

The two other conspicuous α-helices still to be addressed are the ones presented as orange-colored, e.g., in Figure 6C and Supplemental Figures S10B1, S10B2, S11E2, and S11F. Initially, one of them, present in all three homologues, appeared specific for the BLD1; before only here now assigning a corresponding α-helix also to BLD2. In the *Hs*ZC3HC1 BLD1, this α-helix was predicted to start at K75, meaning that all (Kokoszynska *et al*, 2008) or some of this domain's residues (Higashi *et al*, 2005; Figure 1) were already part of the initially defined BLD1 region. Of particular note, several residues of this BLD1 α-helix appear to contribute to the establishment of the abovementioned BLD1:BLD2 interface (Supplemental Figure S10B), while several of its other residues appear to engage in intra-BLD contacts (Supplemental Figure S11F). Moreover, having found that a mutant version of *Hs*ZC3HC1 starting at S72 was well capable of binding to the NE, while deletion of aa 1–81 had abolished such binding (Figure 1), we could now conclude that integrity of this orange-colored α-helix of BLD1, ranging from at least aa K75 to T84, was essential for a functional bimodular NuBaID of *Hs*ZC3HC1 capable of NB-binding. Thus, when defining the boundaries of BLD1, this α-helix needed to be included.

So far, however, a corresponding α-helix apparently associated with BLD2 had not been considered part of this BLD. Instead, the N-terminal BLD2 boundary had been regarded as located at H226 or even further away from BLD1 (also see Figures 1C, 2A1, and 4A). On the other hand, the α-helix we were showing as the orange-colored one of BLD2, as in, e.g., Figure 6C and Supplemental Figures S10B1, S11E2, and S11F, comprises aa A176 to C190. Since we had found deletion mutants lacking either aa 170–210, aa 170–188, or aa 170–178 to all be

incapable of NE-association (Figure 1A and 1B, Supplemental Figure S2A), one could thus consider the integrity of also this BLD2 α-helix as likely essential for NB-binding of *Hs*ZC3HC1.

While this orange-colored α-helix of BLD2, unlike the orange-colored one of BLD1, did not appear to contribute directly to the BLD1:BLD2 interface (Supplemental Figure S10B2), both of these α-helices had one particular feature in common that we regarded as marking them as equivalent nonetheless. This property was their possession of an evolutionarily conserved arginine of apparently similar function. In the human BLD2, we found this arginine positioned at R185, while the corresponding one of BLD1 locates at R81 (Supplemental Figure S11E2), with each appearing to be involved in stabilizing the position of its α-helix relative to the BLD's more central parts. Moreover, each one was predicted to contribute to additionally stabilizing the position of one of the aromatic residues we had studied earlier, namely W158 and W431, and such intra-BLD residue contacts, corresponding to R81:W158 and R185:W431, turned out to be characteristic for *Dd*ZC3HC1 and *Sc*Pml39p too (Supplemental Figure S11F and S11G). Of further note, both this particular α-helix and its evolutionarily conserved arginine residue have an equivalent as part of the BIR domains (Supplemental Figure S11E2 and S11G), thus representing features common to all of the here presented BLDs and BIR domains. For the latter, we have orange-colored this α-helix accordingly (Supplemental Figure S11E1).

Supplemental Information 8. A relationship between *Sc*Pml39p/*Hs*ZC3HC1 and *Sc*Nup157p/*Hs*NUP155?

Pondering on similarities between *Hs*ZC3HC1 and *Sc*Pml39p, we consider it justified to bring a former Y2H screen's reported outcome to mind again. This screen of a yeast genomic library identified Nup157p as another potential binding partner of Pml39p (Palancade *et al*, 2005). With *Sc*Nup157p being the homologue of *Hs*NUP155 (Aitchison *et al*, 1995), this result might perhaps represent another one pointing towards kinship between Pml39p and ZC3HC1, even though our Y2H-screening of a human cDNA library with ZC3HC1 (Gunkel *et al*, manuscript in preparation) had not provided a NUP155 cDNA. We also had not found NUP155 notably co-detached with ZC3HC1 from NEs upon NB disassembly in *Xenopus* oocytes (Gunkel *et al*, 2021), and only minor amounts of NUP155, or none at all, were released concomitantly to the degradation of NBs in human cell lines expressing degron-tagged NB components (Gunkel & Cordes, 2022; our unpublished data). Remarkably, however, when immunoprecipitating ectopically expressed *Hs*ZC3HC1, we found peptides of NUP155 as the only representative of the NPC proper among the co-sedimented materials (our unpublished data).

Our subsequent attempts to illuminate this potential link between ZC3HC1 and NUP155 *in vivo* did not provide much further insight, with both proteins' subcellular positioning not appearing directly affected in the absence of the respective other. This latter finding, though, was again in line with *NUP157* deletion not having affected Pml39p localization either (Palancade *et al*, 2005). Nonetheless, we continue wondering whether the observed interactions between *Sc*Pml39p and *Sc*Nup157p and between *Hs*ZC3HC1 and *Hs*NUP155 might reflect some genuine relationship common to both species or just coincidentally some same type of unspecific interaction.

Supplemental Information 9. Instability of the Mlp-dependent association of *Sc*Pml39p with NPCs under common cell fractionation conditions?

The TPR-dependent association of ZC3HC1, both in humans and amphibians, is sensitive to low temperatures and commonly depends on the presence of bivalent cations, among other conditions, as described earlier (Gunkel *et al*, 2021). By contrast, some of the standard cell fractionation protocols, using ice-cold solutions without adequate amounts of bivalent cations, can cause all or substantial amounts of ZC3HC1 to be detached from the NE, together with the ZC3HC1-dependent population of TPR polypeptides (Gunkel *et al*, 2021). With some of these conditions also employed at specific steps of certain yeast fractionation procedures, we can imagine that sensitivity towards non-physiological conditions could also apply to the interactions between the Pml39 and Mlp polypeptides, causing Pml39p detachment from its Mlp binding partners.

Concerning Pml39p, a notion of a similar kind had already been expressed earlier when authors stated that the Mlp-dependent association of Pml39p with NPCs *"might thus be either transient or unstable under biochemical purification conditions"* (Palancade *et al*, 2005). Along this line, except for two studies (Niepel *et al*, 2013; Bensidoun *et al*, 2021), affinity purifications of Mlp1p or Mlp2p in other investigations appear not to have come along with identifying Pml39p in notable amounts, despite co-isolating other NPC proteins and even nucleocytoplasmic transport factors and mRNA-associated proteins (e.g., Niepel *et al*, 2005; Bretes *et al*, 2014; Saroufim *et al*, 2015; Kim *et al*, 2018). Moreover, just like ZC3HC1 had no longer been detectable among the proteins of purified rat NPCs (Cronshaw *et al*, 2002), reproducibly a consequence of its sensitivity to the conditions mentioned above (Gunkel *et al*, 2021), Pml39p had not been identifiable during the pathbreaking mass spectrometry-based proteomics of purified yeast NPCs either (Rout *et al*, 2000), with the corresponding *YML107C*/*PML39* ORF sequence possibly available at the time (Bowman *et al*, 1997). However, just as

discussed for ZC3HC1 in detail (Gunkel *et al*, 2021), we see no incompatibility in Pml39p being an NB component whose interaction stability with the Mlps can vary under certain non-physiological conditions.

Supplemental Figures

Supplemental Figure S1. Photobleaching experiments with fluorescent protein-tagged proteins ectopically expressed in HeLa WT cells.

Supplemental Figure S2. Characterization of ZC3HC1 deletion and single aa-substituted mutants, ectopically expressed in HeLa WT and ZC3HC1 KO cells, by fluorescence microscopy and FLIP, complemented by additional Y2H experiments.

Supplemental Figure S3. Functional tolerance of *Hs*ZC3HC1 for a C-$X_{(3)}$-C spacing within its first BLD, as commonly present in some fungal ZC3HC1 homologues.

Supplemental Figure S4. Size variations of loop-like sequence insertions within exemplary ZC3HC1 homologues.

Supplemental Figure S5. Complementing the characterization of the *Dictyostelium* homologues of ZC3HC1 and TPR.

Supplemental Figure S6. Complementing the characterization of *Sc*Pml39p and its NuBaID.

Supplemental Figure S7. Complementing studies on the contribution of *Sc*Pml39p in keeping subpopulations of NE-associated Mlp1 polypeptides positioned at the NB and within Mlp1p-containing nuclear foci.

Supplemental Figure S8. Experiments revealing that *Sc*Pml39p and *Hs*ZC3HC1 cannot interact with the respective other species' TPR homologues.

Supplemental Figure S9. Assessment of the contributions of sequence database search-derived MSAs and PDB database-deposited structures as templates for BLD structure predictions.

Supplemental Figure S10. The tertiary structures of *Hs*ZC3HC1, *Dd*ZC3HC1, and *Sc*Pml39p *in toto*, as predicted by AlphaFold2, and closer looks at a BLD1:BLD2 interface and at distinct aromatic amino acids flanking the zinc ion coordination spheres.

Supplemental Figure S11. Comparing the predicted structural characteristics and sequence features of the BLDs of ZC3HC1 with the BIR domains' structures and sequences.

Supplemental Figure S12. *In vivo* and *in silico* deletion mutants of ZC3HC1 homologues and their tertiary structures predicted by AlphaFold2 via ColabFold.

Supplemental Figure S13. Experiments revealing ZC3HC1 deficiency in human cell lines not affecting the cellular amounts and subcellular distribution of FANCD2, in line with no evident robust interaction between ZC3HC1 and FANCD2, neither at the NE nor in cell extracts.

Supplemental Figure S14. Former considerations regarding the zinc ion-coordination topology of ZC3HC1.

Supplemental Figure S15. The BLD2 loop of *Hs*ZC3HC1 as a prime target for phosphorylation.

Supplemental Figure S16. Comparing the crystal structure of an *Sc*Pml39 polypeptide with its tertiary structure as predicted by AlphaFold2.

Supplemental Figure S17. Searching AlphaFold2's protein structure datasets via Foldseek, using ZC3HC1 and BIR protein structures as queries.

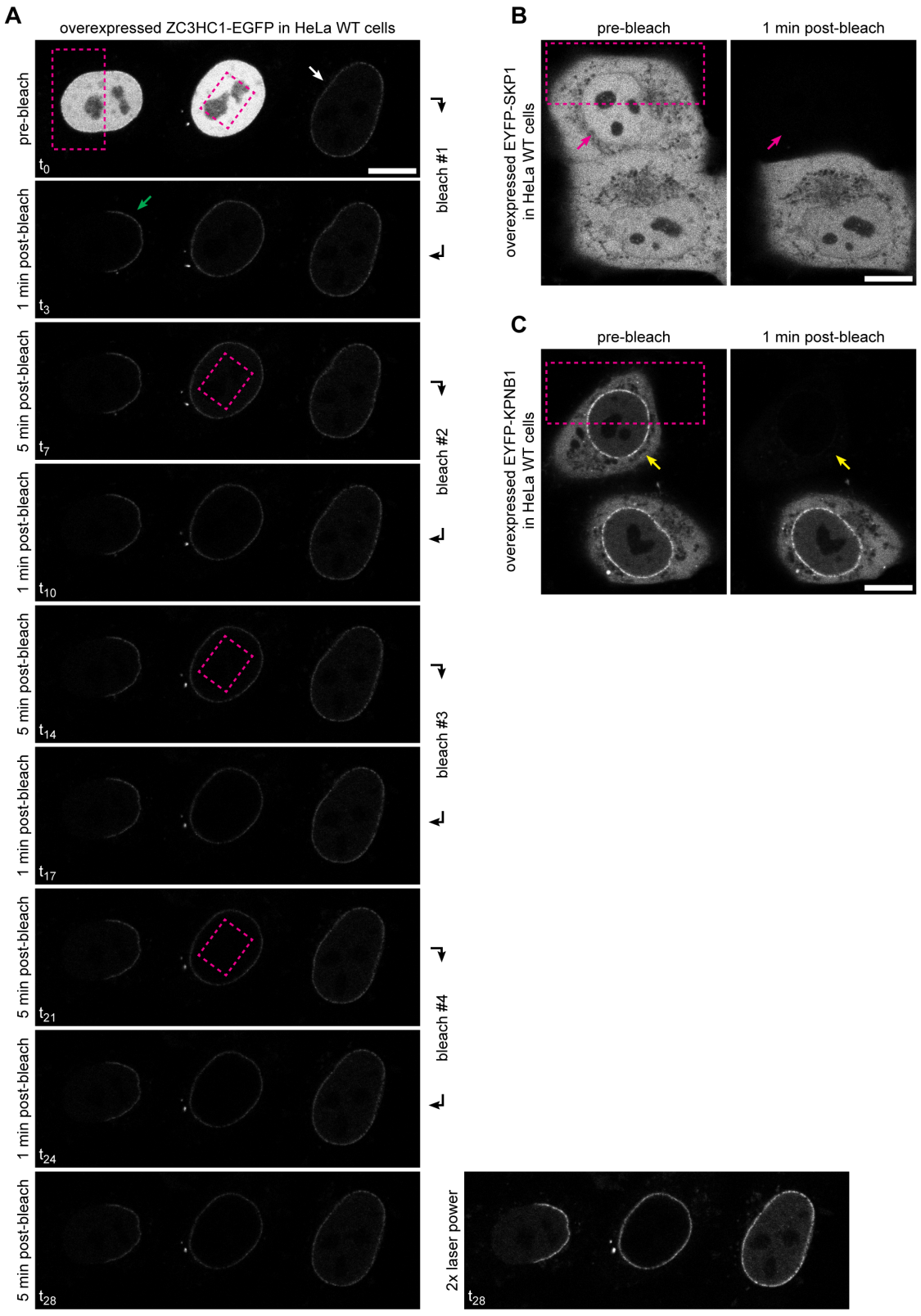

Supplemental Figure S1. Photobleaching experiments with fluorescent protein-tagged proteins ectopically expressed in HeLa WT cells.

Upon constitutive ectopic expression of either an N-terminally EYFP-tagged or a C-terminally EGFP-tagged version of the WT ZC3HC1 protein, we had found such recombinant proteins,

when synthesized only in low amounts, primarily located at the NE, which suggested early on that the NE was a preferred binding site for these tagged versions of ZC3HC1. However, upon further overexpression, we had seen the tagged ZC3HC1 polypeptides distributed throughout the nuclear interior, then resembling the formerly described subcellular localization of ZC3HC1 (Ouyang *et al*, 2003). Such increased levels of ZC3HC1 often made it no longer possible to detect any preferred location at either the NE or any other site within the nucleus, and later we found this issue particularly applying to various mutant versions of ZC3HC1. Live-cell photobleaching of such nuclear pools of tagged ZC3HC1 polypeptides was thus mainly performed to more reliably assess whether specific ZC3HC1 mutants might be capable of binding to the NE. Later on, once ZC3HC1 KO cells had become available, such fluorescence-loss-in-photobleaching (FLIP) experiments were also conducted with the KO cells, with the latter then too ectopically expressing versions of ZC3HC1 tagged with fluorescent proteins (FP), as will be shown further below (see Supplemental Figure S2).

On the other hand, not yet aware at this point that years later, ZC3HC1 would be proven to be a structural element of the NB (Gunkel & Cordes, 2022), the purpose of the initial photobleaching experiments shown here, performed with the EGFP-tagged WT version of ZC3HC1, was to allow for an early assessment as to how durably the ectopically expressed ZC3HC1 polypeptides might be positioned at the NE. Such experiments were thus to provide a first impression regarding the degree of exchange between the NE-located and nuclear pools of ZC3HC1 before addressing this issue at a later time point in more detail by fluorescence recovery after photobleaching (FRAP) experiments, which will be presented elsewhere as part of another study.

Moreover, the initial photobleaching experiments shown here were to be conducted for comparison also with cells expressing other FP-tagged proteins, including the nuclear import factor importin β/KPNB1, which shuttles between the nucleus and cytoplasm (Görlich & Kutay, 1999) and only transiently interacts with the NPC but occurs enriched there in steady-state nonetheless (Görlich *et al*, 1995). In addition, we studied the subcellular distribution of SKP1, being a formerly reported direct binding partner of ZC3HC1 (e.g., Bassermann *et al*, 2005a, 2005b, 2007; Klitzing *et al*, 2011), with this latter notion, though, later refuted (Gunkel *et al*, 2021).

(A) Live-cell fluorescence micrograph of HeLa WT cells transiently transfected with constitutive expression vectors coding for ZC3HC1-EGFP, showing NE-staining in cells expressing only lower amounts of ZC3HC1-EGFP (white arrow) and others in which seemingly

vast amounts were located throughout the nucleus. Photobleaching experiments were performed to assess the extent to which such intranuclear pools of ZC3HC1 might be mobile and to which extent there might be an exchange between this nuclear pool and the ZC3HC1 polypeptides at the NE. The two marked rectangular areas in the pre-bleach image were subjected to pulses of full laser power for 2 min, followed by the acquisition of post-bleach images 1 min and 5 min after the bleaching. The cell shown in the center was then subjected to an immediate next round of bleaching for 2 min, again followed by image acquisition and the repetition of this procedure until four rounds of bleaching and image acquisition had been conducted. For comparison, the cell expressing only low amounts of ZC3HC1-EGFP in the same field of imaging (white arrow) was left unbleached, also in order to assess the degree of signal reduction due to bleaching during image acquisition. Note that the surplus of ZC3HC1 polypeptides deeper within the nuclear interior of the centrally located cell apparently had no immobile natural binding partner that would allow for a longer-lasting interaction. In fact, repeated bleaching of the nuclear interior of this ZC3HC1-overexpressing cell resulted in the quantitative elimination of the nuclear EGFP fluorescence, pointing at a highly mobile pool of nuclear ZC3HC1 polypeptides. On the other hand, the NE of this bleached middle cell concomitantly emerged as the only structure that was still fluorescent even after having bleached its nuclear interior repeatedly. This result indicated a steady and lasting *in vivo* interaction between the NE and a certain amount of ZC3HC1. This conclusion was underscored further by the result relating to the left cell's bleached NE fragment (green arrow), which had remained faded over the monitored period of about 32 min without any remarkable recovery of EGFP fluorescence. This result of such a first type of preliminary FRAP experiment still held when the corresponding image had been acquired with doubled laser power (last image on the right side). As an aside, note that we obtained essentially identical results also after having performed such photobleaching experiments with HeLa cells expressing EYFP-ZC3HC1 (our unpublished data). Bar, 10 µm.
(B, **C)** Live-cell fluorescence micrographs of HeLa WT cells that had been transiently transfected with constitutive expression vectors coding for EYFP-SKP1 and EYFP-KPNB1 and then used for representative photobleaching experiments. In both S1B and S1C, each bleached area (large rectangles) had been subjected once to pulses of full laser power for 2 min. By contrast, the reference cells, one each in S1B and S1C, had been left unbleached to show that the degree of bleaching due to image acquisition prior to and after the actual bleaching procedure was negligible. Especially when compared to the NE-associated pool of ZC3HC1-EGFP in S1A, it was evident that all subcellular populations of these other proteins were far more mobile, yet to a variable extent.

(B) In the case of the EYFP-SKP1-expressing cell, the single round of bleaching of part of its nucleus and cytoplasmic compartment led to a complete loss of this cell's EYFP fluorescence. Note, in particular, that also no traces of signal were seen at the non-bleached NE (magenta-colored arrows), with this suggesting early on that this particular protein does not engage in any lasting interaction with any of the NE's components. As an aside, also note that we obtained essentially identical results after performing such photobleaching experiments with HeLa cells expressing SKP1-EGFP (our unpublished data). Bar, 10 μm.

(C) In the EYFP-KPNB1-expressing cells, the overexpressed protein was not only distributed throughout the nucleus and cytoplasm but also enriched at the NE. However, this did not come as a surprise as such enrichment was known to reflect the naturally occurring subcellular distribution of endogenous KPNB1 (Görlich *et al*, 1995). Nonetheless, just like in the case for EYFP-SKP1, a single round of only bleaching part of the nucleus and the cytoplasmic compartment was sufficient to obliterate all fluorescence from both compartments, in line with KPNB1 being primarily a highly mobile nuclear transport receptor. Furthermore, and in striking contrast to the findings for ZC3HC1-EGFP in S1A, the EYFP-KPNB1 signal at the unbleached part of the NE too (yellow-colored arrows) was nearly abolished, confirming that KPNB1 polypeptides mainly engage in only transient physical interactions with components of the NPC. Bar, 10 μm.

A1

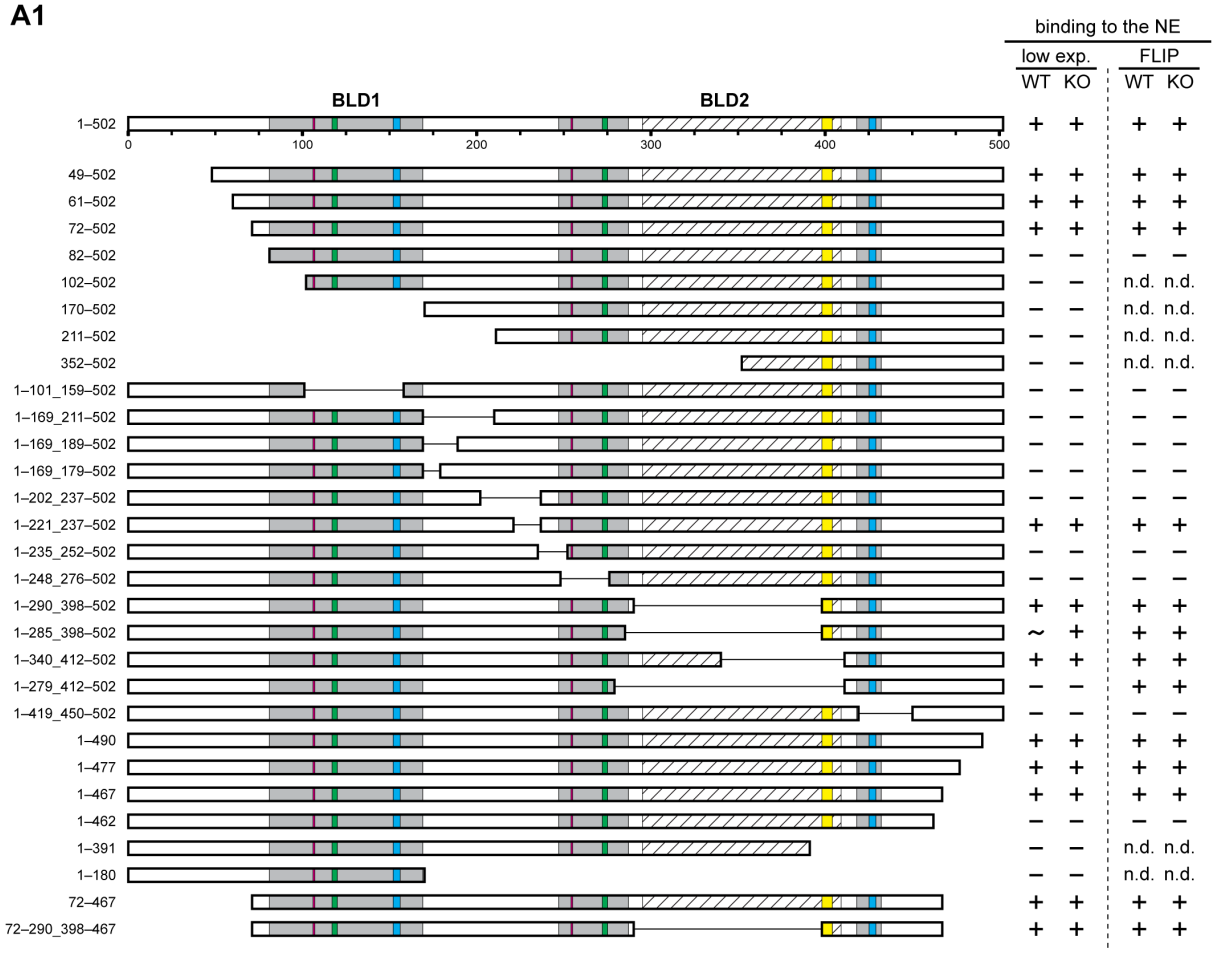
binding to the NE
low exp.
FLIP
WT KO WT KO
BLD1
BLD2
1–502 + + + +
0 100 200 300 400 500
49–502 + + + +
61–502 + + + +
72–502 + + + +
82–502 – – – –
102–502 – – n.d. n.d.
170–502 – – n.d. n.d.
211–502 – – n.d. n.d.
352–502 – – n.d. n.d.
1–101_159–502 – – – –
1–169_211–502 – – – –
1–169_189–502 – – – –
1–169_179–502 – – – –
1–202_237–502 – – – –
1–221_237–502 + + + +
1–235_252–502 – – – –
1–248_276–502 – – – –
1–290_398–502 + + + +
1–285_398–502 ~ + + +
1–340_412–502 + + + +
1–279_412–502 – – + +
1–419_450–502 – – – –
1–490 + + + +
1–477 + + + +
1–467 + + + +
1–462 – – – –
1–391 – – n.d. n.d.
1–180 – – n.d. n.d.
72–467 + + + +
72–290_398–467 + + + +

S2 (1/8)

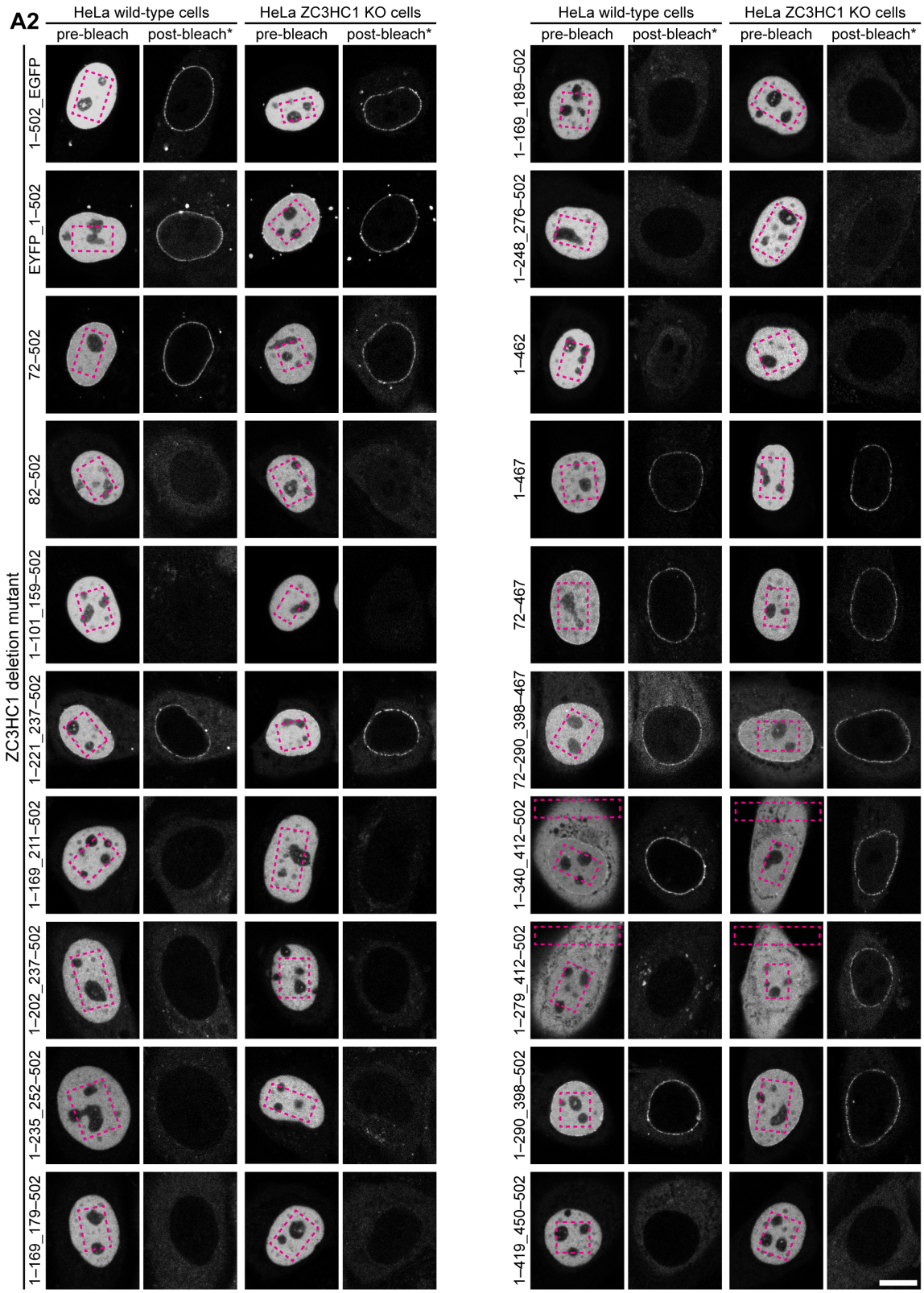
A2
HeLa wild-type cells
HeLa ZC3HC1 KO cells
pre-bleach
post-bleach*
ZC3HC1 deletion mutant
1–502_EGFP
EYFP_1–502
72–502
82–502
1–101_159–502
1–221_237–502
1–169_211–502
1–202_237–502
1–235_252–502
1–169_179–502
1–169_189–502
1–248_276–502
1–462
1–467
72–467
72–290_398–467
1–340_412–502
1–279_412–502
1–290_398–502
1–419_450–502

S2 (2/8)

B1

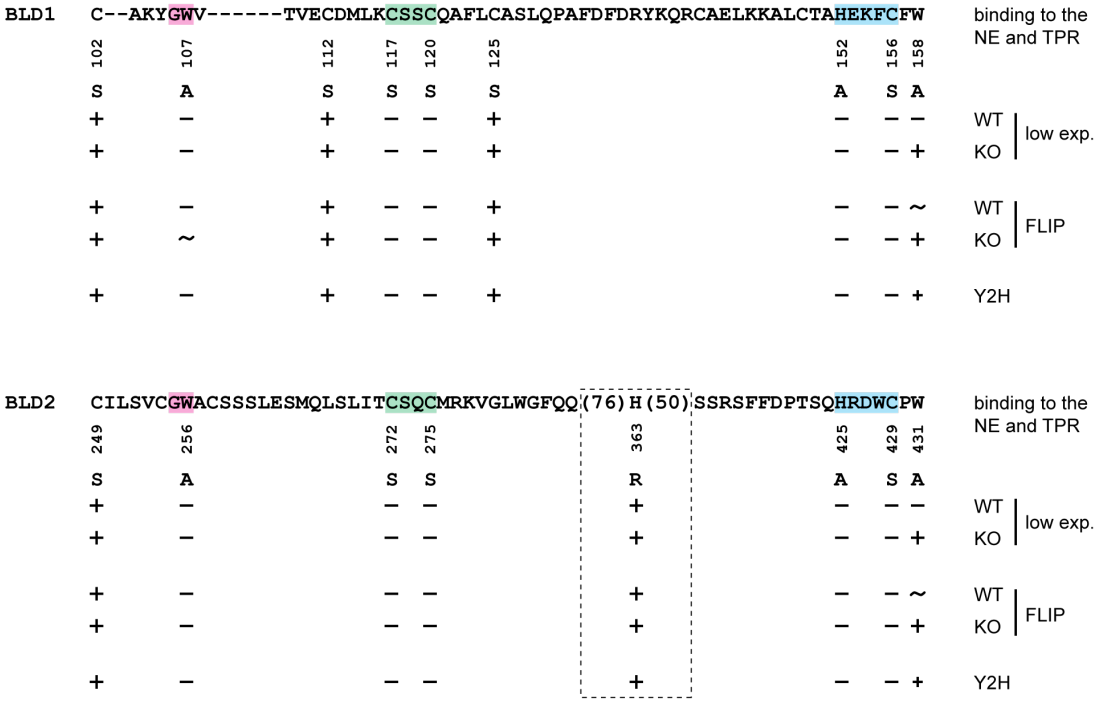
BLD1 C--AKYGWV------TVECDMLKCSSCQAFLCASLQPAFDFDRYKQRCAELKKALCTAHEKFCFW
binding to the NE and TPR
102 107 112 117 120 125 152 156 158
S A S S S S A S A
+ − + − − + − − − WT
+ − + − − + − − + KO
low exp.
+ − + − − + − − ~ WT
+ ~ + − − + − − + KO
FLIP
+ − + − − + − − + Y2H
BLD2 CILSVCGWACSSSLESMQLSLITCSQCMRKVGLWGFQQ(76)H(50)SSRSFFDPTSQHRDWCPW
binding to the NE and TPR
249 256 272 275 363 425 429 431
S A S S R A S A
+ − − − + − − − WT
+ − − − + − − + KO
low exp.
+ − − − + − − ~ WT
+ − − − + − − + KO
FLIP
+ − − − + − − + Y2H

S2 (3/8)

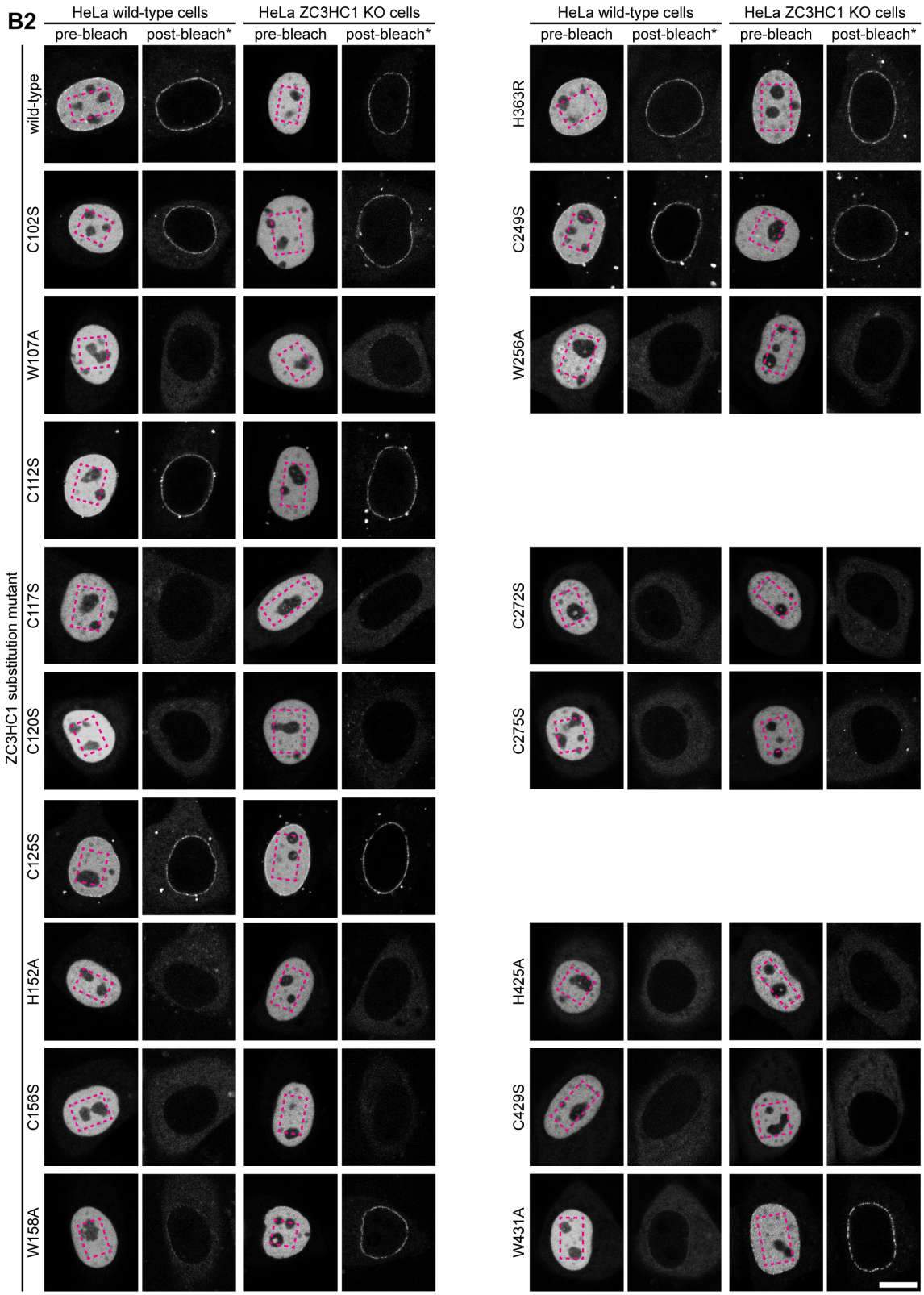
B2
HeLa wild-type cells
HeLa ZC3HC1 KO cells
pre-bleach
post-bleach*
ZC3HC1 substitution mutant
wild-type
C102S
W107A
C112S
C117S
C120S
C125S
H152A
C156S
W158A
H363R
C249S
W256A
C272S
C275S
H425A
C429S
W431A

S2 (4/8)

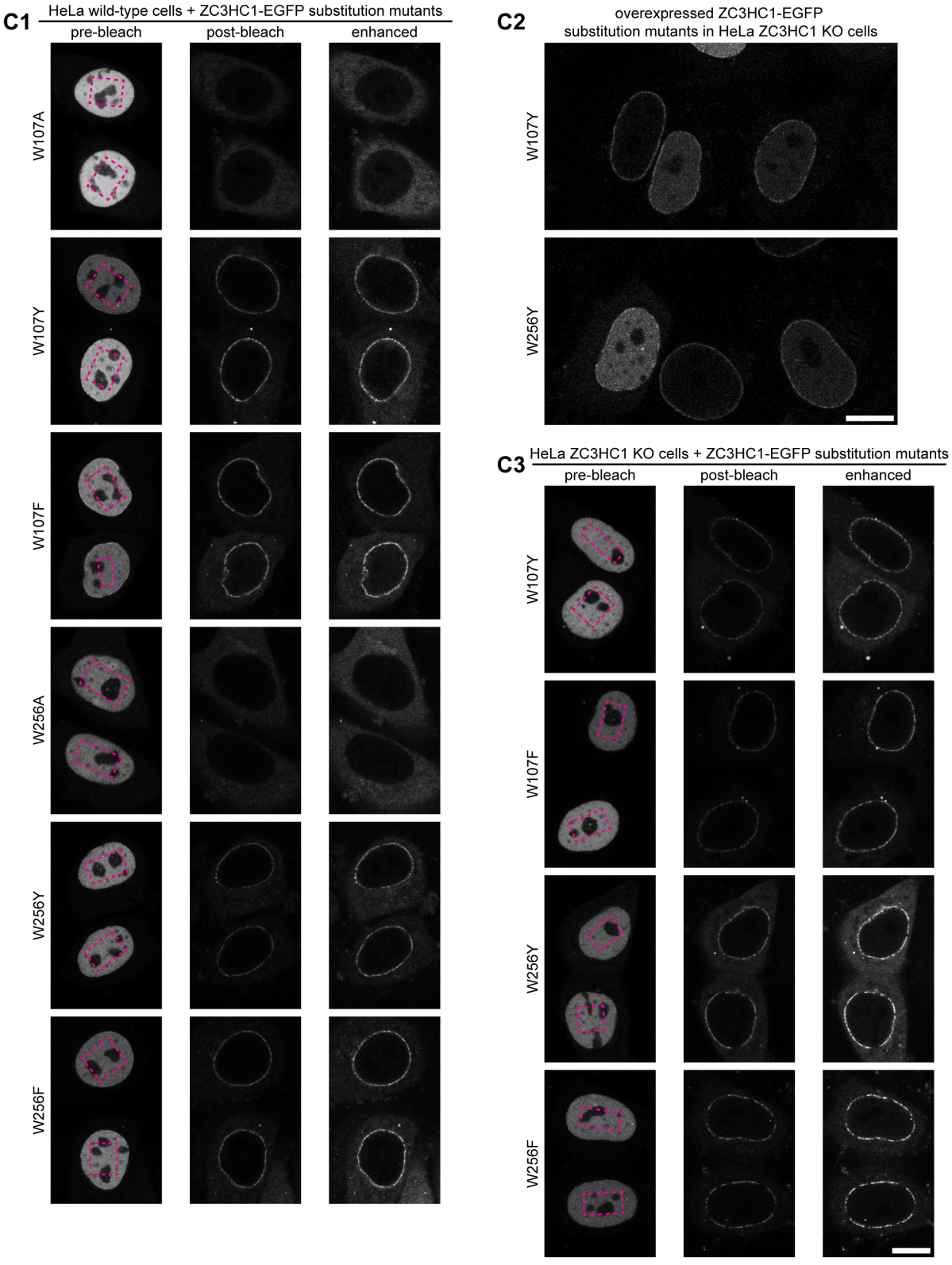
C1
HeLa wild-type cells + ZC3HC1-EGFP substitution mutants
pre-bleach
post-bleach
enhanced
W107A
W107Y
W107F
W256A
W256Y
W256F
C2
overexpressed ZC3HC1-EGFP
substitution mutants in HeLa ZC3HC1 KO cells
W107Y
W256Y
C3
HeLa ZC3HC1 KO cells + ZC3HC1-EGFP substitution mutants
pre-bleach
post-bleach
enhanced
W107Y
W107F
W256Y
W256F

S2 (5/8)

D1

zf-C3HC / PF07967 (Pfam 16 release)

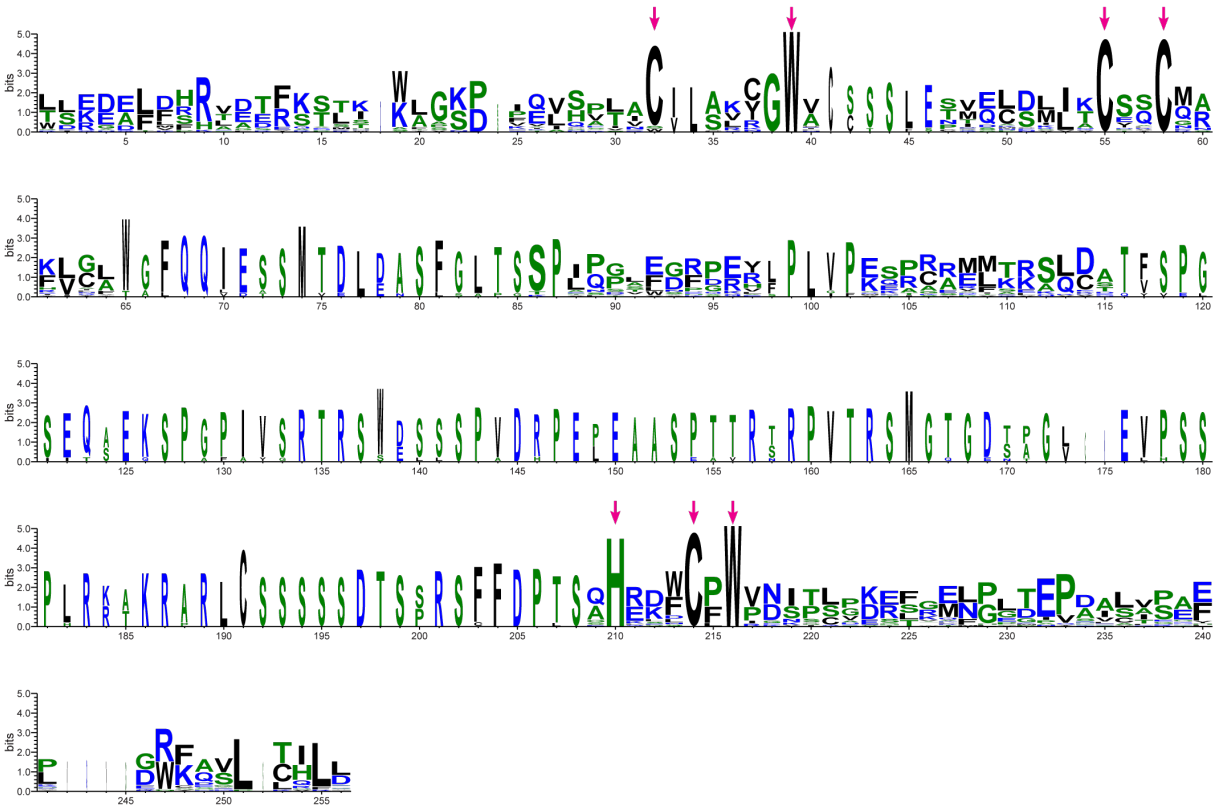

Rsm1 / PF08600 (Pfam 20 release)

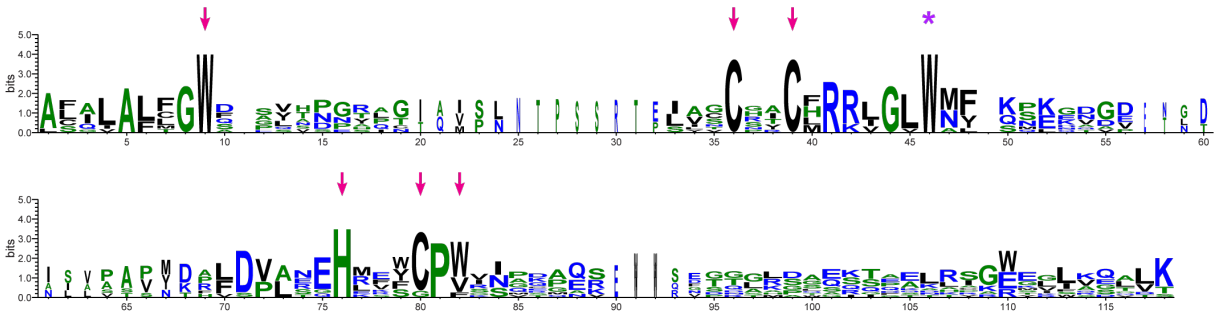

D2

G-[WYF]-$X_{(8,72)}$-C-$X_{(2)}$-C-$X_{(15,524)}$-H-$X_{(3)}$-C-$X_{(62,117)}$-G-[WYF]-$X_{(8,72)}$-C-$X_{(2)}$-C-$X_{(15,524)}$-H-$X_{(3)}$-C

S2 (6/8)

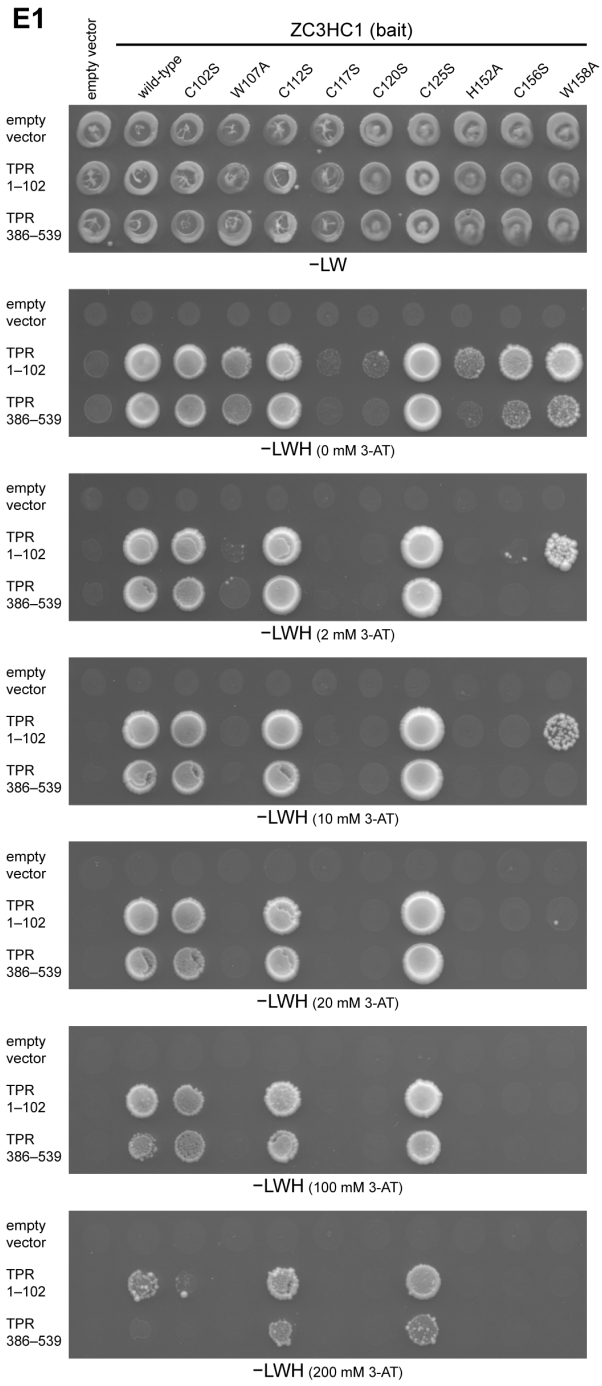
E1
ZC3HC1 (bait)
empty vector
wild-type
C102S
W107A
C112S
C117S
C120S
C125S
H152A
C156S
W158A
empty vector
TPR 1–102
TPR 386–539
−LW
−LWH (0 mM 3-AT)
−LWH (2 mM 3-AT)
−LWH (10 mM 3-AT)
−LWH (20 mM 3-AT)
−LWH (100 mM 3-AT)
−LWH (200 mM 3-AT)

S2 (7/8)

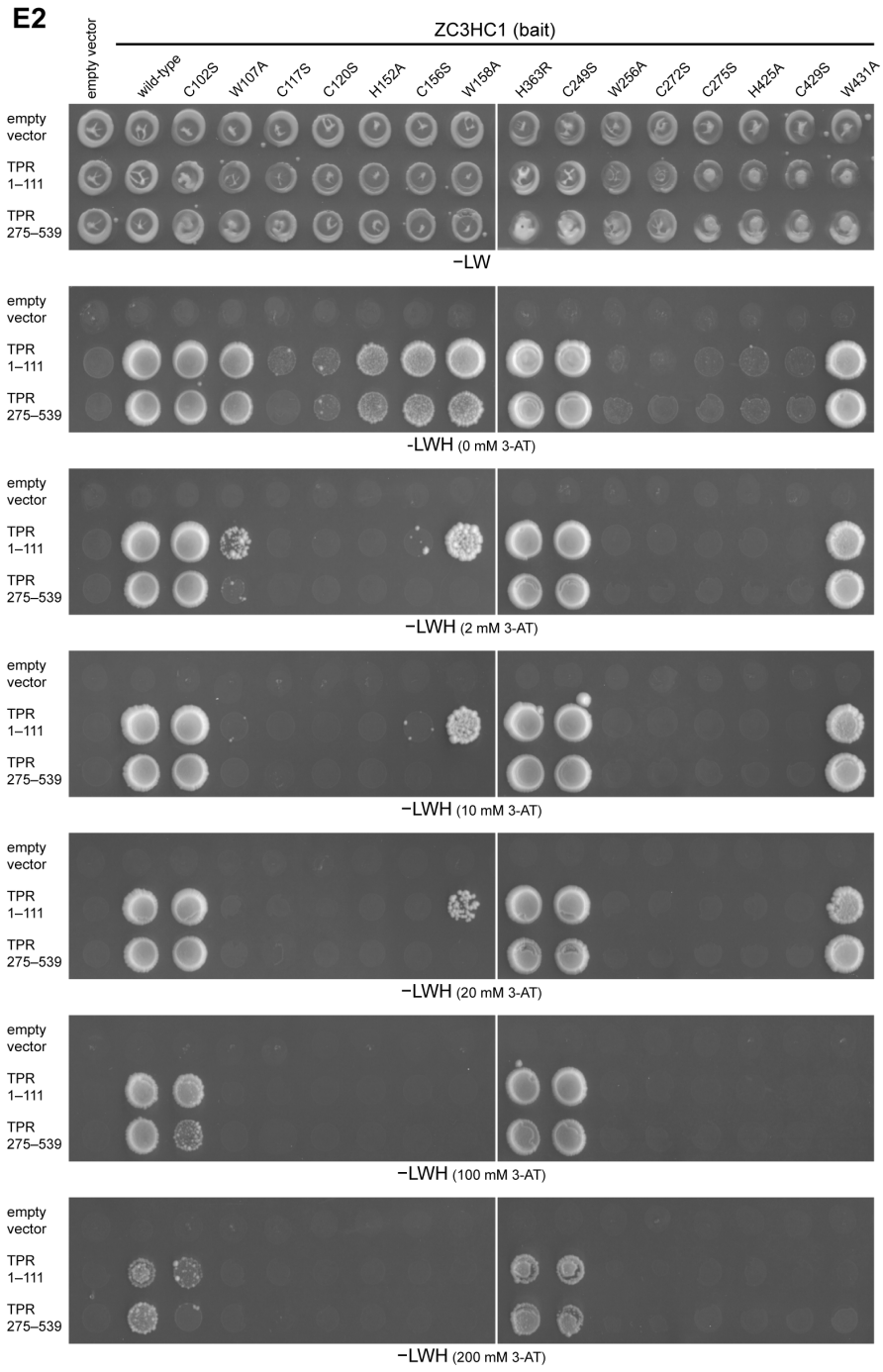

Supplemental Figure S2. Characterization of ZC3HC1 deletion and single aa-substituted mutants, ectopically expressed in HeLa WT and ZC3HC1 KO cells, by fluorescence microscopy and FLIP, complemented by additional Y2H experiments.

In order to specify those parts of ZC3HC1 that enable its initial bonding at the NB and hence to TPR positioned there, we initially studied the subcellular distribution of FP-tagged ZC3HC1 mutants in HeLa WT cells (S2A to S2C). Among those amino acids that we chose as targets for creating single amino acid (aa) substitution mutants were also such that were part of the original

versions of the Pfam motifs zf-C3HC and Rsm1 (S2D). Later, we ectopically expressed these mutants also in ZC3HC1 knockout (KO) cells; once the latter had become available (Supplemental Figure S2A2, S2B2, S2C2, and S2C3). This way of proceeding became possible once we had disrupted the *ZC3HC1* alleles in this cell line by CRISPR/Cas9n methodology (Gunkel *et al*, 2021). The advantage of transfecting such KO cells was that the ZC3HC1 mutants did not need to compete for binding sites with the wild-type ZC3HC1. These experiments in the absence of intact endogenous ZC3HC1 corroborated almost all of the results initially performed in the ZC3HC1 WT cell line. For example, they allowed for underscoring that the likely zinc ion-coordinating residues, namely the total of three cysteines and one histidine residue per BLD, were all essential for NE association. Furthermore, the tryptophan residues W107 and W256 at the N-terminal side of the first and second BLD, respectively, appeared likewise important, with again no NE-binding seen with the W256A mutant and only trace amounts of the W107A mutant at the NE, after having photobleached the protein's soluble nuclear pool. By contrast, however, the mutants W158A and W431A, both appearing incapable of NE-association in WT cells, were found NE-associated in the absence of the endogenous ZC3HC1 protein (S2B2). These findings indicated that W158 and W431, each located at the C-terminal flank of their respective BLD, can support but are not necessarily essential for NE-binding. Later, we would even find that this result explains why a variety of residues present at the corresponding residue positions of apparent ZC3HC1 homologues in other phyla (e.g., Higashi *et al*, 2005; Kokoszynska *et al*, 2008; also see some of the other ZC3HC1 sequences listed further below) are tolerable (our unpublished data). Most notably, though, our findings until then already underscored the two BLDs' commonalities beyond mere sequence similarities, namely by having revealed that signature residues at seemingly invariant positions within both BLDs can also be functionally equivalent.

To investigate interactions between ZC3HC1 and TPR, we performed yeast Y2H experiments (S2E), using TPR segments that we had already mapped and found to comprise ZC3HC1 interaction domains (Gunkel *et al*, manuscript in preparation). While we had initially used TPR segments like, e.g., 1–175 and 172–651 for some of these experiments, all the thereby obtained results were later confirmed and corroborated with also smaller TPR segments thereof, comprising, e.g., aa 1–102 and aa 386–539 (S2E1), as well as aa 1–111 and aa 275–539 (S2E2).

(A, B) Photobleaching experiments with FP-tagged deletion and single aa substitution mutants of ZC3HC1.

(A1) Schematic depiction of expression vector-encoded deletion mutants of ZC3HC1, all containing either an N-terminal EYFP-tag or a C-terminal EGFP-tag, with these tags not depicted though (for details, see Supplemental Table 1). Schemes were designed corresponding to the main Figures 1C and 2A, with the expanse of the central parts of the BLDs highlighted in grey, with these BLDs explained by then and with the BLDs' original boundaries not yet readjusted, as it will later be the case and shown in Figure 6D. Furthermore, each BLD's C-$X_{(2)}$-C tetrapeptide and H-$X_{(3)}$-C pentapeptide, with the putative zinc ion coordinating residues, are highlighted as green and blue boxes, respectively. Areas additionally highlighted represent the positions of evolutionarily conserved G-W dipeptides (magenta-colored boxes) and the protein's NLS (yellow box). The capability of binding to the NE is indicated in the first and second of the four columns at the right margin. Once HeLa ZC3HC1 KO cells became available later in our study (Gunkel *et al*, 2021), we conducted the experiments with them similarly to those initially done with only the HeLa WT cells. Until then, we had not yet been able to exclude that some of the ectopically expressed ZC3HC1 mutants that seemingly were NE-binding-incompetent in HeLa WT cells might merely be unable to successfully compete against the transfected cells' endogenous ZC3HC1 for NB binding sites. All the experiments with the KO cells were thereby correspondingly also carried out once again with the WT cells in parallel to allow for direct data comparability, with these thus repeated WT cell experiments confirming the findings obtained initially with the WT cells only.

Note further that the rating in the first two columns did not relate to those cells in which very high expression levels had resulted in the proteins' distribution throughout the nuclear interior and then even in their notable occurrence in the cytoplasm despite possessing a functional NLS. Furthermore, the third and fourth columns indicate whether NE-localization was still or only notable after photobleaching the nuclear interior of WT and KO cells expressing the recombinant proteins in high amounts, following these cells' transfections with the listed expression vectors. Note that this approach revealed that one of the deletion mutants, ZC3HC1 1–279_412–502, which had not been seen located at the WT cell's NE, can bind to the NE of the ZC3HC1 KO cell, also despite lacking the protein's NLS, the latter comprising at least aa 398–404 (described as 396–402 in Ouyang et al, 2003). Even though the loss of this NLS largely impairs the nuclear import of ZC3HC1, we found small amounts of this mutant protein eventually entering the nucleus nonetheless, which also held for ZC3HC1 1–340_412–502 and which was likely due to NPCs not being perfect permeability barriers (Güttler & Görlich, 2011; Kırlı *et al*, 2015). While we already found it noteworthy at this point that mutants like 1–279_412–502 and 1–340_412–502 were capable of NE-association, we had not yet been able

though to exclude another scenario in which minor amounts of NLS-deficient ZC3HC1 polypeptides would have been co-imported with TPR, as a result of some sporadic binding to TPR already in the cytoplasm. However, a later study (Gunkel & Cordes, 2022) eventually provided unambiguous evidence proving that NB association in the absence of the NLS reflected the intact ZC3HC1 protein's capability of binding to the NB also without engaging in a cytoplasmic interaction with TPR.

Further note that among those ZC3HC1 mutants not listed in the dataset presented in Figure 1 are also such that we had created for further addressing the question as to whether distinct sequence segments of region aa 159–254, located between those parts of the minimal core sequence signature of the first and second BLD found essential for NB-binding, might be required too. This work revealed that even further minor deletions within this area, including the aa segments 170–210, 170–188, 170–178, 203–236, and 236–251, abolished its positioning at the NE, even though these mutants' C-$X_{(2)}$-C and H-$X_{(3)}$-C peptide sequences were intact. These findings indicated that other distinct sequence features or a certain length of this inter-domain region are also needed to allow for an NB-binding interface. We found merely the deletion of one of these short segments (222–236) tolerable. As an aside, also note that FLIP experiments had not been conducted for all of the mutants whose NE-binding incompetence appeared unambiguous early on, here holding for, e.g., 1–180, 1–391, 102–502, 170–502, 211–502, and 352–502.

(A2) Live-cell imaging and photobleaching of HeLa WT and HeLa ZC3HC1 KO cells transiently transfected with the expression vectors encoding the deletion mutants referred to in S2A1. Since it had sometimes turned out difficult to unambiguously judge whether some few of the ectopically expressed mutant versions of FP-tagged ZC3HC1 had actually engaged in some residual interaction with the NE, next to being uniformly distributed throughout the nuclear interior, we bleached this latter pool of polypeptides in order to this then perhaps allow for visualizing some FP-tagged polypeptides at the NE, which otherwise might have remained undetectable due to signal intensities at the NE not exceeding those concomitantly accumulating within the nuclear interior.

Marked rectangular areas in the pre-bleach images of representative cells were subjected to pulses of full laser power, followed by the acquisition of a post-bleach image, with the laser settings then again as for the pre-bleach image. Signal brightness of the here shown post-bleach images was enhanced electronically using the Multiply command in the Math Submenu of the ImageJ/Fiji software, with such enhancement here indicated by an asterisk. Each pixel value was thereby multiplied by the same multiplication factor, allowing the signal intensity

relationships between the electronically brightness-enhanced images to remain essentially the same as between the corresponding raw images beyond their background zero values. The same procedure was also applied to obtain the signal-enhanced images presented in S2B2. Note that after near-quantitative elimination of the nuclear fluorescence, the NEs of many cells ectopically expressing either one or the other mutant version of ZC3HC1 were also not detectable. In contrast, in other cells expressing yet other mutants, the NE emerged as the only structure that was still fluorescent, pointing at an *in vivo* interaction between the NE and the respective ZC3HC1 mutant. As an aside, note that in those cells ectopically expressing the NLS-deficient ZC3HC1 mutants, the cytoplasmic compartment had also been bleached intentionally to render potential signals at the NE better visible. Bar, 10 µm.

(B1) Compilation of the single aa substitutions of *Hs*ZC3HC1 presented or referred to in the current study context. Indicated are the mutations' effects (i) on the protein's capability of binding to the NB, as studied in HeLa WT and ZC3HC1 KO cells with and without photobleaching, as done for the deletion mutants presented in S2A. For example, we found ZC3HC1 with either the single aa substitution W158A or W431A to occur at the NE of a ZC3HC1 KO cell, while both did not appear capable of NE-association when the native ZC3HC1 was present. In experiments without photobleaching, NE-association was rated in cells with a low level of the mutant protein's constitutive expression, while in the FLIP experiments, such cells were bleached in which expression levels were regarded as high. Indicated, furthermore, are the mutations' effects (ii) on the protein's capability of interacting with TPR in Y2H experiments (see further below).

Also note that the dashed rectangle accentuates one particular aa and its substitution, namely R363H, that is not part of one of the actual BLD sequence stretches depicted in grey in S2A1 but whose performance with regard to NB- and TPR-binding we studied nonetheless. Back then, R363H had been reported recently to represent a naturally occurring single aa polymorphism of ZC3HC1 in humans, with pathophysiological phenotypes connected to coronary artery diseases (CAD) assigned to the presence of an arginine at aa position 363. On the other hand, a histidine at the same position instead was regarded as a non-effect residue (Schunkert *et al*, 2011). Positioned within the large, apparently unstructured loop inserted into the second BLD of ZC3HC1 that we had found dispensable for NB association, we nonetheless inspected whether one of the two amino acids at 363 might notably affect the protein's binding to the NB and TPR. However, studying both variants upon their ectopic expression in HeLa cells in parallel, we found both the R363 and H363 versions of full-length ZC3HC1 similarly capable

of binding to the NE. Furthermore, both variants were equally well capable of interacting with both of TPR's ZC3HC1 binding domains in Y2H experiments (see also further below).

Beyond the selection of aa substitutions presented here, some additional ones, at positions beyond the expanse of the minimal signature outlined in Figure 2A3, will be presented elsewhere. Among these is, for example, W458A, which affects NB association notably, yet does not abolish it entirely (our unpublished data).

(B2) Fluorescence microscopy and photobleaching of HeLa WT and HeLa ZC3HC1 KO cells transiently transfected with the expression vectors encoding the aa substitution mutants referred to in S2B1. Experiments were performed, and data were presented, like in S2A2. Bar, 10 µm.

(C) Live-cell imaging and FLIP of HeLa WT (S2C1) and ZC3HC1 KO cells (S2C2 and S2C3) transiently transfected with the expression vectors coding for further ZC3HC1 mutants, with either the single aa substitution W017Y, W107F, W256Y, or W256F. In those experiments initially conducted in the WT cells, FLIP of the aa substitutions W017A and W256A were conducted in parallel for comparison. Note that the W017Y, W107F, W256Y, and W256F substitutions already allowed for NE association in the WT cells, revealing that these aa substitution mutants could successfully compete with the endogenous ZC3HC1 for NB binding sites, in contrast to W107A and W256A. As an aside, note that the here presented experiments in the WT and ZC3HC1 KO cells had been conducted at different time points, in contrast to those presented in S2B2 in which the initial experiments in WT cells later had been repeated, next to the then available KO cells studied in parallel, to identify substitution mutants that were only capable of NE binding in the absence of ZC3HC1. Bars, 10 µm.

(D) Illustration of the sequence signatures of the initial versions of the Pfam zf-C3HC and Rsm1 motifs next to an early low-stringency signature of the BLD-tandem motif. The latter and other versions of the BLD-tandem signature were later collectively referred to as signatures of the nuclear basket-interaction domain (NuBaID; see further below).

(D1) WebLogos (Crooks *et al*, 2004) that we had generated with an online tool (https://weblogo.berkeley.edu/) and the original Pfam MSAs for the zf-C3HC and Rsm1 motifs. The latter had first been described in the Pfam 16.0 and 20.0 releases, respectively, with the underlying MSAs deposited in the corresponding Pfam-A full datasets (http://ftp.ebi.ac.uk/pub/databases/Pfam/releases/Pfam16.0/; http://ftp.ebi.ac.uk/pub/databases/Pfam/releases/Pfam20.0/; e.g., Finn et al, 2006, 2008). For the original version of the Rsm1 motif, the MSA comprised 11 sequence segments from 10 species, of which seven were of fungal origin, including *Sp*Rsm1p, but initially no mammalian sequences. Furthermore, the sequence segments for the Rsm1 motif corresponded only to the second BLD, with one of these sequences

being redundant. On the other hand, for the original zf-C3HC motif, the MSA included a total of 32 sequence segments from seven species, including three vertebrates and *Schizosaccharomyces pombe*, the latter again represented by *Sp*Rsm1p. Furthermore, 18 sequence segments corresponded to the first BLD and 14 to the second BLD, with 9 and 11, respectively, being redundant. Of further note, the zf-C3HC motif had already in the Pfam release 16.0 (released November 2004) been described as representing a domain *"often repeated, with the second domain usually containing a large insert (approximately 90 residues) after the first three cysteine residues"* (http://ftp.ebi.ac.uk/pub/databases/Pfam/releases/Pfam16.0/). Such realization might explain why 14 of the 32 sequence segments initially used for the motif definition represented a BLD2. In other words, for the initial version of the zf-C3HC motif, sequences corresponding to both BLD1 and BLD2 had been used.

In addition to the WebLogos, also note that some residues are marked by magenta-colored arrows, with these residues representing a selection of those for which aa substitutions are presented in the current study. Other aa substitutions, e.g., a tryptophan marked by an asterisk in purple as part of the Rsm1 motif, will be presented in another context elsewhere. Further note that even minimal signature versions deducible from the zf-C3HC motif based on these sequences, like C-$X_{(3,6)}$-G-W-$X_{(9,15)}$-C-$X_{(2)}$-C-$X_{(31,149)}$-H-$X_{(3)}$-C-X-W, would not have allowed for identifying the Pml39 protein of budding yeast, while the ZC3HC1 homologue in *Dictyostelium discoideum* would have been detectable. Regarding the Rsm1 motif, a minimal signature like G-W-$X_{(10,25)}$-C-$X_{(2)}$-C-X-R-$X_{(4)}$-W-$X_{(15,29)}$-H-$X_{(3)}$-C-P-W would have neither allowed for detecting the budding yeast nor the *D. discoideum* homologue.

(D2) The tandem arrangement of the minimal BLD signature referred to in Supplemental Information 2 as signature (2), having taken into account, i.a., the dispensability of C102 of *Hs*ZC3HC1 (S2B) and the replaceability of W for Y or F (e.g., S2C). Furthermore, this BLD-tandem signature had considered the Pfam database's information and the other published data available until then (Higashi *et al*, 2005; Kokoszynska *et al*, 2008), having also deduced from the latter the here chosen spacing between the two identical BLD signatures. Note that while the resulting BLD-tandem signature, G-[WYF]-$X_{(8,72)}$-C-$X_{(2)}$-C-$X_{(15,524)}$-H-$X_{(3)}$-C-$X_{(62,117)}$-G-[WYF]-$X_{(8,72)}$-C-$X_{(2)}$-C-$X_{(15,524)}$-H-$X_{(3)}$-C, allowed for identifying the budding yeast's Pml39 protein via ScanProsite, it did not detect the *D. discoideum* homologue.

(E) Single aa substitution mutants of ZC3HC1 that were studied in Y2H experiments, in combination with two different sets of two ZC3HC1 interaction domain segments of TPR (S2E1 and S2E2). Here, ZC3HC1 was expressed as the Y2H bait, representing a fusion protein including the N-terminally appended GAL4 DNA-binding domain (GAL-BD).

Correspondingly, the empty vector represented the one only expressing the GAL4 DNA-activation domain (GAL4-AD), while the TPR segments, as the Y2H preys, represented GAL4-AD-TPR fusion polypeptides. We chose this approach of identifying TPR interaction domains of ZC3HC1 because the Y2H methodology (Fields & Song, 1989) had already allowed for identifying and mapping interaction domains of TPR in the past (e.g., Hase *et al*, 2001; Hase & Cordes, 2003), which later then also included those for ZC3HC1, as will be described in detail elsewhere (Gunkel *et al*, manuscript in preparation). Furthermore, since we here were studying Y2H interactions monitored via *HIS3* gene expression and subsequent colony growth, we additionally challenged these interactions with various concentrations of 3-amino-1,2,4-triazole (3-AT), a competitive inhibitor of the *HIS3* gene product IGP dehydratase (Brennan & Struhl, 1980; Durfee *et al*, 1993).

The two data sets presented in the following include the presentation of representative colony growth on the selection medium lacking leucine and tryptophan (−LW), and the actual Y2H interactions, after replica-plating onto the selection medium lacking leucine, tryptophan, and histidine (−LWH), supplemented with different concentrations of 3-AT. Some of the data shown here, included for comparison, are also presented in Figure 2C. Note that those single aa substitution mutants of ZC3HC1 that did not impair NE association (in S2B1, those marked with NE+) allowed for colony growth on selective medium minus LHW when paired with ZC3HC1-binding domains of TPR. By contrast, no colony growth on −LHW medium was observed when single aa substitution mutants of ZC3HC1, which have been found incapable of NE association in HeLa cells (NE− in S2B1), had been co-expressed with TPR's ZC3HC1-binding domains. Furthermore, those single aa substitution mutants, like W158A and W431A, that appeared to have failed to bind to the NB in the presence of the ZC3HC1 WT protein but were capable of binding to the NE in ZC3HC1 KO cells were also engaging in Y2H interactions with TPR, which though tolerated only lower concentrations of 3-AT, thus reflecting attenuated interaction. Of additional note, we found ZC3HC1 mutant W158A capable of a seemingly more resistant interaction with those segments of TPR that harbored a ZC3HC1 binding domain located near TPR's NT, here represented by TPR 1–102 (S2E1) and TPR 1–111 (S2E2), while already at a concentration of 2 mM 3-AT, no interaction was observed between ZC3HC1 W158A and either TPR 386–539 (S2E1) or TPR 275–539 (S2E2), both harboring another ZC3HC1 binding site. However, the analysis of this finding in further detail was not considered a topic of the current study.

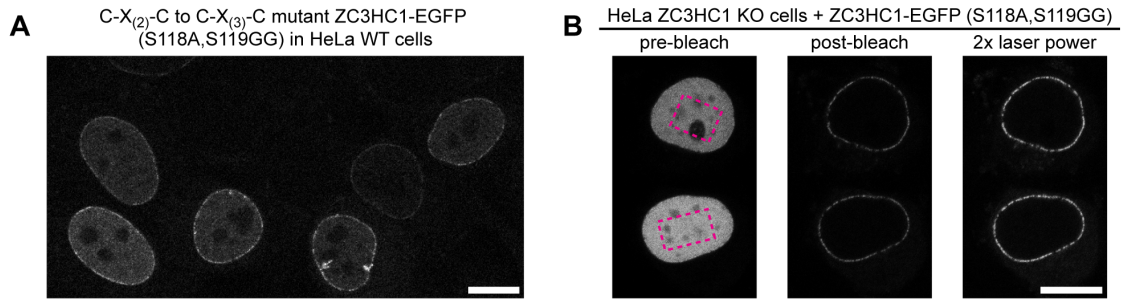

Supplemental Figure S3. Functional tolerance of *Hs*ZC3HC1 for a C-X$_{(3)}$-C spacing within its first BLD, as commonly present in some fungal ZC3HC1 homologues.

Since the potential ZC3HC1 homologues of some fungi, for example, of the genus *Aspergillus*, exhibit a different spacing between the first two cysteines of the first BLD's zinc finger signature, reading C-X$_{(3)}$-C, we had wondered whether such a particular C-X$_{(3)}$-C constellation might still allow for NB-association. To address this question, we created yet additional *Hs*ZC3HC1 mutants, including one in which we exchanged the human homologue's original C-S-S-C sequence between aa 117–120 for the correspondingly positioned sequence C-A-G-G-C, which is present, for example, in *Aspergillus rambellii*.

(**A**) Fluorescence microscopy of HeLa P2 WT cells transiently transfected with an expression vector coding for the mutant version of ZC3HC1 in which the first BLD's sequence C-S-S-C had been replaced by C-A-G-G-C. Note that we found this *Hs*ZC3HC1 mutant, even at low expression levels, well capable of binding to the NE of human cells, with this being so, remarkably enough, even in the presence of the endogenous wild-type version of ZC3HC1.
(**B**) Photobleaching of HeLa ZC3HC1 KO cells transiently transfected with the expression vector encoding the C-X$_{(3)}$-C aa substitution mutant referred to in S3A. Experiments were performed like in Supplemental Figure S2A2, except that the here shown signal-enhanced post-bleach image did not represent the outcome of an electronic signal enhancement but an additional image acquired with doubled laser power after the first post-bleach image had been taken, like also in S1A. The results of these FLIP experiments indicated a steady and lasting *in vivo* interaction between a certain amount of the C-X$_{(3)}$-C mutant and the NE. Bars, 10 µm.

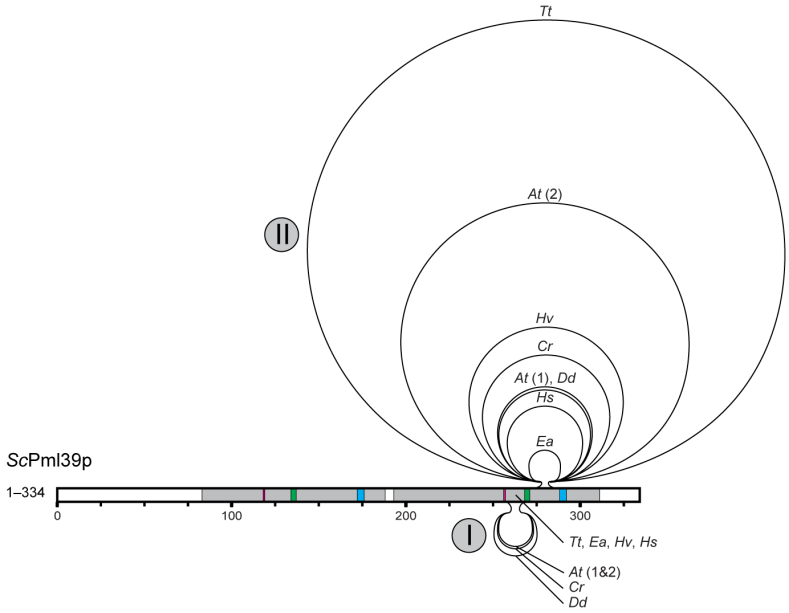

Species		total length (aa)	accession number
Saccharomyces cerevisiae	M-[117]-GW-[14]-CCCC-[34]-HLQKCPW-[_77]-GY-[10]-CTAC-[_16]-HALWCRY-[_40]	334	NP_013600.2
Elsinoe ampelina	M-[138]-GW-[_9]-CKGC-[52]-HSESCPW-[101]-GW-[12]-CDAC-[_69]-HREHCPY-[103]	511	KAF2227358.1
Homo sapiens	M-[104]-GW-[_9]-CSSC-[31]-HEKFCFW-[_96]-GW-[15]-CSQC-[149]-HRDWCPW-[_71]	502	NP_057562.3
Arabidopsis thaliana (1)	M-[113]-GW-[_9]-CESC-[31]-HKLLCPW-[100]-GW-[72]-CKLC-[178]-HRHFCPW-[_64]	594	NP_175325.2
Dictyostelium discoideum	M-[115]-GW-[_9]-CETC-[32]-HRDNCPW-[_93]-GW-[89]-CSYC-[183]-HRWFCPW-[_87]	635	ON368701
Chlamydomonas reinhardtii	M-[_90]-GW-[_9]-CEYC-[29]-HTATCPW-[172]-GW-[76]-CPIC-[243]-HRSWCPW-[_62]	708	PNW78929.1
Hydra vulgaris	M-[_65]-GW-[_9]-CVTC-[31]-HEKLCPW-[_87]-GW-[13]-CTIC-[289]-HRFWCPW-[_69]	590	XP_002154618.2
Arabidopsis thaliana (2)	M-[115]-GW-[_9]-CEYC-[32]-HESSCPW-[_98]-GW-[72]-CSLC-[524]-HNCYCPW-[_81]	958	NP_173164.1
Timema tahoe	M-[_66]-GW-[10]-CTSC-[23]-HYKFCRW-[_75]-GW-[10]-CDFC-[836]-HRYWCIW-[171]	1217	CAD7459619.1

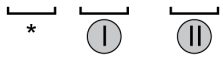

Supplemental Figure S4. Size variations of loop-like sequence insertions within exemplary ZC3HC1 homologues.

In numerous species, we had found the linear sequence of the putative ZC3HC1 homologue's second BLD disrupted by extensive sequence insertions predicted to represent intrinsically disordered loops. Most of these loops did not share any notable sequence similarity, sometimes not even among closely related species. In numerous such potential ZC3HC1 homologues, the length of the BLD2 insertion exceeded the one of *Hs*ZC3HC1 by far. By striking contrast, the putative homologues of other organisms lacked such BLD insertions.

In the following, the wide range of such loops' lengths, as occurring in exemplary ZC3HC1 homologues, is schematically depicted relative to a loop-free ZC3HC1 homologue, here represented by Pml39p, which we identified and characterized as the budding yeast homologue of ZC3HC1, as will be specified later in Figures 4 to 6 and Supplemental Figures S6, S7, S9, S10, and S12.

The here-shown schematic depiction of the two BLDs of *S. cerevisiae* Pml39p as a representative of one of the shortest ZC3HC1 homologues corresponds to a scheme that will later be presented in Figure 6D, where it will base on newly defined BLD boundaries that will have been explained by then. The areas highlighted in grey correspond to those parts that will be shown to constitute the BLD1 and BLD2 of *Sc*Pml39p. The boxes in green and blue, respectively, represent the positions of the C-$X_{(2)}$-C and H-$X_{(3)}$-C sequence elements, and the boxes in magenta depict the position of the evolutionarily conserved dipeptide that in *Sc*Pml39p either reads G-W or G-Y.

Into this scheme for *Sc*Pml39p, the loops of some other exemplary ZC3HC1 homologues are shown inserted. In the latter, such sequence insertions can be found at positions here marked as I and II, with the small selection of loops chosen here comprising the ones from *Elsinoe ampelina* (*Ea*), Homo sapiens (*Hs*), *Arabidopsis thaliana* (*At*) with its two homologues, *Dictyostelium discoideum* (*Dd*), *Chlamydomonas reinhardtii* (*Cr*), *Hydra vulgaris* (*Hv*), and *Timema tahoe* (*Tt*; see also Supplemental List of Sequences for ZC3HC1 Homologues). The lengths of these species' loops are drawn approximately to scale relative to the length of the *Sc*Pml39p scheme.

The alignment of the homologues' corresponding minimal NuBaID sequence signature, including the G-W, C-$X_{(2)}$-C, and H-$X_{(3)}$-C peptides, and the number of residues located between them, next to each homologue's accession number, is provided for comparison. In contrast to loops I and II that are predicted, in numerous cases, to be essentially unstructured in their entirety, other sequence insertions, like those collectively marked with an asterisk, can encompass both structured parts and additional α-helices present in some species while absent in others. Further note that loops inserted at position II appear to be especially large in some species of the insect order Orthoptera, like possibly in *Gryllus bimaculatus* (not shown here) and, in particular, in the order Phasmatodea, here represented by *Timema tahoe*. Protein sequences so far deduced and assembled from whole genome shotgun contigs (WGS) for a range of species of the phasmid genus *Timena* and for species of other stick insect genera, like *Medauroidea extradentata, Clitarchus hookeri*, and *Dryococelus australis* (the two latter not listed in the Supplemental List of Sequences), are currently indicating a possible range of 496 to 994 aa located between the phasmids' second BLD's C-$X_{(2)}$-C, and H-$X_{(3)}$-C peptides. For further thoughts regarding the presence of ZC3HC1 homologues with huge loops in some insects and the seemingly complete absence of a ZC3HC1 homologue in other insects, see Supplemental Discussion 4.

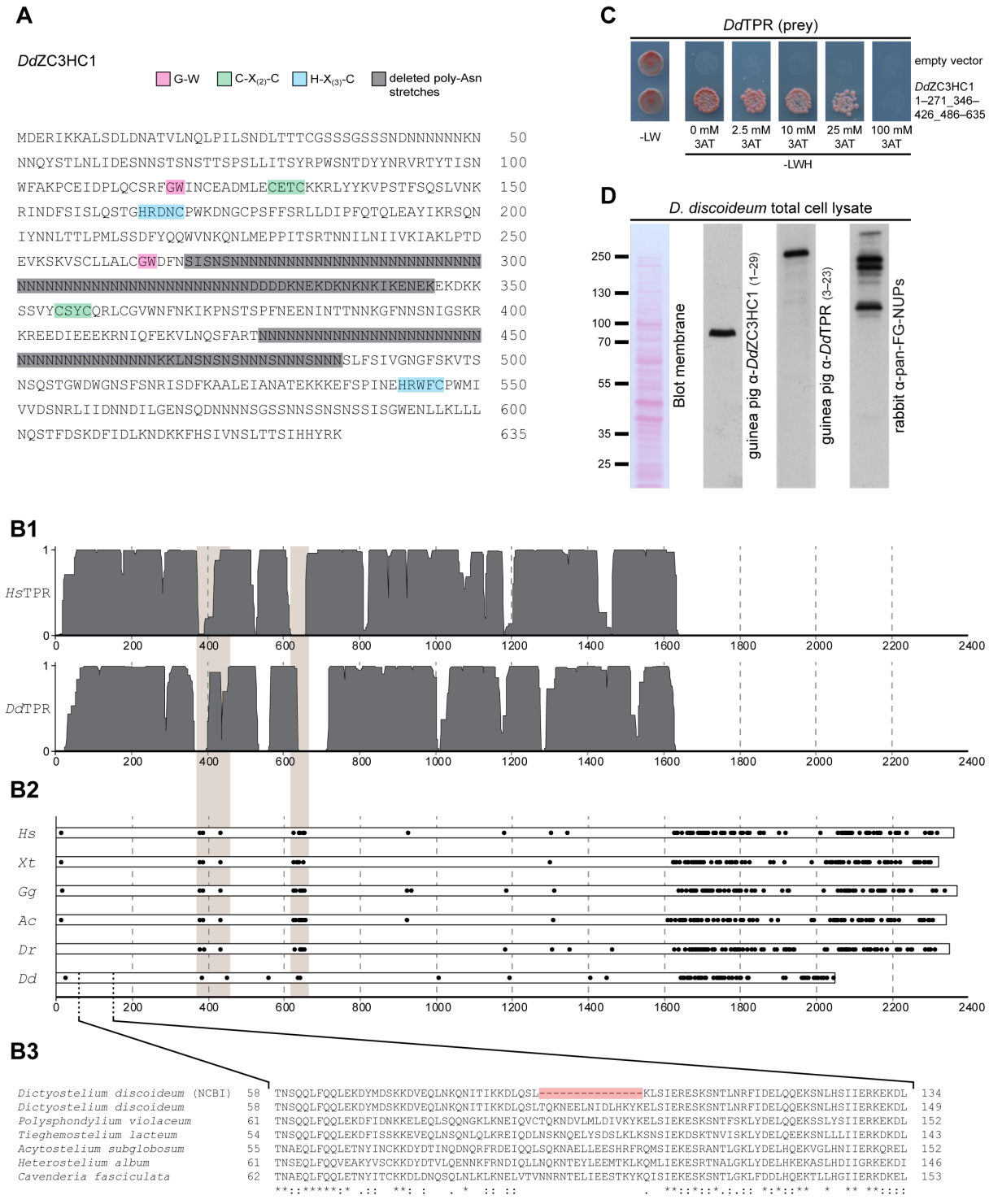

Supplemental Figure S5. Complementing the characterization of the Dictyostelium homologues of ZC3HC1 and TPR.

With *Dd*ZC3HC1, we had at hand a potential homologue possessing a prototypic NuBaID signature in a phylum beyond the opisthokonts and, apart from the NuBaID signature, notably differing in sequence from the ZC3HC1 homologues of other organisms. For example, like some other slime mold proteins, *Dd*ZC3HC1 is a protein featuring sequence clusters of

asparagine residues, which also holds for its large loop-like insertions (S5A). Given the sequence peculiarities of *Dd*ZC3HC1, we considered this alleged homologue well-suited for addressing whether the NuBaID signature might represent the evolutionarily conserved common hallmark of a distinct class of NB- and TPR-interacting proteins.

Furthermore, *D. discoideum* had already been shown to harbor NBs (Beck *et al*, 2004), and this species thus met the requirement of holding ready, in principle, a potential binding site for *Dd*ZC3HC1 at the NE. In fact, we had already found that *D. discoideum* possesses a TPR homologue (S5B1 and S5B2), leading us to cDNA-clone some of its parts, including such to be compared with other amoebic TPR sequences (S5B3) and such to be used for Y2H experiments (S5C) and to raise *Dd*TPR-specific antibodies (S5D). With these antibodies, we had then located the protein at the *Dictyostelium* NPC's nuclear side (e.g., Figure 4C), with this finding now also in line with recent reporting of *Dd*TPR, when tagged with mNeonGreen, to be located at the NE (Mitic *et al*, 2022).

To address whether *Dd*TPR and *Dd*ZC3HC1 can interact, we also cloned the cDNA for *Dd*ZC3HC1 (S5A), which then allowed for conducting Y2H experiments with *Dd*TPR (S5C). Furthermore, to determine where within the slime mold this potential ZC3HC1 homologue would locate, we raised antibodies against *Dd*ZC3HC1 (S5D) and then performed immuno-fluorescence microscopy (IFM; e.g., Figure 4C).

We consider it worth mentioning that generating the required antibodies for *Dd*ZC3HC1 had turned into an unexpectedly challenging enterprise, with each antibody having to be versatile for both IB and IFM while at the same time not allowing it to be cross-reactive with unrelated proteins. Moreover, basic requirements that had to be met by all antibodies selected for double-labeling experiments also included being suitable for at least one same IFM protocol from among the various ones published, including notably different ones reported over time for studying different target proteins in *Dictyostelium*.

After systematically having tested such published IFM protocols and others we had newly conceived for *Dictyostelium*, we realized that none of those of our IB- and IFM-compatible *Dd*TPR and *Dd*ZC3HC1 antibodies that had been raised in different species (here not shown) were sufficiently suitable for being used in combination for double-labeling IFM. One reason was that some of these antibodies performed well only in the one and others only in the other IFM protocol.

However, despite such unanticipated difficulties concerning IFM in *Dictyostelium*, some of the affinity-purified antibodies eventually allowed for the proteins' comparison under identical IFM conditions. Not having managed to generate pairs of antibodies from different species that

would have allowed for conventional double-labeling of *Dd*TPR and *Dd*ZC3HC1 directly within the same specimen, we performed the alternatively possible double-labeling with pan-FG-NUPs antibodies. Applying the same IFM protocol and using the same microscope settings for inspecting all specimens side by side, the positions of *Dd*ZC3HC1 and *Dd*TPR could thus be visualized relative to those of the FG-repeat nucleoporins, which revealed an offset location of *Dd*ZC3HC1 and *Dd*TPR towards the nuclear interior (Figure 4C).

(A) Sequence of the ZC3HC1 homologue of *D. discoideum*. Residues highlighted in magenta, green, and blue represent the positions of the two BLDs' G-W, C-$X_{(2)}$-C, and H-$X_{(3)}$-C sequence elements. Those regions highlighted in grey represent the residues that we removed, by cloning, from some of the *Dd*ZC3HC1 sequences used for expression experiments in budding yeast cells (e.g., in S5C) and in mammalian cells (our unpublished data). The 635 aa-long sequence (NCBI accession number ON368701) results from our RNA isolation from *D. discoideum* Ax4 cells and subsequent cDNA synthesis and sequencing. The protein's C-terminal residues differ from the NCBI-deposited sequence for a 647 aa-long *Dd*ZC3HC1 from Ax4 cells (XP_638576.1), the latter derived from an annotated genomic sequence (NC_007090).
(B) Sequence features of *Dictyostelium discoideum* TPR compared to TPR homologues from other species.
(B1) The coiled-coil (CC)-forming regions of *Dd*TPR compared to those of *Hs*TPR, as here predicted by the PCOILS algorithm (Zimmermann *et al*, 2018; https://toolkit.tuebingen.mpg.de/#/tools/pcoils)based on windows of 28 residues. The CC-forming parts are shown as areas in dark grey. The two vertical rectangles in light brown delineate the area between about aa 400–600 of *Hs*TPR formerly found containing those sequence elements required for TPR's binding to the NE. These elements are flanked by short, hinge-forming sequence stretches involving evolutionary-conserved prolines or other CC-disrupting features at these sites (Hase *et al*, 2001; Kuznetsov *et al*, 2002; Krull *et al*, 2004; Gunkel *et al*, 2021). The 2052 aa-long *Dd*TPR sequence (NCBI accession number ON368702) used for these predictions is the result of RNA isolation from *D. discoideum* Ax4 cells and subsequent cDNA synthesis and sequencing.
(B2) Schemes of vertebrate TPR homologues, comprising the one from humans (*Hs*, accession number NP_003283.2), *Xenopus tropicalis* (*Xt*, XP_002933814.3), *Gallus gallus* (*Gg*, XP_004943365.4), *Anolis carolinensis* (*Ac*, XP_016850554.1) and *Danio rerio* (*Dr*, NP_001025294.1), next to the one for *Dd*TPR (ON368702). The black dots within each of the horizontal rectangles representing the different TPR homologues illustrate the positions of proline residues, of which, as expected, only a few are present within the CC-forming parts. In

particular, though, proline residues flanking the NPC/NB-binding elements of *Hs*TPR and evolutionarily conserved in other vertebrates also exist at similar positions in the CC domain of *Dd*TPR. By contrast, proline residues are abundant in the TPR homologues' carboxy-terminal domains (see also Kuznetsov *et al*, 2002), with this domain shown to be largely unstructured (Hase *et al*, 2001).

(B3) Alignment of a *Dd*TPR aa sequence segment from the N-terminal domain of different amoebic species, including two sequences for *D. discoideum* (accession numbers XP_636884.1 and ON368702, first and second line, respectively), with the first one derived from an annotated genomic sequence (NC_007091), lacking residues evolutionarily conserved in the slime molds. The other aligned sequences stem from hypothetical proteins representing evident TPR homologues of other species of the class Dictyostelia, including *Polysphondylium violaceum* (KAF2071913.1), *Tieghemostelium lacteum* (KYR02800.1), *Acytostelium subglobosum* LB1 (XP_012748738.1), *Cavenderia fasciculata* (XP_004357092.1) and *Heterostelium album* PN500 (XP_020436491.1), with the latter sequence only representing a segment of this species' TPR homologue.

(C) Exemplary Y2H data obtained with expression vectors coding for a GAL4-BD version of *Dd*ZC3HC1 as the bait polypeptide, here with its two BLDs both intact while lacking those asparagine-dominated sequence segments highlighted in grey in S5A. Correspondingly, the empty vector represented the one only expressing the GAL4-BD, while the *Dd*TPR segment used here as the Y2H prey was thus fused to GAL4-AD.

(D) Immunoblotting (IB) of the total of proteins from *D. discoideum* cells of line Ax2, with those IFM-compatible antibodies for *Dd*TPR and *Dd*ZC3HC1 that were also used for the micrographs presented in Figure 4C. IB with pan-FG-NUPs antibodies, cross-reactive with the FG repeat domains of numerous nucleoporins, are shown for comparison. Target regions of *Dd*ZC3HC1 and *Dd*TPR are given in parentheses. Immunolabeling was performed on the representative Ponceau S-stained membrane shown here and on replicates of the identical kind. Note that the *Dd*ZC3HC1 antibodies specifically labeled a single protein with an electrophoretic mobility corresponding to about 80 kDa in total *D. discoideum* cell extracts, in line with the *Dd*ZC3HC1 protein's sequence-deduced molecular mass. In addition, some of the immunoblotting- (IB) and IFM-compatible antibodies that we had raised against *Dd*TPR, including the representative one shown here, allowed for similarly specific labeling of a protein of about 250 kDa. Note, on the other hand, that several *D. discoideum* proteins with molecular masses exceeding 100 kDa were labeled with "pan-FG-NUPs" antibodies that we had generated

for being reactive with various species' NPC proteins (nucleoporins) via the binding to their common FG-repeat domains (for further details, see Supplemental Materials and Methods).

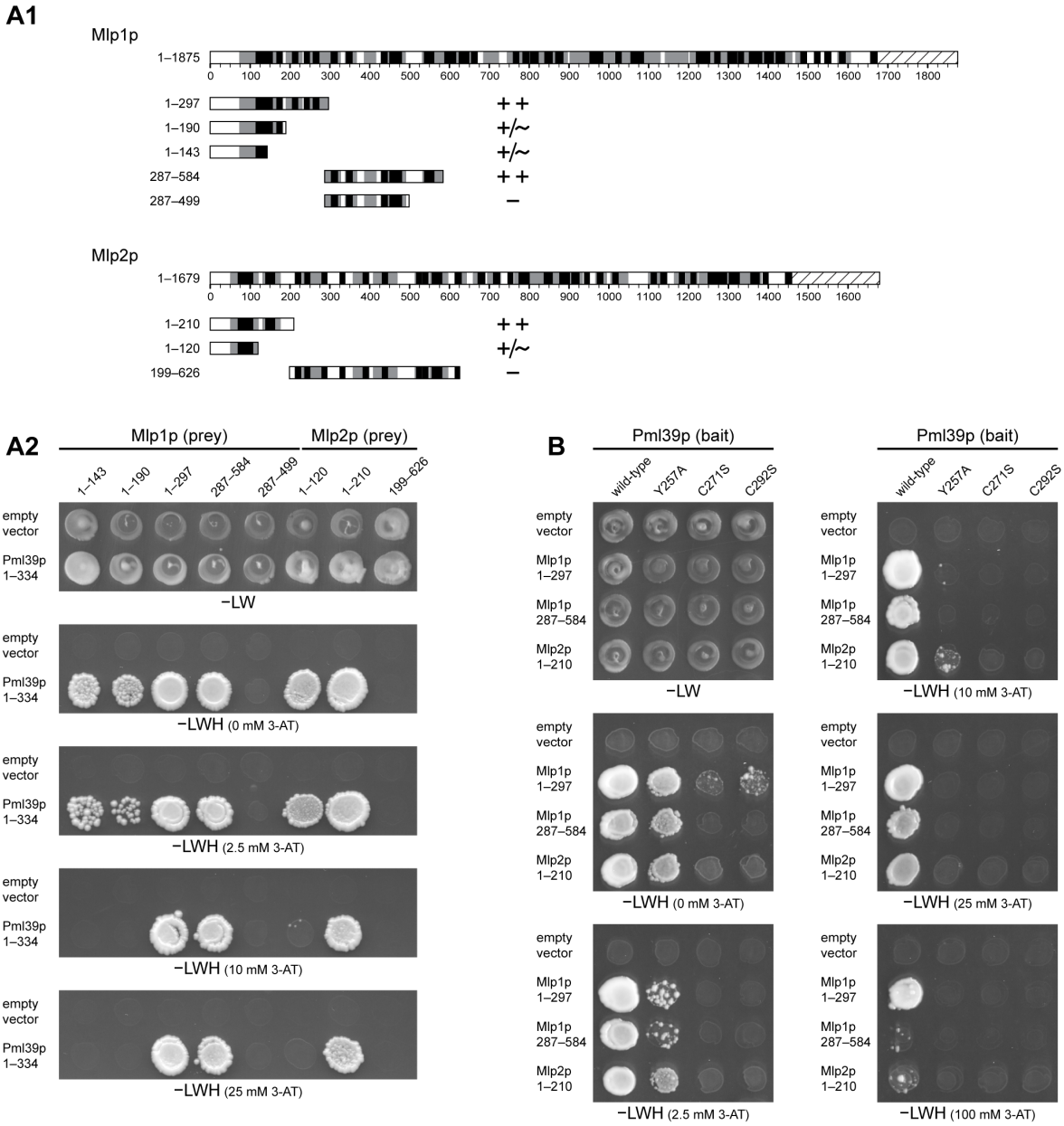
A1
Mlp1p
1–1875
0 100 200 300 400 500 600 700 800 900 1000 1100 1200 1300 1400 1500 1600 1700 1800
1–297 + +
1–190 +/~
1–143 +/~
287–584 + +
287–499 –
Mlp2p
1–1679
0 100 200 300 400 500 600 700 800 900 1000 1100 1200 1300 1400 1500 1600
1–210 + +
1–120 +/~
199–626 –
A2
Mlp1p (prey)
Mlp2p (prey)
1–143 1–190 1–297 287–584 287–499 1–120 1–210 199–626
empty vector
Pml39p 1–334
−LW
−LWH (0 mM 3-AT)
−LWH (2.5 mM 3-AT)
−LWH (10 mM 3-AT)
−LWH (25 mM 3-AT)
B
Pml39p (bait)
wild-type Y257A C271S C292S
Mlp1p 1–297
Mlp1p 287–584
Mlp2p 1–210
−LW
−LWH (0 mM 3-AT)
−LWH (2.5 mM 3-AT)
−LWH (10 mM 3-AT)
−LWH (25 mM 3-AT)
−LWH (100 mM 3-AT)

S6 (1/2)

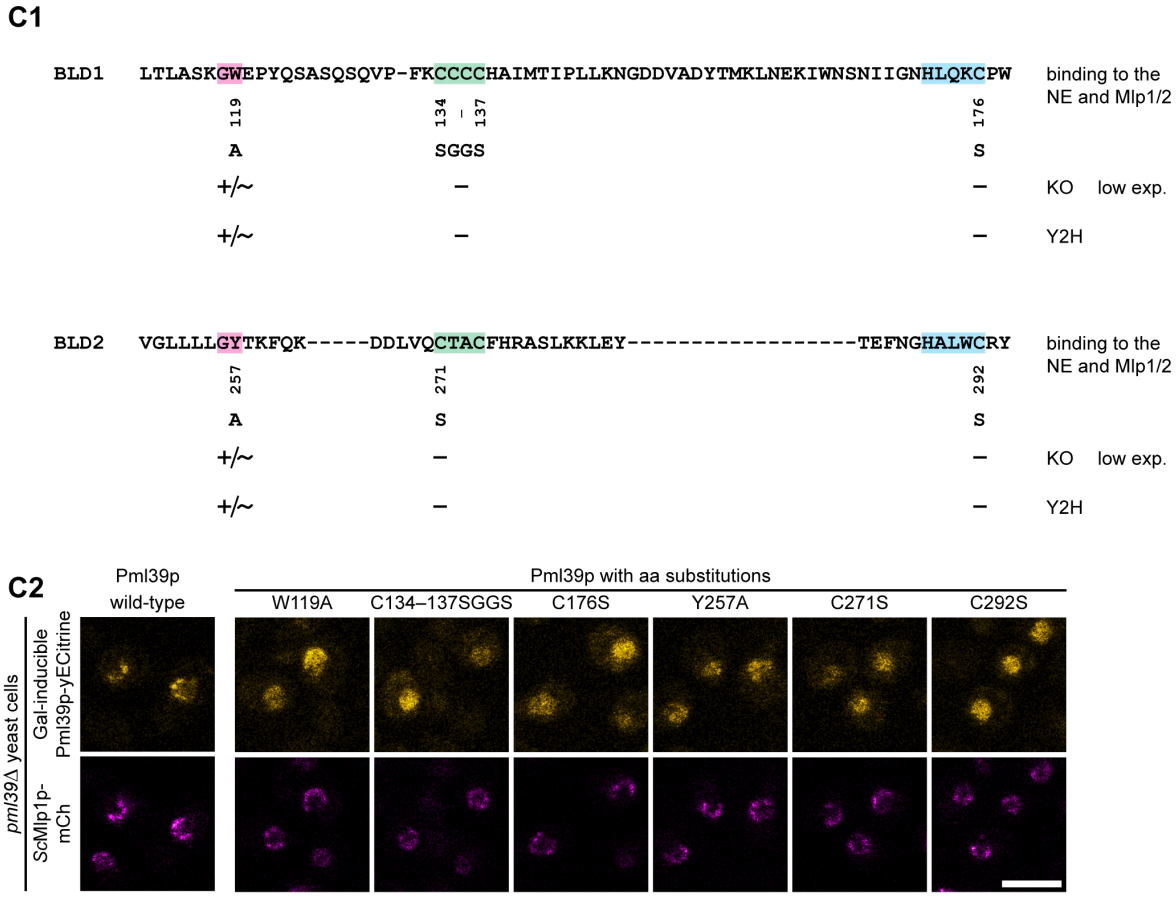

Supplemental Figure S6. Complementing the characterization of *Sc*Pml39p and its NuBaID.

Former screening of a yeast Y2H library with Pml39p as bait had resulted in the isolation of cDNAs coding for segments of Mlp1p and Mlp2p, whose sequence analysis "*revealed two minimal domains of Mlp1 (N1, aa 7–143; N2, aa 287–584) and one domain of Mlp2 (aa 1–120) required for Pml39 interaction"* (Palancade *et al*, 2005). Guided by these findings, we constructed similar Y2H expression vectors coding for different segments of *Sc*Mlp1p and *Sc*Mlp2p (e.g., S6A1), with us aiming to gain insight into whether and which parts of the two Mlps might allow for interactions with Pml39p that would be similarly robust, i.e., tolerating similar concentrations of 3-AT. Furthermore, we examined whether a Y2H interaction between Mlp2p and Pml39p would involve indeed only one Pml39p-binding domain of Mlp2p, in contrast to Mlp1p (e.g., S6A2). Moreover, some of these Y2H expression vectors for Mlp polypeptides were then to be used, in particular, for studying interactions with aa substitution mutants of Pml39p, in order to determine whether the integrity of the Pml39 protein's NuBaID might be essential for such interactions with the Mlps (S6B and S6C1). In addition, we investigated which of these aa substitution mutations of Pml39p might impair binding to the

yeast's NBs (S6C1). To this end, we generated a yeast strain stably expressing all Mlp1p as mCherry-tagged polypeptides in a *pml39*Δ background. This *PML39* deletion strain was used for the galactose-inducible expression of intact and mutant versions of Pml39p tagged with yECitrine, followed by live-cell imaging (S6C2).

(A) Representative Y2H data obtained with expression vectors coding for *Sc*Mlp1p and *Sc*Mlp2p segments, fused to GAL4-AD (prey), and for the intact, WT version of *Sc*Pml39p, fused to GAL4-BD (bait).
(A1) Schemes of full-length Mlp1p and Mlp2p drawn to scale next to segments of Mlp1p and Mlp2p encoded by Y2H expression vectors. The hatched rectangles represent the Mlps' C-terminal domain. The boxes in grey and black represent those parts of each polypeptide for which the probability of forming a coiled-coil is here predicted to be at least 80% by the PCOILS algorithm (Zimmermann *et al*, 2018) within windows of 14 aa (black) and 28 aa (plus grey parts), respectively. Each segment's capability of a Y2H interaction with Pml39p is indicated (++, robust colony growth even in elevated concentrations of 3-AT; +/~, notably attenuated colony growth; −, no colony growth).
(A2) Representative colony growth on selection medium lacking leucine and tryptophan (−LW), revealing successful mating between the yeasts harboring the indicated GAL4-AD and GAL4-BD expression vectors, and visualization of Y2H interactions, after having replica-plated the diploid cells onto selection medium lacking leucine, tryptophan, and histidine (−LWH), either without or with different concentrations of 3-AT as indicated.
(B) Representative Y2H results obtained with prey vectors coding for the three Mlp1p and Mlp2p segments that had allowed for Pml39p interaction in the presence of 25 mM 3-AT (S6A2) and bait vectors encoding the WT version of Pml39p, next to additional Pml39p mutants with single aa substitutions of the NuBaID signature. Some of the data shown here, included for comparison, are also presented in Figure 4D. Note that each of these single aa substitutions abolished the interaction with all three Mlp segments, yet at different concentrations of 3-AT. The Y257A mutant allowed for attenuated Y2H interactions with the Mlps at low 3-AT concentrations, in line with some residual co-localization with Mlp1p at the NE upon ectopic expression of this mutant for live-cell imaging (see S6C2). As an aside, note that other single aa substitutions of the yeast's minimal NuBaID signature again, like Y257W not shown here, which transformed the second BLD's dipeptide G-Y to G-W, thus identical then to the corresponding G-W of *Hs*ZC3HC1, did not notably impair binding to any of the Mlp1p and Mlp2p segments capable of Y2H-interacting with wild-type Pml39p (our unpublished data). As

another aside, note that yet another mutant not shown here, in which we introduced the single aa substitution C134S, was capable of an attenuated Y2H interaction with both Mlp1p and Mlp2p, indicating that the Pml39 protein's three cysteines from C135 to C137 could compensate for the loss of C134 to some extent (our unpublished data).

(C) Summary and presentation of additional live-cell images of *pml39*Δ yeast cells with ectopically expressed versions of yECitrine-tagged Pml39p.

(C1) Sequence segments of Pml39p, representing the corresponding parts of its first and second BLD, together with a compilation of the Pml39p aa substitutions presented in the current study, next to the summary of those data shown in main Figure 4E and here in S6C2. Indicated are the mutations' effects on the protein's capability of binding to the NE, as studied in *pml39*Δ cells, upon the induced ectopic expression of the yECitrine-tagged versions of Pml39p. NE association was rated in cells in which the mutant proteins' expression levels were regarded as still low or only moderate. In addition, the summarizing results of the corresponding Y2H data are provided for comparison, including those presented in Figures 4D and S6B and others not shown as images, reflecting each mutant protein's capability of interacting with the Mlps.

(C2) Live-cell imaging of yeast *pml39*Δ cells with endogenously expressed mCherry-tagged Mlp1 polypeptides and additional, galactose-induced ectopically expressed yECitrine-tagged Pml39p mutant versions, harboring either a single aa substitution of the NuBaID signature or the quadruple aa substitution C134–137SGGS. These additional mutants are here shown next to those micrographs already presented in the main Figure 4E, comprising the ones for the ectopically expressed WT version of the FP-tagged Pml39p and the single aa substitution mutants Y257A, C271S, and C292S. Note that while the wild-type Pml39p primarily accumulated at the NE, all Pml39p mutants but W119A and Y257A were found no longer capable of binding to the NE and instead distributed throughout the nuclear interior. Concerning the W119A and Y257A mutants, we detected some residual co-localization with Mlp1p at the NE, in addition to these mutants' distribution throughout the nuclear interior. This latter finding resembled the attenuated NE association of the corresponding *Hs*ZC3HC1 mutant W107A upon its ectopic expression in HeLa ZC3HC1 KO cells (Supplemental Figure S2B). Furthermore, the residual NE localization of the W119A and Y257A mutants was also in line with these mutants being capable of attenuated Y2H interactions with the Mlps at low 3-AT concentrations (S6B and S6C1). Bar, 5 µm.

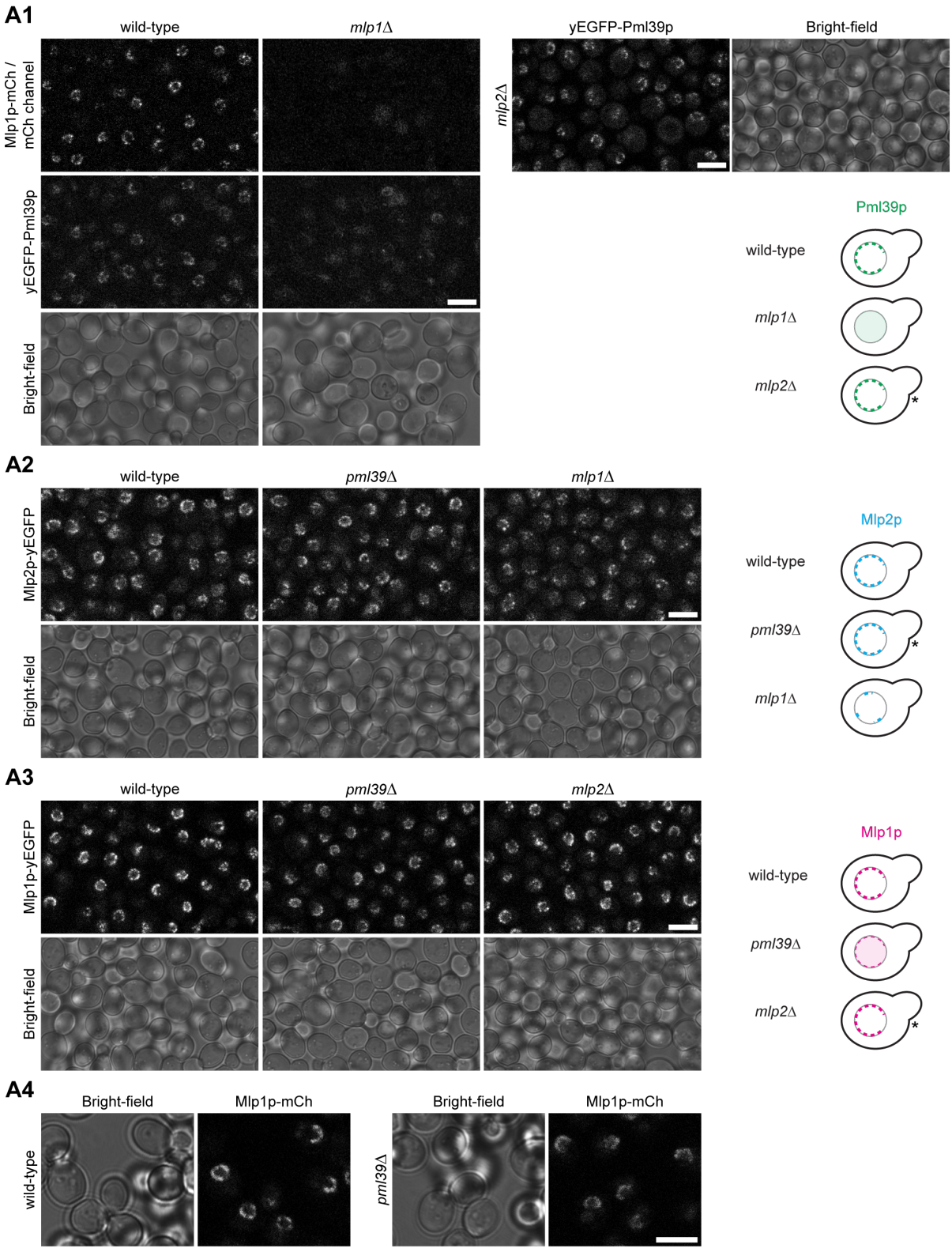
A1
wild-type
mlp1Δ
yEGFP-Pml39p
Bright-field
Mlp1p-mCh / mCh channel
yEGFP-Pml39p
Bright-field
mlp2Δ
Pml39p
wild-type
mlp1Δ
mlp2Δ
A2
wild-type
pml39Δ
mlp1Δ
Mlp2p-yEGFP
Bright-field
Mlp2p
wild-type
pml39Δ
mlp1Δ
A3
wild-type
pml39Δ
mlp2Δ
Mlp1p-yEGFP
Bright-field
Mlp1p
wild-type
pml39Δ
mlp2Δ
A4
Bright-field
Mlp1p-mCh
Bright-field
Mlp1p-mCh
wild-type
pml39Δ

S7 (1/3)

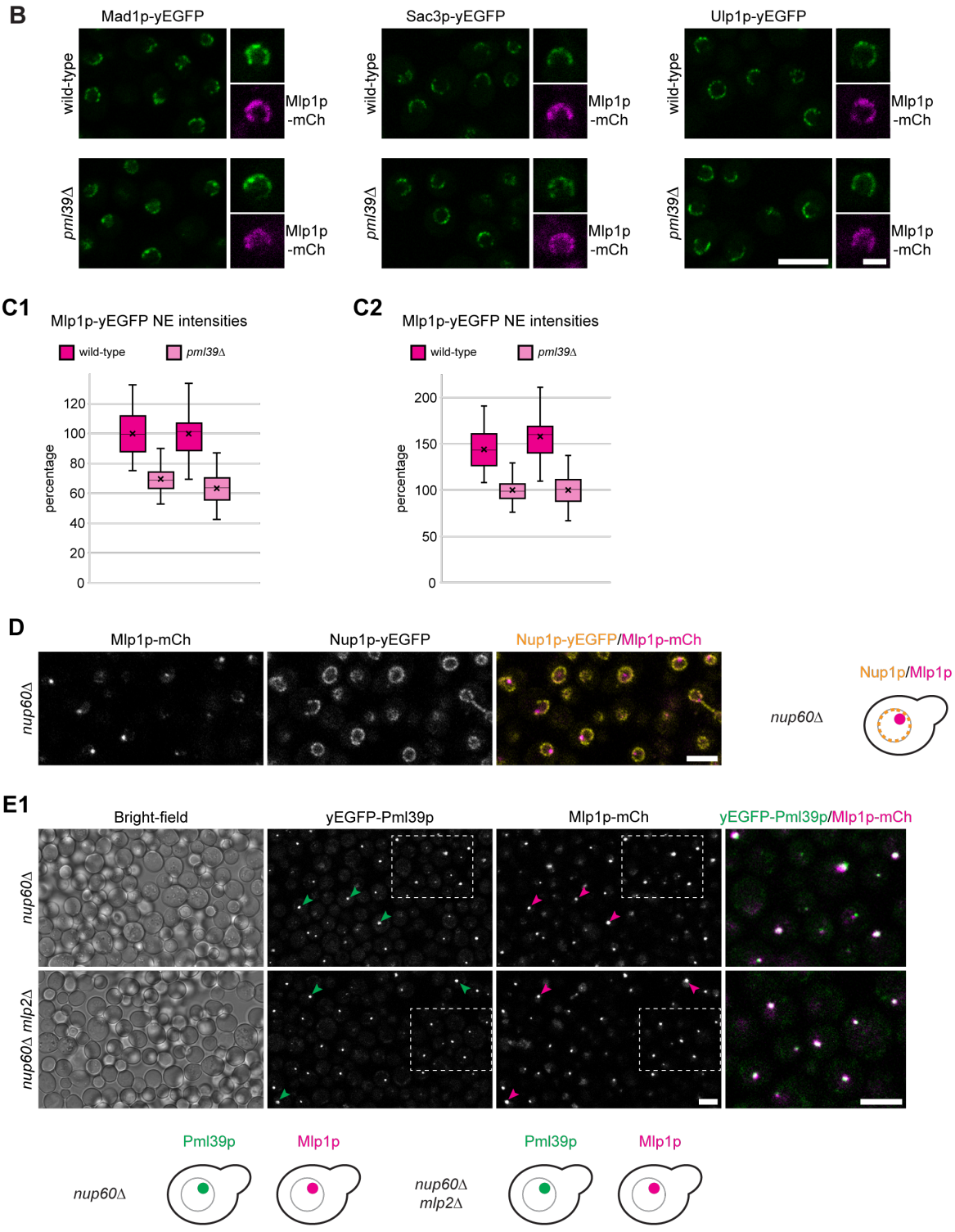
B
Mad1p-yEGFP
Sac3p-yEGFP
Ulp1p-yEGFP
wild-type
pml39Δ
Mlp1p
-mCh
C1
Mlp1p-yEGFP NE intensities
wild-type
pml39Δ
percentage
120
100
80
60
40
20
0
C2
Mlp1p-yEGFP NE intensities
wild-type
pml39Δ
percentage
200
150
100
50
0
D
Mlp1p-mCh
Nup1p-yEGFP
Nup1p-yEGFP/Mlp1p-mCh
nup60Δ
Nup1p/Mlp1p
nup60Δ
E1
Bright-field
yEGFP-Pml39p
Mlp1p-mCh
yEGFP-Pml39p/Mlp1p-mCh
nup60Δ
nup60Δ mlp2Δ
Pml39p
Mlp1p
nup60Δ
Pml39p
Mlp1p
nup60Δ
mlp2Δ

S7 (2/3)

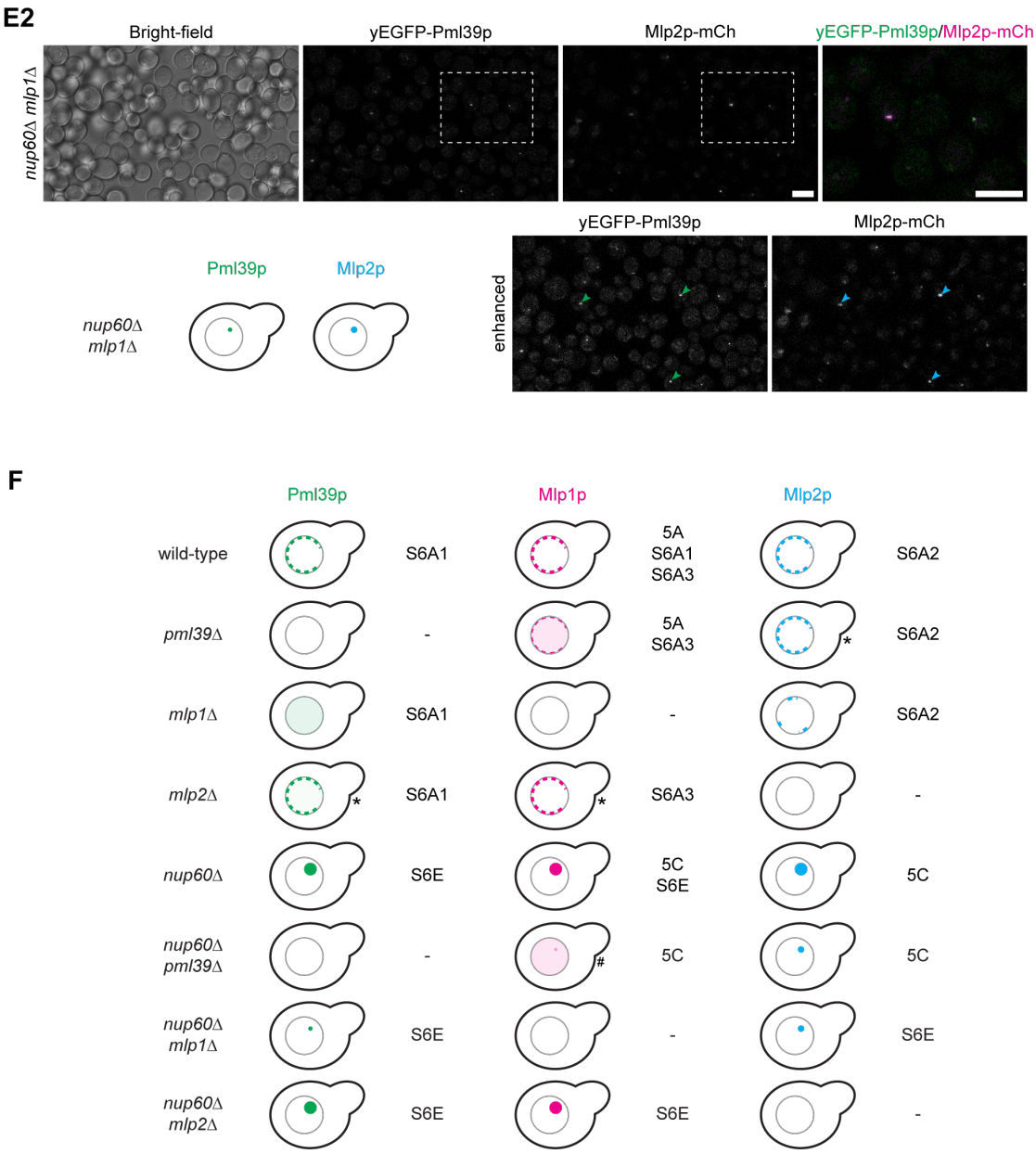

Supplemental Figure S7. Complementing studies on the contribution of *Sc*Pml39p in keeping subpopulations of NE-associated Mlp1 polypeptides positioned at the NB and within Mlp1p-containing nuclear foci.

With (i) Pml39p known to be a protein only located at the NE because of its binding to the Mlps, in particular to Mlp1p (Palancade *et al*, 2005; Supplemental Figure S7A1), with (ii) *Hs*ZC3HC1 known to be a protein whose NB-association depends on its binding to *Hs*TPR (Gunkel *et al*, 2021), and (iii) with both ZC3HC1 and Pml39p sharing a NuBaID sequence signature whose integrity was essential for binding to each species' NBs and TPR homologues, the next inevitable question was apparent. On the one hand, the deletion of *PML39* had been reported as not affecting the NE localization of Mlp1p or Mlp2p (Palancade *et al*, 2005). On

the other, we knew that ZC3HC1 was required for the positioning of subpopulations of TPR polypeptides at the NB (Gunkel *et al*, 2021). Even though one could imagine that the ZC3HC1 homologues in humans and yeasts might not have all functional properties in common, we examined, nonetheless, to what extent Pml39p might differ from ZC3HC1 concerning its role in interconnecting TPR subpopulations.

To this end, we compared the NE-associated signal intensities of FP-tagged Mlp1p and Mlp2p in yeast strains with and without Pml39p (S7A2 and S7A3). Regarding Mlp2p, we noticed hardly any diminishment of its NE-associated amounts in the *pml39*Δ cells (e.g., S7A2). Even after repeatedly inspecting populations of Mlp2p-yEGFP-expressing *PML39wt* and *pml39*Δ cells in parallel and having tested different growth conditions, we only sporadically noted at most some minor diminishment of the NE-associated overall signal intensities for Mlp2p-yEGFP in the *pml39*Δ cells. More commonly, when we had randomly acquired live-cell images with the same microscope settings from populations of *PML39wt* and *pml39*Δ cells, each loaded onto the imaging slides in duplicate, and then coded these images and compiled mixed collections of them, we arrived at the following result: When we attempted to unambiguously sort these coded images of Mlp2p-yEGFP-expressing cells back into groups that, after decoding, would have represented only either *PML39wt* or *pml39*Δ cells, this turned out not to be possible.

By contrast, regarding Mlp1p, the differences in the NE-associated signal intensities were evident enough (e.g., Figure 5A and S7A3) to recurrently allow for unambiguously distinguishing *pml39*Δ from WT cells. In this case, we could sort mixed compilations of coded live-cell micrographs of such Mlp1p-yEGFP-expressing *PML39wt* and *pml39*Δ cells faultlessly back into groups representing each respective strain. Moreover, such a reduction in the NE-associated Mlp1p, accompanied by a nucleoplasmic pool of Mlp1p due to Pml39p deficiency, resembled the effects we had by then noted in human cells, in which knockdown of ZC3HC1 by RNAi had caused a reduction in the NE-associated amounts of TPR, accompanied by a nucleoplasmic pool of TPR. Later, such findings also aligned with similar results in ZC3HC1 KO cells and upon degron-mediated degradation of ZC3HC1 (Gunkel *et al*, 2021; Gunkel & Cordes, 2022). Moreover, they now also resemble the outcome of a study in which degron-mediated Pml39p degradation is shown to affect the NE association of Mlp1p (Bensidoun et al, 2021).

To approximate those amounts of Mlp1p whose positioning at the NE depended on Pml39p, we determined the mean Mlp1p-yEGFP signal intensity of all NEs seen in equatorial focus in randomly acquired live-cell images of WT and *pml39*Δ cells. In doing so, we found the mean

amounts of the Pml39p-dependent Mlp1p subpopulations at the NE reaching up to about one-third of a cell population's ordinarily NE-associated total amount of Mlp1p (Figure 5B and S7C). As such, these amounts were thus lower than the ZC3HC1-dependent amounts of NE-associated TPR, which had been found to represent, on average, about half the total amount of TPR at the NEs of different somatic cell types (Gunkel *et al*, 2021; Gunkel & Cordes, 2022). However, we also noted that the NE-associated Mlp1p signal intensities varied notably between individual *PML39wt* cells. Such cell-to-cell differences were more pronounced than the lower degree of variation noted between TPR's NE-associated relative amounts in human cells, both in synchronized and asynchronous cell populations, with and without ZC3HC1 (Gunkel *et al*, 2021), when having conducted such quantifications in the same manner as for the yeast cells.

We next investigated whether Pml39p might also allow for the interconnection of Mlp1 polypeptides at sites remote from the NPC, perhaps similar to ZC3HC1 being capable of interconnecting TPR polypeptides no longer appended to the NPC. In fact, TPR in human cells was known to accumulate in cytoplasmic and nuclear foci when having knocked down the NPC protein NUP153 by RNAi (e.g., Hase & Cordes, 2003), and later, we had noted that such TPR-containing foci were mostly no longer detectable when both NUP153 and ZC3HC1 had been knocked down by RNAi together. Eventually, we found that such TPR foci also did not arise when knocking down NUP153 in ZC3HC1 KO cells once such cells had become available (Gunkel *et al*, 2021; our unpublished data). Thus, to determine whether the absence of *Sc*Pml39p might have a similar impact on Mlp foci, which typically arise in the absence of *Sc*Nup60p, the latter considered the yeast's homologue of NUP153, we performed a range of yeast experiments corresponding to those conducted in human cells (S7D–F). Eventually, this work revealed that Pml39p could keep Mlp1p place-bound in such foci within *nup60*Δ *cells*.

(A) Subcellular localization of Mlp1p, Mlp2p, and Pml39p in WT and *mlp1*Δ, *mlp2*Δ, and *pml39*Δ cells, with a selection of live-cell images here presenting such cells, endogenously expressing either all Pml39p, Mlp2p, or Mlp1p as yEGFP-tagged polypeptides (S7A1–3) or Mlp1p tagged with mCherrry (S7A1). Bright-field micrographs are shown as a reference. Note that images of *pml39*Δ cells expressing Mlp1p-yEGFP presented in S7A3 and equivalent micrographs in Figure 5A represent different datasets. Further note that images from the different strains presented in S7A2 and S7A3 were acquired on the same day in parallel to each other, using identical microscope settings to allow for adequate comparability of data.

The subcellular distribution of the yEGFP-tagged Mlp and Pml39 polypeptides in the WT and KO strains is again schematically depicted on the right. The asterisks mark those

combinations of KO strains and endogenously expressed FP-tagged proteins for which the results appeared to vary moderately between replicated rounds of inspection. Such ambiguity held for some minor reduction in the amounts of (i) the NE-associated Pml39p in the *mlp2*Δ cells (S7A1), (ii) the NE-associated Mlp2p in the *pml39*Δ cells (S7A2), and (iii) the NE-associated Mlp1p in the *mlp2*Δ cells (S7A3), with us noting such reductions only in some replicates but not others, and with such variations appearing to correlate to some extent with the growth phases of the cell cultures. Further note that not all but most of the results presented in S7A1–3 confirm previously reported findings (Palancade *et al*, 2005).

(A1) Live-cell fluorescence microscopy of WT and *mlp1*Δ cells, with both strains expressing all Pml39p tagged with yEGFP and Mlp1p tagged with mCherry. In addition, an *mlp2*Δ strain expressing yEGFP-tagged Pml39p is shown. Note that Pml39p and Mlp1p co-localize at the WT cells' NEs. Further note that Pml39p was essentially absent from the NEs of the *mlp1*Δ cells and instead primarily distributed diffusely throughout the nuclear interior, next to only some very rarely seen small-sized foci. Pml39p being absent from the NE in *mlp1*Δ cells, even though Pml39p can also bind to Mlp2p (e.g., Figure 4D, and Palancade *et al*, 2005), can be explained as follows: First, apart from some minor subpopulations, including also those Mlp2 polypeptides attached to the yeast's spindle pole body, the positioning of most Mlp2p at the NE depends on Mlp1p occurring NPC-associated (Palancade *et al*, 2005; Niepel *et al*, 2005). The absence of Mlp1p thus comes along with not only Pml39p, but also almost all Mlp2p no longer positioned at the NE (see also S7A2). Second, NE-associated Mlp2p does not appear to attract large amounts of Pml39p *in vivo* anyway, since the absence of Mlp2p in *mlp2*Δ cells appeared to come along with only minor reductions in the NE-associated amounts of Pml39p. Bars, 5µm.

(A2) Live-cell fluorescence microscopy of WT, *pml39*Δ, and *mlp1*Δ cells, with all strains expressing all Mlp2p tagged with yEGFP. Note that while the NE-associated amounts of Mlp2p were notably reduced in *mlp1*Δ cells, the positioning of Mlp2p at the NEs of *pml39*Δ cells appeared barely affected. Bar, 5µm.

(A3) Live-cell fluorescence microscopy of WT, *pml39*Δ, and *mlp2*Δ cells, with all strains expressing all Mlp1p tagged with yEGFP. Note that the positioning of Mlp1p at the NEs of the *mlp2*Δ cells appeared barely affected. By contrast, in many of the cells within the *pml39*Δ population, a subpopulation of the yEGFP-tagged Mlp1 polypeptides appeared distributed diffusely throughout the nuclear interior, a feature generally not noted within the *PML39wt* cells. Moreover, the amounts of the NE-associated Mlp1p-yEGFP appeared notably reduced. These results, which we regarded as unequivocal, were in line with essentially the same observations we made when inspecting Mlp1p-yEGFP-expressing *PML39wt* and *pml39*Δ cells

at higher resolution in a separate experiment (Figure 5A). (Gunkel *et al*, 2021; Gunkel & Cordes, 2022) Bar, 5µm.

(A4) Live-cell fluorescence microscopy of WT and *pml39*Δ cells, with both strains expressing all Mlp1p tagged with mCherry. Note that the subcellular distribution of Mlp1p-mCherry closely resembled the corresponding distributions seen in S7A3, with the NE-associated amounts of Mlp1p-mCherry notably appearing reduced in the *pml39*Δ cells and with some Mlp1p distributed throughout the nucleus instead. Bar, 5µm.

(B) Live-cell fluorescence microscopy for investigating the cellular localization within *pml39*Δ cells of other proteins known to occur NB-associated in WT cells. To study these proteins' fate in the absence of Pml39p, we had created yet further *PML39wt* and *pml39*Δ strains, all endogenously expressing mCherry-tagged Mlp1p and, in addition, either all Mad1p, Sac3p, or Ulp1p as yEGFP-tagged polypeptides. Note that we found the positioning of these other NB-associated proteins at the NE not notably or only very moderately affected in the *pml39*Δ cells compared to their localization at the WT cells' NEs. Bars, 5 µm (overviews) and 2 µm (insets), respectively.

(C) Quantification of signal yields of yEGFP tagged to Mlp1p at the NEs of *PML39wt* and *pml39*Δ cells. The quantification procedure is described in the legend of Figure 5B. The data presented here represent the individual results of the two separate experiments (n = 50 nuclei per dataset), whose means are presented in Figure 5B. The box plots display the relative signal intensity values, with the arithmetic means marked by x and the standard deviations (SD) provided. In S7C1, those arithmetic means set to 100% relate to the *PML39wt* cells, while in S7C2, representing the same measured values, they relate to the *pml39*Δ cells. While both ways of presentation illustrate that the mean Mlp1p-yEGFP signal yields were found notably reduced at the *pml39*Δ cells' NEs, we regard the presentation in S7C2 as perhaps better reflecting the copy number relationships between the different Mlp1p subpopulations at the NE. In fact, we can imagine that those Mlp1 polypeptides anchored to the NPC independently of Pml39p represent a somewhat more homogeneous population in terms of copy numbers than those additionally appended in the presence of Pml39p.

Along the same line, we find it informative that we generally found the signal yields' mean SD values smaller for the population of *pml39*Δ cells than for the WT cells. Again, we regard this finding, too, as in accord with a model in which the Mlp1 polypeptides that occur NPC-anchored independently of Pml39p would reflect an Mlp1p subpopulation with a more defined copy number per NPC. In contrast, the copy numbers of those Mlp1 polypeptides that can be additionally appended to the NB in a Pml39p-dependent manner could, to some extent, be more

variable. In other words, we consider those NBs that remain NPC-appended in the absence of Pml39p to be more similar, regarding their Mlp1p copy numbers, both between cells and between individual NBs within the same cell, than in the presence of Pml39p.

(D) Recapitulating the formation of Mlp-containing nuclear foci in *nup60*Δ cells (e.g., Feuerbach *et al*, 2002) as the prerequisite for later investigating how Pml39p contributes to such foci's occurrence. Here, the formation of such Mlp1p-containing foci, usually a single one per nucleus, is exemplified by the live-cell images of *nup60*Δ cells endogenously expressing mCherry-tagged Mlp1p and the yEGFP-tagged NPC protein Nup1p, the latter shown as a reference protein that remains located at the NE. In the two-color overlay image, note that Mlp1p within such *nup60*Δ cells appeared only detectable within the nuclear foci, with the foci's subcellular location evident as they were surrounded by NPCs labeled with Nup1p-yEGFP. Bar, 5 µm.

(E) Assessing the contribution of Mlp1p and Mlp2p to the formation of the Mlp-containing foci in *nup60*Δ cells.

(E1) Live-cell fluorescence microscopy of *nup60*Δ and *nup60*Δ *mlp2*Δ strains endogenously expressing all Pml39p as yEGFP-tagged polypeptides and all Mlp1p as tagged with mCherry. The overview images demonstrate that the Pml39p- and Mlp1p-containing foci are common within both strains' populations, with some of these foci marked by green- and magenta-colored arrowheads. Furthermore, the images' marked rectangular areas are shown as two-color overlays at higher magnification on the right, revealing quasi-co-localization of Pml39p and Mlp1p in these foci known to be located within these cells' nuclei. Note that signal displacement often observable between the two-color channels was caused by the non-fixed cells' residual mobility during live-cell imaging, even though the cells had been allowed to settle to the wells' bottom. In particular, though, note that the absence of Mlp2p did not prevent the formation of such foci. Further note that the overview images presented here in S7E1 and the following in S7E2 were acquired from specimens all inspected side-by-side, using the same microscope settings, to allow for direct data comparability. Bars, 5 µm.

(E2) Live-cell fluorescence microscopy of a *nup60*Δ *mlp1*Δ strain endogenously expressing all Pml39p as yEGFP-tagged polypeptides and all Mlp2p as tagged with mCherry. The overview images are also shown electronically signal-enhanced, with a multiplication factor of two. Note that hardly any foci, except for a few sporadic ones, were detectable, some of which are marked by green and blue arrowheads, revealing that Pml39p and Mlp2p together are not well capable of forming large foci when Mlp1p is absent. Bars, 5 µm.

(F) Summarizing schematic depiction of the subcellular distribution of the FP-tagged Mlp and Pml39 polypeptides in some of the different yeast strains investigated in the current study (for a list of strains, see Supplemental Table S2). In contrast to the majority of strains, for which we rated the observations as unequivocal, the outcome for a few strains, here marked by asterisks, appeared to vary moderately between replicated rounds of inspection, as mentioned in the legends of Figure 5D and S7A. Figure numbers of micrographs representing the different experiments are provided on the right side of each yeast cell's scheme. Based on the results *in toto*, we regarded it justified to conclude that Pml39p can keep subpopulations of Mlp1p positioned at the NB and even at sites remote from the NB, pointing at Pml39p functioning as a protein connecting Mlp1p polypeptides.

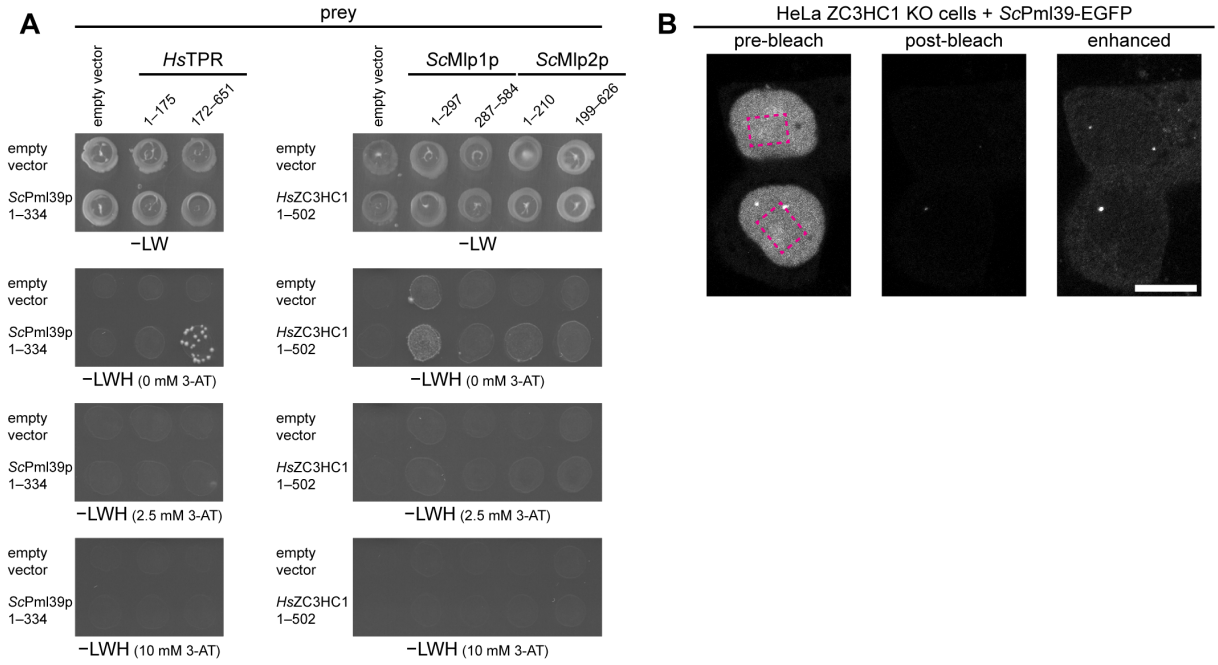

Supplemental Figure S8. Experiments revealing that *Sc*Pml39p and *Hs*ZC3HC1 cannot interact with the respective other species' TPR homologues.

To assess whether Pml39p and ZC3HC1 might interact with the other species' TPR homologues, we performed Y2H experiments and tested whether *Sc*Pml39p, ectopically expressed in HeLa WT and HeLa ZC3HC1 KO cells would be able to bind to the human NB. These experiments revealed that Pml39p could not stably interact with the NBs and *Hs*TPR in human cells, not even in the absence of *Hs*ZC3HC1. Furthermore, we did not find Pml39p capable of a Y2H interaction with the ZC3HC1-binding regions of *Hs*TPR. Similarly, we did not detect a Y2H interaction between *Hs*ZC3HC1 and the Pml39p-binding parts of Mlp1p and Mlp2p. However, we regarded these negative findings of Pml39p and ZC3HC1 as not mutually exchangeable regarding interaction with the other species' TPR homologues as likely explainable by Mlp- and TPR-binding interfaces that probably share only a limited degree of sequence similarity. This explanation appeared even more plausible once it became evident that the proteins' common residues of the minimal NuBaID signature do not engage in intermolecular interactions (Figure 6 and Supplemental Figure S11) and that they, thus, are unlikely to be part of the Mlp- and TPR-binding interfaces.

(A) Representative Y2H data obtained with expression vectors coding for *Hs*TPR, *Sc*Mlp1p, and *Sc*Mlp2p segments, fused to GAL4-AD (prey), and for the intact, WT versions of *Sc*Pml39p and *Hs*ZC3HC1, fused to GAL4-BD (bait). Representative colony growth on selection medium lacking leucine and tryptophan (−LW), revealing successful mating between the yeasts

harboring the indicated GAL4-AD and GAL4-BD expression vectors, and the fate of the diploid cells after having replica-plated them onto selection medium lacking leucine, tryptophan, and histidine (−LWH), either without or with different concentrations of 3-AT as indicated. Note that even in the absence of 3-AT, essentially no growth and thus no Y2H interaction was notable between either *Sc*Pml39p and *Hs*TPR or *Hs*ZC3HC1 and the yeast's Mlps. Further note that each of the here presented Y2H data stems from the same growth plates, with corresponding 3-AT concentration, on which also those colonies were grown that are presented in Supplemental Figure S6A2. The range of Y2H interactions shown in Supplemental Figure S6A2 can thus be regarded as the positive controls for the data presented here.

(B) Live-cell imaging and photobleaching of HeLa ZC3HC1 KO cells transiently transfected with an expression vector encoding EGFP-tagged *Sc*Pml39p. Photobleaching and image acquisition were performed as described in Supplemental Figure S2A2. In brief, marked rectangular areas in the pre-bleach images of representative cells were subjected to pulses of full laser power, followed by the acquisition of a post-bleach image. Note that the ectopically expressed *Sc*Pml39p was never found NE-associated in the HeLa cells. As an aside, further note that the tagged *Sc*Pml39p often appeared within the human cells' nucleoli, in contrast to the accordingly tagged human ZC3HC1 homologue, always found excluded from them (see Supplemental Figure SA2). Bar, 10 µm.

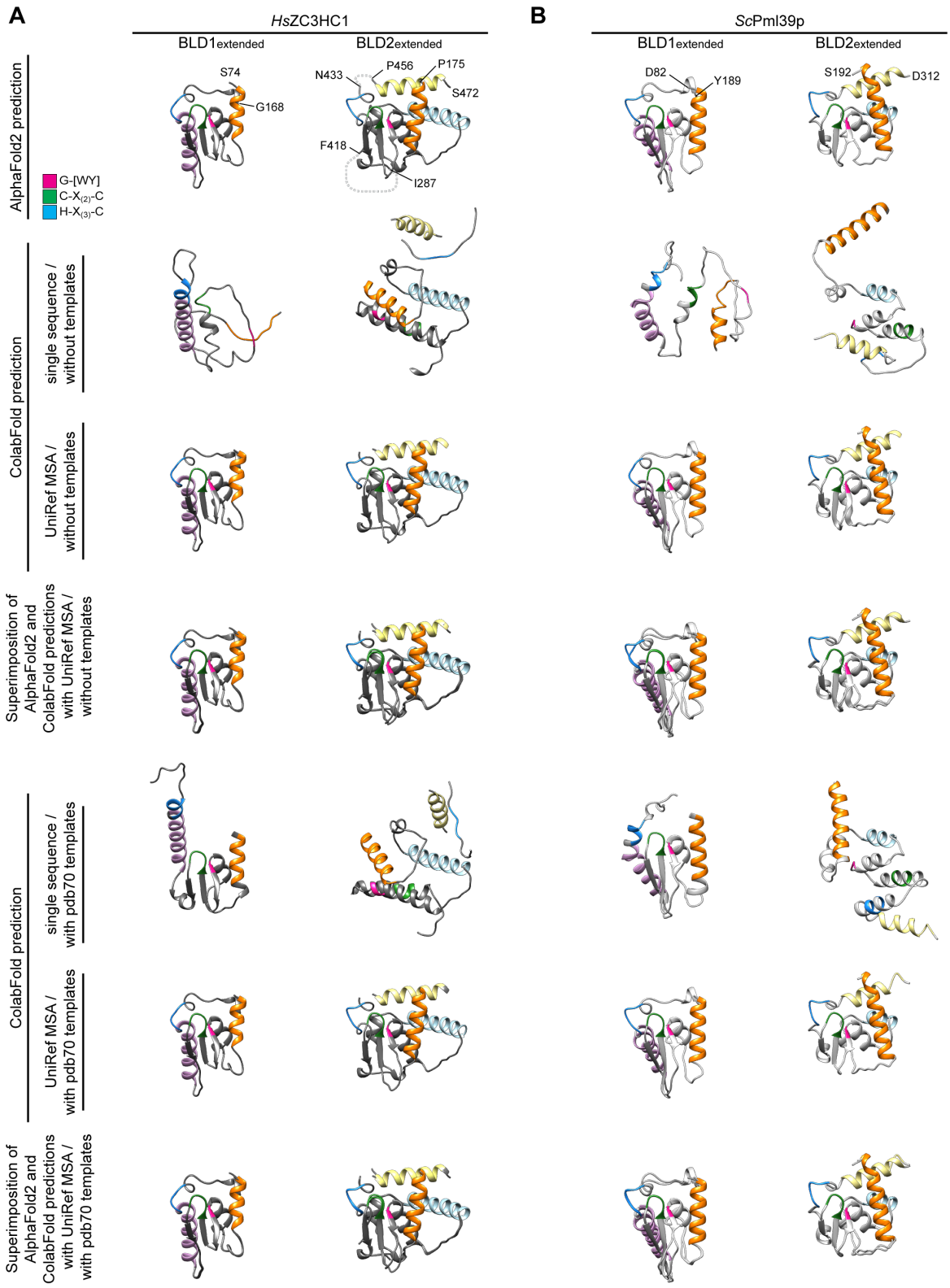
A
HsZC3HC1
BLD1extended
BLD2extended
AlphaFold2 prediction
G-[WY]
C-X(2)-C
H-X(3)-C
S74
G168
N433
P456
P175
S472
F418
I287
ColabFold prediction
single sequence / without templates
UniRef MSA / without templates
Superimposition of AlphaFold2 and ColabFold predictions with UniRef MSA / without templates
ColabFold prediction
single sequence / with pdb70 templates
UniRef MSA / with pdb70 templates
Superimposition of AlphaFold2 and ColabFold predictions with UniRef MSA / with pdb70 templates
B
ScPml39p
BLD1extended
BLD2extended
D82
Y189
S192
D312

S9 (1/2)

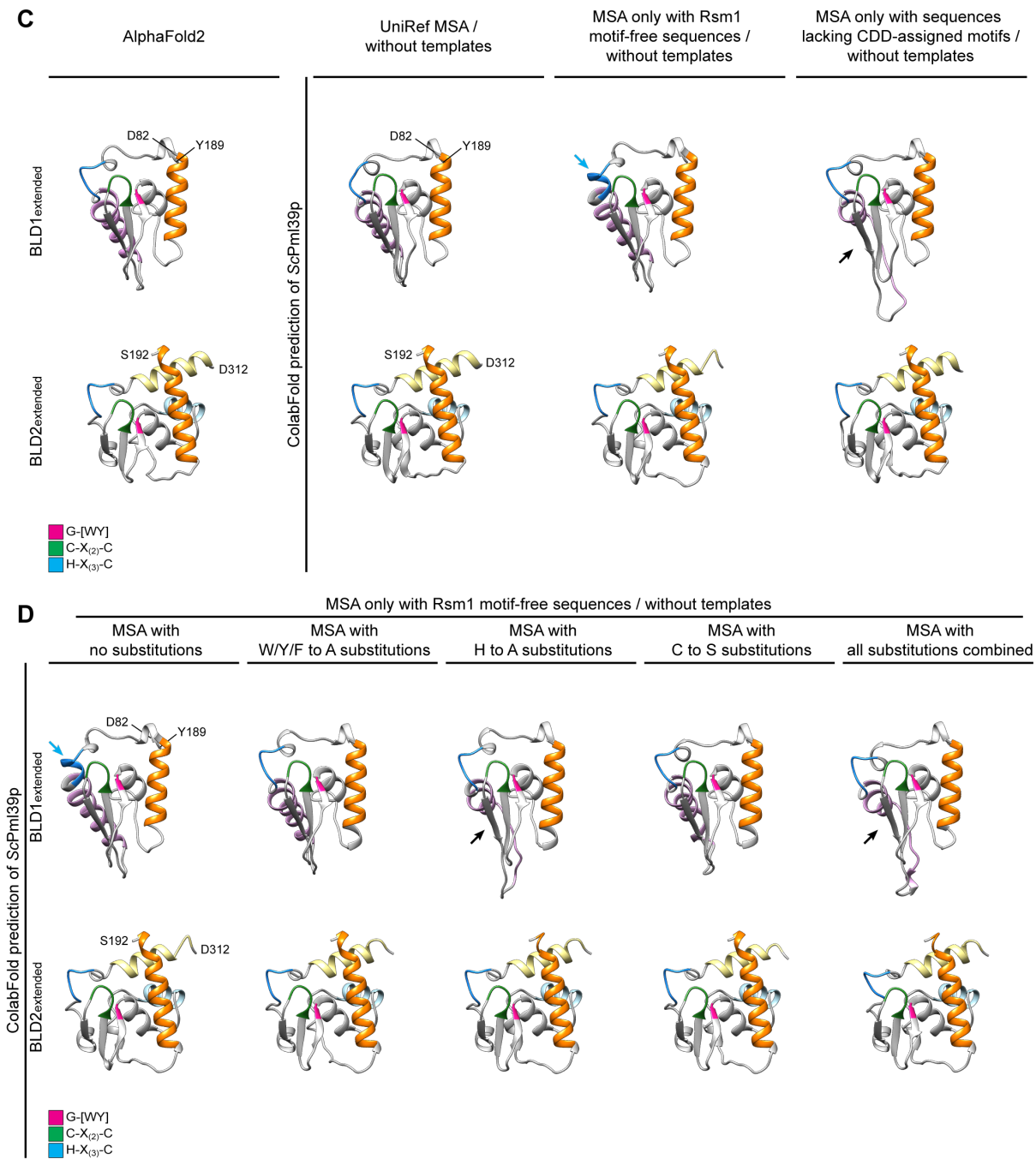

Supplemental Figure S9. Assessment of the contributions of sequence database search-derived MSAs and PDB database-deposited structures as templates for BLD structure predictions.

Since AlphaFold2 uses, as one of the input datasets for predicting a query protein's structure, also PDB-deposited crystal structures as templates in its computations (Jumper *et al*, 2021), we initially had wondered whether such templates might bias the predictions of the BLDs' structures (Supplemental Information 6). Furthermore, we wanted to assess to which extent distinct sequences that were part of the MSAs, the latter representing the other input dataset for

such structure predictions, might influence the outcome of the predictions by introducing some bias. In particular, we were interested to find out whether structure predictions starting from an MSA composed of protein sequences with a Pfam Rsm1 motif already assigned to them would differ from predictions based on an MSA solely composed of sequences without such a pre-existing profile HMM while nonetheless representing ZC3HC1 homologues according to our criteria, which included possession of a NuBaID signature (Supplemental Information 6). Since an Rsm1 motif has not been attributed to *Sc*Pml39p so far, and as this happens to be the case for numerous other proteins too that we consider true ZC3HC1 homologues, including such in other species of the family Saccharomycetaceae, we wondered which structures would be predictable starting from such a "Pfam Rsm1 motif-free" MSA. However, we also noted that tools like HHsearch and HHpred (Söding, 2005; Steinegger et al, 2019; https://toolkit.tuebingen.mpg.de/tools/hhpred) would assign the PDB structures and profile HMM of metazoan BIR domains to such a subset of Pfam motif-free yeast sequences nonetheless. Therefore, we also attempted to mutate the input sequences by *in-silico*-exchanging a small number of residues so that the BIR domains' HMM would no longer be correlatable with the mutated yeast sequences, with this latter approach overlapping with our additional attempt to gain insight also into how AlphaFold2 handles an MSA only composed of mutated sequences (see further below). With such approaches, we aimed to impede the program's access to HMM and PDB template information by which it might correlate *Sc*Pml39p with *Hs*ZC3HC1 or the BIR domains during a user-initiated prediction process, unlike in AlphaFold2's training procedures during which such HMM and crystal structure information had been used (Jumper *et al*, 2021).

In addition, we addressed some of our concerns about the structure predictions of mutant versions of ZC3HC1 (i) that naturally occur *in vivo*, those (ii) that we had constructed and cloned in the course of the current study, and yet additional ones (iii) that we had designed *in silico* in order to test certain aspects of the program's performance. In Supplemental Information 6, the rationale for conducting such trial structure predictions is described in further detail, while exemplary data sets in the following illustrate the outcome of such trials.

(A) Structures predicted for the essentially entire BLD1 and BLD2 modules of *Hs*ZC3HC1, as defined as the "extended" version in Figure 6C. Some of the ColabFold-predicted structures were then superimposed onto those from AlphaFold2. The MMseqs2-derived UniRef MSA used for some of these predictions comprised 799 sequences from various organisms. Note that predictions based on only the protein's own sequence did not allow for any prediction closely

resembling the initial prediction by AlphaFold2 or via ColabFold's default settings (UniRef MSA and without template). Further note, in particular, that including PDB template information did not notably affect the outcome of the ColabFold predictions starting from the UniRef MSA, with such template-considering predictions closely resembling those achieved with the programs' default, "template-free" settings. The additional information provided by the PDB templates only improved the outcome to some extent, though merely for the BLD1, when using only the *Hs*ZC3HC1 sequence as the sequence input.

(B) Structures predicted, as in S9A, for the essentially entire BLD1 and BLD2 modules of *Sc*Pml39p. Some of the ColabFold-predicted structures were again superimposed onto those from AlphaFold2. The UniRef MSA used for some of the here-presented predictions comprised a total of 27 fungal sequences, including two with an Rsm1 motif attributed to them. A zf-C3HC motif had been assigned to 26 of them, as in Pfam release 35.0, while in the CDD, this was the case for only 13 of them. Note that predictions based on the *Sc*Pml39p sequence alone, i.e., without employing an MSA, notably differed from the initial one provided by AlphaFold2. Again, however, just like for *Hs*ZC3HC1, note that the exclusion of PDB template information did not notably affect the outcome of those predictions that only made use of information provided by the UniRef MSA.

(C) ColabFold-predicted structures of the essentially entire BLD1 and BLD2 modules of *Sc*Pml39p, all obtained without accessing the PDB's template information, next to those predicted with AlphaFold2s' default settings. The UniRef MSA used by ColabFold for the structures in the second column, as already presented in S9B, comprised the already abovementioned total of again 27 sequences, among which was also a sequence that would represent a BLD1-mutated version of a Pml39p homologue (XP_037145256.1) and two short segments only comprising part of the respective homologue's BLD1 sequence. Removing these three sequences together with the remaining one with an Rsm1 motif assigned to it resulted in an MSA comprising 23 Rsm1-motif-free sequences, representing ZC3HC1 homologues with an intact BLD1. The BLD1 and BLD2 structures of *Sc*Pml39p computed on the basis of this MSA are presented in the third column. The fourth column then represents those predicted structures obtained after additionally having removed from the MSA all those sequences with a zf-C3HC motif assigned to them in the CDD. Aware that even the remaining sequences still had a zf-C3HC attributed to them by Pfam, we nonetheless considered this structure prediction also noteworthy, for reasons outlined below.

We already regard, though, the BLD2 structure presented in the third column as of particular note. Even without any template information and no Rsm1 profile HMM appertaining to the

input sequences, this ColabFold-predicted BLD2 still closely resembled the initial one based on the UniRef MSA, with this again essentially identical to those from the AlphaFold2 structure database. However, one also needs to know that a program like HHpred (Zimmermann et al, 2018; https://toolkit.tuebingen.mpg.de/tools/hhpred), even though it, back then, did not detect ZC3HC1 homologues of other phyla when using the Rsm1-motif-free yeast sequences, would still correlate the MSA composed of these sequences with the PDB-deposited structure and HMM profile of BIR domains. In other words, some profile comparison tools using such Rsm1-motif-free yeast sequences would still detect similarity with the BIR domains' profile even when the closer kinship of these yeast proteins remained undetectable. In this context, we also regard it as noteworthy that the removal of the Rsm1 motif-containing sequences resulted in a BLD1 prediction, which then, in some part, more closely resembled a BIR domain: In fact, the pink-colored α-helix of the BLD1 was then predicted C-terminally extended (blue arrow), with the histidine of the first BLD's H-$X_{(3)}$-C pentapeptide then part of this α-helix, just like the histidine of the BIR domains' H-$X_{(6)}$-C octapeptide is part of an α-helix similarly positioned relative to the domain's centrally positioned β-sheets.

Furthermore, we consider it noteworthy that a total of only 13 remaining sequences had turned out sufficient to predict a structure whose appearance was still very similar to the one predicted when starting from the UniRef MSA, with about twice as many sequences. Merely the prediction of the pink-colored α-helix of BLD1, then no longer predicted as such in its entirety, differed notably (here marked by a black arrow). Initially, we had been uncertain whether such a small number of very similar sequences, all from the same family Saccharomycetaceae, would provide a bandwidth of non-conserved residues high enough to accentuate those evolutionarily conserved residues that were the structurally most relevant ones. In other words, we initially were doubtful whether such a small dataset would suffice because Alphafold2's prediction accuracy had been mentioned to decrease notably when an MSA was composed of less than 30 sequences (Jumper *et al*, 2021).

(D) ColabFold-predicted structures of wild-type and mutant versions of *Sc*Pml39p, all obtained without accessing the PDB's template information. The MSA for predicting the wild-type structure on the left, as already presented in S9C, again comprised the abovementioned 23 yeast sequences that we regarded as representing functionally intact ZC3HC1 homologues, including *Sc*Pml39p, while all of them lacked an Rsm1 signature as defined by the Pfam database. For predicting the structure of various mutant versions of *Sc*Pml39p, we exchanged distinct residues both within the *Sc*Pml39p input sequence and at the corresponding positions of the other 22 sequences for either alanine or serine, with these MSAs and their modified sequences to be then

used for the mutant *Sc*Pml39p's structure prediction. The residues exchanged corresponded, in the case of *Sc*Pml39p, to H172A and H288A of the two BLDs' H-$X_{(3)}$-C pentapeptides (H to A), and to W119A and Y257A of the G-W and G-Y dipeptides, with one of the other yeast sequences having featured a G-F at the corresponding position instead, which was changed accordingly (W/Y/F to A). Furthermore, for another mutant *in silico*, all cysteine residues of the two BLDs' C-$X_{(2)}$-C tetrapeptides and H-$X_{(3)}$-C pentapeptides involved in zinc coordination were exchanged for serine, resulting in C134S, C137S, C176S, C268S, C272S, and C292S (C to S). Finally, all these mutations were combined (W/Y/F to A, C to S, and H to A). It needs to be remarked that upon introducing the W/Y/F to A mutations or the H to A mutations, the high-sensitivity tool HHpred would still correlate these MSAs with BIR domain structures. However, this was no longer the case for the MSA representing the C to S mutations when initially using HHpred, i.e., before the HHpred web server updates in 2022, and the same applied to the one whose sequences combined all the substitutions. Furthermore, while other tools like HHblits (Remmert *et al*, 2011) and HMMER3 (Eddy, 2011), used by AlphaFold2 too (Jumper *et al*, 2021), would still allow for identifying a few fungal wild-type ZC3HC1 homologues when using some of the mutant sequences as query, no homologues were immediately identifiable beyond the Mycota kingdom during first-round searches. The latter also held when conducting such searches with the other search tools mentioned in the current study.

The findings outlined in S9D conveyed to us the following impressions. First, we initially considered it reassuringly remarkable that the *Sc*Pml39p BLD structures predicted on the following terms were still strikingly similar to those of *Hs*ZC3HC1. These terms had comprised (i) the *Sc*Pml39p sequence being part of a subtracted MSA, which at first appeared no longer alignable with BIR domain structures when we had initially conducted such computations, and (ii) such an MSA neither then nor currently allowing for direct detection of ZC3HC1 homologues beyond the fungi.

Second, we were surprised, though, that after having introduced aa substitutions in all 23 sequences that would have abolished the establishment of a zinc ion coordination sphere, the AlphaFold2/ColabFold-predicted structures for these mutants appeared only very moderately affected. We regarded this observation as particularly noteworthy since we already knew that each individual substitution mutation, already on its own, abolished or severely attenuated *Sc*Pml39p binding to the NB (this study), with at least some of them also known to prevent proper folding of *Hs*ZC3HC1 (Gunkel & Cordes, 2022, and our unpublished data). Even though we were aware that AlphaFold2 had been mentioned not to have been trained for predicting the effect of substitution mutations within a query sequence, we were nonetheless amazed that even

manifoldly mutating all the sequences of an MSA would hardly affect the outcome of a prediction process. We considered it enigmatic that even in the case of those BLD1 and BLD2 mutants that each included five aa substitutions, the program still predicted the three centrally positioned conspicuous β-sheets and those positions usually occupied by residues involved in establishing the zinc coordination sphere to remain essentially unchanged. With these central arrangements predicted unaffected, the only finding no longer a surprise to us was that the positioning of the BLDs' α-helices relative to these central structures was then predicted to have remained unchanged too, with this also in contrast to what we would expect based on our experimental data. Therefore, in light of such trial predictions of the kind exemplified here and the insight they had allowed us to gain, we considered it justified to exert some caution when interpreting some of the structure predictions by AlphaFold2; to avoid misinterpretations and not draw conclusions from computed structures that this prediction tool had not been trained for providing.

A

*Hs*ZC3HC1 full length AlphaFold2 prediction

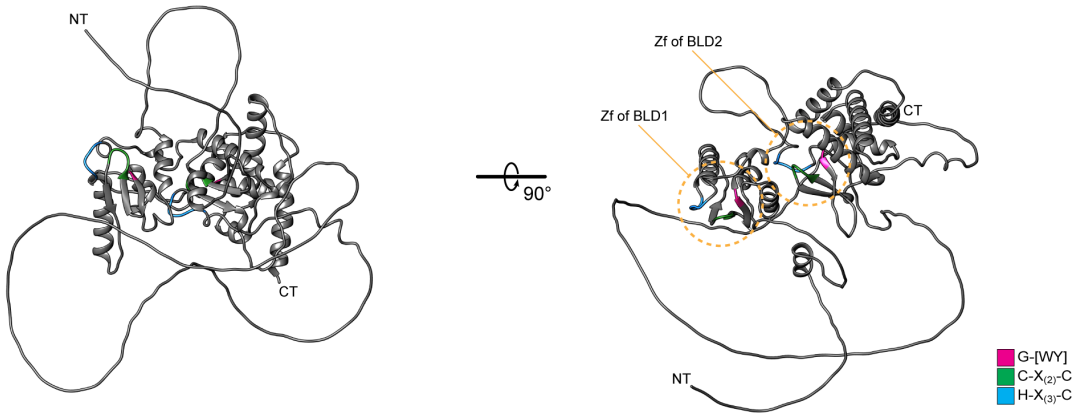

*Dd*ZC3HC1 full length AlphaFold2 prediction

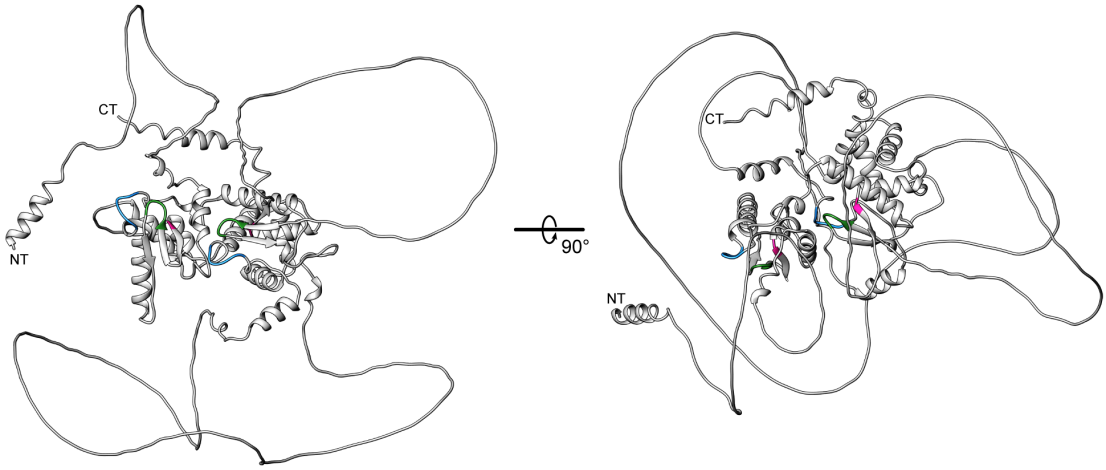

*Sc*Pml39p full length AlphaFold2 prediction

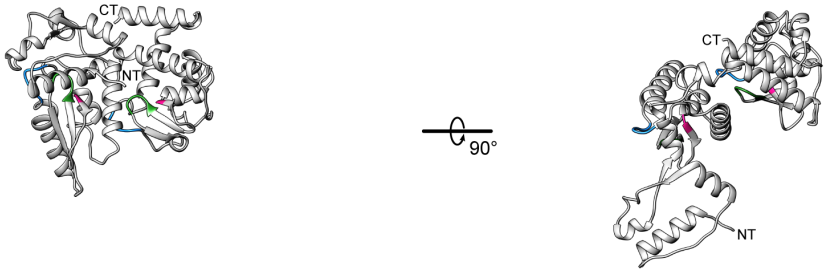

S10 (1/3)

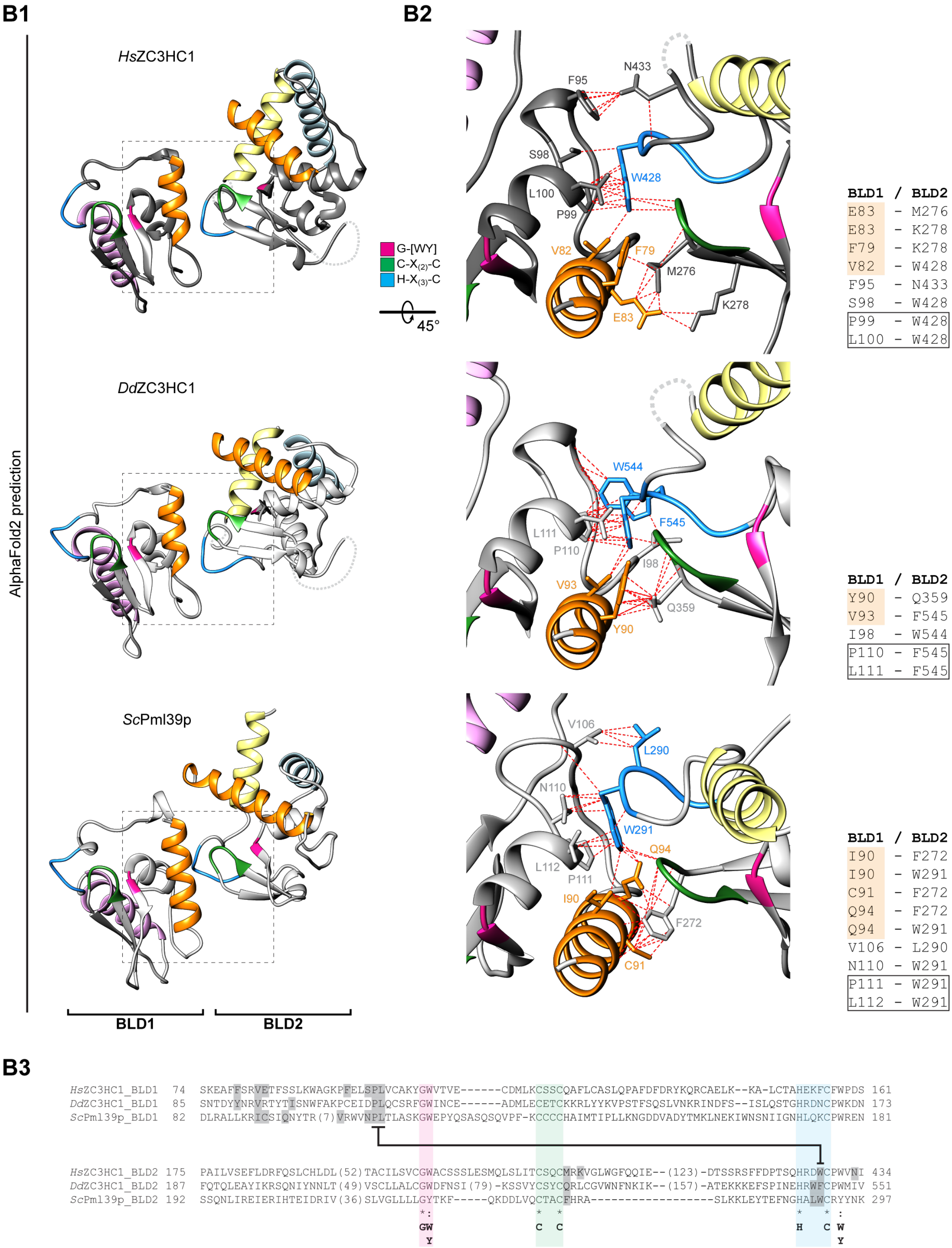

B1
B2
HsZC3HC1
DdZC3HC1
ScPml39p
AlphaFold2 prediction
BLD1
BLD2
G-[WY]
C-X(2)-C
H-X(3)-C
45°
F95
N433
S98
W428
L100
P99
V82
F79
M276
E83
K278
W544
F545
L111
P110
I98
V93
Q359
Y90
V106
L290
N110
W291
Q94
L112
P111
I90
F272
C91
BLD1 / BLD2
E83 - M276
E83 - K278
F79 - K278
V82 - W428
F95 - N433
S98 - W428
P99 - W428
L100 - W428
BLD1 / BLD2
Y90 - Q359
V93 - F545
I98 - W544
P110 - F545
L111 - F545
BLD1 / BLD2
I90 - F272
I90 - W291
C91 - F272
Q94 - F272
Q94 - W291
V106 - L290
N110 - W291
P111 - W291
L112 - W291
B3
HsZC3HC1_BLD1 74 SKEAFFSRVETFSSLKWAGKPFELSPLVCAKYGWVTVE------CDMLKCSSCQAFLCASLQPAFDFDRYKQRCAELK--KA-LCTAHEKFCFWPDS 161
DdZC3HC1_BLD1 85 SNTDYYNRVRTYTISNWFAKPCEIDPLQCSRFGWINCE------ADMLECETCKKRLYYKVPSTFSQSLVNKRINDFS--ISLQSTGHRDNCPWKDN 173
ScPml39p_BLD1 82 DLRALLKRICSIQNYTR(7)VRWVNPLTLASKGWEPYQSASQSQVPF-KCCCCHAIMTIPLLKNGDDVADYTMKLNEKIWNSNIIGNHLQKCPWREN 181
HsZC3HC1_BLD2 175 PAILVSEFLDRFQSLCHLDL(52)TACILSVCGWACSSSLESMQLSLITCSQCMRKVGLWGFQQIE--(123)-DTSSRSFFDPTSQHRDWCPWVNI 434
DdZC3HC1_BLD2 187 FQTQLEAYIKRSQNIYNNLT(49)VSCLLALCGWDFNSI(79)-KSSVYCSYCQRLCGVWNFNKIK--(157)-ATEKKKEFSPINEHRWFCPWMIV 551
ScPml39p_BLD2 192 SSQNLIREIERIHTEIDRIV(36)SLVGLLLLGYTKF-----QKDDLVQCTACFHRA-------------------SLKKLEYTEFNGHALWCRYYNK 297
*:
GW
Y
* *
C C
* * :
H C W
Y

S10 (2/3)

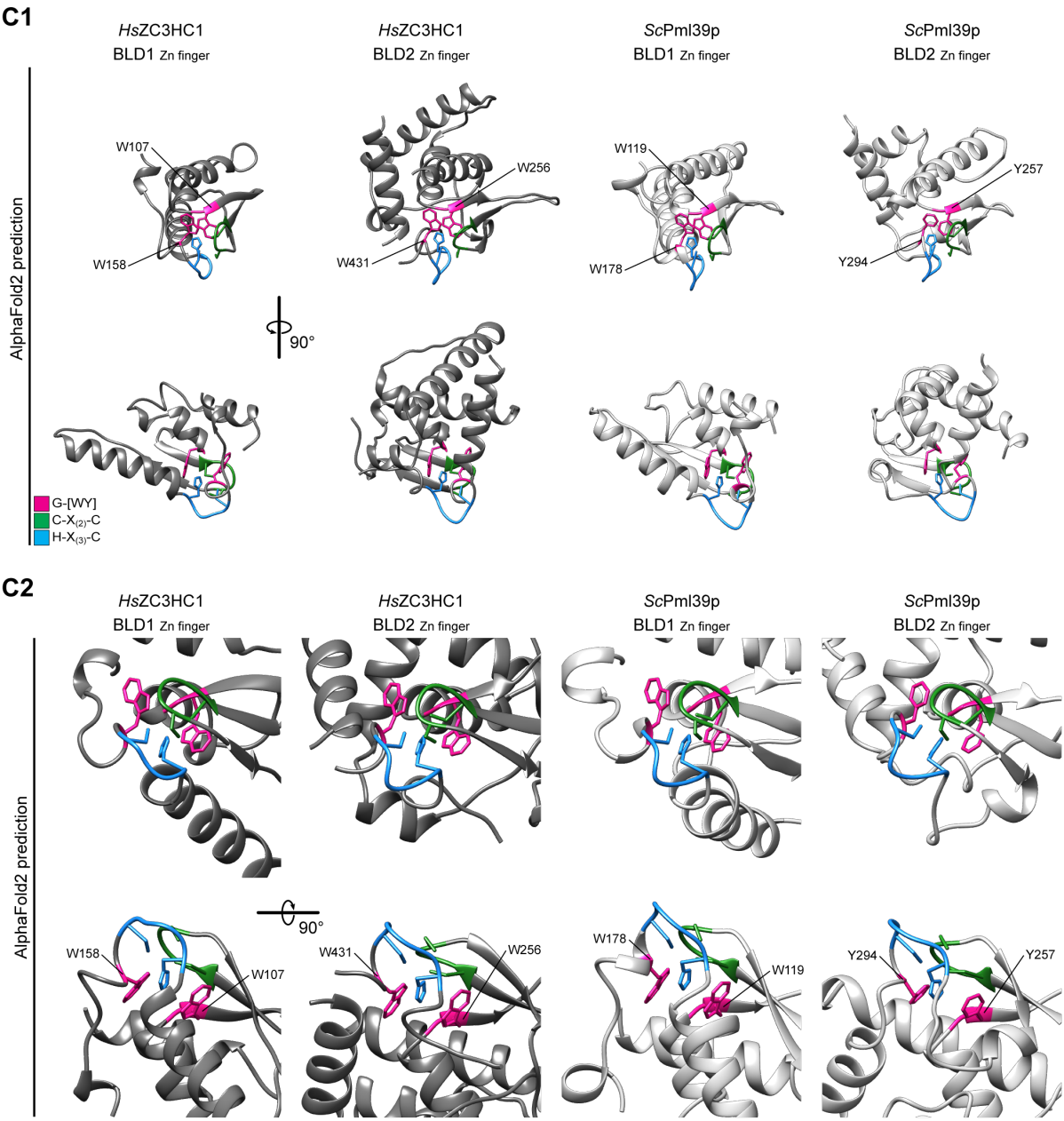

Supplemental Figure S10. The tertiary structures of *Hs*ZC3HC1, *Dd*ZC3HC1, and *Sc*Pml39p *in toto*, as predicted by AlphaFold2, and closer looks at a BLD1:BLD2 interface and at distinct aromatic amino acids flanking the zinc ion coordination spheres.

To allow for a comparison of the at first sight notably different appearance of the human, amoebic and budding yeast ZC3HC1 homologue, AlphaFold2's predictions for each of these proteins' entirety are presented in S10A. Furthermore, an evolutionarily conserved BLD1:BLD2 binding interface unveiled by these predictions, with distinct inter-BLD contacts, is shown in S10B. In addition, conspicuous intra-BLD arrangements, including evolutionarily conserved aromatic acids, and these residues' positions relative to the zinc ion coordination spheres, are outlined in S10C.

(A) AlphaFold2's predictions for *Hs*ZC3HC1, *Dd*ZC3HC1, and *Sc*Pml39p, with each homologue's predicted structure aligned to those of the other via each homologue's first BLD and there, in particular, to the zinc coordination sphere and the neighboring β-sheets. In addition, the structures are shown in two different perspectives, allowing for visualizing additional α-helices, seemingly also evolutionarily conserved, beyond the BLDs' boundaries, as newly defined in this study further below. The functions of some of these non-BLD α-helices, a research topic beyond the scope of the current study, will be presented elsewhere.
(B) Structure and sequence characteristics of the BLD1:BLD2 interface of *Hs*ZC3HC1, *Dd*ZC3HC1, and *Sc*Pml39p.
(B1) AlphaFold2's predictions for *Hs*ZC3HC1, *Dd*ZC3HC1, and *Sc*Pml39p as in S10A, with the BLDs' positions relative to each other remaining the same, but here having blinded out all those parts not regarded as belonging to the BLDs structural parts, the latter essentially as defined in Figure 6C. Also in contrast to S10A, the BLDs are here shown colored, corresponding to their coloring in Figure 6C. The dashed squares mark those parts shown at higher magnification in S10B2.
(B2) BLD1 and BLD2 residues of the BLD1:BLD2 interface are shown at higher magnification and tilted by 45°. Structures and side chains are colored as in S10B1. Chimera's structural analysis tool was used to compute and illustrate potential contacts of designated atoms of selected aa side chains with neighboring aa residues. On the basis of atom-to-atom distances of ≤ 4 Å, several possible contacts are here depicted as dashed red lines. Note that among the residues most likely involved in such inter-BLD contacts were aromatic ones positioned between the histidine and cysteine of the H-$X_{(3)}$-C pentapeptide of BLD2, with these then in contact with a distinct P-L dipeptide as part of the three ZC3HC1 homologues' BLD1. In the case of, e.g., *Hs*ZC3HC1, the corresponding aromatic residue of BLD2 is W428, while the P-L dipeptide is composed of P99 and L100. Corresponding residues are also present in *Dd*ZC3HC1 and *Sc*Pml39p, where AlphaFold2 also predicts them to contribute to a BLD1:BLD2 interface, with such residues and their potential contacts here also shown cataloged on the right side. As an aside, these aromatic residues are not among those for which substitution mutants were presented in the current study.

Additional residues seemingly contributing to the BLD1:BLD2 contacts are part of a BLD1 α-helix that is here shown orange-colored, representing the same BLD1 α-helix also shown orange-colored, e.g., in Figure 6C. In *Hs*ZC3HC1, the BLD1 α-helix residues whose side chains point towards BLD2 include F79, V82, and E83, with these then potentially in contact with

M276, K278, and W428. Furthermore, contacts that can be regarded as corresponding ones are also evident at the BLD1:BLD2 interfaces of *Dd*ZC3HC1 and *Sc*Pml39p.

While an α-helix equivalent to this particular one in the BLD1 also exists in the BLD2 (see, e.g., Figure 6C) and even in the BIR domains (e.g., Supplemental Figure S11E), where they are then also shown orange-colored, neither the BLD2 nor the BIR domains' orange-colored α-helices contribute to the BLD1:BLD2 nor a BIR:BIR domain interface, respectively. Instead, the common feature of all of the BLD and BIR domains' orange-colored α-helices, which defines their equivalence, are those helix residues, also including an evolutionarily conserved arginine, that are oriented towards the domains' central parts where they allow for distinct intra-BLD contacts (e.g., Supplemental Figure S11F and S11G).

In toto, the predicted proximity of each homologue's two BLDs to each other and the numerous potential inter-BLD contacts, with the resulting overarching arrangement then reminiscent of two BLDs tethered to each other, confers the impression of a NuBaID that represents a compact entity of two adjoining modules. As such, it differs notably from the BIR domains within, e.g., those human BIR proteins that possess more than one BIR domain, namely *Hs*BIRC1 to *Hs*BIRC4. In the latter, the BIR domains are predicted to either exhibit no inter-BIR domain contacts at all or only such that appear relatively loose, as specified further below.
(B3) Alignment of the three homologues' BLD1 and BLD2, plus some additional BLD-flanking sequence segments. The highlighting of the G-[WY] dipeptides, the C-$X_{(2)}$-C tetrapeptide, and the H-$X_{(3)}$-C pentapeptide is like in Figure 4B, while those residues highlighted in grey are the ones predicted potentially capable of inter-BLD contacts. Those contacts between the P-L dipeptide of each of the three homologues' BLD1 on the one hand and the aromatic residues positioned between the histidine and cysteine of the H-$X_{(3)}$-C pentapeptide of BLD2 on the other are accentuated by a connector line.

It is worth mentioning that the BLD1:BLD2 interface appears notably distinct from the few predicted BIR:BIR domain contacts within the four human BIRC proteins in which more than one BIR domain exists. In the case of *Hs*BIRC1 (https://alphafold.ebi.ac.uk/entry/Q13075), we found only a few contacts predicted to occur between the *Hs*BIRC1 protein's BIR1 and BIR2 domain, with these contacts notably dissimilar from those of the BLD1:BLD2 interface. In *Hs*BIRC2 and *Hs*BIRC3 (https://alphafold.ebi.ac.uk/entry/Q13490; https://alphafold.ebi.ac.uk/entry/Q13489), the BIR domains were predicted so far apart from each other that contact between them appeared unlikely. Merely for *Hs*BIRC4 (https://alphafold.ebi.ac.uk/entry/P98170) some likely contacts were predicted to occur between its BIR2 and BIR3 domain that involved (i) an aromatic residue located between the histidine and cysteine of the H-$X_{(6)}$-C

octapeptide of BIR3 and (ii) residues of an adjacent α-helix of BIR2. This BIR2 α-helix, though, is not equivalent to the orange-colored one of BLD1. This latter BLD1 α-helix is equivalent instead to yet another α-helix of the BIR domains, as described further below, where this other BIR domain α-helix is then also shown as orange-colored (Supplemental Figure S11E). Note also that the BLD1:BLD2 interface does not overlap with the IBM-reminiscent groove of the human BLD1 (see later Supplemental Figure S11D), with this particular groove located on the BLD1 surface side opposite to the one contributing to the BLD1:BLD2 interface.

(C) The positioning of the evolutionarily conserved aromatic residues flanking the zinc ion coordination spheres of BLD1 and BLD2.

(C1) Structures predicted for central regions of the BLD1 and BLD2 modules of *Hs*ZC3HC1 and *Sc*Pml39p. The outer boundaries of the here shown part of BLD1 are S74 and G168 for *Hs*ZC3HC1 and D82 and Y189 for *Sc*Pml39p. The outer boundaries of the BLD2 part shown here correspond to P175 and S472 of *Hs*ZC3HC1 and S192 and D312 of *Sc*Pml39p. The major loop-like insertion (E288 to S417) and a minor loop (I434 to E455) of the human homologue's BLD2 have been blanked out, as in Figure 6C. Side chains are shown for those histidines (highlighted in blue) and cysteines (green) that are engaged in the likely zinc ion coordination and for the flanking tryptophans' or tyrosines' side chains (highlighted in magenta). These aromatic residues are W107, W158, W256, and W431 in *Hs*ZC3HC1 and W119, W178, Y257, and Y294 in *Sc*Pml39p. Note that the tryptophans' indole and the tyrosines' phenol rings are predicted to be similarly positioned relative to the histidines' imidazole ring and the center of the zinc ion coordination spheres.

(C2) Residues flanking the zinc coordination spheres of both homologues' two BLDs, shown at higher magnification with side chains colored as in S10C1. Note that the *Hs*ZC3HC1 residues W107 and W256 and the *Sc*Pml39p residues W119 and Y257, which we had found crucial for NE-association and TPR/Mlp-binding (Figures 2 and 4; Supplemental Figures S2 and S6), appear to be involved in protecting and shielding the histidines of the zinc ion coordination spheres, with the histidines' and cysteines' side chains again shown as well. In addition, we found the now-emerging role of two *Hs*ZC3HC1 NuBaID signature residues, W158 and W431, and the corresponding ones from *Sc*Pml39p, namely W178 and Y294, of particular interest. In our single aa substitution experiments, the loss of the tryptophan's indole ring at such a position had been found to still allow for the mutant proteins' NE-association in ZC3HC1 KO cells and impaired binding to TPR (Figure 2; Supplemental Figure S2). Now, AlphaFold2's structure predictions indicate that these residues, while also located within the BLDs' central regions, do not appear to be engaging in such types of BLD core-stabilizing intramolecular interactions

with other side chains that one would instantaneously regard as being essential. In other words, these particular residues appear less required than others for maintaining the structural integrity of the BLDs' core structures. While the indole ring of both W158 and W431, and correspondingly the W178 indole and Y294 phenol ring of *Sc*Pml39p, do appear to be in contact with an evolutionarily conserved arginine of a particular α-helix occurring in both BLD1 and BLD2 (see later Supplemental Figure S11F and S11G), such contacts rather provide the impression of primarily keeping the aromatic residues in place. There, they appear to occupy, like a lid, a hollow space at the "entrance" to the zinc coordination sphere in a manner that would shield this entrance, suggesting that the function of these residues might be the seemingly less crucial protection of the coordinated zinc ion from water.

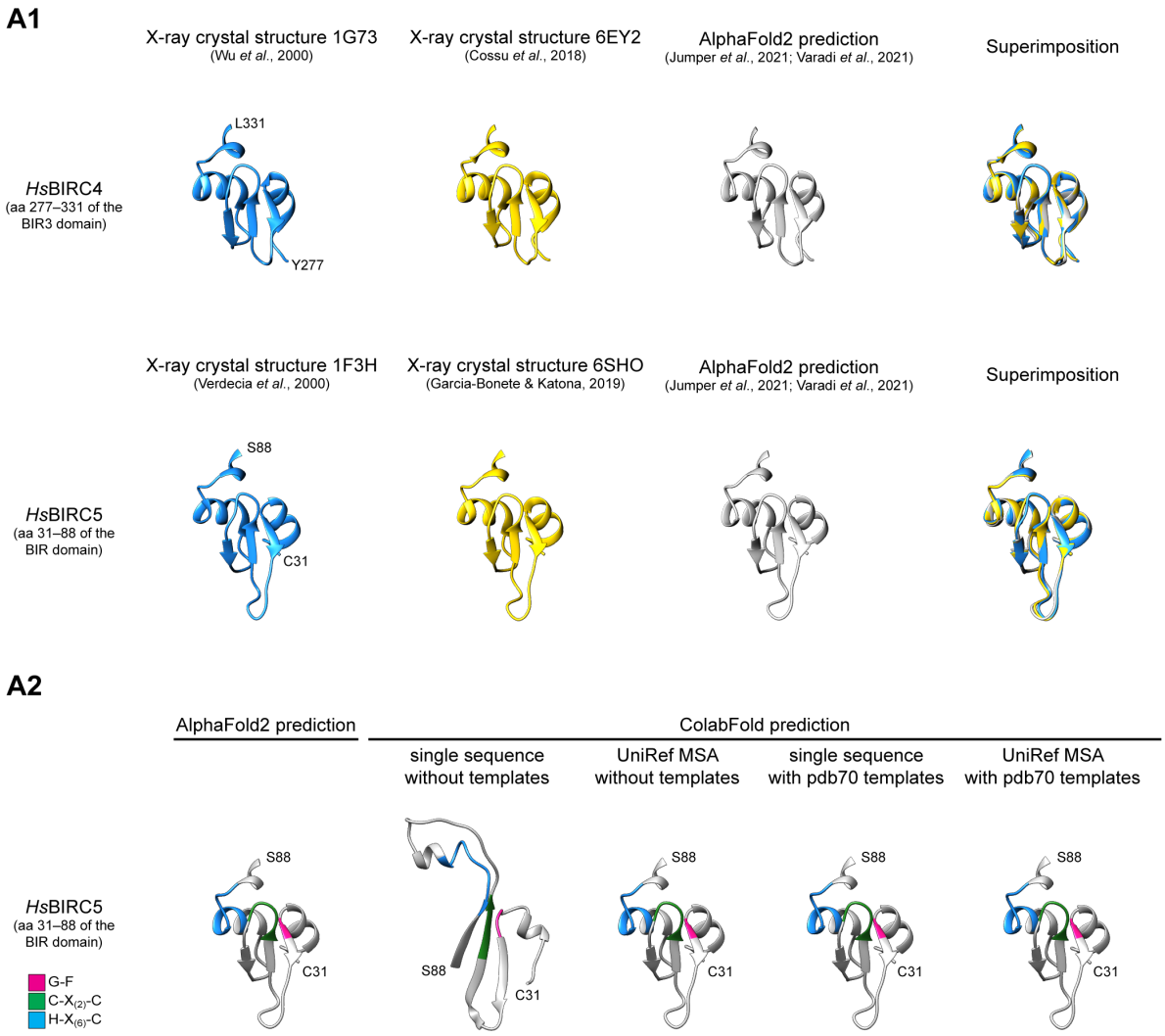
A1
X-ray crystal structure 1G73
(Wu et al., 2000)
X-ray crystal structure 6EY2
(Cossu et al., 2018)
AlphaFold2 prediction
(Jumper et al., 2021; Varadi et al., 2021)
Superimposition
HsBIRC4
(aa 277–331 of the
BIR3 domain)
L331
Y277
X-ray crystal structure 1F3H
(Verdecia et al., 2000)
X-ray crystal structure 6SHO
(Garcia-Bonete & Katona, 2019)
AlphaFold2 prediction
(Jumper et al., 2021; Varadi et al., 2021)
Superimposition
HsBIRC5
(aa 31–88 of the
BIR domain)
S88
C31
A2
AlphaFold2 prediction
ColabFold prediction
single sequence
without templates
UniRef MSA
without templates
single sequence
with pdb70 templates
UniRef MSA
with pdb70 templates
HsBIRC5
(aa 31–88 of the
BIR domain)
G-F
C-X(2)-C
H-X(6)-C
S88
C31

S11 (1/7)

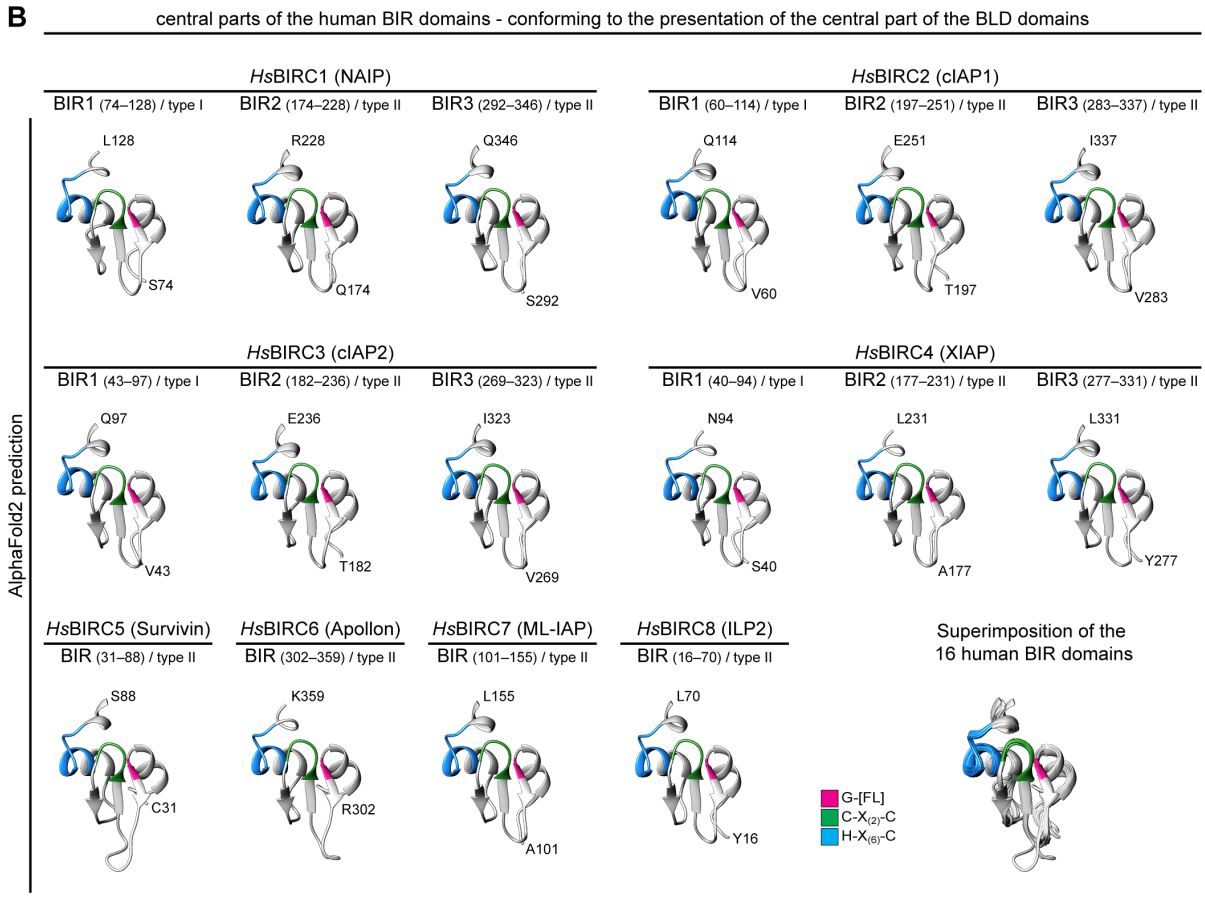
B
central parts of the human BIR domains - conforming to the presentation of the central part of the BLD domains
AlphaFold2 prediction
HsBIRC1 (NAIP)
BIR1 (74–128) / type I
BIR2 (174–228) / type II
BIR3 (292–346) / type II
L128
S74
R228
Q174
Q346
S292
HsBIRC2 (cIAP1)
BIR1 (60–114) / type I
BIR2 (197–251) / type II
BIR3 (283–337) / type II
Q114
V60
E251
T197
I337
V283
HsBIRC3 (cIAP2)
BIR1 (43–97) / type I
BIR2 (182–236) / type II
BIR3 (269–323) / type II
Q97
V43
E236
T182
I323
V269
HsBIRC4 (XIAP)
BIR1 (40–94) / type I
BIR2 (177–231) / type II
BIR3 (277–331) / type II
N94
S40
L231
A177
L331
Y277
HsBIRC5 (Survivin)
BIR (31–88) / type II
S88
C31
HsBIRC6 (Apollon)
BIR (302–359) / type II
K359
R302
HsBIRC7 (ML-IAP)
BIR (101–155) / type II
L155
A101
HsBIRC8 (ILP2)
BIR (16–70) / type II
L70
Y16
G-[FL]
C-X(2)-C
H-X(6)-C
Superimposition of the
16 human BIR domains

S11 (2/7)

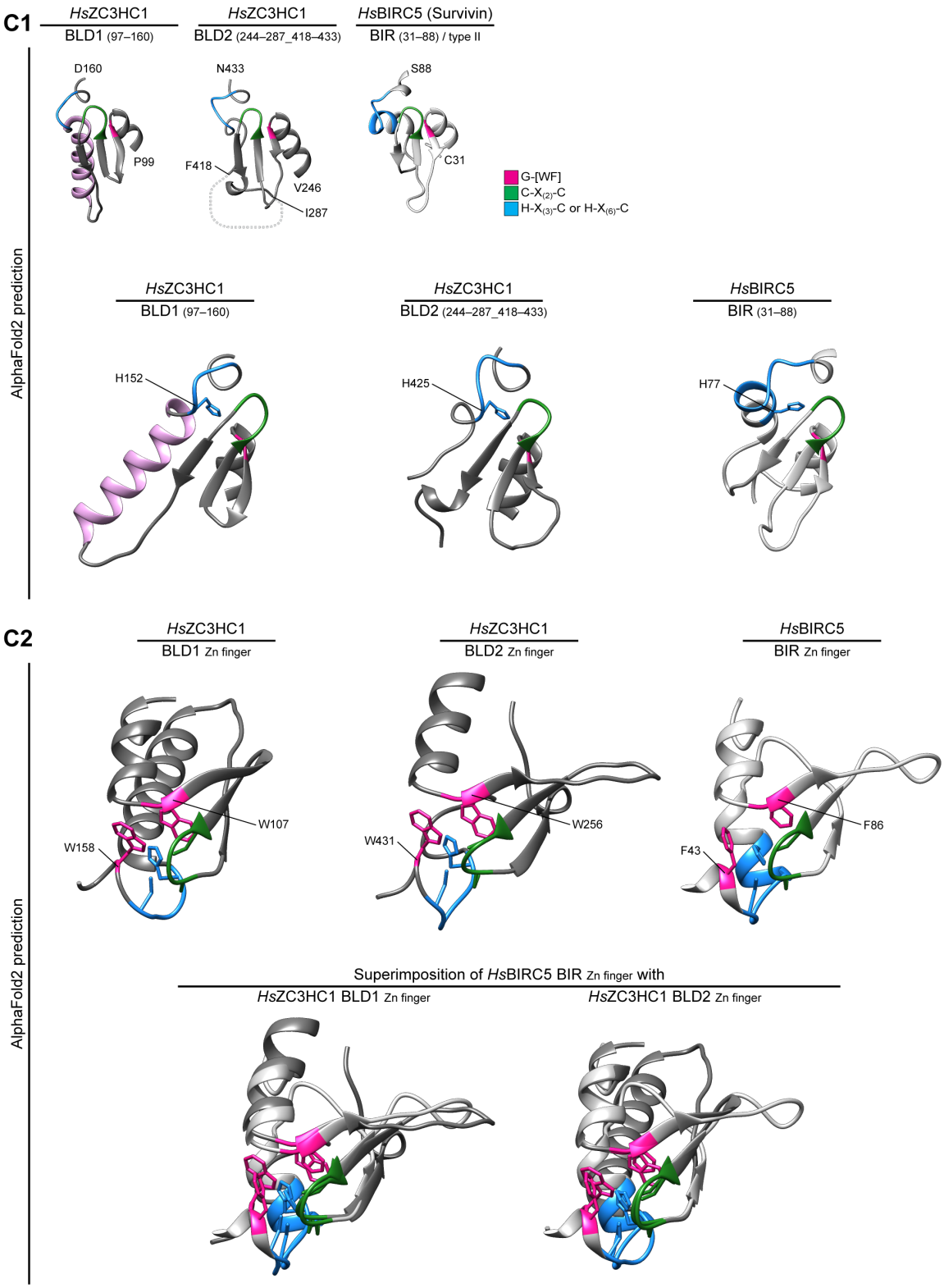
C1
HsZC3HC1
BLD1 (97–160)
HsZC3HC1
BLD2 (244–287_418–433)
HsBIRC5 (Survivin)
BIR (31–88) / type II
D160
P99
N433
F418
V246
I287
S88
C31
G-[WF]
C-X(2)-C
H-X(3)-C or H-X(6)-C
AlphaFold2 prediction
HsZC3HC1
BLD1 (97–160)
HsZC3HC1
BLD2 (244–287_418–433)
HsBIRC5
BIR (31–88)
H152
H425
H77
C2
HsZC3HC1
BLD1 Zn finger
HsZC3HC1
BLD2 Zn finger
HsBIRC5
BIR Zn finger
W107
W158
W256
W431
F86
F43
AlphaFold2 prediction
Superimposition of HsBIRC5 BIR Zn finger with
HsZC3HC1 BLD1 Zn finger
HsZC3HC1 BLD2 Zn finger

S11 (3/7)

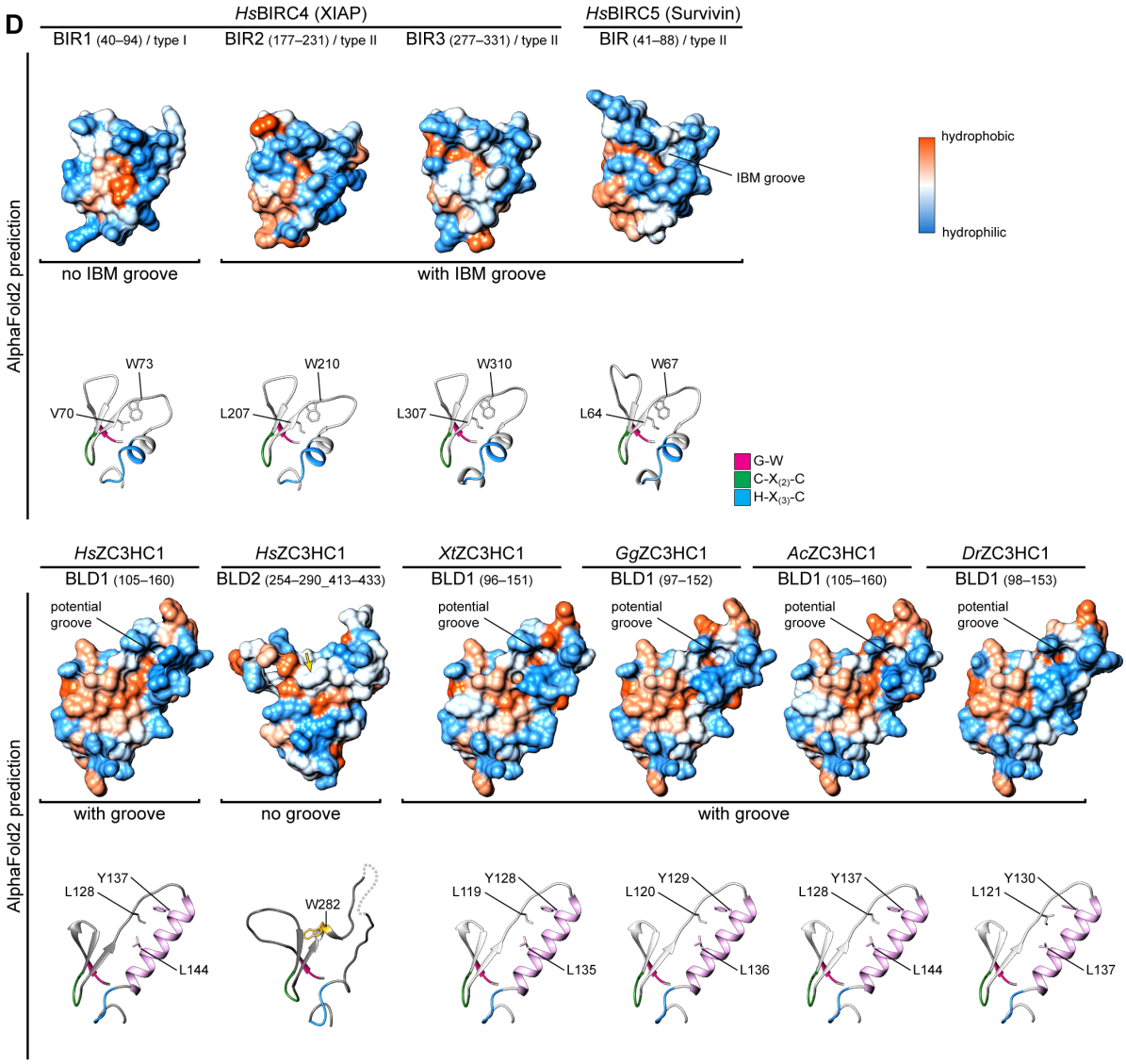
D
HsBIRC4 (XIAP)
HsBIRC5 (Survivin)
BIR1 (40–94) / type I
BIR2 (177–231) / type II
BIR3 (277–331) / type II
BIR (41–88) / type II
AlphaFold2 prediction
IBM groove
hydrophobic
hydrophilic
no IBM groove
with IBM groove
W73
V70
W210
L207
W310
L307
W67
L64
G-W
C-X(2)-C
H-X(3)-C
HsZC3HC1
BLD1 (105–160)
HsZC3HC1
BLD2 (254–290_413–433)
XtZC3HC1
BLD1 (96–151)
GgZC3HC1
BLD1 (97–152)
AcZC3HC1
BLD1 (105–160)
DrZC3HC1
BLD1 (98–153)
potential groove
with groove
no groove
with groove
Y137
L128
L144
W282
Y128
L119
L135
Y129
L120
L136
Y137
L128
L144
Y130
L121
L137

S11 (4/7)

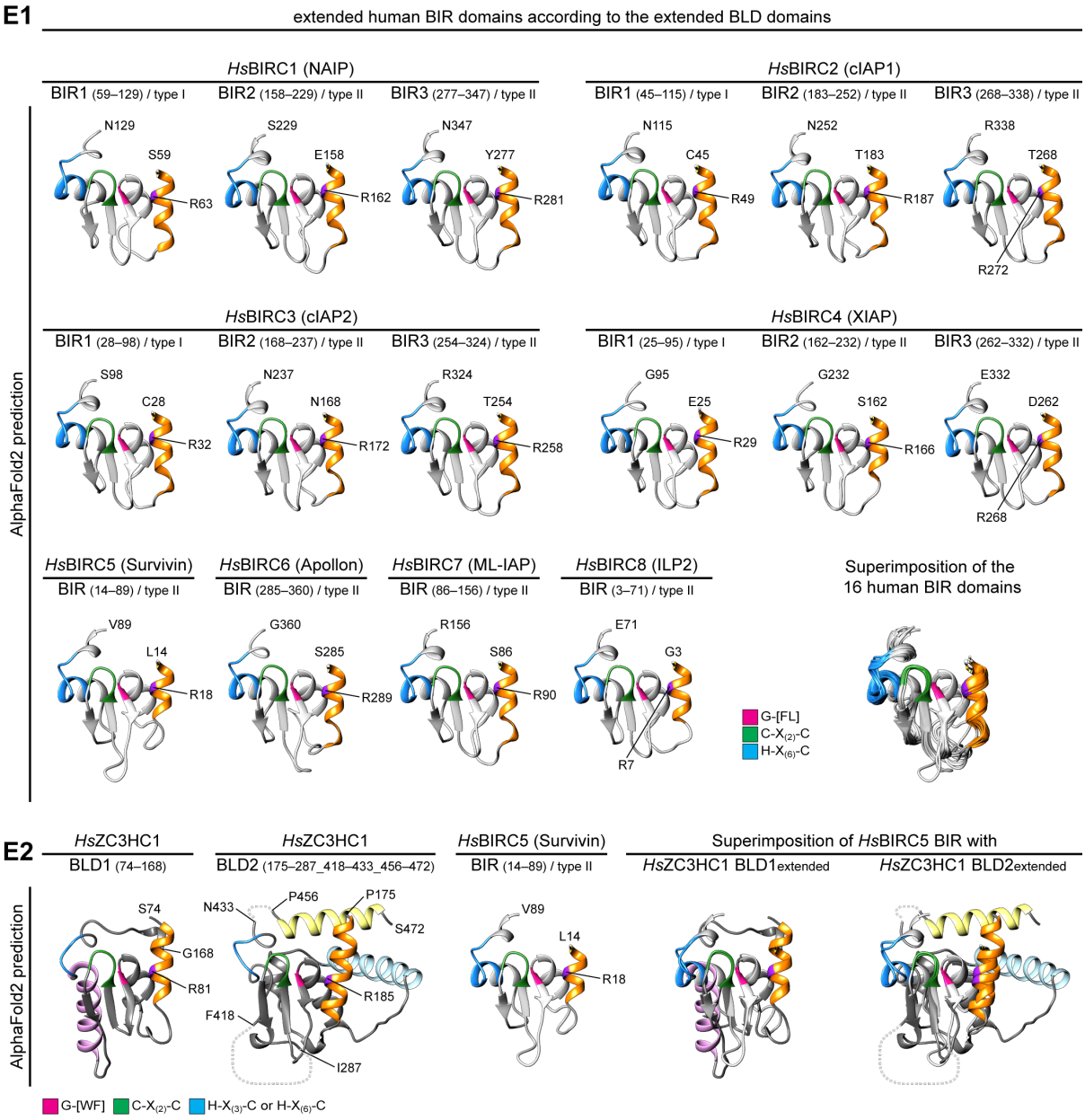
E1
extended human BIR domains according to the extended BLD domains
AlphaFold2 prediction
HsBIRC1 (NAIP)
BIR1 (59–129) / type I
BIR2 (158–229) / type II
BIR3 (277–347) / type II
N129
S59
R63
S229
E158
R162
N347
Y277
R281
HsBIRC2 (cIAP1)
BIR1 (45–115) / type I
BIR2 (183–252) / type II
BIR3 (268–338) / type II
N115
C45
R49
N252
T183
R187
R338
T268
R272
HsBIRC3 (cIAP2)
BIR1 (28–98) / type I
BIR2 (168–237) / type II
BIR3 (254–324) / type II
S98
C28
R32
N237
N168
R172
R324
T254
R258
HsBIRC4 (XIAP)
BIR1 (25–95) / type I
BIR2 (162–232) / type II
BIR3 (262–332) / type II
G95
E25
R29
G232
S162
R166
E332
D262
R268
HsBIRC5 (Survivin)
BIR (14–89) / type II
V89
L14
R18
HsBIRC6 (Apollon)
BIR (285–360) / type II
G360
S285
R289
HsBIRC7 (ML-IAP)
BIR (86–156) / type II
R156
S86
R90
HsBIRC8 (ILP2)
BIR (3–71) / type II
E71
G3
R7
G-[FL]
C-X(2)-C
H-X(6)-C
Superimposition of the
16 human BIR domains
E2
AlphaFold2 prediction
HsZC3HC1
BLD1 (74–168)
S74
G168
R81
HsZC3HC1
BLD2 (175–287_418–433_456–472)
N433
P456
P175
S472
R185
F418
I287
HsBIRC5 (Survivin)
BIR (14–89) / type II
V89
L14
R18
Superimposition of HsBIRC5 BIR with
HsZC3HC1 BLD1extended
HsZC3HC1 BLD2extended
G-[WF]
C-X(2)-C
H-X(3)-C or H-X(6)-C

S11 (5/7)

F

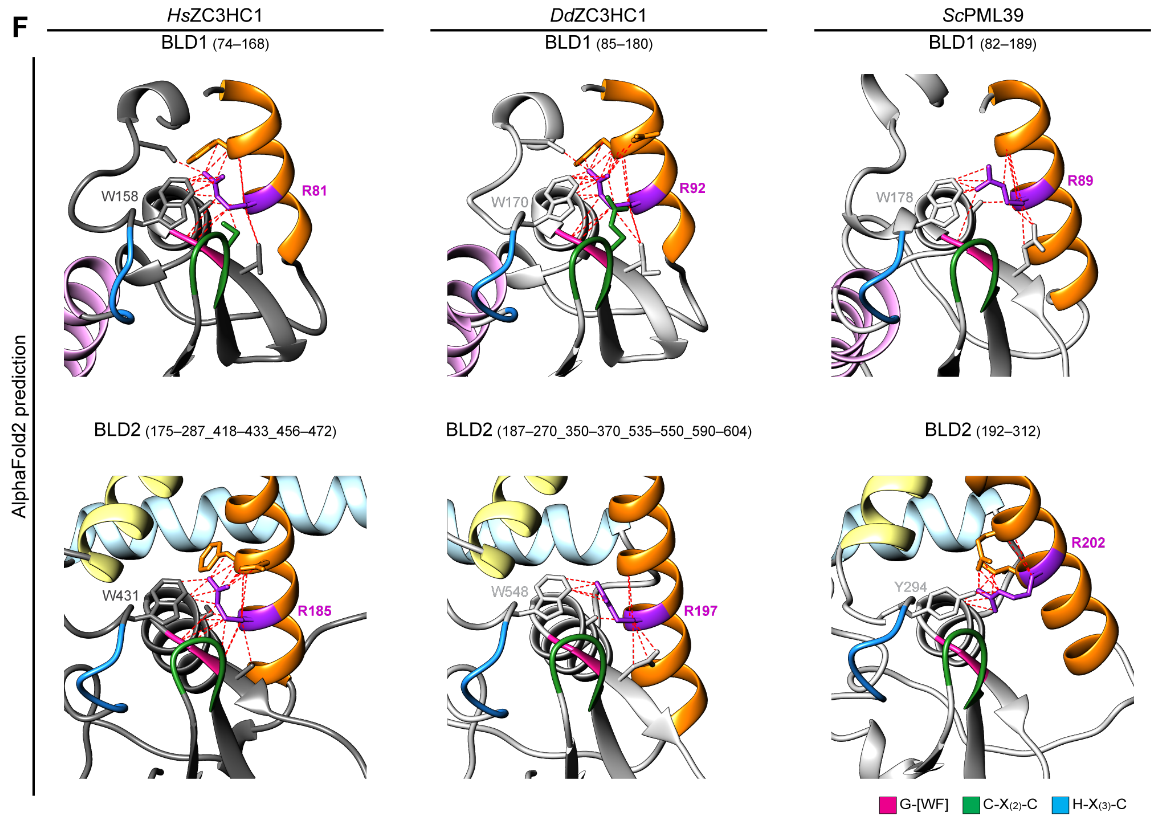

G

BIR domains (Pfam)

```
HsBIRC1_BIR1    59  SEAKRLKTFVTYEPYS---SWIPQEMAAAGFYFT-----GVKSGIQCFCCSLI--------------------LFGAGLTR------LPIEDHKRFHPDCGFLLN 129
HsBIRC1_BIR2   158  EEEARLASFRNWPFYV--QGISPCVLSEAGFVFT-----GKQDTVQCFSCGGC--------------------LGNWEEGD------DPWKEHAKWFPKCEFLRS 229
HsBIRC1_BIR3   277  YEELRLDSFKDWPRES---AVGVAALAKAGLFYT-----GIKDIVQCFSCGGC--------------------LEKWQEGD------DPLDDHTRCFPNCPFLQN 347
HsBIRC2_BIR1    45  CELYRMSTYSTFPAGV---PVSERSLARAGFYYT-----GVNDKVKCFCCGLM--------------------LDNWKLGD------SPIQKHKQLYPSCSFIQN 115
HsBIRC2_BIR2   183  TEEARFLTYHMWPL-T---FLSPSELARAGFYYI-----GPGDRVACFACGGK--------------------LSNWEPKD------DAMSEHRRHFPNCPFLEN 252
HsBIRC2_BIR3   268  THAARMRTFMYWPSSV---PVQPEQLASAGFYYV-----GRNDDVKCFCCDGG--------------------LRCWESGD------DPWVEHAKWFPRCEFLIR 338
HsBIRC3_BIR1    28  CELYRMSTYSTFPAGV---PVSERSLARAGFYYT-----GVNDKVKCFCCGLM--------------------LDNWKRGD------SPTEKHKKLYPSCRFVQS  98
HsBIRC3_BIR2   168  NENARLLTFQTWPL-T---FLSPTDLAKAGFYYI-----GPGDRVACFACGGK--------------------LSNWEPKD------NAMSEHLRHFPKCPFIEN 237
HsBIRC3_BIR3   254  THAARFKTFFNWPSSV---LVNPEQLASAGFYYV-----GNSDDVKCFCCDGG--------------------LRCWESGD------DPWVQHAKWFPRCEYLIR 324
HsBIRC4_BIR1    25  EEFNRLKTFANFPSGS---PVSASTLARAGFLYT-----GEGDTVRCFSCHAA--------------------VDRWQYGD------SAVGRHRKVSPNCRFING  95
HsBIRC4_BIR2   162  SEAARLKSFQNWPDYA---HLTPRELASAGLYYT-----GIGDQVQCFCCGGK--------------------LKNWEPCD------RAWSEHRRHFPNCFFVLG 232
HsBIRC4_BIR3   262  DYEARIFTFGTWIYSV-----NKEQLARAGFYAL-----GEGDKVKCFHCGGG--------------------LTDWKPSE------DPWEQHAKWYPGCKYLLE 332
HsBIRC5_BIR     14  LKDHRISTFKNWPFLE-GCACTPERMAEAGFIHCP--TENEPDLAQCFFCFKE--------------------LEGWEPDD------DPIEEHKKHSSGCAFLSV  89
HsBIRC6_BIR    285  SEANRRETFTSWPHVG-YRWAQPDPMAQAGFYHQP--ASSGDDRAMCFTCSVC--------------------LVCWEPTD------EPWSEHERHSPNCPFVKG 360
HsBIRC7_BIR     86  SEELRLASFYDWPLTA---EVPPELLAAAGFFHT-----GHQDKVRCFFCYGG--------------------LQSWKRGD------DPWTEHAKWFPSCQFLLR 156
HsBIRC8_BIR      3  GYEARLITFGTWMYSV-----NKEQLARAGFYAI-----GQEDKVQCFHCGGG--------------------LANWKPKE------DPWEQHAKWYPGCKYLLE  71
```

BLD domains

```
HsZC3HC1_BLD1   77  AFFSRVETFSSLKWAGKPFELSPLVCAKYGWVTVE------CDMLKCSSCQAFLCASLQPAFD----------FDRYKQRCAELKKAL-CTAHEKF---CFWPDS 161
HsZC3HC1_BLD2  181  EFLDRFQSLCHLDLQLPS(49)ACILSVCGWACSSSLESMQLSLITCSQCMRK--------------------VGLWGFQQ(132)FDPTSQHRDW---CPWVNI 434
ScPml39p_BLD1   85  ALLKRICSIQNYTRHV(7)WVNPLTLASKGWEPYQSASQSQVPF-KCCCCHAIMTIPLLKNGDDVADYTMKLNEKIWNSNI--------IGNHLQK---CPWREN 181
ScPml39p_BLD2  198  REIERIHTEIDRIVSGS(33)SLVGLLLLGYTKF-----QKDDLVQCTACFHR--------------------ASLKKLEY------TEFNGHALW---CRYYNK 297
DdZC3HC1_BLD1   88  DYYNRVRTYTISNWFAKPCEIDPLQCSRFGWINCE------ADMLECETCKKRLYYKVPSTFS----------QSLVNKRINDFSISLQSTGHRDN---CPWKDN 173
DdZC3HC1_BLD2  193  AYIKRSQNIYNNLTT(46)SKVSCLLALCGWDFNSI(79)-KSSVYCSYCQRL--------------------CGVWNFNK(166)FSPINEHRWF---CPWMIV 551
                        *  .                  *               *  *                                               *     * :
                        R                     GW              C  C                                               H     C W
                                               Y                                                                         Y
                                               F                                                                         F
                                               L
```

S11 (6/7)

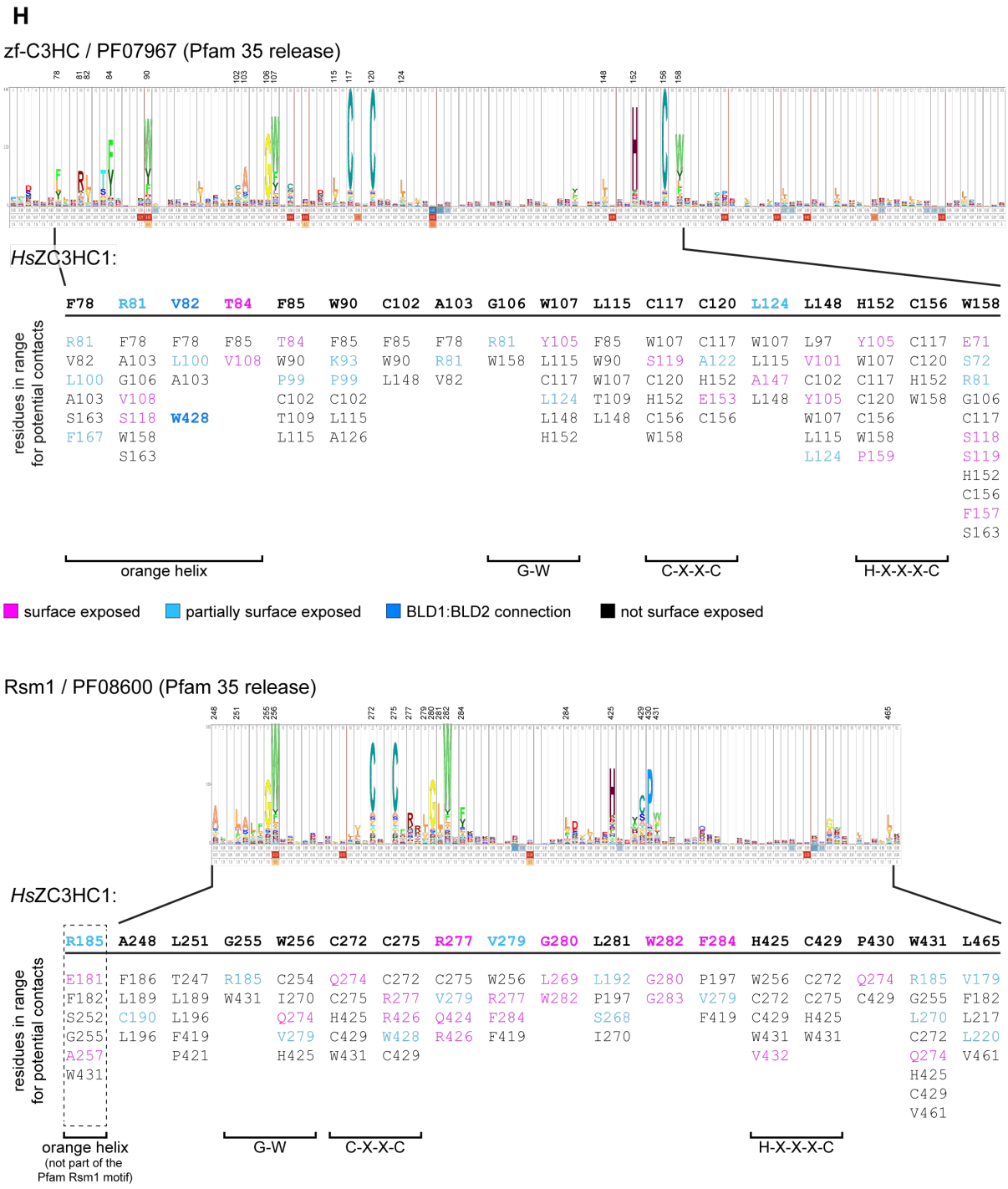

Supplemental Figure S11. Comparing the predicted structural characteristics and sequence features of the BLDs of ZC3HC1 with the BIR domains' structures and sequences.

Altogether, the structural features of the BLDs' central parts, as predicted by AlphaFold2, turned out similar to those characterizing the BIR domains of the IAPs, the latter exemplified further below by the eight BIR domain-containing proteins in humans. However, despite structural similarities common to both BIR domains and BLDs, all of the BIR domains

nonetheless turned out structurally more similar among themselves than the ZC3HC1 homologues' BLD1 and BLD2 domains compared to each other. While both BIR domains and BLDs share several essentially identical structural elements, as will be illustrated in the following, it is also apparent, especially when regarding the newly defined entirety of each of the two BLDs, that each one also exhibits its unique characteristics, distinguishing one from the other and both from the related BIR domains.

We, humans, possess a total of 16 different BIR domains, of which four belong to the so-called type I and twelve to the type II of BIR domains (e.g., Oberoi-Khanuja *et al*, 2013). Such type I and II BIR domains exhibit some differences, like a binding groove of physiological relevance that exists in the type II BIR domains while absent in type I (e.g., Cossu et al, 2019, and see further below). However, apart from such a few relatively minor structural differences, the overall construction of all these 16 BIR domains, particularly the construction of their zinc coordination spheres, was already known to be highly similar to each other (e.g., Cossu *et al*, 2019). In the following, such similarity is now illustrated by these BIR domains' AlphaFold2-predicted structures, presented in S11B and S11E. Furthermore, the close similarity between some exemplary BIR domain structures, as determined by X-ray crystallography and predicted by AlphaFold2, is shown in S11A1. In addition, S11A2 shows a representative comparison of a BIR domain, as present in the AlphaFold2 database, with the same domain's structures predicted via the ColabFold platform, having used either only this domain's sequence alone or an UniRef MSA, with and without additional consideration of PDB70 templates, as outlined in Supplemental Figure S9. The rationale for this approach, namely assessing the contributions of the sequence database search-derived MSAs, on the one hand, and the PDB-deposited structures as templates, on the other, to the computationally predicted BIR domains' structures, has been described further above (Supplemental Information 6 and Supplemental Figure S9).

In line with the former proposal that the BIR domain of human survivin/BIRC5 and the BLD1 of *Hs*ZC3HC1 are most likely to be structurally very similar (Higashi *et al*, 2005), the outcome of the here-presented comparisons of the AlphaFold2/ColabFold-predicted structures illustrates that the BIR domains' structural elements, and their arrangements relative to each other, resemble the BLDs' corresponding parts. In the following, in S11C, this is exemplified by the comparison of the two AlphaFold2-predicted structures of the *Hs*ZC3HC1 BLDs' central parts with those of the three BIR domains of *Hs*XIAP/BIRC4 and the single one of *Hs*BIRC5.

Furthermore, the predictions of the BLDs' structures by Alphafold2 allowed for unveiling yet other features shared by the one or other BLD with either the BIR type I or type II domain beyond the similarities of their central, zinc ion coordination spheres. Among such features are,

e.g., a conspicuous groove in the vertebrate homologues' BLD1, located on the side opposite the abovementioned BLD1:BLD2 interface with its hydrophobic residues. This groove appears akin to the so-called IAP binding motif (IBM) peptide-binding groove that characterizes the type II BIR domain, where it functions as a binding site for IAP antagonists (e.g., Cossu *et al*, 2019). On the other hand, such a groove is absent from the type I BIR domains, and we found it to appear similarly absent, altered, or masked in the ZC3HC1 homologues' BLD2. In the latter, a few surface-exposed protruding residues, evolutionarily relatively conserved, are predicted to be positioned at the IBM and BLD1 groove-corresponding positions instead. Of note, though, the BIR domains of type II nonetheless share notable sequence similarities with the BLD2 at precisely those positions that correspond to the IBM groove, with a tryptophan forming the bottom of the BIR domains' IBM groove being equivalent to a tryptophan instead protruding from the BLD2 surface, here W282 of *Hs*ZC3HC1. S11D illustrates the grooves' absence and presence in the different BLD and BIR domains, thereby pointing to also some of the residues involved.

Then, comparing the other structural elements of the BLDs and BIR domains beyond the central parts focused on in S11C, we noted, apart from some apparent differences, also yet another evident similarity. Having identified the *Hs*ZC3HC1 α-helix aa 175–190 as a structural element of the BLD2 within its newly defined boundaries (e.g., Figure 6D), equivalent to a corresponding α-helix in the human BLD1, and the two latter as also correspondingly present in the amoebic and budding yeast homologue's BLDs (e.g., orange-colored α-helices in Figure 6C), we noted these to be potentially equivalent to an α-helix that represents an extension of the BIR domain at its N-terminus. Since part of this α-helix extends beyond the BIR domains' currently defined boundaries, we now propose redefining the BIR domain's N-terminal boundary accordingly. This additional structural similarity is illustrated in S11E, where these particular α-helices are again shown as orange-colored.

Of particular note, the orange-colored α-helices share an evolutionarily conserved arginine of apparently similar function. In the ZC3HC1 homologues, this arginine appears to be involved in stabilizing the position of its α-helix relative to the BLD's more central parts. Moreover, the same arginine is also predicted to contribute to additionally stabilizing the position of one of those aromatic residues we had already studied in our single aa substitution experiments. These potential intra-BLD contacts that this particular arginine might be capable of are illustrated in S11F.

Furthermore, based on such structural similarities and our reinspection of the BLD and BIR domains' sequences, we present the corresponding sequence alignments in S11G. For such

alignments, we had considered the newly defined BLD boundaries and the orange-colored α-helices now rated as equivalent, which in turn allowed for revealing the additional sequence similarity we regard as noteworthy.

Finally, regarding those residues of the zf-C3HC and Rsm1 motifs that appear evolutionarily most conserved, according to current Pfam release 35.0 information, we present the corresponding HMM logos and these residues' positions relative to the BLDs' central parts and surfaces in S11H, thereby allowing to assess which of these residues are more likely to permit intra-BLD and inter-BLD contacts or such between a BLD and other proteins.

(A) Comparison of representative BIR domains' crystal structures with structures predictable by AlphaFold2 and ColabFold using default and altered parameter settings.

(A1) Comparison of the central parts of the structures of BIR3 of *Hs*BIRC4 and the single BIR domain of *Hs*BIRC5, as predicted by AlphaFold2, with the same domains' structural elements formerly determined as part of the *Hs*BIRC4 and *Hs*BIRC5 proteins by X-ray crystallography (Wu *et al*, 2000; Verdecia *et al*, 2000; Corti *et al*, 2018; Garcia-Bonete & Katona, 2019). For clarity, only the BIR domain segments aa 277–331 of *Hs*BIRC4 and aa 31–88 of *Hs*BIRC5 are shown for comparison, with the protein's other parts, including some side chains presented as parts of the PDB-deposited crystal structures, rendered invisible. As an aside, note that for these BIR domain examples, the Pfam database' BIR motif (https://pfam.xfam.org/family/BIR) comprises aa 268–331 for the BIR3 of *Hs*BIRC4 and aa 18–88 for *Hs*BIRHC5, with the here presented structures thus lacking several BIR signature residues at their N-terminus. The crystallographic data represent parts of the structures found with the identifiers 1G73, 6EY2, 1F3H, and 6SHO in the PDB database (https://www.rcsb.org). Superimposition of the structures was again achieved with Chimera's MatchMaker tool. Note that the close similarity between the structures determined by crystallography and the one predicted by AlphaFold2 appears evident.

(A2) Assessment of the contributions of the MSA, on the one hand, and the PDB database-deposited structures as templates, on the other, in BIR structure predictions by AlphaFold2 via ColabFold. The AlphaFold2-predicted structure of the *Hs*BIRC5 BIR domain is shown next to the structures predicted via the ColabFold platform, having used either only the BIR domain's sequence without further alignment with other sequences or having started the prediction from the UniRef MSA provided by ColabFold, with and without additional consideration of the PDB70 templates, which include the BIR domains' crystal structures. Note that using neither the MSA nor the template information resulted in a prediction that strongly deviates from the domain's actual structure. By contrast, predictions based either merely on the information

provided by the MSA or by the templates alone resulted in structures that appear highly similar, if not hardly distinguishable, from those initially determined by X-ray crystallography, as shown in S11A1.

(B) The AlphaFold2-predicted structures of the central parts of the sixteen BIR domains existing in humans, comprising the three BIR domains each of *Hs*BIRC1 (NAIP), *Hs*BIRC2 (cIAP1), *Hs*BIRC3 (cIAP2), and *Hs*BIRC4 (XIAP), and the only one single BIR domain-containing proteins *Hs*BIRC5 (Survivin), *Hs*BIRC6 (Apollon), *Hs*BIRC7 (ML-IAP), and *Hs*BIRC8 (ILP2). Note that all but one of the BIR domain structures were retrieved from the AlphaFold2 database (https://alphafold.ebi.ac.uk), except for *Hs*BIRC6, which was predicted via ColabFold. Further note that those parts of these structures that are actually shown correspond to the following parts of the Pfam database's BIR signature (Pfam release 35). For *Hs*BIRC1, aa 74–128 of 63–128 for BIR1, 174–228 of 162–228 for BIR2, and 292–346 of 281–346 for BIR3. For *Hs*BIRC2, 60–114 of 49–114 for BIR1, 197–251 of 187–251 for BIR2, and 283–337 of 272–337 for BIR3. For *Hs*BIRC3, 43–97 of 32–97 for BIR1, 182–236 of 172–236 for BIR2, and 269–323 of 258–323 for BIR3. For *Hs*BIRC4, 40–94 of 29–94 for BIR1, 177–231 of 166–231 for BIR2, and 277–331 of 268–331 for BIR3. For *Hs*BIRC5, 31–88 of 18–88; for *Hs*BIRC6, 302–359 of 289–359; for *Hs*BIRC7, 101–155 of 90–155; for *Hs*BIRC8, 16–70 of 7–70. These central parts of each BIR domain are presented individually and again superimposed onto each other, once again illustrating the domains' evident structural similarity.

(C) Comparison of the BIR domain of BIRC5 with the two BLDs of human ZC3HC1.

(C1) The AlphaFold2-predicted structures of the central parts of the two BLDs of *Hs*ZC3HC1, as identically presented in Figure 6A, and here compared with the corresponding central part of the representative BIR domain of *Hs*BIRC5. The structures are shown in two different magnifications and perspectives (upper and lower row), with the lower row also presenting the side chain of the histidine of the BLDs' H-$X_{(3)}$-C pentapeptide and the BIR domain's H-$X_{(6)}$-C octapeptide. Note the structural similarity of these domains' most central parts, including the anti-parallel arrangement of several β-sheets and one of the flanking α-helices, the latter here colored in grey, which corresponds to those α-helices that also are shown in grey in Figures 6C and 6D, among the BLDs' other α-helices there presented as colored. However, in addition to such similarities, a conspicuous difference is also evident, relating to the prominent α-helix of BLD1 that flanks the domain's central zinc coordination sphere on the other side. This α-helix, colored in light pink, as in Figure 6, cannot be regarded as likely equivalent to the BIR domain's short α-helix here partially colored in blue, with this blue-colored part reflecting the H-$X_{(6)}$-C. This octapeptide's histidine is positioned in the middle of this short α-helix, in contrast to the

BLDs' zinc ion-coordinating histidines that locate beyond the BLDs' α-helix. Further note that additional BLD-specific α-helices distinguishing the one and other BLD from the BIR domains are presented in S11E.

(C2) Aromatic residues flanking the zinc coordination spheres of the two BLDs of *Hs*ZC3HC1, shown at higher magnification, compared to corresponding residues in the BIR domains, the latter here again exemplified by the one from *Hs*BIRC5. Note that the aromatic side chains W107, W158, W256, and W431 of *Hs*ZC3HC1 and F43 and F86 of *Hs*BIRC5, all highlighted in magenta, appear relatively similarly arranged to each other and the zinc ion-coordinating residues, with such equivalent positioning here also illustrated by superimposition.

(D) Space-filling surface presentations of parts of the type I and type II BIR domains, here represented by those of *Hs*BIRC4 and *Hs*BIRC5, compared to surfaces of parts of the BLD1 and BLD2 of *Hs*ZC3HC1, next to the BLD1 domains of other vertebrates. The BIR domains' structures shown correspond to the following parts of the BIR signature. For *Hs*BIRC4, 40–94 of 29–94 for BIR1, 177–231 of 166–231 for BIR2, and 277–331 of 268–331 for BIR3. For *Hs*BIRC5, 41–88 of 18–88. Surface coloring is according to hydrophobicity, with hydrophobic residues in orange and hydrophilic in blue. For *Hs*BIRC5, the so-called IAP binding motif (IBM) peptide-binding groove is marked, the latter characterizing the type II BIR domain while absent from the type I BIR domains. Also marked is a conspicuous groove in the BLD1 of *Hs*ZC3HC1. Such a groove is also detectable in the BLD1 of the other vertebrate homologues**.** However, it is neither conspicuous in the BLD1 of *Dd*ZC3HC1 and *Sc*Pml39p nor evident in the BLD2 of *Hs*ZC3HC1 and the other vertebrates. In the latter, an evolutionarily relatively well-conserved group of residues (see also S11H), including a surface-exposed, protruding tryptophan, W282 in *Hs*ZC3HC1, here marked by a yellow arrow, which corresponds to W365 in *Dd*ZC3HC1 (not shown here), is predicted to be located at the BLD1 groove-corresponding position instead.

Tempting to regard it as playing a distinct role in the interaction with TPR homologues, such a tryptophan appears evolutionarily conserved in the majority of ZC3HC1 homologues and, as such, it is also part of the Rsm1 motif signature (see also Supplemental Figures S2D1 and S11H). Some homologues, though, exhibit another protruding residue at this position instead, like in *Sc*Pml39p, where this position appears occupied by K278 (not shown here).

The corresponding parts of the BLDs and BIR domains are also presented as ribbons to facilitate correlating the surfaces with the domains' secondary structures. For further orientation, the α-helix of the ZC3HC1 homologues' BLD1 is colored in light pink, corresponding to the coloring of this α-helix in, e.g., S11C1 and Figure 6. Moreover, those side

chains shown additionally as part of the ribbons are the W282 of the *Hs*ZC3HC1 BLD2 and those residues located at each groove's central bottom, which in the BLD1 and BIR domains' grooves represent a residue with an aromatic side chain. In the *Hs*ZC3HC1 BLD1, where residues between L128 and L144 form this groove, a tyrosine, Y137, is centrally positioned at the groove's bottom. Such a tyrosine at the corresponding position is evolutionarily conserved in all vertebrates. In the type II BIR domains, the IBM groove harbors a tryptophan at the groove's dip, for example, W67, in the case of BIRC5. Of note, in the BIR domains, this tryptophan is positioned at the same site relative to the C-$X_{(2)}$-C tetrapeptide as W282 is in the human ZC3HC1 BLD2 (e.g., S11G).

Furthermore, since the IBM grooves are known to interact with IAP antagonists like Smac/DIABLO (see Supplemental Discussion 1 for further information), we consider it noteworthy that minor amounts of Smac/DIABLO, beyond background levels, had been among those materials that we found co-sedimented with immunoprecipitated FP-tagged ZC3HC1 polypeptides (our unpublished data). However, whether this might also point to a naturally occurring interaction of physiological relevance still needs to be determined.

(E) The AlphaFold2-predicted structures of the two BLDs of *Hs*ZC3HC1 in their entirety, as identically presented in Figure 6C, and here compared with the human BIR domains, as defined by the Pfam database's BIR motif, with now additionally considered BIR motif-flanking aa residues, causing us to refer to these structures as the BIR domains' extended versions.

(E1) The AlphaFold2-predicted structures of the central parts of the sixteen BIR domains in humans, here now shown in the extended version. Note that the presented structures include additional residues flanking the BIR signature, the latter so far having started at its N-terminal side with an evolutionarily conserved arginine, here colored in purple. For *Hs*BIRC1, the predicted structure corresponds to aa 59–129 instead of 63–128 for only the BIR signature of BIR1. For BIR2, it is 158–229 instead of 162–228, and for BIR3, 277–347 instead of 281–346. For *Hs*BIRC2, it is 45–115 instead of 49–114 for BIR1, 183–252 instead of 187–251 for BIR2, and 268–338 instead of 272–337 for BIR3. For *Hs*BIRC3, it is 28–98 instead of 32–97 for BIR1, 168–237 instead of 172–236 for BIR2, and 254-324 instead of 258–323 for BIR3. For *Hs*BIRC4, it is 25–95 instead of 29–94 for BIR1, 162-232 instead of 166–231 for BIR2, and 262–332 of 268–331 for BIR3. For *Hs*BIRC5, it is 14–89 instead of 18–88; for *Hs*BIRC6, 285–360 instead of 289–359; for *Hs*BIRC7, 86–156 instead of 90–155; for *Hs*BIRC8, 3–71 instead of 7–70. These extended versions of each BIR domain are here presented individually and again superimposed onto each other, once again illustrating the domains' evident structural similarity. Note that the inclusion of additional aa residues at the N-terminal side of the BIR signature

allowed for a prominent α-helix (colored in orange) to become apparent in all of the BIR domains.

(E2) Comparison of the AlphaFold2-predicted structures of the *Hs*ZC3HC1 BLDs, as presented in Figure 6C and defined in Figure 6D, with the extended versions of the human BIR domains. Note that the orange-colored α-helix as part of both BLDs appears equivalent to the BIR domains' orange-colored α-helix (see S11E1), despite the latter being shorter than in the BLDs. Further note that this particular α-helix, positioned in the proximity of the BLDs' and BIR domains' G-[WF] dipeptide, possesses an arginine, again colored in purple, whose presence appears obligatory for both BLDs and as such equivalent to the BIR domains' arginine already highlighted in purple in S11E1. Here in S11E2, these arginines are represented by R81 in BLD1, R185 in BLD2, and R18 in BIRC5. Each of these BLD and BIR domains' arginine residues appears involved in stabilizing the position of the neighboring α-helix that leads over to the BLDs' and BIR domains' first β-sheet.

Beyond such similarity between the BLDs and BIR domains, further note, though, that both BLD1 and BLD2 also possess BLD-specific α-helices, present in the one BLD while absent from the other BLD and from the BIR domains. These α-helices include the light pink-colored one of BLD1 and the yellow- and light-blue-colored ones of BLD2. The functions of these single BLD-specific features will need to be dissected in future work. Such studies will also have to clarify which parts of the two BLDs engage in direct interactions with TPR as part of the ZC3HC1 protein's TPR-binding interface. Here, we already consider it conceivable that one or the other of each BLD's α-helices will have a penchant for parts of TPR's homodimeric coiled coils, as it will also be discussed from the TPR protein's viewpoint elsewhere (Gunkel *et al*, manuscript in preparation).

(F) The evolutionarily conserved arginines that are part of the orange-colored α-helices common to both BLDs are here shown enlarged and colored in purple. Other parts of the BLDs in these image sections are colored as in the preceding Figures. Chimera's structural analysis tool was used to compute and illustrate potential contacts between the conserved arginines' side chain atoms and neighboring residues. Several possible contacts, based on atom-to-atom distances being ≤ 4 Å, are depicted as dashed red lines. Note that among the residues predicted most likely involved in such intra-BLD contacts are the aromatic ones positioned two residues after each BLD's H-$X_{(3)}$-C pentapeptide (see also S11G). In the case of, e.g., *Hs*ZC3HC1, such intra-BLD residue contacts would be R81:W158 and R185:W431, with these aromatic residues also described in Supplemental Figure S10C, and corresponding ones here now shown also present in *Dd*ZC3Hc1 and *Sc*Pml39p. The contacts between one of these aromatic residues and

the arginine's side chain provide the impression of a "lid", represented by either the tryptophan's indole ring or the tyrosine's phenol ring, which the arginine appears to contribute to keeping in place (in this context, see also Supplemental Figure S10C2). Apart from that, some of these arginines also appear to engage in additional intra-BLD interactions that would keep the orange-colored α-helix in a distinct position relative to the BLD core, just like some other residues of this α-helix too (not shown here). Again other residues of this α-helix though, are predicted to contribute to the inter-BLD contacts of the BLD1:BLD2 interface described in Supplemental Figure S10B2. As an aside, also note that W158 and W431 of *Hs*ZC3HC1 were among the residues for which single aa substitutions were presented in the current study (see Supplemental Figure S2B). Further note that for the BIR domains, the predictions do not position their orange-colored-α-helix-positioned arginines in direct contact with those aromatic residues located two aa after each BIR domain's H-$X_{(6)}$-C octapeptide that would be the ones equivalent to those in the BLDs. Nonetheless, in this case, the predictions indicate an indirect, i.e., two-step contact via a phenylalanine residue positioned between the two cysteines of the BIR domain's C-$X_{(2)}$-C tetrapeptide (not shown here, but see S11G for further details).

(G) Multiple aa sequence alignment of the human BIR domain sequences with BLD sequences of *Hs*ZC3HC1, *Dd*ZC3HC1, and *Sc*Pml39p, having first used for such purpose Clustal Omega (https://www.ebi.ac.uk/Tools/msa/clustalo/), followed by some manual readjustments. While the BIR domain sequences comprise those defined by the Pfam database's BIR motif in their entirety, plus some additionally flanking aa residues, the BLD sequences lack a few residues close to those BLDs' boundaries defined in Figure 6D. The BIR domains' N-terminal α-helix, which has been shown orange-colored in S11E, is here schematically depicted next to the corresponding BIR sequences, with this meant to facilitate correlating parts of the aligned sequences with the structural elements presented. Note that the identification of the *Hs*ZC3HC1 α-helix located between aa 176–190 and its assignment to BLD2, where it would thus be equivalent to the α-helix of BLD1 comprising at least aa 75–83 (Figure 6C and 6D), was followed by relating these α-helices with the BIR domains' orange-colored one. The latter, in turn, allowed for unveiling the here highlighted arginine residue, as part of these α-helices, as another commonality of the BLD and BIR domains. More precisely, in the *Hs*ZC3HC1 BLD1, this arginine, R81, was already part of the Pfam database's zf-C3HC motif, just like R92 of *Dd*ZC3HC1. In addition, we now found such arginine evolutionarily conserved in *Sc*Pml39p too. Furthermore, we also found such an arginine at the corresponding position of the BLD2 domains, like, for example, the R185 as part of the BLD2 α-helix of *Hs*ZC3HC1. Such correspondence of R185 to R81 had escaped detection during all the alignments between

segments of primary ZC3HC1 sequences conducted till then. Subsequent comparison of the BLD and BIR domain structures allowed us to correlate these BLD1 and BLD2 arginines with the arginine at the corresponding position of the BIR domain, like, for example, at R18 of *Hs*BIRC5, where it was already part of the Pfam database's BIR motif. Therefore, we regarded these findings as further supporting our conclusion that the orange-colored α-helices of BLD1 and BLD2 could now be considered equivalent to a likewise positioned shorter α-helix of the BIR domains. Moreover, this finding provided further justification for our new definition of the N-terminal boundary of BLD2, as presented in Figure 6D. As an aside, though, we also need to mention that not all ZC3HC1 homologues harbor such an arginine equivalent to R81 of *Hs*ZC3HC1, with it being absent in a few organisms, like, for example, in C49H3.9, the ZC3HC1 homologue noted for *C. elegans* (Higashi *et al*, 2005; Gunkel *et al*, 2021) and some other roundworms, while again present in other nematodes (our unpublished data).

Furthermore, note that one of the connector lines, here colored in grey, marks the predicted direct contact between a BLD's orange-colored-α-helix-positioned arginine and an aromatic residue located two aa after the same BLD's H-$X_{(6)}$-C octapeptide. In the case of the BIR domains, two of such connector lines indicate an indirect contact between the BIR domains' corresponding residues via a phenylalanine residue that is part of the C-$X_{(2)}$-C tetrapeptide.
(H) HMM logos of the zf-C3HC and Rsm1 motifs, based on current seed sequences retrievable from the Pfam website. A selection of residues formerly (see Supplemental Figure S2D1) and currently regarded as evolutionarily relatively conserved are numbered corresponding to their position within the *Hs*ZC3HC1 protein sequence. Those conserved residues (bold lettering) that are predicted to be exposed and accessible on the surface of the BLDs are written in magenta, while those appearing only partially exposed outwardly are in light blue. By contrast, those conserved residues embedded within the BLDs are written in black. In addition, *Hs*ZC3HC1 Y82 and W428, the latter evolutionarily somewhat less well conserved while contributing to the BLD1:BLD2 interface, are written in dark blue. Those conserved residues that are part of the BLDs' G-[WYF] dipeptides, C-$X_{(2)}$-C tetrapeptides, and H-$X_{(3)}$-C pentapeptides, are marked by brackets, as are those residues that are part of both BLDs' orange-colored α-helix. Even though this particular α-helix is not yet part of a current Pfam Rsm1 motif, we here assign the evolutionarily conserved R185 of *Hs*ZC3HC1 to this motif's N-terminal side (hatched rectangle). Moreover, other *Hs*ZC3HC1 residues that could be in contact with the listed conserved residues' side chains are specified, having again used Chimera's structural analysis tool for computing potential contacts, based on atom-to-atom distances being ≤ 4 Å, between side chains only.

Note that only relatively few of the evolutionarily conserved residues are predicted to be exposed on the surface of either one or the other BLD. Most of these belong to a cluster of conserved residues that are part of Pfam's Rsm1 motif. These BLD2 residues are located between the C-X(2)-C tetrapeptide and the site where the additional, non-conserved sequence loops are commonly inserted into this BLD. W282, as one of these conserved residues, has already been described in S11D as exposed on the surface of the *Hs*ZC2HC1 BLD2. Of further note, these residues are located at the position corresponding to the IBM-like groove of the BLD1. These residues and their exposed side chains will need to be the topic of a study to be presented elsewhere.

The side chains of the majority of the other most conserved residues are predicted not to be exposed on the BLDs surface but located within the BLDs. These residues appear either projecting towards the abutting BLD or embedded within each BLD, where they contribute to intra-BLD arrangements. These zf-C3HC and Rsm1 motif residues are also part of the NuBaID signature's minimal versions, which in turn allows us to conclude that the current NuBaID signature residues are not likely to engage in intermolecular interactions and thus are unlikely to represent residues of the Mlp- and TPR-binding interfaces.

A1


HsZC3HC1
G-W
C-X(2)-C
H-X(3)-C
deleted parts
MAAPCEGQAFAVGVEKNWGAVVRSPEGTPQKIRQLIDEGIAPEEGGVDAK 50
DTSATSQSVNGSPQAEQPSLESTSKEAFFSRVETFSSLKWAGKPFELSPL 100
VCAKYGWVTVECDMLKCSSCQAFLCASLQPAFDFDRYKQRCAELKKALCT 150
AHEKFCFWPDSPSPDRFGMLPLDEPAILVSEFLDRFQSLCHLDLQLPSLR 200
PEDLKTMCLTEDKISLLLHLLEDELDHRTDERKTTIKLGSDIQVHVTACI 250
LSVCGWACSSSLESMQLSLITCSQCMRKVGLWGFQQIESSMTDLDASFGL 300
TSSPIPGLEGRPERLPLVPESPRRMMTRSQDATFSPGSEQAEKSPGPIVS 350
RTRSWDSSSPVDRPEPEAASPTTRTRPVTRSMGTGDTPGLEVPSSPLRKA 400
KRARLCSSSSDTSSRSFFDPTSQHRDWCPWVNITLGKESRENGGTEPDA 450
SAPAEPGWKAVLTILLAHKQSSQPAETDSMSLSEKSRKVFRIFRQWESLC 500
SC 502

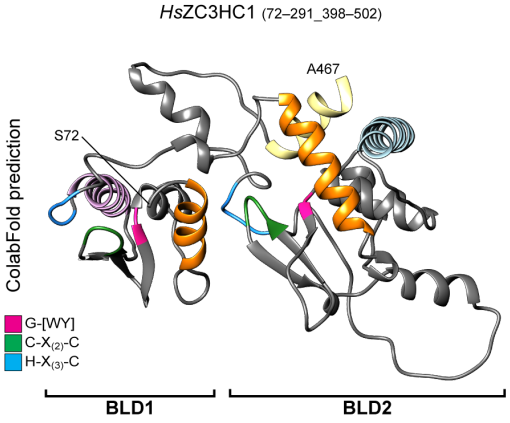
HsZC3HC1 (72–291_398–502)
A467
S72
ColabFold prediction
G-[WY]
C-X(2)-C
H-X(3)-C
BLD1
BLD2

A2

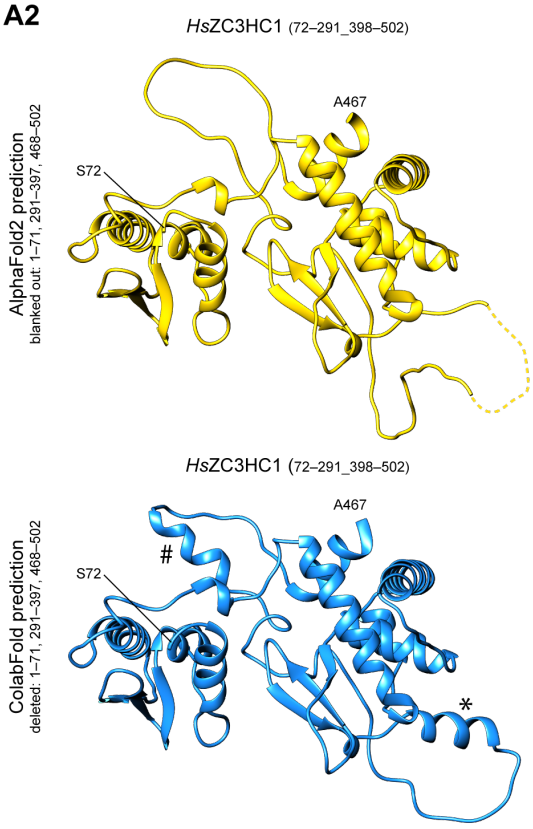
HsZC3HC1 (72–291_398–502)
AlphaFold2 prediction
blanked out: 1–71, 291–397, 468–502
A467
S72
HsZC3HC1 (72–291_398–502)
ColabFold prediction
deleted: 1–71, 291–397, 468–502
A467
S72
#
*

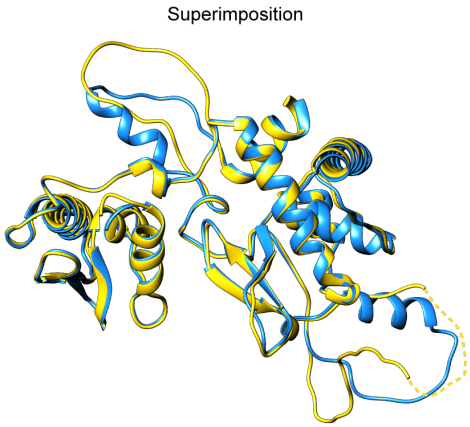
Superimposition

S12 (1/2)

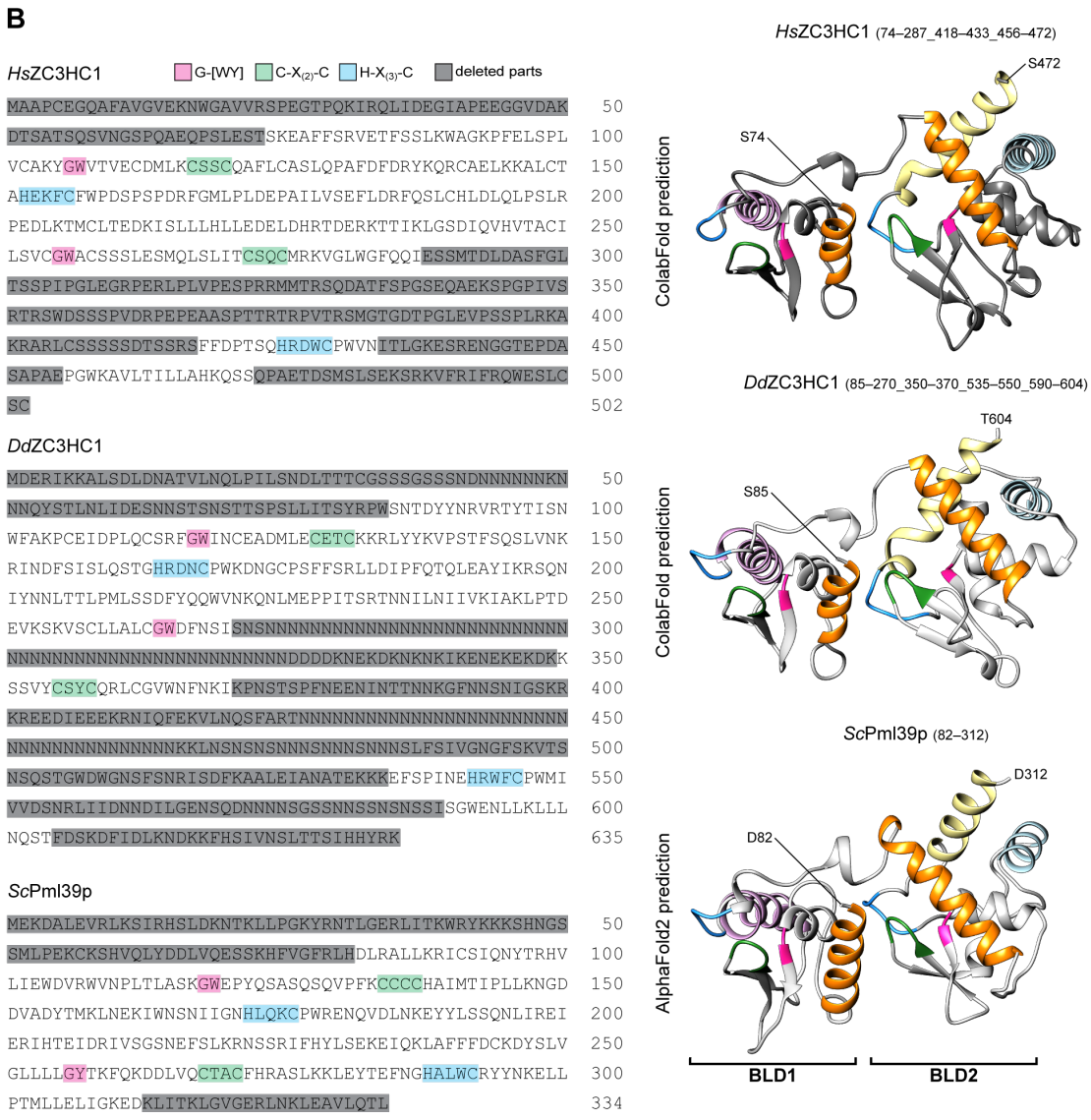

Supplemental Figure S12. *In vivo* and *in silico* deletion mutants of ZC3HC1 homologues and their tertiary structures predicted by AlphaFold2 via ColabFold.

The ColabFold platform allowed for the structure of the experimentally determined NB-binding-competent *Hs*ZC3HC1 deletion mutant 72–290_398–467 to be predicted by AlphaFold2, with this structure to be then compared with the intact protein's predicted structure. Furthermore, this corporal mutant's predicted structure was to be compared with the accordingly-predicted structures of ZC3HC1 deletion mutants we had created *in silico*.

(A1) The sequence of the still NB-binding-competent *Hs*ZC3HC1 deletion mutant 72–290_398–467 (Δ1–71_Δ291–397_Δ468–502) and the corresponding structure for this residual sequence as predicted by AlphaFold2 via ColabFold. Those regions highlighted in grey represent the residues removed by cloning and thus excluded also from this structure prediction. Residues highlighted in magenta, green, and blue again represent the positions of the two BLDs'

G-W, C-$X_{(2)}$-C, and H-$X_{(3)}$-C sequence elements. The coloring of the α-helices corresponds to the same helices' colors in Figure 6C and Supplemental Figures S9, S10, and S11. Note that the structure predicted for this mutant, comprising only 289 aa and mainly encompassing the two BLDs of *Hs*ZC3HC1, resembles a compact version of a ZC3HC1 homologue, reminiscent, e.g., of the central parts of *Sc*Pml39p with its two BLDs, with its second one lacking large sequence insertions. Such prediction further underscored the conclusion that the integrity of the two BLDs is essential and sufficient for the initial binding of *Hs*ZC3HC1 to the NB.

(A2) Comparison of the ColabFold-predicted structure of (i) the same *Hs*ZC3HC1 deletion mutant as shown in S12A1, yet here colored in blue, with (ii) the AlphaFold2-predicted structure (yellow) for the intact full-length *Hs*ZC3HC1, of which we blanked out those parts corresponding to those missing in the deletion mutant. Note that the minimal binding-competent mutant exhibits a high degree of structural similarity with the wild-type protein, except for two α-helices only predicted for the deletion mutant. One of these, marked by an asterisk, appears to result from having deleted most of the BLD2-inserted loop. The other α-helix, which is marked by a hash and would correspond to aa 436–434 of the wild-type protein, represents a prediction peculiarity, the latter only noted when predicting the structures of N-terminally deleted ZC3HC1 mutants via ColabFold but not when only C-terminal parts are missing.

(B) Sequences of *in silico*-created deletion mutants of *Hs*ZC3HC1, *Dd*ZC3HC1, and *Sc*Pml39p and the corresponding structures predicted by either AlphaFold2 or via ColabFold. The largely "loop-free" versions of each homologue here presented, primarily comprising the BLD-corresponding sequences according to the newly defined BLD boundaries, include a mutant, only 247 aa long, of *Hs*ZC3HC1 (74–287_418–433_456–472) and a 238 aa-long *Dd*ZC3HC1 mutant 85–270_350–370_535–550_590–604. In addition, the naturally "loop-less" *Sc*Pml39p, which here though lacks its N- and C-terminal parts, thus representing an *in silico* mutant of *Sc*Pml39p only comprising 231 aa (Δ1–81_Δ313–334), is shown for comparison. Note that all three deletion mutants represent polypeptides of about similar length. Further note, in particular, that despite the still relatively low end-to-end sequence identities between the three mutants' sequences (see below), their predicted structures appear once again very similar, with each homologue's two BLDs as separate yet closely abutting entities now particularly evident.

While such a finding was no longer unexpected, we regarded these structural similarities as nonetheless remarkable, given the homologues' low degree of sequence identity that still manifested itself after having aligned pairwise only these residual sequences representing the different homologues' redefined pairs of BLDs. In fact, some standard sequence alignment tools even then did not find any significant similarity between the residual 247 aa-long sequence of

*Hs*ZC3HC1 74–287_418–433_456–472 (Δ1–73_Δ288–417_Δ434–455_Δ473–502) and the residual 231 aa of *Sc*Pml39p 82–312 (Δ1–81_Δ313–334). We considered this finding to add to a plausible explanation (see also Supplemental Information 5) for the former reporting that a ZC3HC1 homologue had not been detectable in *S. cerevisiae* when data mining primary sequences (Higashi *et al*, 2005).

Again other tools aligned the residual *Hs*ZC3HC1 and *Sc*Pml39p sequences almost correctly, like the EMBOSS local alignment program Water (https://www.ebi.ac.uk/Tools/psa/emboss_water/) and the end-to-end global alignment tools Needle (https://www.ebi.ac.uk/Tools/psa/emboss_needle/) and GGSEARCH2SEQ (https://www.ebi.ac.uk/Tools/psa/ggsearch2seq/), but then only yielded end-to-end sequence identities of about 16.5–18.4%.

Moreover, even some of these mentioned tools did not allow for a proper pairwise alignment when attempting to match the residual 238 aa-long, largely "loop-free" and primarily BLD-corresponding sequence of *Dd*ZC3HC1 85–270_350–370_535–550_590–604 (Δ1–84_Δ271–349_Δ371–534_Δ551–589_Δ605–635) with that of Pml39p 82–312. Again others, like the GGSEARCH2SEQ program, provided an almost correct alignment of the two homologues' NuBaID signatures but with an end-to-end sequence identity again of only 17.3%.

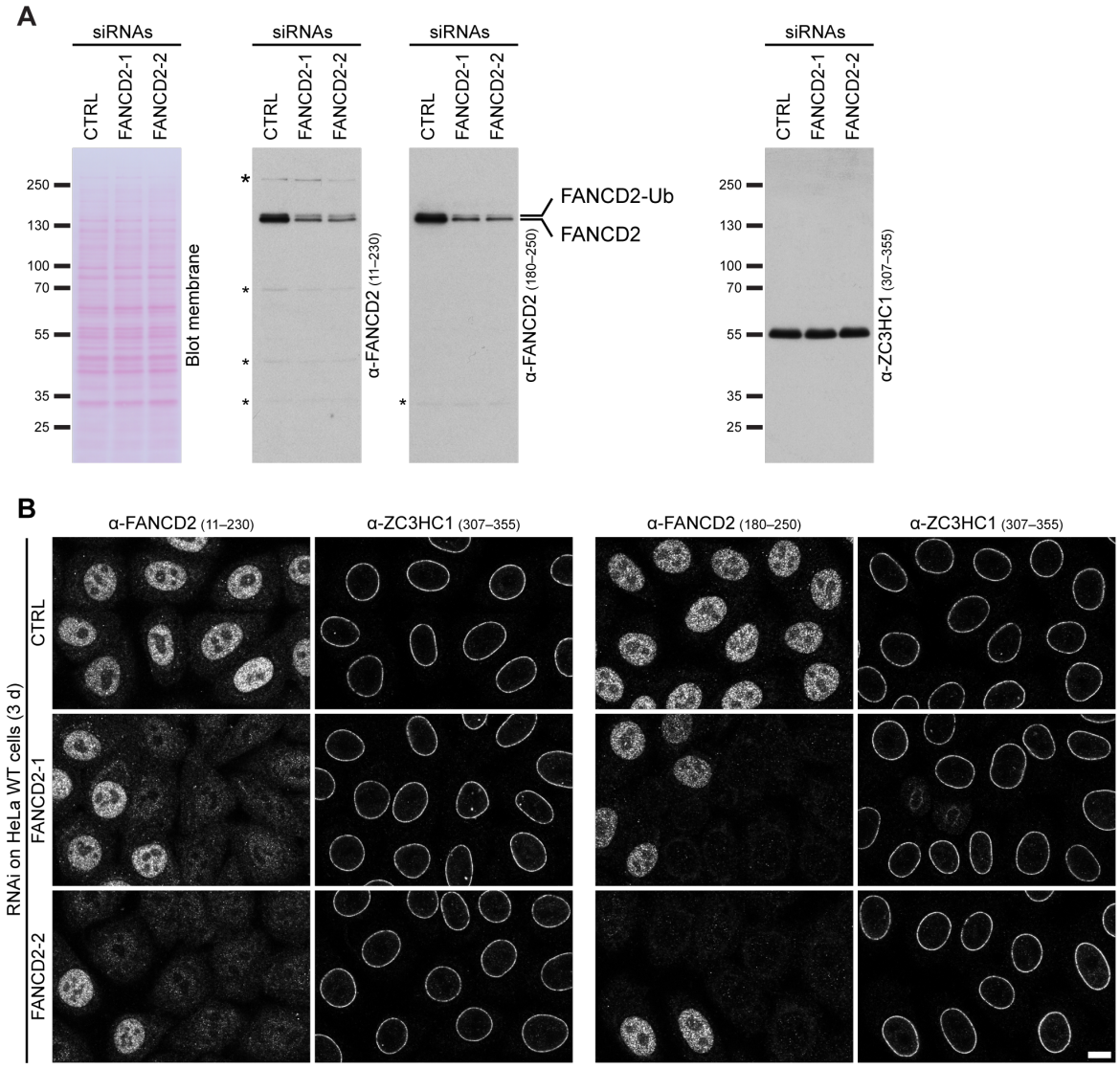
A
siRNAs
CTRL
FANCD2-1
FANCD2-2
250
130
100
70
55
35
25
Blot membrane
α-FANCD2 (11–230)
α-FANCD2 (180–250)
FANCD2-Ub
FANCD2
α-ZC3HC1 (307–355)
B
α-FANCD2 (11–230)
α-ZC3HC1 (307–355)
α-FANCD2 (180–250)
α-ZC3HC1 (307–355)
RNAi on HeLa WT cells (3 d)
CTRL
FANCD2-1
FANCD2-2

S13 (1/3)

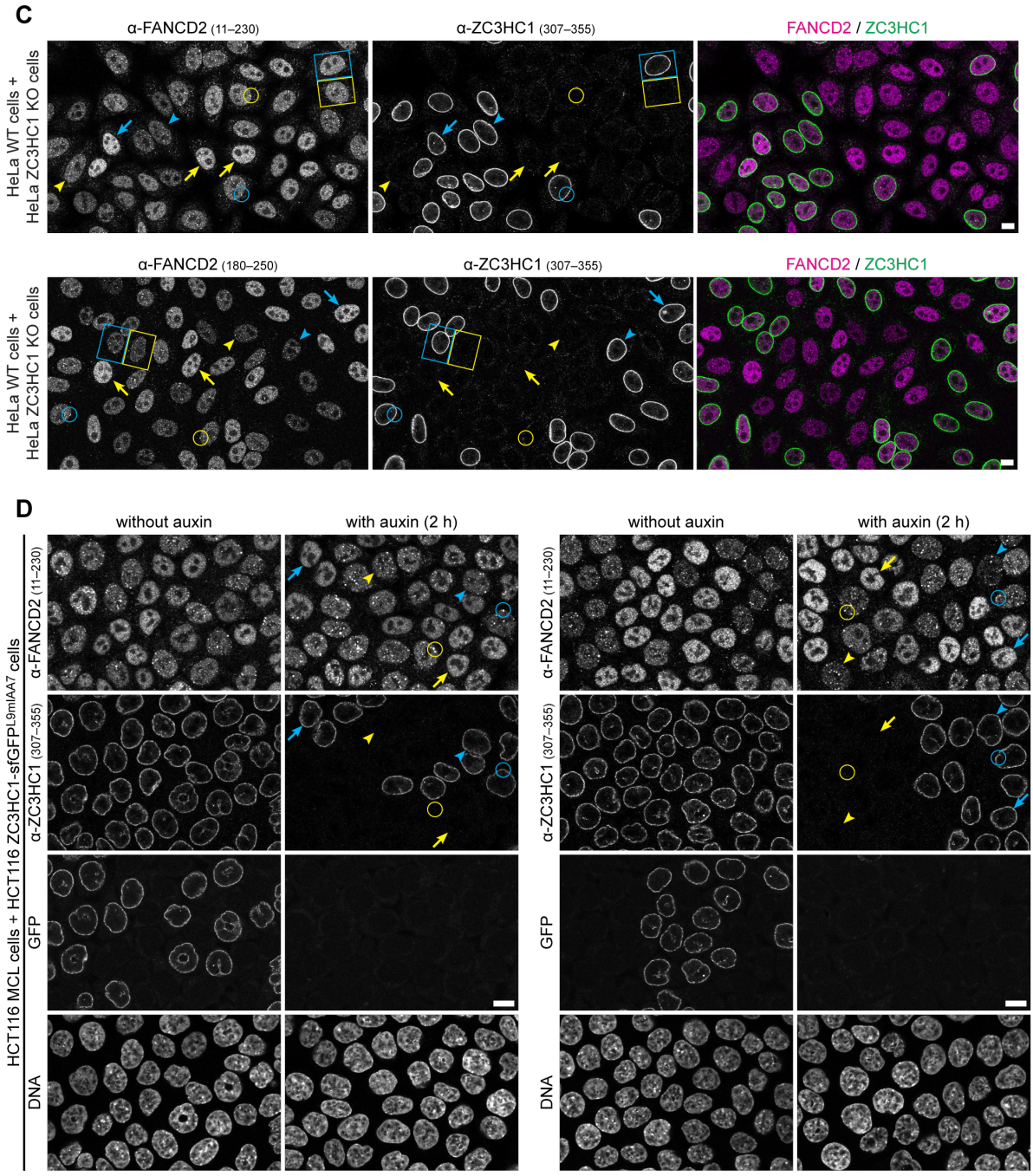
C
α-FANCD2 (11–230)
α-ZC3HC1 (307–355)
FANCD2 / ZC3HC1
HeLa WT cells +
HeLa ZC3HC1 KO cells
α-FANCD2 (180–250)
α-ZC3HC1 (307–355)
FANCD2 / ZC3HC1
HeLa WT cells +
HeLa ZC3HC1 KO cells
D
without auxin
with auxin (2 h)
without auxin
with auxin (2 h)
HCT116 MCL cells + HCT116 ZC3HC1-sfGFP^9mIAA7 cells
α-FANCD2 (11–230)
α-ZC3HC1 (307–355)
GFP
DNA
α-FANCD2 (11–230)
α-ZC3HC1 (307–355)
GFP
DNA

S13 (2/3)

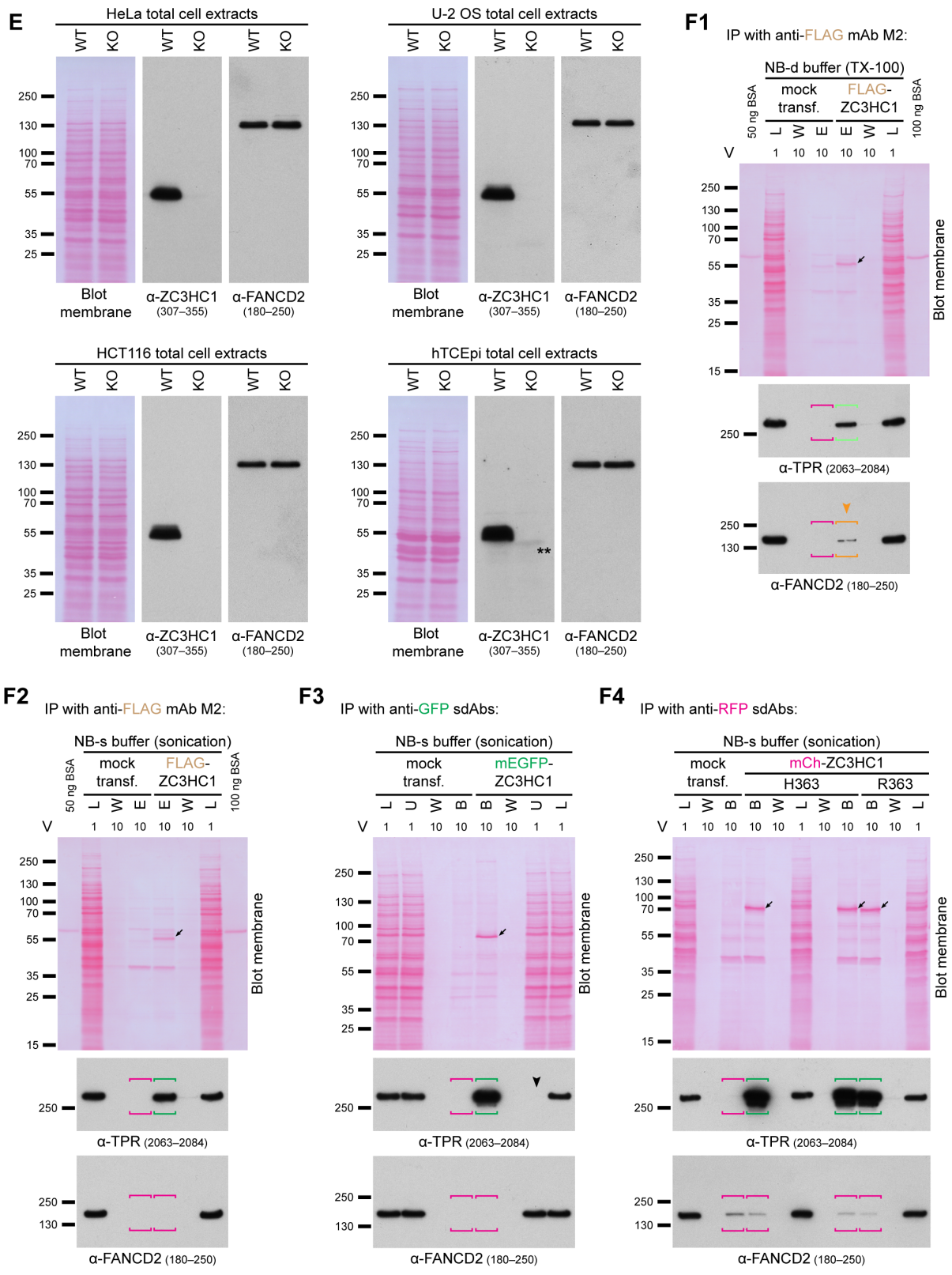

Supplemental Figure S13. Experiments revealing ZC3HC1 deficiency in human cell lines not affecting the cellular amounts and subcellular distribution of FANCD2, in line with no evident robust interaction between ZC3HC1 and FANCD2, neither at the NE nor in cell extracts.

In a recent study, FANCD2, a protein of 164 kD in humans, has been described as a binding partner of NIPA (Kreutmair *et al*, 2020), the latter protein also known as ZC3HC1. Among this study's data, ZC3HC1 knockdown in HeLa cells was reported to cause a significant reduction of FANCD2 protein levels in total cell extracts, as was presented by IB, and in the HeLa cells' nuclei, as shown by IFM. Moreover, immunoprecipitation (IP) of ectopically expressed, FLAG-tagged ZC3HC1 from HEK293T Phoenix cells was reported resulting in co-IP of endogenous FANCD2, then regarded as representing a robust ZC3HC1:FANCD2 interaction (Kreutmair *et al*, 2020). The authors considered ZC3HC1 necessary for FANCD2 protein stability and half-life, with ZC3HC1 acting as a scaffold protein for FANCD2 and stabilizing its nuclear abundance.

On the other hand, we had till then not encountered evidence indicating an interaction between ZC3HC1 and FANCD2 in our studies. We had neither found FANCD2 to be a component of manually isolated and then mass spectrometrically analyzed *Xenopus laevis* and *Xenopus tropicalis* oocyte NEs, even though database-deposited *Xenopus* FANCD2 sequences were already available at the time. Therefore, we had also not detected this protein among those co-detached with *Xenopus* ZC3HC1 and other proteins after disassembling the oocytes' NBs by physicochemical means (Gunkel *et al*, 2021, and our unpublished data). Similarly, we had neither found FANCD2 among those proteins that one could identify, via comparative proteomics, to have been detached from the NEs of CRISPR/Cas9-edited human cell lines expressing degron-tagged versions of TPR after having, and not having, auxin-induced the degradation of TPR (Gunkel & Cordes, 2022, and our unpublished data). Furthermore, following the IP of FP-tagged versions of *Hs*ZC3HC1, protein FANCD2 had not been detectable by mass spectrometry among those materials co-sedimented with ZC3HC1 (our unpublished data).

However, to assess whether we might have overlooked a ZC3HC1:FANCD2 interaction, we addressed this question more thoroughly. To this end, we used the two commercial FANCD2 antibodies (S13A and S13B) that had also been employed in the recent study on ZC3HC1 and FANCD2 (Kreutmair *et al*, 2020). With these antibodies, we investigated the fate of FANCD2 in human cell lines, including HeLa P2, HCT116, U-2 OS, and hTCEpi (for cell line details, see Gunkel *et al*, 2021) in the absence of ZC3HC1 (e.g., S13C to S13E). Furthermore, we investigated whether the IP of ectopically expressed FLAG-tagged and FP-tagged versions of ZC3HC1 from HEK293T cells would allow for detecting co-immunoprecipitated FANCD2 (S13F). In parallel, we also addressed whether the absence of FANCD2 itself might affect the cellular amounts and the positioning of ZC3HC1 at the NB (S13A and S13B).

In the course of these experiments, we applied various IFM and IP protocols, including those used earlier (Kreutmair *et al*, 2020; Gunkel *et al*, 2021). For some of the FANCD2 immunoblots (S13E and S13F), we eventually decided to use the same cellular materials and nitrocellulose membranes (Gunkel *et al*, 2021) that we had already used for investigating the interaction between ZC3HC1 and TPR and between ZC3HC1 and other proteins formerly reported binding partners of ZC3HC1. These materials thus allowed for directly comparing the here presented data with those we had obtained earlier. Furthermore, since the underlying rationale for our former experiments and their procedural details, followed by an in-depth discussion of the conclusions to be drawn from such experiments' results, had already been outlined in all detail (Gunkel *et al*, 2021), this further allowed for here confining oneself to a brief description of the experimental specifics and the here obtained data related to FANCD2. A representative selection of these data is presented in the following.

(A) IB of whole-protein extracts from HeLa P2 cells that had been transfected with control siRNAs (CTRL) and two pairs of FANCD2 siRNAs (FANCD2-1 and FANCD2-2). The RNAi experiments presented in S13A were conducted (i) to confirm FANCD2 antibody performance and (ii) to assess whether a reduction in the cellular amounts of FANCD2 might also affect those of ZC3HC1. Immunolabeling for the three immunoblots shown on the right was performed on the Ponceau S-stained uncut membrane shown here on the left and on an identical duplicate, comprising the entire length of gel-electrophoretic sample separation, in order to also illustrate each of the FANCD2 antibodies' degree of target-specificity, apart from their target-verification by RNAi. The membranes were first incubated with the FANCD2 antibodies, then recovered by quantitatively detaching the bound antibodies through incubation at low pH, and then re-incubated with the ZC3HC1 antibodies. Asterisks mark minor cross-reactions with yet unknown polypeptides. The band marked as FANCD2-Ub represents a minor subpopulation of mono-ubiquitinated FANCD2 polypeptides (e.g., Vandenberg *et al*, 2003). Note that the reduction in the total cellular amounts of FANCD2 did not appear to have affected the cellular amounts of ZC3HC1. As an aside, IB of total cell extracts from HeLa cells treated with ZC3HC1 siRNAs, resulting in a substantial KD in total ZC3HC1 amounts, did not have a notable effect on the cellular amounts of FANCD2 either (our unpublished data), with these findings equivalent to those with cell extracts of ZC3HC1 KO cells, presented further below in S13E.

(B) Double-labeling IFM of ZC3HC1 and FANCD2 in HeLa P2 WT cells. The cells had been treated with either control siRNAs or the two pairs of siRNAs targeting FANCD2 and then harvested on day 3 post-transfection. FANCD2 and ZC3HC1 were detected with the antibodies presented in S13A. Some cells not transfected with the FANCD2 siRNAs are shown as a

reference. Note the characteristic dotted staining for FANCD2 throughout the nuclear interior, except for the nucleoli, in the control cells. By contrast, in the cell populations treated with the FANCD2 siRNAs, such staining is only visible in the subpopulation of cells that apparently had remained untransfected. Also, note that the knockdown of FANCD2 had not affected the presence and immunolabeling intensity of ZC3HC1 at the NE. Bar, 10 µm.

(C) IFM of asynchronous HeLa P2 WT cells grown together with cells of a stable HeLa cell line in which all *ZC3HC1* alleles have been disrupted by CRISPR/Cas9n technology. Allowing for a side-by-side comparison of the WT and ZC3HC1 KO cells on the same coverslip, the mixed cell populations were double-immunolabeled with the FANCD2 and ZC3HC1 antibodies also used for S13A. Some HeLa WT cells are marked by blue arrows and arrowheads, while arrows and arrowheads in yellow mark some ZC3HC1 KO cells. The arrows mark those cells in which the signal intensities for nuclear FANCD2 appear especially pronounced, while the arrowheads mark some representative cells with less intense nuclear FANCD2 immunolabeling. Furthermore, blue and yellow circles mark some similarly conspicuous FANCD2 foci at the NEs of both the WT and ZC3HC1 KO cells. In addition, pairs of rectangles, again in blue and yellow, mark some cell pairs, consisting of one WT and one neighboring ZC3HC1 KO cell, in which nuclear FANCD2 levels appear very similar. These arrows, arrowheads, circles, and rectangles are also included same-positioned on the micrographs showing the ZC3HC1 immunolabeling, allowing for directly comparing FANCD2 with ZC3HC1. Furthermore, the same FANCD2 and ZC3HC1 micrographs are also shown as overlays on the right side.

Note that, when regarding these mixed populations of WT and ZC3HC1 KO cells as a whole, neither the cellular amounts nor the subcellular location of FANCD2 appeared altered by the absence of ZC3HC1, with immunolabeling of FANCD2 varying between individual WT cells to the same extent as between individual ZC3HC1 KO cells, accompanied by FANCD2-containing NE-associated foci being similarly evident in the presence and absence of ZC3HC1. As an aside, when using a formerly described protocol for cell fixation and permeabilization (Kreutmair *et al*, 2020), we could not detect any evident difference between the WT and ZC3HC1 KO cells of a mixed population of cells immunolabeled for FANCD2 in such a way either (our unpublished data). Furthermore, we could also not detect any evident difference following ZC3HC1 RNAi in HeLa WT cells when comparing the siRNA-transfected cells with (i) those cells that had remained non-transfected within the same population and with (ii) a separate population of cells that we had transfected with control siRNAs (our unpublished data). Bars, 10 µm.

(D) IFM of cells from an HCT116 progenitor cell line expressing the naturally tag-free ZC3HC1

and cells of a homozygous HCT116 progeny line, in which all ZC3HC1 polypeptides were C-terminally tagged with a GFP-degron tag, called sfGFP^{L9mIAA7} (for details regarding these cell lines and the sfGFPL9mIAA7-tag, see Gunkel & Cordes, 2022). These cells had been co-cultured as mixed populations together on the same coverslip, followed by an additional incubation of 2h in the absence or presence of auxin, the latter inducing the rapid proteasomal degradation of ZC3HC1 (for details, see Gunkel & Cordes, 2022). Specimens were then double-immunolabeled for ZC3HC1 and FANCD2 and analyzed in parallel, using identical microscope settings. Assigned to the same features as in S13C, the blue arrows, arrowheads, and circles mark the nuclei of some progenitor cells, i.e., those expressing the tag-free version of ZC3HC1, while the yellow arrows, arrowheads, and circles mark some of the progeny cells' nuclei, i.e., those with the sfGFP-tagged ZC3HC1. Note that the auxin treatment resulted in the elimination of NE-associated GFP and immunostaining for ZC3HC1 in those cells that had been expressing the tagged version of ZC3HC1, while the progenitor cells' untagged ZC3HC1 remained unaffected. Further note that the elimination of the tagged ZC3HC1 neither affected the nuclear amounts nor the subcellular distribution of FANCD2 notably. In particular, note that upon also the rapid loss of ZC3HC1, the more finely punctate nuclear staining for FANCD2 remained largely unchanged, with no evident more diffuse distribution throughout the nuclear interior, in contrast to what a model might have expected in which ZC3HC1 would act as a FANCD2-protecting scaffold. Bars, 10 μm

(E) IB of total cell extracts from HeLa P2, HCT116, U-2 OS, and hTCEpi WT and ZC3HC1 KO cells. The Ponceau S-labeled membranes and the IBs for ZC3HC1 are identical to those already presented earlier (see Figures 6B and S15H in Gunkel *et al*, 2021). The double asterisk marks a cross-reaction of the polyclonal guinea-pig ZC3HC1 antibodies, just beneath the band for ZC3HC1, which was only seen in hTCEpi cell extracts and which also arose when only using secondary antibodies (for further details, see S15I in Gunkel *et al*, 2021). Here, these membranes were recovered by quantitatively detaching the bound ZC3HC1 antibodies through incubation at low pH, followed by re-incubating such membranes with rabbit antibodies for FANCD2. Note that while ZC3HC1 had not been detectable in any of the KO cells' extracts, with each cell type's pair of KO and WT cell extracts representing about the same number of cells, the cellular amounts of FANCD2 appeared highly similar in the WT and KO cells of each cell line. Altogether, these data demonstrated that the integrity of FANCD2 in three aneuploid tumor cell lines of different tissue origins (HeLa, HCT116, and U-2 OS) and a non-tumor cell line of normal diploid karyotype (hTCEpi) does not depend on ZC3HC1 being present.

(F) A representative selection of IP experiments that had been performed with HEK293T cell extracts containing differently tagged versions of ectopically expressed intact *Hs*ZC3HC1. The Ponceau S-labeled membranes and the IBs for TPR presented in S13F1–4 are identical to those already presented earlier (see Figure S11D2 and S11D3 in Gunkel *et al*, 2021). Here, these membranes were recovered by quantitatively detaching the bound TPR antibodies through incubation at low pH, followed by re-incubating such membranes with rabbit antibodies for FANCD2. Buffers used for the actual IP experiments included such that we had found to result in the destabilization of the nuclear basket (NB-d buffers), with the composition of these buffers, and the mode of their application, being notably different in several aspects from the physicochemical conditions within the living mammalian cell. The composition of the NB-d buffer for the here presented IP experiment in S13F1 lacked, for example, Mg cations while containing high concentrations, i.e., 1%, of Triton X-100. As such, this buffer and the corresponding IP protocol (for further details, see Gunkel *et al*, 2021) were representatives of very similar or essentially identical IP buffers and protocols used for earlier studies on ZC3HC1 and its alleged interactions with other proteins (e.g., Bassermann *et al*, 2005a, 2007; Illert *et al*, 2012; Kreutmair *et al*, 2020). Other buffers and protocols used for our IP experiments allowed for maintaining the NB's integrity, with the corresponding buffers termed NB-stabilizing (NB-s; Gunkel *et al*, 2021). Of note, while the use of the NB-d buffers only resulted in minor amounts of TPR being co-immunoprecipitated upon IP of tagged versions of ZC3HC1, as exemplified in S13F1, the NB-s buffers, more closely resembling the physiological conditions within the cell, often allowed for a quantitative co-IP of TPR. Figure S13F3 exemplifies such removal of all soluble TPR from the cell extract due to co-IP with the immunoprecipitated ZC3HC1 (for further details, again see Gunkel *et al*, 2021). By contrast, as outlined further below, we did not find FANCD2 co-immunoprecipitated in amounts that we would regard as significant with any of these and other buffers in any combination with different IP protocols.

(F1) IB of materials obtained from an IP experiment with anti-FLAG IgG-coated immuno-magnetic beads, following ectopic expression of FLAG-tagged ZC3HC1, and subsequent cell extract preparation and incubation under NB-d conditions (for details, see the Supplemental Materials and Methods section of Gunkel *et al*, 2021). Lanes had been loaded for SDS-PAGE with an aliquot of the total soluble cell proteins not yet treated with the magnetic immunoaffinity beads (L, for load), with an aliquot of those materials released during the third of three successive washing steps (W), and with the proteins obtained after final elution (E). The arrow on the image of the Ponceau S-stained membrane shown here, like on those presented in S13F2–4, marks the immunoprecipitated tagged ZC3HC1 polypeptides. Loadings in L

represented one volume fraction of the respective samples' total amount (1 V), while the loadings in lanes W and E represented ten-fold higher relative amounts (10 V). TPR regarded as inefficiently co-immunoprecipitated with the FLAG-tagged ZC3HC1, as the IP's actual target protein, is framed with brackets in light green, while those cases in which no co-IP had occurred, like upon incubating FLAG-ZC3HC1-deficient cell extracts with the anti-FLAG IgG-coated immuno-magnetic beads, are accentuated by brackets in magenta. The orange-colored brackets frame some trace amounts of FANCD2, also marked by an arrowhead. Note that trace amounts like those seen here in S13F1 represent what one had been able to detect at most in such kinds of experiments relative to the total FANCD2 amounts in the corresponding cell extracts. Even though one might consider such trace amounts of co-sedimented FANCD2 as having been co-immunoprecipitated with the FLAG-tagged ZC3HC1 specifically, one needs to look at the actual numbers of these FANCD2 polypeptides in the context with the numbers of the ectopically expressed ZC3HC1 polypeptides; the latter determined to be present in millions, on average, within a transfected cell at the time of harvest (Gunkel *et al*, 2021). In fact, the availability of quantitative mass spectrometric data for HEK293 cells (Bekker-Jensen *et al*, 2017), paired with the knowledge of the absolute copy numbers within HEK293 cells for some representative NPC proteins, allowed us to deduce the HEK293T cell's approximate total number of FANCD2 polypeptides and thus also the approximate number of the few FANCD2 polypeptides co-sedimented together with FLAG-ZC3HC1. This information, in turn, allowed us to conclude that, at most, only a few hundred FANCD2 polypeptides per transfected cell had been co-sedimented during the IP of the same cell's millions of ectopically expressed ZC3HC1 polypeptides. In other words, for every 10,000 FLAG-ZC3HC1 polypeptides immunoprecipitated, only about one endogenous FANCD2 polypeptide had been co-sedimented.

(F2) IB of materials obtained from an IP experiment with anti-FLAG IgG-coated immuno-magnetic beads, following ectopic expression of FLAG-tagged ZC3HC1, subsequent cell extract preparation, and incubation for IP under NB-s conditions more closely resembling the physicochemical conditions within the cells' cytoplasm and nucleoplasm (for further details, also regarding cell extract preparation, see the Supplemental Materials and Methods section of Gunkel *et al*, 2021). While not yet reaching the quantitative co-IP of TPR achievable via "nano-trapping", i.e., when using single-domain antibodies (sdAbs) in combination with NB-s buffers (see S13F3 and S13F4 below), these NB-s conditions already allowed for recurrently co-immunoprecipitating notably higher TPR amounts, here now framed by dark green brackets,

when immunoprecipitating FLAG-ZC3HC1. Further note, in particular, that no co-IP of FANCD2 was detected.

(F3) IB of materials obtained from IP experiments with anti-GFP sdAb-coated agarose beads, after ectopically having expressed a monomeric EGFP-tagged version of ZC3HC1, followed by cell extract preparation and incubation for IP under NB-s conditions. Like in S13F1 and S13F2, lanes had been loaded for SDS-PAGE with an aliquot of the total soluble cell proteins not yet treated with the sdAb-coated immunoaffinity beads (L), with an aliquot of those materials released during the third of three successive washing steps (W), and with the proteins obtained after final elution (E). In addition, we had here also loaded the proteins that had remained unbound after incubation with such beads (U). Loadings in L and U represented one volume fraction of the respective samples' total amount (1 V), while the loadings in lanes W and E represented ten-fold higher relative amounts (10 V). Note that these IP conditions had allowed for quantitative co-IP of all soluble TPR polypeptides initially present in interphase cell extracts (L), which were then absent from such extracts (position marked by arrowhead) after the incubation (U) with the anti-GFP beads. By striking contrast, no co-IP of FANCD2 was detected.

(F4) IB of materials obtained from IP experiments with anti-RFP sdAb-coated agarose beads, after ectopically having expressed two versions of ZC3HC1, namely the H363 and the R363 variants, here both tagged with mCherry. Note that both ZC3HC1 variants allowed for quantitative co-IP of TPR, while trace amounts of FANCD2 had been co-sedimented in this experiment with the sdAb-coated agarose beads even after their incubation with cell extracts lacking ectopically-expressed ZC3HC1.

Finally, not having intentionally stressed the cells for our FANCD2-related experiments, we need to remark that our current results do not yet permit excluding scenarios in which FANCD2 might engage in stress-induced interactions with some structures at the NE. For example, one might conceive such interactions as a result of DNA replication stress or DNA damage-induced stresses and localization of DNA lesions to the NPC (e.g., Freudenreich & Su, 2016; Lamm *et al*, 2021; Whalen & Freudenreich, 2020). However, based on our current FANCD2 results, including those presented here in S13, we regard it justified to conclude that FANCD2 is not a regular, customary binding partner of ZC3HC1 in different human cell lines, neither at the NE nor elsewhere within such cells in interphase, and that ZC3HC1 does not function as a regular scaffold protein for FANCD2.

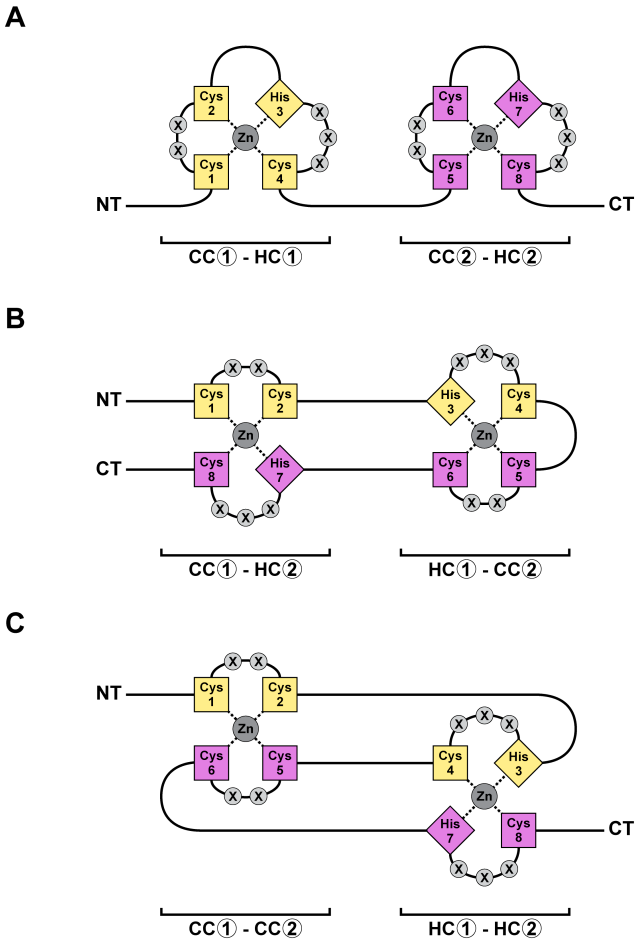

Supplemental Figure S14. Former considerations regarding the zinc ion-coordination topology of ZC3HC1.

Speculating in the early stages of our research on ZC3HC1 how the protein's two pairs of each one C-$X_{(2)}$-C tetrapeptide and one H-$X_{(3)}$-C pentapeptide are arranged relative to each other, each in order to coordinate a zinc ion likely in a tetrahedral manner, we had initially considered different constellations hypothetically conceivable. Even though the NuBaID signature early on suggested an arrangement of two zinc finger modules one after the other, here also paraphrased as CC①-HC① and CC②-HC② and schematically depicted as such in S14A, and even though this appeared in line with a zinc coordination sphere already proposed for BLD1 (Higashi *et al*, 2005), we at times had not yet regarded it as justified to exclude other scenarios categorically. Such mind games also took place in light of the variety of arrangements within different proteins that, by then, were known to allow for binding zinc ions in a tetrahedral geometry.

For example, configurations with pairs of zinc ion-coordinating residues belonging to different parts of the primary sequence, separated from each other by other pairs of residues involved in coordinating yet another zinc ion, had been described for some zinc fingers of the

RING/FYVE/PHD-types (e.g., Capili et al, 2001; Legge et al, 2004; Houben et al, 2005; Gamsjaeger et al., 2007; Kandias et al, 2009; Deshaies & Joazeiro, 2009; Wei & Sun, 2010) and for some other types of zinc fingers too (e.g., He *et al*, 2007; Massiah *et al*, 2007). These proteins were characterized by the especially pronounced winding of their aa chains to achieve an interleaved arrangement of the zinc ion-coordinating residues, also referred to as a cross-braced configuration.

Furthermore, while the coordination of a zinc ion by two cysteines and two histidines was known to commonly occur in a non-interleaved manner in numerous zinc finger proteins harboring a C2H2 zinc finger domain (e.g., Brayer & Segal, 2008), zinc ion coordination involving two histidines had also been found occurring within cross-braced arrangements. For example, in some B-box zinc finger proteins (e.g., Massiah *et al*, 2006; He *et al*, 2007). If such latter coordination topology had applied for ZC3HC1, the *Hs*ZC3HC1 protein's two pairs of C-$X_{(2)}$-C tetrapeptides and H-$X_{(3)}$-C pentapeptides would have had to allow for an interleaved CC①-CC② and HC①-HC② configuration, as schematically depicted in S14C. Furthermore, we also did not want to discard yet another scenario too early in which the protein would adopt a clothespin-like CC①-HC② and CC②-HC① configuration, as outlined in S14B.

In principle, our finding that eliminating a single one of the BLDs' zinc-coordinating residues had been sufficient for abolishing TPR-binding would have been reconcilable with all three scenarios. Thus, without crystallographic data for ZC3HC1 at hand, we had initially conceived it inappropriate to take the CC①-HC①_CC②-HC② configuration already for granted. In other words, even though sequence similarities between the BLDs and the related BIR domains, for which crystal structures were already available (e.g., Supplemental Figure S11), were pointing attractively towards the CC①-HC①_CC②-HC② version, we had initially refrained from categorically ruling out the other scenarios.

Eventually, though, we considered it reasonable to treat the CC①-HC①_CC②-HC② configuration as the one genuinely existing in all probability. This conclusion was based on AlphaFold2 predicting such a configuration (Figure 6, Supplemental Figure S10) not only for *Hs*ZC3HC1 but also for other homologues with which the human one barely shared any aa sequence identity, like *Sc*Pml39p (see in this context also Supplemental Information 6 and Supplemental Figure S9). In particular, the finding of an evolutionarily conserved BLD1:BLD2 binding interface (Supplemental Figure S10B) contributed to this conclusion substantially, with the latter then based on the following considerations: On the one hand, regarding the similarity of the BLDs' predicted central structures with the BIR domains' crystal structures, we had initially considered it appropriate to interpret such similarities with caution, as reasoned further

above (e.g., Supplemental Information 6). On the other hand, though, the BIR domains' AlphaFold2-predicted arrangements relative to each other, for example, in the four human proteins that contain more than one BIR domain (BIRC1 to BIRC4), appeared dissimilar from the BLD1:BLD2 interface of the three here presented ZC3HC1 homologues. This, then again, meant that the three homologues' BLD1:BLD2 interface similarities were less likely to have been influenced by some structural similarity with the BIR domains and thus by an initially considered "discussible level of bias" affecting the BLD structure predictions (Supplemental Information 6).

Nonetheless, even though all current evidence argues for the NuBaID's CC①-HC①_CC②-HC② configuration, we still consider it adequate to illustrate the other initially imagined constellations for comparison in the following. The tetrahedrally coordinated zinc ions are thereby presented as dark grey spheres in these schematic depictions. The zinc ion-coordinating residues of the first and second BLD are depicted as squares and rhombuses, representing cysteine and histidine residues, with those corresponding to the first BLD colored in yellow and those of the second in purple. In addition, the numbers 1–8 displayed within these quadrilaterals correspond to the total of eight zinc ion-coordinating residues of the two BLDs and reflect their order relative to each other along the protein's linear sequence of amino acids.

(A) Depiction of the two BLDs of ZC3HC1 as two separate zinc-binding modules consecutively arranged one after the other in tandem. The coordinating residues of the first and second BLD conform with the order CC①-HC①_CC②-HC② and the arithmetic sequence 1,2,3,4,5,6,7,8. Note that this arrangement is in line with AlphaFold2's structure predictions for ZC3HC1 homologues like *Hs*ZC3HC1 (https://alphafold.ebi.ac.uk/entry/Q86WB0) and *Sc*Pml39p (https://alphafold.ebi.ac.uk/entry/Q03760). As such, they closely resemble the consecutive arrangements of zinc fingers that are part of the BIR domain-containing proteins, the latter compared with the BLDs' structures in Supplemental Figure S11, with the ZC3HC1 homologues' BLDs though exhibiting an evolutionarily conserved BLD1:BLD2 interface (Supplemental Figure S10B). By contrast, in the single BIR domain-containing human proteins BIRC5 to BIRC8, an equivalent BIR:BIR interface is self-evidently absent, while in the human BIRC1 to BIRC4 (https://alphafold.ebi.ac.uk/entry/Q13075; https://alphafold.ebi.ac.uk/entry/Q13490; https://alphafold.ebi.ac.uk/entry/Q13489; https://alphafold.ebi.ac.uk/entry/P98170), with three BIR domains each, their arrangements relative to each other appear notably different (see also further comments in the legend to Supplemental Figure S10B).

(B) Depiction of a zipper-like arrangement that could have arisen when the second half of the ZC3HC1 protein, harboring the second BLD, would have folded back onto itself. Such constellation could then have allowed positioning each of the one BLD's two pairs of zinc ion-coordinating residues face-to-face with each of the other BLD's two pairs, resulting in a CC①-HC②_CC②-HC① arrangement and the number order 1,2,7,8,3,4,5,6. As this would possibly have positioned the protein's N- and C-terminal parts next to each other, such a constellation might have created the impression also of a clothespin-like arrangement.

(C) Depiction of an interleaved, cross-braced type of arrangement, which would have required marked winding of the aa chain to achieve such a conformation. In contrast to the scenarios in S14A and S14B, this model of a CC①-CC②_HC①-HC② arrangement, equivalent to a number order of 1,2,5,6,3,4,7,8, would have demanded that the first zinc ion would have been coordinated only by cysteine residues while both histidine residues would have been involved in the coordination of the second zinc ion.

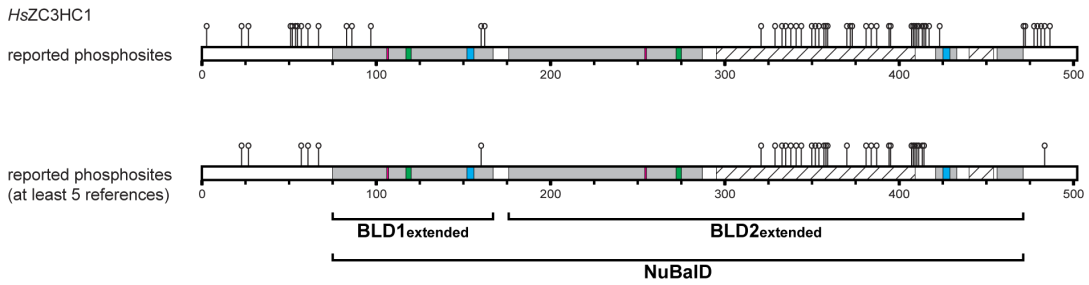

Supplemental Figure S15. The BLD2 loop of *Hs*ZC3HC1 as a prime target for phosphorylation.

Endogenous ZC3HC1 polypeptides in mammals have been recurrently identified as being specifically and varyingly phosphorylated at specific sites during cell cycle progression (Bassermann *et al*, 2005a; Dephoure *et al*, 2008; Blethrow *et al*, 2008; Chi *et al*, 2008; Weintz *et al*, 2010; Illert *et al*, 2012; Zhou *et al*, 2013; Robitaille *et al*, 2013; Sharma *et al*, 2014; Sos *et al*, 2014; Hu *et al*, 2015), yet not only then. In fact, ZC3HC1 and, in particular, its BLD2-embedded loop, were also found phosphorylated upon a range of different stimuli and the activation of kinases that operate in different cell signaling pathways (e.g., Christensen *et al*, 2010; Moritz *et al*, 2010; Yu *et al*, 2011). For some scenarios regarding the potential roles of such ZC3HC1 phosphorylation, see Supplemental Discussion 5.

Here, we have correlated the schematic scheme of *Hs*ZC3HC1 with its newly defined BLDs, corresponding to the scheme presented in Figure 6D, with the serine and threonine residues of *Hs*ZC3HC1 so far reported to have been found phosphorylated (https://www.phosphosite. org/ proteinAction.action?id=3471&showAllSites=true). The upper scheme depicts all phosphosites identified to date (July 2022), while the lower scheme comprises those for which at least five datasets have been deposited at https://www.phosphosite.org.

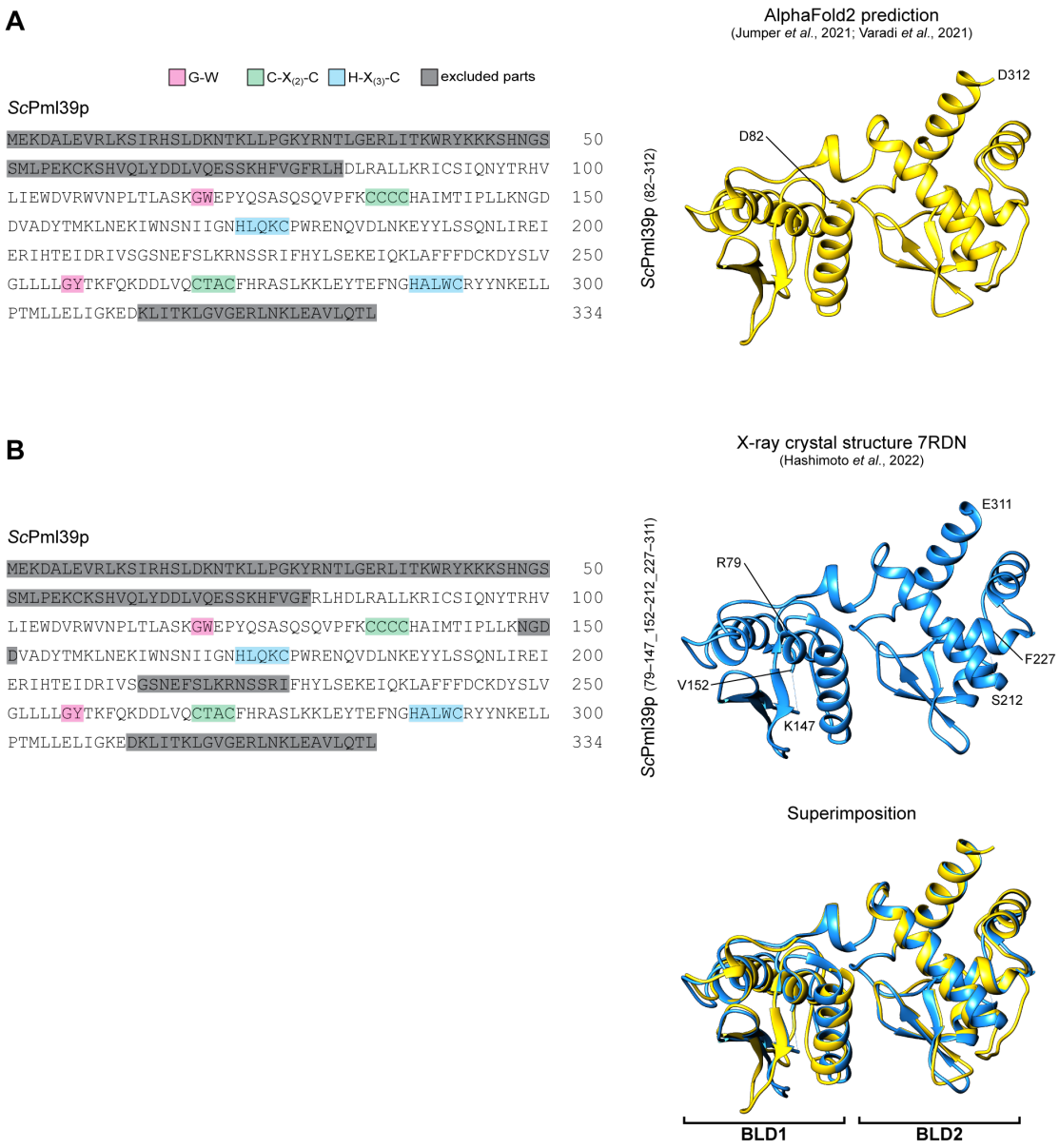

Supplemental Figure S16. Comparing the crystal structure of an *Sc*Pml39 polypeptide with its tertiary structure as predicted by AlphaFold2.

With Pml39p of *Saccharomyces cerevisiae* and Rsm1p of *Schizosaccharomyces pombe* having been stated to be "*the unequivocal homologues of ZC3HC1 in these species*" (Gunkel *et al*, 2021), crystal data available for *Sc*Pml39p have now been correlated with AlphaFold2's structure predictions for ZC3HC1 recently (Hashimoto *et al*, 2022). Here, we also compare this crystal structure of *Sc*Pml39p with its corresponding one predicted by AlphaFold2.

(A) The sequence of *Sc*Pml39p and its structure predicted by AlphaFold2, with those predicted parts corresponding to the sequence segments highlighted in grey blanked out. Residues highlighted in magenta, green, and blue represent the positions of the two BLDs' G-W, C-$X_{(2)}$-

C, and H-$X_{(3)}$-C sequence elements. Note that this presented structure (aa 82–312) for the two BLDs of *Sc*Pml39p is identical to the one in Supplemental Figure S12B.

(B) The sequence of *Sc*Pml39p and the structure of an *Sc*Pml39 polypeptide, comprising aa 77–317, determined by X-ray crystallography. Sequence segments highlighted in grey include the N- and C-terminally truncated parts and short segments found to be disordered, with the presented structure describable as 79–147_152–212_227–311 (Δ1–78_Δ148–151_Δ213–226_Δ312-334). Note that the superimposition of this crystal structure onto the AlphaFold2-predicted structure revealed a high degree of similarity.

Identified structures:			Query structures:													
			*Hs*ZC3HC1		*Hs*ZC3HC1_minimal		*Dd*ZC3HC1		*Dd*ZC3HC1_minimal		*Sc*Pml39p		*Sc*Pml39p_minimal		*Dm*Diap2	
Target species	Identifier (afdb-proteome)	Protein name	Score	TM-score	Score	TM-score	Score	TM-score	Score	TM-score	Score	TM-score	Score	TM-score	Score	TM-score
Homo sapiens	**AF-Q86WB0-F1-model_v2**	**ZC3HC1**	**3458**	**5,56E-78**	**1635**	**4,25E-35**	**757**	**8,90E-16**	**649**	**6,89E-14**	**383**	**4,03E-07**	**348**	**1,88E-06**	197	9,67E-03
Homo sapiens	AF-Q13075-F1-model_v2	BIRC1	-	-	-	-	-	-	-	-	188	1,57E-02	184	1,62E-02	844	5,66E-18
Homo sapiens	AF-Q13490-F1-model_v2	BIRC2	-	-	-	-	-	-	-	-	172	3,75E-02	156	7,59E-02	1398	5,12E-31
Homo sapiens	AF-Q13489-F1-model_v2	BIRC3	-	-	-	-	-	-	151	8,92E-02	173	3,55E-02	158	6,80E-02	1454	2,46E-32
Homo sapiens	AF-P98170-F1-model_v2	BIRC4	-	-	200	1,26E-02	-	-	204	4,58E-03	248	6,09E-04	200	6,68E-03	**1550**	**1,35E-34**
Homo sapiens	AF-O15392-F1-model_v2	BIRC5	-	-	-	-	-	-	-	-	-	-	-	-	260	3,18E-04
Homo sapiens	AF-Q9NR09-F2-model_v2	BIRC6	-	-	-	-	-	-	-	-	-	-	-	-	221	2,63E-03
Homo sapiens	AF-Q9NR09-F1-model_v2	BIRC6	-	-	-	-	-	-	-	-	-	-	-	-	207	5,62E-03
Homo sapiens	AF-Q96CA5-F1-model_v2	BIRC7	-	-	-	-	-	-	-	-	-	-	-	-	696	1,73E-14
Homo sapiens	AF-Q96P09-F1-model_v2	BIRC8	-	-	-	-	-	-	-	-	-	-	-	-	797	7,23E-17
Homo sapiens	AF-Q99675-F1-model_v2	CGRF1	-	-	-	-	-	-	-	-	-	-	-	-	189	1,49E-02
Homo sapiens	AF-Q6UWE0-F1-model_v2	LRSAM1	-	-	-	-	-	-	-	-	-	-	-	-	215	3,64E-03
Homo sapiens	AF-Q6ZN04-F1-model_v2	MEX3B	-	-	-	-	-	-	-	-	-	-	-	-	165	5,48E-02
Homo sapiens	AF-Q86YT6-F1-model_v2	MIB1	-	-	-	-	-	-	-	-	-	-	-	-	221	2,63E-03
Homo sapiens	AF-Q969V5-F1-model_v2	MUL1	-	-	-	-	-	-	-	-	-	-	-	-	210	4,78E-03
Homo sapiens	AF-Q8WZ73-F1-model_v2	RFFL	-	-	-	-	-	-	-	-	-	-	-	-	224	2,24E-03
Homo sapiens	AF-Q5VTB9-F1-model_v2	RNF220	-	-	-	-	-	-	-	-	-	-	-	-	161	6,81E-02
Homo sapiens	AF-Q9BY78-F1-model_v2	RNF26	-	-	-	-	-	-	-	-	-	-	-	-	269	1,95E-04
Dictyostelium discoideum	**AF-Q54PS8-F1-model_v2**	**ZC3HC1**	**835**	**2,17E-17**	**607**	**7,75E-12**	**4037**	**2,35E-92**	**1385**	**8,68E-32**	**284**	**8,64E-05**	**250**	**4,22E-04**	-	-
Dictyostelium discoideum	AF-Q55EJ5-F1-model_v2	MYLIP	-	-	-	-	-	-	-	-	-	-	-	-	207	5,62E-03
Saccharomyces cerevisiae	**AF-Q03760-F1-model_v2**	**Pml39p**	-	-	**405**	**2,88E-07**	-	-	**388**	**1,54E-07**	**2786**	**1,07E-63**	**1927**	**2,48E-44**	**220**	**2,78E-03**
Saccharomyces cerevisiae	AF-P47134-F1-model_v2	Bir1p	-	-	-	-	-	-	155	7,13E-02	191	1,34E-02	178	2,25E-02	269	1,95E-04
Saccharomyces cerevisiae	AF-P54074-F1-model_v2	Asi1p	-	-	-	-	-	-	-	-	-	-	-	-	200	8,22E-03
Drosophila melanogaster	**AF-Q24307-F1-model_v2**	**Diap2**	-	-	**210**	**7,45E-03**	-	-	**211**	**3,10E-03**	**225**	**2,12E-03**	**223**	**1,88E-03**	**4007**	**1,92E-92**
Drosophila melanogaster	AF-Q24306-F1-model_v2	Diap1	-	-	-	-	-	-	-	-	-	-	-	-	1030	2,36E-22
Drosophila melanogaster	AF-Q9VEM2-F1-model_v2	Deterin	-	-	-	-	-	-	-	-	-	-	-	-	265	2,42E-04
Drosophila melanogaster	AF-Q9VCV3-F1-model_v2	RNF220	-	-	-	-	-	-	-	-	-	-	-	-	208	5,32E-03
Drosophila melanogaster	AF-Q9VUX2-F1-model_v2	Mib1	-	-	-	-	-	-	-	-	-	-	-	-	187	1,66E-02
Drosophila melanogaster	AF-Q9VZJ9-F1-model_v2	Mul1	-	-	-	-	-	-	-	-	-	-	-	-	208	5,32E-03
Drosophila melanogaster	AF-P29503-F1-model_v2	Neur	-	-	-	-	-	-	-	-	-	-	-	-	179	2,57E-02
Drosophila melanogaster	AF-P20193-F1-model_v2	Su(var)3-7	-	-	-	-	-	-	-	-	-	-	-	-	199	8,67E-03
Drosophila melanogaster	AF-Q9VIK5-F1-model_v2	CG2617	-	-	-	-	-	-	-	-	-	-	-	-	186	1,76E-02

Supplemental Figure S17. Searching AlphaFold2's protein structure datasets via Foldseek, using ZC3HC1 and BIR protein structures as queries.

In order to search for proteins with ZC3HC1-reminiscent structures in those insect species, like *Drosophila melanogaster*, that appear to lack a homologue of ZC3HC1 recognizable as such at the protein sequence level, we used the Foldseek tool (https://search.foldseek.com/search; van Kempen *et al*, 2022) for conducting some first searches among the PDB files of the AlphaFold/ Proteome v2 database (here abbreviated as afdb-proteome). As query structures, we used those of the human, amoebic and budding yeast ZC3HC1 homologues (Uniprot identifiers Q86WB0, Q54PS8, and Q03760, respectively), which we also used in their truncated versions (here referred to as the minimal structures), corresponding to those presented in Supplemental Figure S12B, lacking the loops and most of the other parts not regarded as belonging to the NuBaID. In addition, we used the *Drosophila melanogaster* BIR protein Diap2 (Q24307) as a query structure for comparison. Searches via Foldseek were conducted in the 3Di/AA mode, using the taxonomic filter for the respective other species, with searches among the *D. melanogaster* structures having been complemented by searching the human, amoebic and budding yeast structure datasets for comparison. All identified structures and their scores, as obtained with the default settings of Foldseek and retrieved from Foldseek's web server, are presented. Note that these searches, for now, did not reveal a *Drosophila* protein structure that we would regard as a likely ZC3HC1 equivalent, with the only non-ZC3HC1 structures identified with the ZC3HC1 query structures being known BIR proteins. By contrast, when searching the database-deposited human, amoebic, and budding yeast structures with either the *Hs*ZC3HC1, *Dd*ZC3HC1, or

*Sc*Pml39p structure as the only query, the two other species' ZC3HC1 structures were in each case identifiable as the best matches when using the homologues' loop-free NuBaID structures.

Supplemental Discussion

Supplemental Discussion 1. The NuBaID and BIR domains as characteristic constituents of their holders.

Supplemental Discussion 2. Some pending questions regarding the two or more ZC3HC1 paralogues in those species that have undergone genome duplication events.

Supplemental Discussion 3. Considerations regarding the Pfam motifs zf-C3HC and Rsm1, together with a suggestion for a single, all-characteristics-encompassing novel signature describing the bimodular construction of prototypic ZC3HC1 homologues.

Supplemental Discussion 4. Thoughts on ZC3HC1 homologues with conspicuously long BLD2-inserted loops in some insects, while ZC3HC1 appears absent in others, and on remarkable length differences between loops of ZC3HC1 paralogues in plants.

Supplemental Discussion 5. Considerations regarding the multisite-phosphorylation of ZC3HC1 and its BLD2-embedded loop in interphase.

Supplemental Discussion 6. *Sc*Pml39p and *Hs*ZC3HC1: A kinship of two bona fide NB proteins long unrecognized.

Supplemental Discussion 7. An alternative approach to interpreting specific phenotypes upon excess or absence of Pml39p?

Supplemental Discussion 8. Further thoughts regarding the presence of ZC3HC1 in many organisms and its absence in others.

Supplemental Discussion 9. The existence of NBs in ZC3HC1-deficient insects and the inevitable question regarding the positioning of the ZC3HC1-dependent TPR polypeptides in other species.

Supplemental Discussion 10. To have or have not: Extended considerations regarding trade-offs underlying the absence of a ZC3HC1 homologue in some species and its presence in others.

Supplemental Discussion 1. The NuBaID and BIR domains as characteristic constituents of their holders.

The BIR domains have been described as comprising approximately 70 amino acids, including three invariant cysteine residues plus one histidine for tetrahedrally coordinating a zinc ion (Birnbaum *et al*, 1994). They are a characteristic feature of the IAPs, which also exist in insects (e.g., Orme & Meier, 2009; Berthelet & Dubrez, 2013) while absent in plants (e.g., Higashi *et al*, 2005; Cao *et al*, 2008; https://pfam.xfam.org/family/BIR). Each of the IAPs possesses at least one and often two or three of these zinc finger modules, and in some rare cases, perhaps more (e.g., Mace *et al*, 2010a; Silke & Vucic, 2014; Sharma *et al*, 2017; https://pfam.xfam.org/family/BIR).

Even though we found them to lack certain BLD-specific α-helices, it appears evident that the BIR domains share a common ancestor with the BLDs of the NuBaID, with such kinship already proposed in the past (Higashi *et al*, 2005; Kokoszynska *et al*, 2008) and with such notion now substantiated by further findings. While the BIR domain's most common H-$X_{(6)}$-C spacing of its zinc-coordinating histidine and third cysteine distinguishes it from the H-$X_{(3)}$-C arrangement of the NuBaID's two zinc finger modules, it had been noted early on that the BIR domain shares some additional, seemingly conserved residues with either the one or the other or both of the two potential zinc finger modules of several ZC3HC1 homologues. Based on such similarity, and since BIR domain-containing IAPs are absent in plants, the two ILP proteins in *Arabidopsis* had even been considered to take on tasks equivalent to those of the IAPs in other species (Higashi *et al*, 2005). Furthermore, such local similarities between the BIR domains' and the ZC3HC1 homologues' sequences thus led to naming each of the latter's two zinc finger modules a BLD (Higashi *et al*, 2005; Kokoszynska *et al*, 2008). The BLDs had also been described as containing two zinc fingers of the C2HC-type, but such former designations should neither be confused with the likewise called C2HC-type of zinc fingers, with its minimal consensus C-$X_{(4)}$-C-$X_{(12)}$-H-$X_{(5)}$-C (Kim & Hudson, 1992), nor with the so-called CCHC-type of zinc finger, also known as the zinc knuckle, with its minimal consensus C-$X_{(2)}$-C-$X_{(4)}$-H-$X_{(4)}$-C (Green & Berg, 1989).

As we now know, some of the NuBaID residues common to both the BLDs and BIR domains are essential for *Hs*ZC3HC1 and *Sc*Pml39p to adopt a conformation enabling them to bind to the NB. However, as has been reasoned in this study's main text, these BLD residues, among which are also the invariant ones of the NuBaID's minimal sequence signature, are likely not directly interacting with TPR. Instead, in line with a former homology model of the BLD1 of *Hs*ZC3HC1 (Higashi *et al*, 2005) and now also according to AlphaFold2's predictions, these

residues appear to participate in intramolecular interactions and to play, like the BIR domains' corresponding ones (Supplemental Figures S10C and S11C2), both direct and indirect roles in the establishment of shielded zinc ion coordination spheres. Such a similarity between the central parts of the BLDs and the BIR domain's core construction appeared particularly evident after having compared the BLD and BIR domains' structure predictions provided by AlphaFold2 (Supplemental Figure S11C and S11E), and these with the BIR domains' structures determined by X-ray crystallography (e.g., Cossu *et al*, 2019; https://www.rcsb.org; Supplemental Figure S11A). Therefore, even though the current version of the NuBaID signature allows for distinguishing the ZC3HC1 homologues of numerous, if not most, species from their BIR domain-possessing proteins, one must keep in mind that such a distinction via this signature only relates to a few residue preferences and their spacing within the core structures of these two related domains.

With the current versions of the here presented NuBaID signature thus not describing a TPR-binding interface, we expect that reports to come will unveil those sequence elements that define the BLDs' specificity for TPR and distinguish the BLDs' binding interfaces from those of the BIR domains. Some of these target specificity-defining sequence features are possibly already conjecturable from the HMMs of the Pfam database's zf-C3HC and Rsm1 motifs, and we can imagine them becoming even more evident once the sequences of the loop-free BLDs, in their newly defined boundaries, are taken into account for updating such motifs (also see Supplemental Discussion 3).

The NPC-associated TPR protein being a specific binding partner of the NuBaID and rather not a target of any BIR domain, was actually in line with us not having found any of the eight vertebrate IAP/BIR proteins (e.g., Deveraux & Reed, 1999; Dubrez-Daloz *et al*, 2008) as naturally interacting with TPR at the NB, neither in *Xenopus* oocytes nor in human tumor cell lines in standard growth conditions (our unpublished data). Furthermore, we also did not find ZC3HC1 stably binding to any other protein than TPR in normally growing human cells in interphase (our unpublished data; but see also Gunkel *et al*, 2021), and neither did we find ZC3HC1 to act as an inhibitor of apoptosis, at least not in its typical physiological concentrations within the cell (Gunkel *et al*, 2021).

However, we currently cannot exclude the possibility that one or the other of the ZC3HC1 BLDs might transiently interact with one or another of those proteins interacting with the IAPs, or with proteins equivalent to such IAP-interacting ones. We consider it tempting to speculate that the IAPs and ZC3HC1 might use similar mechanisms to regulate the interplay with their respective binding partners. In this context, we also have those proteins in mind that act as IAP

antagonists and that, upon stress stimulation, bind to the IBM groove of the type II BIR domains, like in the case of the natural BIRC4 antagonist Smac/DIABLO and thereby displace an IAP's actual binding partner (e.g., Verhagen *et al*, 2001; Gyrd-Hansen & Meier, 2010; Damgaard & Gyrd-Hansen, 2011; Cossu *et al*, 2019). Again in this context, we regard it as noteworthy that the BLD1, too, possesses a similarly positioned conspicuous groove (Supplemental Figure S11D). We now wonder whether the BLD1 groove might have a function equivalent to that of the IBM groove, perhaps allowing for modulating the interaction between ZC3HC1 and TPR at the NB as part of a cellular stress response.

This notion was also inspired by a few Smac/DIABLO polypeptides that we had found among those proteins co-precipitated with soluble ZC3HC1 when the latter had been immunoprecipitated from cell extracts (Gunkel *et al*, 2021, and our unpublished data). However, it still needs to be determined whether such findings reflect an interaction of physiological relevance. Nonetheless, we already propose to test the IBM antagonist molecules used for cancer research (e.g., Cossu *et al*, 2019) to investigate whether these might interact with ZC3HC1 and perhaps result in destabilization or even displacement of ZC3HC1 and TPR polypeptides from the NB.

Furthermore, even though such a groove at the BLD1-corresponding position is not to be seen in the BLD2, we noted those residues at the BLD2 position directly corresponding to the BIR domains' IBM groove to be conspicuously similar to those defining the IBM groove. We can imagine that these BLD2 residues, evolutionarily rather well conserved even among distant ZC3HC1 homologues, contribute to a ZC3HC1:TPR binding interface and that this region can be a target for certain compounds that would allow for some signal-induced modulation of ZC3HC1:TPR interactions.

However, apart from the evident similarities and those possibly still to emerge, the BLDs and the BIR domains characterize proteins that nonetheless conspicuously differ in several respects. Such differences not only relate to the BLDs being the characterizing feature of a generally unique, one-of-a-kind protein per species with a non-duplicated genome, in contrast to the BIRs, which can be part of several different proteins. Beyond that, the BIR domains are known to interact with different primary binding partners. In mammals, for example, such binding partners include, among others, tumor necrosis factor (TNF) receptor-associated factors (TRAFs), which interact with type I BIR domains, and effector caspases, which bind to the BIR domains of type II (e.g., Rothe *et al*, 1995; Roy *et al*, 1997; Takahashi *et al*, 1998; Chai *et al*, 2001; Huang *et al*, 2001; Riedl *et al*, 2001; Samuel *et al*, 2006; Gyrd-Hansen & Meier, 2010; Mace *et al*, 2010a, 2010b; Silke & Vucic, 2014; Lalaoui & Vaux, 2018). By contrast, current

evidence does not suggest that the BLDs of the vertebrate ZC3HC1 homologues stably bind directly to a regular binding partner other than TPR, also since other proteins formerly proposed as regular ZC3HC1 binding partners (e.g., Bassermann *et al*, 2005a, 2007; Kreutmair *et al*, 2020) were refuted (Gunkel *et al*, 2021) or assessed as unlikely (Supplemental Figure S13). In other words, while the BIR domains act as binding modules for several different proteins within a given species, the NuBaID with its two BLDs currently appears monogamous for only one stably to be bound target protein, namely TPR.

Furthermore, some of the IAP's BIR domains have been shown capable of forming homodimers, with examples, among others, including the BIR1 and the BIR3 domain of protein BIRC4 (Lu *et al*, 2007; Lin *et al*, 2007; Mastrangelo *et al*, 2008). However, whether such a capability of homodimerization would further distinguish the BIRs from the BLDs remains uncertain. So far, neither our experimental data in this context nor predictions by AlphaFold2 have allowed us to answer for sure whether ZC3HC1 can genuinely dimerize or not.

Clearly, however, another property again distinguishes the IAPs and their BIR domains from ZC3HC1 with its two BLDs strikingly: An individual BIR domain, either as a naturally occurring one as part of a single-BIR domain IAP or when part of an IAP with several of them, represents an autonomous binding unit. Even when separated from their neighboring BIR domains, the individual ones of an IAP, like BIRC4, can still interact with their respective target proteins (e.g., Mace *et al*, 2010a). By contrast, even though each of the two BLDs of ZC3HC1 on their own could well be capable of zinc ion coordination, neither of them when separated from each other, is capable of a sufficiently robust standalone interaction with TPR *in vivo*, which in the current study even held for the Y2H interactions in yeast cells. Our findings thus confirmed the conclusions of the study in which the BLDs had been described first (Higashi *et al*, 2005) and where the BLD repeat, i.e., the existence of two BLDs, had been predicted to be essential for the ILPs', i.e., the ZC3HC1 homologues' function.

In other words, while the affinity between one BIR domain and its regular target protein suffices for a lasting interaction, the bipartite NuBaID only allows for a lasting interaction with its corresponding TPR homologue, at least in humans and yeast, when both of its two BLDs are intact and connected. Again, in other words, while an IAP with several BIR domains does not necessarily require cooperativity between its different BIR domains for target protein binding, the two BLDs need to act in concert, either by both contributing to one complex TPR binding interface or by each binding separately but cooperatively to the NPC-anchored homodimers of TPR. Only the avidity of such a bivalent interaction might provide the required strength of interaction that allows for a lasting engagement of ZC3HC1 with TPR *in vivo*.

Furthermore, yet another criterion distinguishes the ZC3HC1 homologues from numerous members of the eukaryotic realm's IAPs. Many of the latter possess not only one or several BIR domains but also one or several other types of domains, among which are some that additionally enable homodimerization, allow for interaction with yet other proteins, or play a role in ubiquitination (e.g., Oberoi-Khanuja *et al*, 2013; Silke & Vaux, 2015; Cossu *et al*, 2019). The presence of such other domains applies, for example, to seven of the eight IAPs in humans, with only the small, single BIR domain-possessing BIRC5 lacking such an additional one. Five human IAPs even possess yet another type of zinc ion coordination system, namely the RING finger (e.g., Oberoi-Khanuja *et al*, 2013). By striking contrast, hardly any of the eukaryotic realm's ZC3HC1 homologues appear to possess, next to their BLDs, an additional protein domain of those currently known. In fact, upon careful inspection of the relatively few sequences corresponding to those illustrations that show, in the Pfam database, a zf-C3HC or an Rsm1 motif as part of a protein possessing different types of domains (https://pfam.xfam.org/family/zf-C3HC, https://pfam.xfam.org/family/Rsm1), we found most of these assemblages explainable differently. The underlying sequences, the majority of which were genomic, harbored computational errors in sequence interpretation, including misassembled sequences, wrongly predicted or assigned exons, or other types of errors (our unpublished data). Therefore, we conclude that, at least in higher eukaryotes, a genuine ZC3HC1 homologue can also be described by its lack of other known protein domains, thereby further distinguishing it from many of the BIR-possessing IAPs.

Finally, the other prominent feature that distinguishes the IAPs from many ZC3HC1 homologues is the latters' capability to harbor large sequence inserts at different sites within their bounds, including loop-like insertions within their second BLD that can be extraordinarily long, with only a few examples presented in the current study (Supplemental Figure S4). Even though such loops are also missing in some ZC3HC1 homologues, like in *Sc*Pml39p, they appear absent in the BIR domains far more commonly, if not categorically (see also https://pfam.xfam.org/family/BIR).

Supplemental Discussion 2. Some pending questions regarding the two or more ZC3HC1 paralogues in those species that have undergone genome duplication events.

It remains to be clarified whether all of the two or more ZC3HC1 paralogues in those species in which genome duplications have occurred represent TPR-binding proteins. The latter question holds, for example, for the *Arabidopsis* ILP proteins At1g17210 and At1g48950 (e.g., Higashi *et al*, 2005), and it holds even more so for the three or more ZC3HC1 paralogues found

in a few species, as in plant genera that have undergone several rounds of genome duplication. The resistance of at least two such plant ZC3HC1 paralogues and their NuBaID signatures against the pressure of evolutionary elimination could mean that one of the two has acquired yet another BLD-involving function, the latter then possibly plant-specific, as also considered for other pairs of paralogues that have persisted in plants (e.g., Blanc & Wolfe, 2004; Veitia, 2005). In this context, we regard it as of note that one of the *Arabidopsis* paralogues of ZC3HC1, At1g48950, was isolated in a genetic screen for proteins involved in the regulation of DNA demethylation pathways, with the gene's inactivation leading to hypermethylation phenotypes and to naming the protein MEM1 (methylation elevated mutant 1; Lu *et al*, 2020). Further investigations from the same laboratory then reported that MEM1 is also involved in preventing genomic DNA damage (Wang *et al*, 2022). We now consider it of particular interest whether MEM1, which represents the 594 aa-long and thus shorter one of the two ZC3HC1 paralogues in *Arabidopsis*, will turn out located at the plant's NBs, in order to there fulfill its function. Moreover, we currently wonder (i) whether the longer paralogue of 958 aa, with its conspicuously long loop-like insertion (Supplemental Figure S4; Supplemental List of Sequences), might exhibit similar or other properties (in this context, also see Supplemental Discussion 4), (ii) where it will turn out located, and (iii) whether both paralogues interact with the *Arabidopsis* homologue of TPR or with different proteins. So far, though, AlphaFold2's predictions of the BLDs of the two *Arabidopsis* paralogues have not revealed pronounced differences that would hint at one of them unambiguously no longer being able to bind to TPR. Both paralogues' BLD1 and BLD2 domains appear similarly constructed and equipped with the BLD-characteristic α-helices that are also part of the corresponding BLDs of *Hs*ZC3HC1, *Dd*ZC3HC1, and *Sc*Pml39p (our unpublished data). Nonetheless, without full knowledge of all prerequisites required for a functional TPR binding interface, it remains a matter of speculation whether both bind to the NB or not.

Supplemental Discussion 3. Considerations regarding the Pfam motifs zf-C3HC and Rsm1, together with a suggestion for a single, all-characteristics-encompassing novel signature describing the bimodular construction of prototypic ZC3HC1 homologues.

The first half of the NuBaID signature, applying to the first of the predicted two zinc fingers, resembles, to some extent, the Pfam database's zinc finger motif called zf-C3HC (Finn *et al*, 2006; http://pfam.xfam.org/family/zf-C3HC). Indicating a total of four specific cysteines (see also Supplemental Figure S2D1), we can imagine that this motif's name had been eponymic for the gene's name *ZC3HC1* (zinc finger C3HC-type protein 1; https://www.genenames.org/data/

gene-symbol-report/#!/hgnc_id/HGNC:29913). The NuBaID signature, however, does not include this fourth cysteine, as we found it dispensable for NE-binding and TPR interaction. Moreover, numerous proteins across the eukaryotic realm that we consider prototypic ZC3HC1 homologues do not possess such a fourth cysteine (also see Supplemental Figure S11H).

Furthermore, when we database-mined protein sequences from all across the eukaryotic realm for such that likely represent ZC3HC1 homologues, it became evident that the second half of the NuBaID signature, applying to the predicted other zinc finger, was often but not always predicted to overlap with sequence segments that included the Pfam signature called the Rsm1 motif, or parts thereof. This motif's name stemmed from the fission yeast protein Rsm1p (Yoon, 2004) that we, like others (Higashi *et al*, 2005), regard being the homologue of *Hs*ZC3HC1 in *Schizosaccharomyces pombe,* with *Sp*Rsm1 too containing a prototypic NuBaID signature, and now also a structure (https://alphafold.ebi.ac.uk/entry/O94506), as predicted by AlphaFold2, whose BLDs resemble those of *Sc*Pml39p.

Our finding that not all prototypic NuBaID proteins, though, are predicted to possess an Rsm1 motif might, in some cases, be explainable by the highly variable spacing between the C-$X_{(2)}$-C tetrapeptide and the H-$X_{(3)}$-C pentapeptide of the NuBaID's second zinc finger. These insertions, mainly representing connecting sequences coding for unstructured loops, are sometimes so extraordinarily long that the Rsm1 consensus might not always tolerate them. Furthermore, in some homologues, long sequence insertions also exist between the G-W dipeptide and the C-$X_{(2)}$-C tetrapeptide of the BLD2, e.g., in *D. discoideum*, *A. thaliana*, and *C. reinharditii* (see also Supplemental Figure S4 and Supplemental List of Sequences), and these insertions too might sometimes prevent the assignment of an Rsm1 motif to these ZC3HC1 homologues. On the other hand, it is noteworthy that the Rsm1 motif is also not detected in some of the other genuine NuBaID proteins in which the spacer sequence is very short, like in the case of *Sc*Pml39p, where it consists of only 16 amino acids. In again other cases, though, the reason for an Rsm1 motif not being detectable would simply be that the corresponding ZC3HC1 homologue has been mutated in the course of evolution and lacks a BLD2 domain (e.g., Figure 3B1 and Supplemental List of Sequences), as will also be discussed further below.

Clearly, though, whenever a sequence was predicted to possess a zf-C3HC signature together with an Rsm1 motif, or even when only one of the two was part of an incomplete sequence in hands, we eventually were able to class the corresponding protein as a ZC3HC1 homologue, or at least as a fragment thereof, next to some also naturally occurring mutated versions of ZC3HC1. Such assignment was based on the protein's possession of a prototypic NuBaID signature or at least unquestionable parts thereof, the latter then usually affirmed by a few

additional residues, which too are characteristic for this type of protein, even though some are evolutionarily less conserved and mostly specific for either only BLD1 or BLD2 (e.g., Supplemental Figures S2D1 and S11H). However, apart from such a minimal NuBaID sequence signature and the few other residues, the degree of sequence conservation between more distantly related ZC3HC1 homologues appeared, in general, relatively poor. With such findings suggesting early on that it is primarily the NuBaID that defines the properties common to such predicted homologues, we could confirm this actually to be the case, as we could demonstrate that *Dd*ZC3HC1 and *Sc*Pml39p are genuine homologues of *Hs*ZC3HC1.

Moreover, structure predictions then allowed us to redefine each BLD's expanse, with this, in turn, revealing that the C-terminal part of the BLD1 domain's zf-C3HC motif corresponds, in actual fact, to the N-terminal part of the adjacent BLD2. On the other hand, we found the Rsm1 motif to only relate to parts of the BLD2 of some homologues, like *Hs*ZC3HC1, while missing other structural elements of the BLD2 (Figure 6D).

Therefore, with the zf-C3HC motif not exclusively referring only to the BLD1 and with the Rsm1 motif only describing a short part of the BLD2, one might now consider redefining the expanse of the sequence stretches for which these signatures should hold. For example, one of the BLD2 residues one could now newly assign to an Rsm1 motif would be R185 of *Hs*ZC3HC1, as part of an α-helix that we had newly attributed to the BLD2 (e.g., Supplemental Figure S11G). Furthermore, we found R185 corresponding to R81 of the BLD1 of *Hs*ZC3HC1, with an arginine also present in a corresponding BLD1 α-helix of *Dd*ZC3HC1 and *Sc*Pml39p. Such an arginine had already been notable within the HMM logo of Pfam's zf-C3HC motif, too (Supplemental Figure S11H).

Moreover, one might consider adapting the Rsm1 motif's consensus sequence so that it would eventually describe the BLD2 of ideally all ZC3HC1 homologues since the current motif is insufficient for identifying every homologue regarded as prototypic. For example, both *Dd*ZC3HC1 and *Sc*Pml39p have not been assigned an Rsm1 motif to date.

Furthermore, one might also consider renaming the zf-C3HC motif since it indicates a total of four specific cysteines, of which one is absent in the vast majority of likely ZC3HC1 homologues. Moreover, one might even consider combining the zf-C3HC and Rsm1 motifs into one to encompass the ZC3HC1 homologues' entire NuBaID and then represent a more complex version of the current study's NuBaID signatures. In effect, this means we wish to propose to those with corresponding expertise to consider merging the NuBaID, the zf-C3HC, and the Rsm1 signatures into a single, all-characteristics-encompassing and then again freely database-

accessible novel signature, as present knowledge now allows us to argue that the individual signatures all represent the same one-of-a-kind type of protein.

With one reservation, though, regarding the resulting signature's name: as long as we cannot tell for sure that the current study's NuBaID signatures will eventually turn out to mark every ZC3HC1 paralogue with such a motif as a nuclear basket-interacting protein, one could conceive another, more universally applicable naming for this signature, without already assigning a function to it. Alternative names, for example, might be the zf-C2HC-tandem, the BLD-bimodule, or simply the zf-(C2HC)2 motif.

Supplemental Discussion 4. Thoughts on ZC3HC1 homologues with conspicuously long BLD2-inserted loops in some insects, while ZC3HC1 appears absent in others, and on remarkable length differences between loops of ZC3HC1 paralogues in plants.

As evident from the data presented in the current study, a necessity for flexible linkers cannot explain the large loops' persistence in a wide range of species. In fact, short flexible stretches like those located between the different structural elements of the BLDs of the NB-binding-competent *Hs*ZC3HC1 mutant 72–290_398–467 and, in particular, between the corresponding structural parts of *Sc*Pml39p suffice as the unstructured elements that all ZC3HC1 homologues would require for allowing their NuBaIDs to fold into their final conformation, including the inter-BLD interactions at the BLD1:BLD2 interface. Therefore, with evolution having tolerated such ZC3HC1 loops evolving in numerous species, we are currently wondering whether and which tasks there might be at the NB for such loops to fulfill (in this context, also see Supplemental Discussion 5), with demand and possibly accompanying antagonistic properties (also see Supplemental Discussion 8) then varying between different species.

The existence of huge loops in only a few insect orders of the cohort Polyneoptera, like in the Orthoptera and Phasmatodea, while ZC3HC1 homologues appear to have been lost altogether in most others, is cause for some additional thought. First, the seeming absence of ZC3HC1 in most insects probably reflects the outcome of separate evolutionary events, perhaps even with different underlying causes. As can be deduced from Figure 3B2, at least one *ZC3HC1* gene loss event appears to have occurred along the evolutionary path leading to Paleoptera like the Odonata, while another one would have happened at some point early in the evolution of the Neoptera, prior to the arising of the Eumetabola, the latter including for example Diptera like *Drosophila melanogaster*. Concerning the gene's loss during the Dipterans' evolution, one could now speculate how this might have come about and whether

loop-like insertions within the BLD2 of early Dipterans might have played a role, as outlined in the following.

Such a scenario would be based on several assumptions. One would be that ZC3HC1 would always have been a non-essential protein whose existence reflected the outcome of an evolutionary balancing act (also see Supplemental Discussion 8). Another one would be that a loop-free ZC3HC1 would represent the initial version of this protein, already functioning as an interconnector of TPR polypeptides at the NB, while the insertion of a loop-forming sequence into a BLD2 would represent an event that happened later. Then, at some point, possibly when beyond a certain length, such a loop would have turned into playing an additional role at the NB, meaning that the protein would have acquired a second functional property. Next, further expansion of the loop's length would have been advantageous concerning the protein's ability to execute the second function. However, beyond a certain length, with the loops in the Orthoptera perhaps defining the length possibly just so still acceptable, such a loop would also gradually come along with increasing problems in correctly assembling the BLD's zinc ion coordination sphere, with the second H-$X_{(3)}$-C pentapeptide widely separated from its corresponding C-$X_{(2)}$-C tetrapeptide. In other words, the loop's evolutionary expansion, to exploit the advantages such a loop could provide, would thus have been expedited at the cost of the protein's functionality regarding its initial task as a structural element of the NB. In again other words, gradually increasing the proportion of those ZC3HC1 polypeptides that no longer function correctly as structural NB components would eventually have neutralized the advantageous effects of an increasingly long loop. Provided then such a neutral point had been reached or overstepped if too many NB binding-incompetent ZC3HC1 polypeptides would represent a handicap, it is imaginable, both with and without adaptive forces at work, that the protein and its large loop would turn into a target for mutations. These could then, e.g., include such that would cause losing the second H-$X_{(3)}$-C pentapeptide, thereby eliminating a functional BLD2 and thus the protein's central function depending on its bimodular construction. Depending on whether the resulting truncated polypeptides would then be more readily tolerable as "molecular garbage" or still represent a problem for the cell, evolution could then dispose of these remnants more gradually or rapidly, blurring and eventually obliterating the traces of the insects' *ZC3HC1* gene over time.

Now, we wonder whether this or yet other speculative scenarios might recapitulate the fate that ZC3HC1 experienced very early in Neoptera evolution, near the lineage splitting point, about 260–250 million years ago (e.g., Thomas *et al*, 2013), beyond which the Orthoptera still continued possessing a ZC3HC1 homologue while the other Neoptera had lost their ZC3HC1.

Furthermore, as part of another mind game, we are also wondering whether such thoughts regarding the loop's advantages and disadvantages can also be adapted for the Viridiplantae that have undergone genome duplication events and now possess two ZC3HC1 paralogues. We consider it particularly remarkable that the loop of their one paralogue is of rather "normal length", similar to that in many other organisms, whilst the other paralogue's loop is always far longer (see Supplemental Figure S4 and Supplemental List of Sequences). Even though generally not reaching the extreme lengths in some Phasmatodea, the loop of the plants' second ZC3HC1 paralogue is generally several hundred residues longer than the other paralogue's loop. We now wonder whether such plants, having two ZC3HC1 paralogues at their disposal, take advantage of both opportunities, with perhaps the "normal-loop" paralogue readily fulfilling its task as a structural element at the NB. The second paralogue might then additionally or even solely exploit the longer loops' advantages. In combination, such task sharing might require less balancing between the two functions.

Supplemental Discussion 5. Considerations regarding the multisite-phosphorylation of ZC3HC1 and its BLD2-embedded loop in interphase.

Some of the ZC3HC1 phosphorylation events at the onset of mitosis might play a role in one of the steps eventually leading to complete ZC3HC1 solubilization along with NB disassembly. However, the multisite-phosphorylation of ZC3HC1 during interphase in response to extracellular stimuli suggests that ZC3HC1, in general, and the loop, in particular, could play some role in cellular stress response and along specific signal transduction pathways. One could, among several scenarios, imagine that some of those phosphorylation sites flanking the NLS of *Hs*ZC3HC1, the latter located between aa 398–404, could play a role in regulating the protein's nuclear import in certain situations. In this context, it is noteworthy that residues often detected phosphorylated are located between S395 and S411, with S407, in particular, appearing to be a prime target for kinases (https://www.phosphosite.org/proteinAction. action ?id=3471&showAllSites=true; also see Supplemental Figure S15).

In addition, once ZC3HC1 has been appended to the NB, one could imagine that the loop either surrounds the NB's terminal ring on its outer side or projects towards the NB's longitudinal mid-axis. In both cases, this would then, in turn, allow for further conceiving scenarios in which the loop would contribute in one way or the other to promoting or preventing some specific steps in nucleocytoplasmic transport. Phosphorylation of the loop at one or several of its numerous phosphorylation sites, also located between S321 and S395, would then

allow for regulating such steps on demand, with a more or less phosphorylated loop, for example, repelling specific molecules more or less efficiently.

Furthermore, and in addition to TPR, which is a target for stress-activatable phosphatases (Yadav *et al*, 2017; Wigington *et al*, 2020), we deem it possible that ZC3HC1, which also possesses prototypic binding sites for stress-activated phosphatases, like, e.g., for calcineurin at aa 390–393, might eventually turn out being a target too for such phosphatases, and other enzymes, in interphase.

Supplemental Discussion 6. *Sc*Pml39p and *Hs*ZC3HC1: A kinship of two bona fide NB proteins long unrecognized.

ZC3HC1 not having been identified earlier as a Pml39p homologue might have had several reasons. One of them, already mentioned further above (e.g., Supplemental Information 5), will have been the poor sequence similarity between *Sc*Pml39p and *Hs*ZC3HC1, which prevented finding the other species' homologue through standard primary sequence alignment searches, with this in line with the former reporting of a ZC3HC1 homologue not having been detectable in *S. cerevisiae* (Higashi *et al*, 2005).

Another reason will have been that ZC3HC1 had formerly been described as a protein of entirely different function and as constructed of completely different domains, with neither such domains nor function indicating any relation to the NPC or the protein's actual BLDs. Formerly named NIPA, ZC3HC1 had instead been reported as a nucleoplasmic F-box protein with a CCNB1 binding domain, to primarily occur as a regular part of an SCF-type (SKP1, CUL1, F-box) of multiprotein E3 ubiquitin ligase complexes, and to be directly involved in CCNB1 degradation and cell cycle regulation (e.g., Bassermann *et al*, 2005a, 2005b, 2007; Klitzing *et al*, 2011; Illert *et al*, 2012). These features have then been listed in several knowledgebases as the characteristics of ZC3HC1/NIPA ever since (e.g., https://www.genecards.org/cgi-bin/carddisp.pl?gene=ZC3HC1; https://www.uniprot.org/uniprotkb/Q86WB0/entry#names_and_taxonomy; https://www.ncbi.nlm.nih.gov/gene/51530). None of these functions and domains hinted at Pml39p, excluding ZC3HC1 for long as a possible candidate for a Pml39p homologue. Only recently, the abovementioned data relating to ZC3HC1 as an F-box and SCF protein have been refuted (Gunkel *et al*, 2021), with this information now also considered in some knowledgebases (e.g., https://omim.org/entry/619746).

In theory, yet another reason might have been that *Hs*ZC3HC1 had been assigned yet another function, namely as an anti-apoptotic protein (Higashi *et al*, 2005), further distinguishing it from *Sc*Pml39p. Again, experiments scrutinizing the role of ZC3HC1 in apoptosis have been reported

only recently (Gunkel *et al*, 2021). Moreover, with *Hs*ZC3HC1 initially considered an anti-apoptotic protein and thereby named ILP1 (Higashi *et al*, 2005), this name, in this context, might have also been misleading, as ILP1 represents an alias for the human anti-apoptotic BIR protein XIAP/BIRC4 (e.g., Duckett *et al*, 1996; Richter *et al*, 2001; https://www.genecards.org/cgi-bin/carddisp.pl?gene=ZC3HC1). However, it could also be that such confusion had never occurred – simply because this first paper describing the construction of ILP1 as a likely bimodular protein composed of two BLDs (Higashi *et al*, 2005) is not identifiable in NCBI-Pubmed anyhow when searching this literature database (https://pubmed.ncbi.nlm.nih.gov/) for ZC3HC1, NIPA, or its other listed aliases (https://www.genecards.org/cgi-bin/carddisp.pl?gene=ZC3HC1; https://www.uniprot.org/uniprotkb/Q86WB0/entry#names_and_taxonomy). The impossibility of identifying this particular study in a direct search for ZC3HC1/NIPA may also have been the reason why it had not been cited in the sequence analysis study of Kokoszynska *et al*, 2008. Then, in turn, regarding this latter study, it is of further note that NIPA had been described there as a prototypic BIR domain protein, additionally equipped with the alleged F-box and CCNB1-binding domain reported by others. Any consideration of this presentation of NIPA as a multidomain protein composed of four modules (Kokoszysnka *et al*, 2008) would have distinguished this protein from Pml39 even further.

The reason why Pml39p itself, identified in a synthetic lethal screen with a *nup133*Δ mutant (Palancade *et al*, 2005), appears not to have been generally considered a bona fide NB protein (Köhler & Hurt, 2007, 2010; Grossman *et al*, 2012; Niepel *et al*, 2013; Floch *et al*, 2014; Ptak *et al*, 2014; Obado *et al*, 2016; Lin & Hoelz, 2019; Fernandez-Martinez & Rout, 2021; Dultz *et al*, 2022) might be similar to the reason which for long prevented detecting *Hs*ZC3HC1 as an NB protein: While ZC3HC1 is a protein stably bound to the NB under physiological conditions, it is rapidly detached when exposed to the non-physiological conditions of standard cell fractionation protocols (Gunkel *et al*, 2021; Gunkel & Cordes, 2022). Furthermore, once the genuine *in vivo* interactions between native TPR and ZC3HC1 polypeptides have been disrupted in such a way, notable amounts of these parted proteins do not appear inclined to readily re-associate again *in vitro*, even when having re-instated conditions that more closely again resemble those within cells. Since common yeast and mammalian cell fractionation protocols share non-physiological similarities, we can now imagine that sensitivity towards such conditions also applies to the interactions between the Pml39 and Mlp polypeptides (for further comments along this line, also see Supplemental Information 9).

Supplemental Discussion 7. An alternative approach to interpreting specific phenotypes upon excess or absence of Pml39p?

Formerly, different phenotypes observed upon the overexpression of Pml39p or its absence in *pml39*Δ cells have been directly attributed to Pml39p itself, the latter imagined to interact directly with mRNP proteins or the splicing machinery (Palancade *et al*, 2005). We can, however, also imagine interpreting some of the phenotypes formerly observed in yeast in an alternative manner, which might assign Pml39p only an indirect contribution. Instead of conceiving Pml39p as directly interacting with different RNA-binding proteins, we consider it imaginable that some of the phenotypes observed upon the absence and overexpression of Pml39p might have reflected a consequence of subpopulations of Mlp1 polypeptides then having occurred mislocalized. A scenario in which not only the absence but also an excess of Pml39p causes Mlp1p mislocalization would be similar to what we noted in human cells, in which subpopulations of TPR can be found mislocalized both when ZC3HC1 is absent and when highly overexpressed (Gunkel *et al*, 2021; Gunkel & Cordes, 2022). However, one should also keep in mind that neither the nucleoplasmic Mlp1p amounts in the *pml39*Δ cells (Figure 5A) nor the large nucleoplasmic pools of soluble TPR in different ZC3HC1 KO cell lines (Gunkel & Cordes, 2022) appear to interfere with normal cell cycle progression, which argues against some TPR/Mlp1p-interacting proteins being mislocalized or sequestered within these cells' nucleoplasm in pivotal amounts.

Supplemental Discussion 8. Further thoughts regarding the presence of ZC3HC1 in many organisms and its absence in others.

While in some organisms, like in most insect orders, all signs of a former ZC3HC1 and its NuBaID signature appear to have disappeared, suggesting the protein's ultimate loss, other organisms possess ZC3HC1 homologues with aa substitutions or deletions that would render the human homologue incapable of binding to the NB and TPR. Notably, these potential mutant versions of ZC3HC1 so far appear mostly impaired with regard to their BLD2, with parts of the latter sometimes still recognizable in some species and absent in others *in toto*, while the appertaining BLD1 appears unaffected. Moreover, having scrutinized those database-deposited sequences that suggested the existence of truncated ZC3HC1 versions comprising only BLD2 while lacking an intact BLD1, we found these BLD2-only versions of ZC3HC1 to be incomplete merely for procedural reasons, as we could identify an associated BLD1 for each of them (our unpublished data). Among these seemingly BLD2-only versions were also 48 cases

listed till then in the Pfam database for the Rsm1 motif (https://pfam.xfam.org/family/PF08600).

Based on these findings, we initially thought that it was mostly the BLD2 that had been a target for mutations in those species in which they appeared to have occurred, like in several unicellular organisms and some marine invertebrates. For example, in all tunicates for which sequence information was available by the end of this study, like for the genus *Ciona* of the class Ascidiacea, some of the second BLD's zinc ion-coordinating residues were found exchanged for such not capable of zinc ion coordination. In other tunicates again, like in the genus *Oikopleura* of the class Appendicularia, the second BLD appeared to have been entirely lost.

We further noted such putative signs of ZC3HC1 homologues being in a state of disintegration, by either a complete loss of their BLD2 or by accumulating mutations that one would regard as abolishing their former zinc ion coordination ability, to exist also in very different organisms. Among them are, as another example, the xerophilic fungi of the genus *Wallemia*, in which we additionally confirmed the second BLD's absence by cDNA cloning and sequencing of the "residual" ZC3HC1 homologue of *Wallemia mellicola*, thereby supporting an already database-deposited sequence (see Supplemental List of Sequences).

We also need to note, though, that we do not exclude the existence of naturally occurring single aa substitution mutations also within the BLD1, as exemplified by the ZC3HC1 homologue from *Zygosaccharomyces mrakii* (XP_037145256.1; see Supplemental List of Sequences), which despite its sequence mutation, has a Pfam zf-C3HC motif assigned to it nonetheless. Assuming this sequence can be confirmed to be correct, one could further imagine this homologue no longer capable of binding to an NB, with this assumption based on presuming that this species' aa substitution, when introduced into *Hs*ZC3HC1, would abolish the NB-binding capability of the latter, with this particular substitution though still having to be tested.

Apart from that, it certainly will require further efforts to systematically screen and verify the sequences of ZC3HC1 homologues for those that harbor aa substitutions that might abolish a homologue's ability to bind to the NB. Currently, we can only tell that the frequency of potential NB-binding-competence-abolishing mutations as yet noted within the different species' BLD domains appears conspicuously higher in the BLD2 when compared to the then relatively few potential ones so far detected in sequences encoding the BLD1.

Such findings and conclusions, though, then raise further questions. For example, if the functions of *Hs*ZC3HC1 and *Sc*Pml39p, and the sequence prerequisites for a NuBaID with two

BLDs both required for binding TPR and Mlp1p, would also hold for other species' ZC3HC1 homologues, and if one of the latter would then be destined for decay by evolution for whatever reasons, one might not necessarily expect the detectable mutations in some clades primarily occurring within or even confined to the BLD2 alone. One could, therefore, ask whether the remaining, seemingly intact BLD1 might still be good for something in these organisms. If this were the case, one could imagine the single-BLD version having compensated for the second BLD's loss and evolved the means to bind to TPR on its own, thus still allowing for fulfilling distinct tasks at the NB. Of course, one could also imagine such a single-BLD ZC3HC1 variant to be located somewhere else within the cell, where it might fulfill an NB-unrelated function instead of spending merely a non-functional existence as molecular garbage prior to its complete elimination over time. Studying organisms in which such seemingly truncated ZC3HC1 versions exist, and determining their subcellular locations, should now rather straightforwardly allow distinguishing between some of these possibilities.

However, if the seemingly mutated ZC3HC1 versions reflect a state of ongoing evolutionary decay, or even if they represent polypeptides with some residual functional activity or novel tasks, this brings us back to the question of why no selective pressure has preserved the protein's original version and function. One could further ask whether the ZC3HC1 homologue's original might merely have been lost incidentally or whether evolutionary forces might actually have been selecting against it in certain species. Such questions, of course, also apply to those organisms in which ZC3HC1 homologues are no longer detectable at all.

In one scenario, the protein would simply no longer have been of use for a particular species during its replicative lifespan or reproductive phase, with no remaining selective pressure maintaining its existence as a functionally intact protein. Even if minor deficits might have come along with its absence, one could imagine these to have been compensated for by co-evolved counter-steering adaptations of other proteins**.** In other words, during the adaptation to its current environment, such a species' ZC3HC1 homologue, formerly favorable in another environment, would have turned into a gene whose contribution to the species' fitness would eventually have been neutral, with this then also describable as conditional neutrality (e.g., Bargiello & Grossfield, 1979; Anderson *et al*, 2013).

In a different scenario, the presence of a species' ZC3HC1 homologue, while again advantageous in some situations, would be disadvantageous in others, resulting in fitness trade-offs. Evolutionary forces would then have expedited the gene's elimination once the disadvantages started overwhelming, with this reflecting the concept of antagonistic pleiotropy (e.g., Roff & Fairbairn, 2007; Anderson *et al*, 2011; see also Carter & Nguyen, 2011). The

absence of ZC3HC1 in some organisms would then no longer be interpretable as the fate of a gene that has turned out useless and no longer required at some point. Instead, it then would reflect a gene whose protein has turned into being more detrimental than advantageous, eventually exhibiting an unbearable property that demanded to be selected against in order to be disposed of by evolution.

Related to these notions, we wonder whether the existence of the extremely long BLD2 insertions in the ZC3HC1 homologues of the Orthoptera might hint at one scenario of how such a fate of becoming dispensable or disadvantageous over time might have come to pass and eventually have led to the ZC3HC1 homologues' absence in the other insect orders of the Neoptera (also see Supplemental Discussion 4 and Supplemental Figure S4).

However, we do not regard either one or the other of these different scenarios as solely possible, and we can imagine that ZC3HC1 homologues in different organisms have been lost for different reasons. Summarizing the abovementioned scenarios, the homologues in some species would have become dispensable once their possession no longer provided a fitness advantage, resulting in the accumulation of incidental mutations over time. And in other species, a trade-off between the ZC3HC1 homologues' pros and cons would have tilted to the disadvantageous side, causing evolutionary forces to exert selective pressure for achieving the protein's elimination.

In the main Discussion, we also regarded it as noteworthy that Pml39p belongs to a minor group of less than 4% of all protein-coding yeast genes whose deletion notably extends the yeast's replicative lifespan (McCormick *et al*, 2015). Here we now further suggest that the absence of a ZC3HC1 homologue may also have some moderate life span-prolonging effect in mammals, with some indications coming from studies in ZC3HC1 KO mice (e.g., Aherrahrou *et al*, 2021). Such effect would be in line with elderly ZC3HC1 KO mice outperforming, concerning some physiological parameters, their wild-type siblings with whom they shared a cage for year-long periods, and with such KO mice featuring, for example, viscera that often appear seemingly young, even at old age (our unpublished data).

Such observations of ZC3HC1 KO mice possibly being slightly more long-living, despite the deficits they had to live with since they were young, and then barely exhibiting additional deficits at a higher age, in contrast to their ZC3HC1-possessing siblings, underscores the notion that lacking a ZC3HC1 homologue does not only need to come along with irrelevance in some species and disadvantages in others, but can also have its advantages. The benefits would then manifest themselves later in life. Conversely, regarding the WT mice, ZC3HC1 would thus manifest most of its advantages in young adults, but start revealing its disadvantages at an older

age, with such a change in the weighting of properties conforming to the original definition for antagonistic pleiotropy (Williams, 1957; see also, e.g., Gavrilov & Gavrilova, 2002; Montano & Long, 2011).

However, even if ZC3HC1 might eventually turn out to be the product of a trade-off gene, exhibiting advantages and disadvantages in different environmental conditions, and causing antagonistic pleiotropic effects in the young and old, one will still need to find out how these effects can be explained by ZC3HC1 and TPR being structural proteins and correlated with their presence at the NB.

Finally, we propose ZC3HC1 also as a general model for studying different aspects of both adaptive and neutral protein evolution (e.g., Akashi *et al*, 2012; Galtier, 2016; Albalat & Cañestro, 2016) by gaining insight into which types of evolutionary causes have affected the different ZC3HC1 homologues' evolutionary history. Being a protein (i) probably non-essential in most organisms, (ii) nonetheless existing as a functional version in many species while appearing mutated or absent in others, (iii) exhibiting some features strikingly different among species, like a sprawling BLD2-inserted loop in some and its complete lack in others, while at the same time (iv) featuring an evolutionarily conserved centerpiece, ZC3HC1 combines all the ingredients that compose a challenging riddle posed by evolution, with such riddle now demanding to be solved.

Supplemental Discussion 9. The existence of NBs in ZC3HC1-deficient insects and the inevitable question regarding the positioning of the ZC3HC1-dependent TPR polypeptides in other species.

ZC3HC1-deficient organisms can still possess an NB, attested by its presence in insects. In these, the NBs have been studied in the relatively large nuclei of the salivary gland cells of the midge *Chironomus tentans* (Kiseleva *et al*, 1996, 1998), which belongs like *Drosophila* to the order Diptera, possesses a TPR homologue (e.g., Soop *et al*, 2005) just as likely all insects do, but lacks an identifiable ZC3HC1 homologue, just as it is the case for most insect orders. Nonetheless, the midge's NB structure appears similar to the NB commonly regarded as prototypic in the ZC3HC1-containing vertebrate oocyte. Even though the reported length and diameter of the insect's NB fibrils (Kiseleva *et al*, 1996) would have them be shorter and thicker than those in vertebrates, there described as more extended and notably thinner (e.g., Ris, 1991, 1997; Jarnik & Aebi, 1991; Gunkel *et al*, 2021), these differences likely reflect, to a large part, the outcome of different sample preparation procedures. Some of the latter included, for

example, coating the specimens with relatively thick layers of heavy metals, which other protocols did not.

However, if one assumes that no conspicuously different structures are hidden beneath such coats of metal that would distinguish the insects' from the vertebrates' NB fibrils, this raises the next inevitable question. Namely, where are those TPR polypeptides positioned that are appended to the vertebrate NB by ZC3HC1? And the same question also applies to yeast and its Pml39p-dependent Mlp1p subpopulation.

In theory, a thinkable answer would sketch a scenario in which there actually are no significant differences between the insects' and the vertebrates' NBs, simply because insects would still possess a ZC3HC1 homologue whose NuBaID signature merely diverged from the current consensus beyond recognizability during insect evolution, while still acting as a TPR-interlinking structural NB component nonetheless. One could then speculate whether this might have come along with, for example, other combinations of cysteine and histidine residues or with residues like aspartate and glutamate as zinc ion coordinating ligands (Laitaoja *et al*, 2013) instead of one or the other of the NuBaID's cysteines and histidines. Along a similar line, one could alternatively also conceive that the function of ZC3HC1 at the NB has been taken over by another yet unknown insect protein capable of binding to the NB and of NB-appending TPR polypeptides in a manner analogous to ZC3HC1.

However, while we deem such scenarios not yet proven ruled out, we regard the other signs pointing at a ZC3HC1 homologue having been lost without substitution in various organisms, including insects, as more compelling. We felt this assumption underscored by the outcome of searching AlphaFold's database with the recently available protein structure search tool Foldseek (van Kempen *et al*, 2022). The latter allowed us to seek protein structures of *Drosophila melanogaster* that might come into question as structural homologues of *Hs*ZC3HC1, *Dd*ZC3HC1, or *Sc*Pml39p. However, other than known BIR proteins, these searches, for now, did not reveal *Drosophila* structures that we would instantaneously regard as likely candidates. By contrast, when searching the database-deposited human, amoebic, and budding yeast structures with either the *Hs*ZC3HC1, *Dd*ZC3HC1, or *Sc*Pml39p structure as the only query, the two other species' ZC3HC1 structures were in each case readily identifiable as the best matches (Supplemental Figure S17).

This situation, though, would momentarily leave us with neither a homologue nor an analog of ZC3HC1 in insects, and consequently with no additional TPR amounts appended to the insects' NB, while at the same time, we would remain confronted by micrographs of similarly looking NBs in both insects and vertebrates. This seeming riddle thus leaves us now with the

task of providing an answer elsewhere (Gunkel *et al*, manuscript in preparation) as to how at least the ZC3HC1-dependent TPR polypeptides in vertebrates are arranged at the NB.

Supplemental Discussion 10. To have or have not: Extended considerations regarding trade-offs underlying the absence of a ZC3HC1 homologue in some species and its presence in others.

The presence of ZC3HC1 in many organisms and its absence in others raise questions. Some are addressed in Supplemental Discussions 4, 8, and 9, and others in the following.

In this context, one needs to know that ZC3HC1 homologues are non-essential in different organisms, including budding and fission yeast (Yoon, 2004; Palancade *et al*, 2005), the nematode *C. elegans* (Rual *et al*, 2004; Sönnichsen *et al*, 2005), and mice (e.g., Illert *et al*, 2012; Aherrahrou *et al*, 2021; our unpublished data). Moreover, CRISPR/Cas9n-mediated inactivation of the human *ZC3HC1* gene did not notably affect cell growth and normal cell cycle progression of tumor and non-tumor cell lines (e.g., Hart *et al*, 2015; Gunkel *et al*, 2021).

However, male ZC3HC1 KO mice are infertile (Illert *et al*, 2012), and both sexes exhibit several other phenotypes and limitations. Some of them would likely prevent such mice from surviving in a competitive natural environment. For example, although ZC3HC1-deficient mice often appear lively and metabolically in a seemingly favorable condition, they are generally far more slender and fine-boned than their wild-type kin. Such phenotypes are sometimes accompanied by, e.g., one or the other kind of skeletal abnormality (our unpublished data; see also www.mousephenotype.org/data/genes/MGI:1916023; www.informatics.jax.org/marker/MGI:1916023). In other organisms, though, the experimental removal of ZC3HC1 did not lead to overt detrimental phenotypes. And those organisms that seem to have naturally lost a functional ZC3HC1 homologue during evolution also survive in its absence.

On the one hand, this raises the question of what species-spanning general advantage does ZC3HC1 provide in the numerous organisms, in which selection pressure ensures persistence of this protein. And, on the other hand, why it had become dispensable or perhaps even disadvantageous for those organisms that lost it during evolution.

These questions inevitably come along with yet another one. *TPR* in some organisms, including mammals and insects, is an essential gene, meaning that those TPR polypeptides appended to the NPC independently of ZC3HC1 are indispensable. The latter also appears to be the case in proliferating human cells, as we could not generate TPR KO cell lines by CRISPR/Cas9n technology. However, NB-appendage of TPR by ZC3HC1 is not essential, as currently known ZC3HC1 KO organisms are viable. Furthermore, one could assume that the

ZC3HC1 deficiency caused by evolution could also have come with the inability to attach additional TPR to the NBs. Thus, one needs to ask why such TPR subpopulations would be dispensable for the ZC3HC1-deficient organisms. These species can still have TPR-containing NBs, as attested in insects of the order Diptera (Kiseleva *et al*, 1996; Soop *et al*, 2005; for further considerations, see Supplemental Discussion 9). While such insects were initially considered ZC3HC1-deficient only based on sequence searches, potential homologues were now also not found with structure search tools like Foldseek (van Kempen *et al*, 2022; Supplemental Figure S17).

Assuming these eukaryotes once had a functional ZC3HC1 homologue, this brings us back to how and why they lost it. In one scenario (for further considerations, see Supplemental Discussions 4, 8, and 9), the protein would have become disadvantageous for some species in certain situations and environments, with evolutionary forces then expediting its elimination. Such a notion of a trade-off between advantages and disadvantages finds support in several systematic studies in *S. cerevisiae*. In these, homozygous *pml39*Δ cells were found viable in various growth conditions considered approximations of typical environments experienced by wild, domesticated, and laboratory yeast strains. Pml39p deficiency in these conditions did not or only minimally affect the competitive fitness of the KO cells compared to the WT strains (e.g., Breslow *et al*, 2008; Qian *et al*, 2012). However, when exposed to a plethora of chemical, physical or nutritional stress conditions, the competitive fitness of *PML39w*t and *pml39*Δ cells differed significantly in some of these conditions. While the *pml39*Δ cells were more sensitive to certain types of acute stress and the triggering of distinct signal transduction pathways, they outclassed the *PML39w*t cells by being more tolerant of nutritional deficiencies and other types of stress (Brown *et al*, 2006; Hillenmeyer *et al*, 2008). Overall, these screening data suggest that the existence of Pml39p in free-living yeasts reflects a balancing act between pros and cons.

We also find it remarkable that many prominent phenotypes observed with the *pml39*Δ strains were similarly pronounced in *mlp1*Δ strains. By contrast, such phenotypes were notably different from those of the homozygous or heterozygous deletion strains of other known NB-associated proteins like Mad1p, Sac3p, Ulp1p, and, in particular, also Mlp2p (Hillenmeyer *et al*, 2008). These findings are consistent with our idea of a special structural-functional relationship between Pml39p and Mlp1p. Although a few other phenotypes appeared *pml39*Δ-specific, which could indicate some additional, standalone functions of Pml39p, such findings could instead reflect the absence of those Mlp1p subpopulations that usually occur NB-attached via Pml39p. In fact, one can expect that some tasks of these Mlp1 polypeptides differ from those fulfilled by Mlp1p that occurs NPC-anchored independently of Pml39p. Furthermore, we also

consider it noteworthy that some disadvantages caused by homozygous *PML39* deletion are also observed, though less pronounced, in the heterozygous *pml39*Δ cells (Hillenmeyer *et al*, 2008). Such findings indicate haploinsufficiency and the need for sufficient copy numbers of Pml39p to fulfill its function properly.

In the context of trade-offs between advantages and disadvantages in different situations and life stages, it is interesting that Pml39p belongs to those less than 4% of all protein-coding yeast genes, whose deletion notably extends yeast replicative lifespan (McCormick *et al*, 2015). This finding raises the question of whether this phenotype could result from the enhanced oxidative stress tolerance of *pml39*Δ cells (Brown *et al*, 2006; Hillenmeyer *et al*, 2008).

Furthermore, we can imagine that losing a *ZC3HC1* gene may also be advantageous for other organisms at some time. For example, some physiological phenotypes observed with elderly ZC3HC1 KO mice (also see Supplemental Discussion 8) may be related to certain phenotypes observed upon Pml39p deficiency. Overall, we can imagine that the existence of a unique but non-essential *ZC3HC1*/*PML39* gene in some organisms and its absence in others reflects a dynamic balance between advantages in some situations and life stages and disadvantages in others. *ZC3HC1* would then conform to the current definition of a gene with multiple opposing effects on fitness, and thus with antagonistic pleiotropy (e.g., Kirkwood, 2002; Elena & Lenski, 2003; Mitchell-Olds *et al*, 2007; Anderson *et al*, 2011; Qian *et al*, 2012; Austad & Hoffman, 2018).

In conclusion, while future research might naturally focus on elucidating the advantages that ZC3HC1, and the TPR it attaches to the NB, will provide to those with a ZC3HC1 homologue, we argue there may also be a dark side to possessing this protein and the ZC3HC1-dependent TPR at the NB. However, even if ZC3HC1 were the product of a trade-off gene, future work would still need to unveil how the structural arrangements of ZC3HC1 and TPR at the NB could cause both positive and negative effects.

Supplemental Materials and Methods

Antibodies

Mouse monoclonal antibody 203-37 against *Hs*TPR (Cordes *et al*, 1997), whose epitope was mapped to a region comprising aa 1462–1500 (Hase *et al*, 2001; Gunkel *et al*, 2021), has been described earlier. Similarly, guinea pig peptide antibodies against *Hs*TPR aa 2063–2084 (Cordes *et al*, 1997) and *Hs*ZC3HC1 aa 307–355 (Gunkel *et al*, 2021) have been described. The same pool of pan-FG-NUPs rabbit antibodies already used earlier (Göttfert *et al*, 2013) represented antibodies obtained after immunization with the FG-repeat domain of the *Xenopus* oocyte NB-associated protein *Xl*GANP. From these anti-*Xl*GANP sera, we had isolated by sequential affinity-chromatography, using a series of overlapping FG domain peptides and recombinant proteins, as illustrated for other proteins (Gunkel *et al*, 2021), antibody subpopulations either specific for xlGANP or cross-reactive with numerous FG-NUPs. The most broadly cross-reactive ones of these pan-FG antibodies targeted all of a comprehensive collection of bacterially expressed and purified FG-repeat domains of *Xenopus* and mammalian FG-NUPs. Novel peptide antibodies against synthetic peptides (Peptide Specialty Laboratories, Heidelberg, Germany), coupled via a C-terminal (i) or N-terminal (ii) cysteine to keyhole limpet hemocyanin, were raised in guinea pigs, followed by peptide affinity purifications using standard procedures. These peptides included such corresponding to aa 3–23 of *Dd*TPR (accession number ON368702) and aa 1–29 of *Dd*ZC3HC1 (ON368701). Rabbit polyclonal antibodies against *Hs*FANCD2, raised against aa 11–230 (NB100-182, Novus Biologicals, Abingdon, UK), and rabbit monoclonal antibody EPR2302, against an *Hs*FANCD2 epitope located between aa 180–250 (ab108928, Abcam, Cambridge, UK), were commercially obtained and had already been verified to target FANCD2, by using FANCD2 KO cells, according to the suppliers' information. All secondary antibodies were from Jackson ImmunoResearch (Cambridgeshire, United Kingdom), as listed earlier (Gunkel *et al*, 2021).

Culturing of cell lines and transfection with siRNAs for IFM and IB

Culturing of HeLa and HCT116 cells was performed as described (Gunkel *et al*, 2021). Cell lines were routinely tested and confirmed free of contaminations by mycoplasmas and other microorganisms. HeLa cell transfections with small interfering RNAs (siRNAs; see Supplemental Figure S13; CTRL siRNA, Ambion Silencer Select negative control #2 [cat. no. 4390846] | FANCD2-1 siRNA, Ambion Silencer Select s4988 [GCACCGUAUUCAAGUAC AA] | FANCD2-2 siRNA, Ambion Silencer Select s4989 [CAGCCUACCUGAGAUCCUA],

Thermo Fisher Scientific Waltham, MA, USA), using HiPerFect (QIAGEN, Hilden, Germany), followed by cell harvest at three days post-transfection and subsequent IFM, were performed as described, as were immunoblottings of cell extracts (Gunkel *et al*, 2021).

Sequence database mining and generation of sequence logos

The ScanProsite tool (de Castro et al, 2006; https://prosite.expasy.org/scanprosite) was commonly used for scanning the Swiss-Prot and TrEMBL protein sequence databases (Bairoch & Apweiler, 1997; https://www.uniprot.org/help/uniprotkb sections), while the original BLAST tools (Altschul *et al*, 1990) were used for the mining of NCBI's nucleotide and protein sequence databases. In addition, BLASTP was also used for reverse BLAST approaches to identify false positive sequences within whole genome sequencing (WGS) datasets, e.g., contaminating DNAs from a species' food sources or fungal or other evident contaminations. Furthermore, searches were conducted with tools using position-specific score matrices (PSSMs) like position-specific iterated (PSI)-BLAST (Altschul *et al*, 1997), via pattern hit-initiated (PHI)-BLAST (Zhang *et al*, 1998), and via domain-enhanced lookup time-accelerated (DELTA)-BLAST (Boratyn *et al*, 2012). In addition, other profile-based tools like pHMMER (Finn *et al*, 2011; Potter *et al*, 2018), next to others making use of HMMs; see Supplemental Information 3), were used for other profile-based approaches. WebLogos (Crooks *et al*, 2004) were generated with an online tool (https://weblogo.berkeley.edu/) using for this the original Pfam MSAs from the Pfam-A full datasets of different releases (http://ftp.ebi.ac.uk/pub/databases/Pfam/releases/), retrieved from Pfam database's FTP server (http://ftp.ebi.ac.uk/pub/databases/Pfam/). For generating HMM logos as vector graphics, Pfam seed sequences retrievable from the Pfam website (https://pfam.xfam.org/) were processed with the Skylign tool (Wheeler *et al*, 2014; http://skylign.org/).

Use of the UCSF Chimera system for structure analyses

Structural alignments, which in turn generated new sequence alignments, were performed with the Match-Align tool of the Chimera system. For the superimposition of the different homologues' BLD modules onto each other, Chimera's superimposition tools, including MatchMaker, were used. Chimera's structural analysis tool was used to compute and illustrate potential contacts of designated atoms of an aa side chain with neighboring aa residues (distance ≤ 4 Å). The UCSF Chimera tools enabling molecular graphics and analyses have been developed, with support from NIH P41-GM103311, by the Resource for Biocomputing, Visualization, and Informatics at the University of California, San Francisco.

Fast structural comparisons via Foldseek

The PDB files from the AlphaFold database for the human, amoebic and budding yeast ZC3HC1 homologues (Uniprot identifiers Q86WB0, Q54PS8, and Q03760) and the *Drosophila melanogaster* Diap2 protein (Q24307) were used as query structures for performing fast structural comparisons of these datasets on the Foldseek web server (https://search.foldseek.com/search; van Kempen *et al*, 2022). Foldseek searches for structures within the AlphaFold/Proteome v2 database were conducted in the 3Di/AA mode, using the taxonomic filter for the respective other species.

Supplemental Tables

Supplemental Table S1: Expression vectors

Description (promoter > expressed protein)	Backbone (resistance)	Source
ADH1>GAL4-BD (empty vector)	pGBT9 (Amp)	Clontech, Mountain View CA, USA
ADH1>GAL4-BD-*Dd*ZC3HC1(1–271_346–426_486–635)	pGBT9 (Amp)	This study
ADH1>GAL4-BD-*Hs*ZC3HC1(1–502)	pGBT9 (Amp)	This study
ADH1>GAL4-BD-*Hs*ZC3HC1(1–502 | C102S)	pGBT9 (Amp)	This study
ADH1>GAL4-BD-*Hs*ZC3HC1(1–502 | W107A)	pGBT9 (Amp)	This study
ADH1>GAL4-BD-*Hs*ZC3HC1(1–502 | C112S)	pGBT9 (Amp)	This study
ADH1>GAL4-BD-*Hs*ZC3HC1(1–502 | C117S)	pGBT9 (Amp)	This study
ADH1>GAL4-BD-*Hs*ZC3HC1(1–502 | C120S)	pGBT9 (Amp)	This study
ADH1>GAL4-BD-*Hs*ZC3HC1(1–502 | C125S)	pGBT9 (Amp)	This study
ADH1>GAL4-BD-*Hs*ZC3HC1(1–502 | H152A)	pGBT9 (Amp)	This study
ADH1>GAL4-BD-*Hs*ZC3HC1(1–502 | C156S)	pGBT9 (Amp)	This study
ADH1>GAL4-BD-*Hs*ZC3HC1(1–502 | W158A)	pGBT9 (Amp)	This study
ADH1>GAL4-BD-*Hs*ZC3HC1(1–502 | C249S)	pGBT9 (Amp)	This study
ADH1>GAL4-BD-*Hs*ZC3HC1(1–502 | W256A)	pGBT9 (Amp)	This study
ADH1>GAL4-BD-*Hs*ZC3HC1(1–502 | C272S)	pGBT9 (Amp)	This study
ADH1>GAL4-BD-*Hs*ZC3HC1(1–502 | C275S)	pGBT9 (Amp)	This study
ADH1>GAL4-BD-*Hs*ZC3HC1(1–502 | H363R)	pGBT9 (Amp)	This study
ADH1>GAL4-BD-*Hs*ZC3HC1(1–502 | H425A)	pGBT9 (Amp)	This study
ADH1>GAL4-BD-*Hs*ZC3HC1(1–502 | C429S)	pGBT9 (Amp)	This study
ADH1>GAL4-BD-*Hs*ZC3HC1(1–502 | W431A)	pGBT9 (Amp)	This study
ADH1>GAL4-AD (empty vector)	pGAD424 (Amp)	Clontech, Mountain View CA, USA
ADH1>GAL4-AD-*Sc*Mlp1p(1–143)	pGAD424 (Amp)	This study
ADH1>GAL4-AD-*Sc*Mlp1p(1–190)	pGAD424 (Amp)	This study
ADH1>GAL4-AD-*Sc*Mlp1p(1–297)	pGAD424 (Amp)	This study
ADH1>GAL4-AD-*Sc*Mlp1p(287–499)	pGAD424 (Amp)	This study
ADH1>GAL4-AD-*Sc*Mlp1p(287–584)	pGAD424 (Amp)	This study
ADH1>GAL4-AD-*Sc*Mlp2p(1–120)	pGAD424 (Amp)	This study
ADH1>GAL4-AD-*Sc*Mlp2p(1–210)	pGAD424 (Amp)	This study
ADH1>GAL4-AD-*Sc*Mlp2p(199–626)	pGAD424 (Amp)	This study
ADH1>GAL4-BD-*Sc*Pml39p(1–334)	pGBT9 (Amp)	This study
ADH1>GAL4-BD-*Sc*Pml39p(1–334 | W119A)	pGBT9 (Amp)	This study
ADH1>GAL4-BD-*Sc*Pml39p(1–334 | C134S)	pGBT9 (Amp)	This study
ADH1>GAL4-BD-*Sc*Pml39p(1–334 | C134–137SGGS)	pGBT9 (Amp)	This study
ADH1>GAL4-BD-*Sc*Pml39p(1–334 | C176S)	pGBT9 (Amp)	This study
ADH1>GAL4-BD-*Sc*Pml39p(1–334 | Y257A)	pGBT9 (Amp)	This study
ADH1>GAL4-BD-*Sc*Pml39p(1–334 | Y257W)	pGBT9 (Amp)	This study
ADH1>GAL4-BD-*Sc*Pml39p(1–334 | C271S)	pGBT9 (Amp)	This study
ADH1>GAL4-BD-*Sc*Pml39p(1–334 | C292S)	pGBT9 (Amp)	This study
ADH1>GAL4-AD-*Hs*TPR(1–60)	pGAD424 (Amp)	This study
ADH1>GAL4-AD-*Hs*TPR(1–74)	pGAD424 (Amp)	This study
ADH1>GAL4-AD-*Hs*TPR(1–88)	pGAD424 (Amp)	This study
ADH1>GAL4-AD-*Hs*TPR(1–102)	pGAD424 (Amp)	This study
ADH1>GAL4-AD-*Hs*TPR(1–111)	pGAD424 (Amp)	This study
ADH1>GAL4-AD-*Hs*TPR(1–175)	pGAD424 (Amp)	This study
ADH1>GAL4-AD-*Hs*TPR(11–109)	pGAD424 (Amp)	This study
ADH1>GAL4-AD-*Hs*TPR(20–111)	pGAD424 (Amp)	This study
ADH1>GAL4-AD-*Hs*TPR(29–175)	pGAD424 (Amp)	This study
ADH1>GAL4-AD-*Hs*TPR(43–175)	pGAD424 (Amp)	This study
ADH1>GAL4-AD-*Hs*TPR(54–175)	pGAD424 (Amp)	This study
ADH1>GAL4-AD-*Hs*TPR(110–342)	pGAD424 (Amp)	This study
ADH1>GAL4-AD-*Hs*TPR(110–377)	pGAD424 (Amp)	This study
ADH1>GAL4-AD-*Hs*TPR(172–651)	pGAD424 (Amp)	This study
ADH1>GAL4-AD-*Hs*TPR(233–342)	pGAD424 (Amp)	This study
ADH1>GAL4-AD-*Hs*TPR(233–499)	pGAD424 (Amp)	This study
ADH1>GAL4-AD-*Hs*TPR(275–450)	pGAD424 (Amp)	This study
ADH1>GAL4-AD-*Hs*TPR(275–481)	pGAD424 (Amp)	This study
ADH1>GAL4-AD-*Hs*TPR(275–539)	pGAD424 (Amp)	This study
ADH1>GAL4-AD-*Hs*TPR(347–499)	pGAD424 (Amp)	This study
ADH1>GAL4-AD-*Hs*TPR(347–543)	pGAD424 (Amp)	This study
ADH1>GAL4-AD-*Hs*TPR(361–539)	pGAD424 (Amp)	This study
ADH1>GAL4-AD-*Hs*TPR(386–481)	pGAD424 (Amp)	This study
ADH1>GAL4-AD-*Hs*TPR(386–539)	pGAD424 (Amp)	This study
ADH1>GAL4-AD-*Hs*TPR(411–539)	pGAD424 (Amp)	This study

ADH1>GAL4-AD-*Hs*TPR(432–539)	pGAD424 (Amp)	This study
ADH1>GAL4-AD-*Hs*TPR(450–543)	pGAD424 (Amp)	This study
ADH1>GAL4-AD-*Hs*TPR(608–940)	pGAD424 (Amp)	This study
ADH1>GAL4-AD-*Hs*TPR(926–1178)	pGAD424 (Amp)	This study
ADH1>GAL4-AD-*Hs*TPR(1129–1632)	pGAD424 (Amp)	This study
ADH1>GAL4-AD-*Hs*TPR(1177–1632)	pGAD424 (Amp)	This study
ADH1>GAL4-AD-*Hs*TPR(1618–1917)	pGAD424 (Amp)	This study
ADH1>GAL4-AD-*Hs*TPR(1894–2138)	pGAD424 (Amp)	This study
ADH1>GAL4-AD-*Hs*TPR(2110–2363)	pGAD424 (Amp)	This study
CMV>EYFP-*Hs*KPNB1(1–876)	pEYFP-C1 (Kan)	This study
CMV>EYFP-*Hs*SKP1(1–163)	pEYFP-C1 (Kan)	This study
CMV>EYFP-*Hs*ZC3HC1(1–502)	pEYFP-C1 (Kan)	This study
CMV>EYFP-*Hs*ZC3HC1(102–502)	pEYFP-C1 (Kan)	This study
CMV>EYFP-*Hs*ZC3HC1(170–502)	pEYFP-C1 (Kan)	This study
CMV>EYFP-*Hs*ZC3HC1(211–502)	pEYFP-C1 (Kan)	This study
CMV>EYFP-*Hs*ZC3HC1(352–502)	pEYFP-C1 (Kan)	This study
CMV>EYFP-*Hs*ZC3HC1(1–490)	pEYFP-C1 (Kan)	This study
CMV>EYFP-*Hs*ZC3HC1(1–477)	pEYFP-C1 (Kan)	This study
CMV>EYFP-*Hs*ZC3HC1(1–467)	pEYFP-C1 (Kan)	This study
CMV>EYFP-*Hs*ZC3HC1(1–462)	pEYFP-C1 (Kan)	This study
CMV>EYFP-*Hs*ZC3HC1(1–462)	pEYFP-C1 (Kan)	This study
CMV>EYFP-*Hs*ZC3HC1(1–391)	pEYFP-C1 (Kan)	This study
CMV>EYFP-*Hs*ZC3HC1(1–180)	pEYFP-C1 (Kan)	This study
CMV>*Hs*SKP1(1–163)-EGFP	pEYFP-C1 (Kan)	This study
eEF1α>*Hs*ZC3HC1(1–502)-EGFP	pEGFP-N1 (Kan)	This study
eEF1α>*Hs*ZC3HC1(1–502 | C102S)-EGFP	pEGFP-N1 (Kan)	This study
eEF1α>*Hs*ZC3HC1(1–502 | W107A)-EGFP	pEGFP-N1 (Kan)	This study
eEF1α>*Hs*ZC3HC1(1–502 | W107F)-EGFP	pEGFP-N1 (Kan)	This study
eEF1α>*Hs*ZC3HC1(1–502 | W107Y)-EGFP	pEGFP-N1 (Kan)	This study
eEF1α>*Hs*ZC3HC1(1–502 | C112S)-EGFP	pEGFP-N1 (Kan)	This study
eEF1α>*Hs*ZC3HC1(1–502 | C117S)-EGFP	pEGFP-N1 (Kan)	This study
eEF1α>*Hs*ZC3HC1(1–502 | S118A,S119GG)-EGFP	pEGFP-N1 (Kan)	This study
eEF1α>*Hs*ZC3HC1(1–502 | C120S)-EGFP	pEGFP-N1 (Kan)	This study
eEF1α>*Hs*ZC3HC1(1–502 | C125S)-EGFP	pEGFP-N1 (Kan)	This study
eEF1α>*Hs*ZC3HC1(1–502 | H152A)-EGFP	pEGFP-N1 (Kan)	This study
eEF1α>*Hs*ZC3HC1(1–502 | C156S)-EGFP	pEGFP-N1 (Kan)	This study
eEF1α>*Hs*ZC3HC1(1–502 | W158A)-EGFP	pEGFP-N1 (Kan)	This study
eEF1α>*Hs*ZC3HC1(1–502 | C249S)-EGFP	pEGFP-N1 (Kan)	This study
eEF1α>*Hs*ZC3HC1(1–502 | W256A)-EGFP	pEGFP-N1 (Kan)	This study
eEF1α>*Hs*ZC3HC1(1–502 | W256F)-EGFP	pEGFP-N1 (Kan)	This study
eEF1α>*Hs*ZC3HC1(1–502 | W256Y)-EGFP	pEGFP-N1 (Kan)	This study
eEF1α>*Hs*ZC3HC1(1–502 | C272S)-EGFP	pEGFP-N1 (Kan)	This study
eEF1α>*Hs*ZC3HC1(1–502 | C275S)-EGFP	pEGFP-N1 (Kan)	This study
eEF1α>*Hs*ZC3HC1(1–502 | H363R)-EGFP	pEGFP-N1 (Kan)	This study
eEF1α>*Hs*ZC3HC1(1–502 | H425A)-EGFP	pEGFP-N1 (Kan)	This study
eEF1α>*Hs*ZC3HC1(1–502 | C429S)-EGFP	pEGFP-N1 (Kan)	This study
eEF1α>*Hs*ZC3HC1(1–502 | W431A)-EGFP	pEGFP-N1 (Kan)	This study
eEF1α>*Hs*ZC3HC1(1–502 | W458A)-EGFP	pEGFP-N1 (Kan)	This study
eEF1α>*Hs*ZC3HC1(49–502)-EGFP	pEGFP-N1 (Kan)	This study
eEF1α>*Hs*ZC3HC1(61–502)-EGFP	pEGFP-N1 (Kan)	This study
eEF1α>*Hs*ZC3HC1(72–502)-EGFP	pEGFP-N1 (Kan)	This study
eEF1α>*Hs*ZC3HC1(82–502)-EGFP	pEGFP-N1 (Kan)	This study
eEF1α>*Hs*ZC3HC1(1–101_159–502)-EGFP	pEGFP-N1 (Kan)	This study
eEF1α>*Hs*ZC3HC1(1–169_211–502)-EGFP	pEGFP-N1 (Kan)	This study
eEF1α>*Hs*ZC3HC1(1–169_189–502)-EGFP	pEGFP-N1 (Kan)	This study
eEF1α>*Hs*ZC3HC1(1–169_179–502)-EGFP	pEGFP-N1 (Kan)	This study
eEF1α>*Hs*ZC3HC1(1–202_237–502)-EGFP	pEGFP-N1 (Kan)	This study
eEF1α>*Hs*ZC3HC1(1–221_237–502)-EGFP	pEGFP-N1 (Kan)	This study
eEF1α>*Hs*ZC3HC1(1–235_252–502)-EGFP	pEGFP-N1 (Kan)	This study
eEF1α>*Hs*ZC3HC1(1–248_276–502)-EGFP	pEGFP-N1 (Kan)	This study
eEF1α>*Hs*ZC3HC1(1–290_398–502)-EGFP	pEGFP-N1 (Kan)	This study
eEF1α>*Hs*ZC3HC1(1–285_398–502)-EGFP	pEGFP-N1 (Kan)	This study
eEF1α>*Hs*ZC3HC1(1–340_412–502)-EGFP	pEGFP-N1 (Kan)	This study
eEF1α>*Hs*ZC3HC1(1–279_412–502)-EGFP	pEGFP-N1 (Kan)	This study
eEF1α>*Hs*ZC3HC1(1–419_450–502)-EGFP	pEGFP-N1 (Kan)	This study
eEF1α>*Hs*ZC3HC1(72–467)-EGFP	pEGFP-N1 (Kan)	This study
eEF1α>*Hs*ZC3HC1(72–290_398–467)-EGFP	pEGFP-N1 (Kan)	This study
eEF1α>*Sc*Pml39p(1–334)-EGFP	pEGFP-N1 (Kan)	This study
GAL1>yECitrine / TEF>hphNT1	2μ/pMB1 (Amp)	This study
GAL1>yECitrine-*Sc*Pml39p(1–334) / TEF>hphNT1	2μ/pMB1 (Amp)	This study
GAL1>yECitrine-*Sc*Pml39p(1–334 | W119A) / TEF>hphNT1	2μ/pMB1 (Amp)	This study
GAL1>yECitrine-*Sc*Pml39p(1–334 | C134–137SGGS) / TEF>hphNT1	2μ/pMB1 (Amp)	This study

GAL1>yECitrine-*Sc*Pml39p(1–334 | C176S) / TEF>hphNT1	2µ/pMB1 (Amp)	This study
GAL1>yECitrine-*Sc*Pml39p(1–334 | Y257A) / TEF>hphNT1	2µ/pMB1 (Amp)	This study
GAL1>yECitrine-*Sc*Pml39p(1–334 | C271S) / TEF>hphNT1	2µ/pMB1 (Amp)	This study
GAL1>yECitrine-*Sc*Pml39p(1–334 | C292S) / TEF>hphNT1	2µ/pMB1 (Amp)	This study
yEGFP / TEF>hphNT1	pYM25 (Amp)	(Janke *et al*, 2004)
yEGFP / TEF>kanMX4	pYM27 (Amp)	(Janke *et al*, 2004)
mCh / TEF>natNT2	based on pYM43 (Amp)	This study (based on Janke *et al*, 2004)

Supplemental Table S2: Yeast strains

Description	Genotype	Source
Y187	*MATα*, *ura3-52*, *his3-200*, *ade2-101*, *trp1-901*, *leu2-3,112*, *gal4*Δ, *met–*, *gal80*Δ, *URA3*::*GAL1*$_{UAS}$-*GAL1*$_{TATA}$-*lacZ*	Clontech
CG-1945	*MATa*, *ura3-52*, *his3-200*, *ade2-101*, *lys2-801*, *trp1-901*, *leu2-3,112*, *gal4-542*, *gal80-538*, *cyhr2*, *LYS2*::*GAL1*$_{UAS}$-*GAL1*$_{TATA}$-*HIS3*, *URA3*::*GAL4*$_{17\text{-}mers(x3)}$-*CYC1*$_{TATA}$-*lacZ*	Clontech
AH109	*MATa*, *trp1-901*, *leu2-3*, *112*, *ura3-52*, *his3-200*, *gal4*Δ, *gal80*Δ, *LYS2*::*GAL1UAS-GAL1*$_{TATA}$-*HIS3*, *GAL2*$_{UAS}$-*GAL2*$_{TATA}$-*ADE2*, *URA3*::*MEL1*$_{UAS}$-*MEL1*$_{TATA}$-*lacZ*	Clontech
wild-type (BY4742)	*MATα*, *his3*Δ1, *leu2*Δ0, *lys2*Δ0, *ura3*Δ0	Dharmacon (Lafayette, CO, USA)
***pml39*Δ (BY4742)**	*MATα*, *his3*Δ1, *leu2*Δ0, *lys2*Δ0, *ura3*Δ0, *pml39*::*kanMX4*	Clone ID 16507 (Dharmacon; Winzeler *et al*, 1999)
***nup60*Δ (BY4739)**	*MATα*, *leu2*Δ0, *lys2*Δ0, *ura3*Δ0, *nup60*::*kanMX4*	Clone ID 10407 (Dharmacon; Winzeler *et al*, 1999)
***mlp1*Δ (BY4742)**	*MATα*, *his3*Δ1, *leu2*Δ0, *lys2*Δ0, *ura3*Δ0, *mlp1*::*kanMX4*	Clone ID 17104 (Dharmacon; Winzeler *et al*, 1999)
***mlp2*Δ (BY4742)**	*MATα*, *his3*Δ1, *leu2*Δ0, *lys2*Δ0, *ura3*Δ0, *mlp2*::*kanMX4*	Clone ID 12308 (Dharmacon; Winzeler *et al*, 1999)
wild-type Mlp1p-mCh	*MATα*, *his3*Δ1, *leu2*Δ0, *lys2*Δ0, *ura3*Δ0, *MLP1-mCh*:*natNT2*	This study
***pml39*Δ Mlp1p-mCh**	*MATα*, *his3*Δ1, *leu2*Δ0, *lys2*Δ0, *ura3*Δ0, *pml39*::*kanMX4*, *MLP1-mCh*:*natNT2*	This study
***nup60*Δ Mlp1p-mCh**	*MATα*, *leu2*Δ0, *lys2*Δ0, *ura3*Δ0, *nup60*::*kanMX4*, *MLP1-mCh*:*natNT2*	This study
***nup60*Δ *mlp1*Δ yEGFP-Pml39p**	*MATα*, *leu2*Δ0, *lys2*Δ0, *ura3*Δ0, *nup60*::*kanMX4*, *mlp1*::*URA3*, *yEGFP-PML39*:*hphNT1*	This study
wild-type Mlp1p-yEGFP	*MATα*, *his3*Δ1, *leu2*Δ0, *lys2*Δ0, *ura3*Δ0, *MLP1-yEGFP*:*hphNT1*	This study
***pml39*Δ Mlp1p-yEGFP**	*MATα*, *his3*Δ1, *leu2*Δ0, *lys2*Δ0, *ura3*Δ0, *pml39*::*kanMX4*, *MLP1-yEGFP*:*hphNT1*	This study
wild-type Mlp1p-yEGFP, Mlp2p-mCh	*MATα*, *his3*Δ1, *leu2*Δ0, *lys2*Δ0, *ura3*Δ0, *MLP1-yEGFP*:*hphNT1*, *MLP2-mCh*:*natNT2*	This study
***pml39*Δ Mlp1p-yEGFP, Mlp2p-mCh**	*MATα*, *his3*Δ1, *leu2*Δ0, *lys2*Δ0, *ura3*Δ0, *pml39*::*kanMX4*, *MLP1-yEGFP*:*hphNT1*, *MLP2-mCh*:*natNT2*	This study
***nup60*Δ Mlp2p-yEGFP, Mlp1p-mCh**	*MATα*, *his3*Δ1, *leu2*Δ0, *lys2*Δ0, *ura3*Δ0, *nup60*::*URA3*, *MLP2-yEGFP*:*hphNT1*, *MLP1-mCh*:*natNT2*	This study
***nup60*Δ Mlp2p-yEGFP, Mlp1p-mCh**	*MATα leu2*Δ0 *lys2*Δ0 *ura3*Δ0, *nup60*::*kanMX4*, *MLP2-yEGFP*:*hphNT1*, *MLP1-mCh*:*natNT2*	This study
***nup60*Δ *pml39*Δ Mlp2p-yEGFP, Mlp1p-mCh**	*MATα*, *his3*Δ1, *leu2*Δ0, *lys2*Δ0, *ura3*Δ0, *nup60*::*URA3*, *pml39*::*kanMX4*, *MLP2-yEGFP*:*hphNT1*, *MLP1-mCh*:*natNT2*	This study
wild-type Mad1p-yEGFP, Mlp1p-mCh	*MATα*, *his3*Δ1, *leu2*Δ0, *lys2*Δ0, *ura3*Δ0, *MAD1-yEGFP*:*hphNT1*, *MLP1-mCh*:*natNT2*	This study
wild-type Ulp1p-yEGFP, Mlp1p-mCh	*MATα*, *his3*Δ1, *leu2*Δ0, *lys2*Δ0, *ura3*Δ0, *ULP1-yEGFP*:*hphNT1*, *MLP1-mCh*:*natNT2*	This study
wild-type Sac3p-yEGFP, Mlp1p-mCh	*MATα*, *his3*Δ1, *leu2*Δ0, *lys2*Δ0, *ura3*Δ0, *SAC3-yEGFP*:*hphNT1*, *MLP1-mCh*:*natNT2*	This study
***pml39*Δ Mad1p-yEGFP, Mlp1p-mCh**	*MATα*, *his3*Δ1, *leu2*Δ0, *lys2*Δ0, *ura3*Δ0, *pml39*::*kanMX4*, *MAD1-yEGFP*:*hphNT1*, *MLP1-mCh*:*natNT2*	This study
***pml39*Δ Ulp1p-yEGFP, Mlp1p-mCh**	*MATα*, *his3*Δ1, *leu2*Δ0, *lys2*Δ0, *ura3*Δ0, *pml39*::*kanMX4*, *ULP1-yEGFP*:*hphNT1*, *MLP1-mCh*:*natNT2*	This study

***pml39*Δ Sac3p-yEGFP, Mlp1p-mCh**	*MATα*, *his3*Δ1, *leu2*Δ0, *lys2*Δ0, *ura3*Δ0, *pml39*::*kanMX4*, *SAC3-yEGFP*:*hphNT1*, *MLP1-mCh*:*natNT2*	This study
***mlp2*Δ Mlp1p-yEGFP**	*MATα*, *his3*Δ1, *leu2*Δ0, *lys2*Δ0, *ura3*Δ0, *mlp2*::*URA3*, *MLP1-yEGFP*:*hphNT1*	This study
wild-type Mlp2p-yEGFP	*MATα*, *his3*Δ1, *leu2*Δ0, *lys2*Δ0, *ura3*Δ0, *MLP2-yEGFP*:*hphNT1*	This study
***pml39*Δ Mlp2p-yEGFP**	*MATα*, *his3*Δ1, *leu2*Δ0, *lys2*Δ0, *ura3*Δ0, *pml39*::*kanMX4*, *MLP2-yEGFP*:*hphNT1*	This study
***mlp1*Δ Mlp2p-yEGFP**	*MATα*, *his3*Δ1, *leu2*Δ0, *lys2*Δ0, *ura3*Δ0, *mlp1*::*URA3*, *MLP2-yEGFP*:*hphNT1*	This study
wild-type Mlp2p-yEGFP, Mlp1p-mCh	*MATα*, *his3*Δ1, *leu2*Δ0, *lys2*Δ0, *ura3*Δ0, *MLP2-yEGFP*:*hphNT1*, *MLP1-mCh*:*natNT2*	This study
***pml39*Δ Mlp2p-yEGFP, Mlp1p-mCh**	*MATα*, *his3*Δ1, *leu2*Δ0, *lys2*Δ0, *ura3*Δ0, *pml39*::*kanMX4*, *MLP2-yEGFP*:*hphNT1*, *MLP1-mCh*:*natNT2*	This study
wild-type yEGFP-Pml39p, Mlp1p-mCh	*MATα*, *his3*Δ1, *leu2*Δ0, *lys2*Δ0, *ura3*Δ0, *yEGFP-PML39*:*hphNT1*, *MLP1-mCh*:*natNT2*	This study
***mlp2*Δ yEGFP-Pml39p, Mlp1p-mCh**	*MATα*, *his3*Δ1, *leu2*Δ0, *lys2*Δ0, *ura3*Δ0, *mlp2*::*URA3*, *yEGFP-PML39*:*hphNT1*, *MLP1-mCh*:*natNT2*	This study
***mlp1*Δ yEGFP-Pml39p**	*MATα*, *his3*Δ1, *leu2*Δ0, *lys2*Δ0, *ura3*Δ0, *mlp1*::*URA3*, *yEGFP-PML39*:*hphNT1*	This study
***nup60*Δ yEGFP-Pml39p, Mlp1p-mCh**	*MATα leu2*Δ0 *lys2*Δ0 *ura3*Δ0 *nup60*::*kanMX4*, *yEGFP-PML39*:*hphNT1*, *MLP1-mCh*:*natNT2*	This study
***nup60*Δ *mlp2*Δ yEGFP-Pml39p, Mlp1p-mCh**	*MATα*, *leu2*Δ0, *lys2*Δ0, *ura3*Δ0, *nup60*::*kanMX4*, *mlp2*::*URA3*, *yEGFP-PML39*:*hphNT1*, *MLP1-mCh*:*natNT2*	This study
***nup60*Δ *mlp1*Δ yEGFP-Pml39p, Mlp2p-mCh**	*MATα*, *leu2*Δ0, *lys2*Δ0, *ura3*Δ0, *nup60*::*kanMX4*, *mlp1*::*URA3*, *yEGFP-PML39*:*hphNT1*, *MLP2-mCh*:*natNT2*	This study
***nup60*Δ yEGFP-Pml39p**	*MATα*, *his3*Δ1, *leu2*Δ0, *lys2*Δ0, *ura3*Δ0, *nup60*::*URA3*, *yEGFP-PML39*:*hphNT1*	This study
***nup60*Δ *mlp1*Δ Mlp2p-yEGFP**	*MATα*, *leu2*Δ0, *lys2*Δ0, *ura3*Δ0, *nup60*::*kanMX4, mlp1*::*URA3*, *MLP2-yEGFP*:*hphNT1*	This study
***nup60*Δ *mlp2*Δ Mlp1p-mCh**	*MATα*, *leu2*Δ0, *lys2*Δ0, *ura3*Δ0, *nup60*::*kanMX4, mlp2*::*URA3*, *MLP1-mCh*:*natNT2*	This study
***nup60*Δ *pml39*Δ *mlp1*Δ Mlp2p-yEGFP**	*MATα*, *his3*Δ1, *leu2*Δ0, *lys2*Δ0, *ura3*Δ0, *nup60*::*URA3*, *pml39*::*kanMX4*, *mlp1*::*HIS3*, *MLP2-yEGFP*:*hphNT1*	This study
***nup60*Δ *pml39*Δ *mlp2*Δ Mlp1p-mCh**	*MATα*, *his3*Δ1, *leu2*Δ0, *lys2*Δ0, *ura3*Δ0, *nup60*::*URA3*, *pml39*::*kanMX4*, *mlp2*::*HIS3*, *MLP1-mCh*:*natNT2*	This study
***nup60*Δ Mad1p-yEGFP, Mlp1p-mCh**	*MATα*, *leu2*Δ0, *lys2*Δ0, *ura3*Δ0, *nup60*::*kanMX4*, *MAD1-yEGFP*:*hphNT1*, *MLP1-mCh*:*natNT2*	This study
***nup60*Δ *mad1*Δ Mlp1p-mCh**	*MATα*, *leu2*Δ0, *lys2*Δ0, *ura3*Δ0, *nup60*::*kanMX4*, *mad1*::*LEU2*, *MLP1-mCh*:*natNT2*	This study
***nup60*Δ *mlp1*Δ Mad1p-yEGFP**	*MATα*, *leu2*Δ0, *lys2*Δ0, *ura3*Δ0, *nup60*::*kanMX4*, *mlp1*::*URA3*, *MAD1-yEGFP*:*hphNT1*	This study
***nup60*Δ *pml39*Δ Mad1p-yEGFP, Mlp1p-mCh**	*MATα*, *his3*Δ1, *leu2*Δ0, *lys2*Δ0, *ura3*Δ0, *nup60*::*URA3*, *pml39*::*kanMX4*, *MAD1-yEGFP*:*hphNT1*, *MLP1-mCh*:*natNT2*	This study
wild-type Nup1p-yEGFP, Mlp1p-mCh	*MATα*, *his3*Δ1, *leu2*Δ0, *lys2*Δ0, *ura3*Δ0, *NUP1-yEGFP*:*hphNT1*, *MLP1-mCh*:*natNT2*	This study
***nup60*Δ Nup1p-yEGFP, Mlp1p-mCh**	*MATα*, *his3*Δ1, *leu2*Δ0, *lys2*Δ0, *ura3*Δ0, *nup60*::*URA3*, *NUP1-yEGFP*:*hphNT1*, *MLP1-mCh*:*natNT2*	This study

Supplemental Table S3: Primer sequences

Target	Sequence
*Dd*ZC3HC1_for1	ATGGATGAGAGAATTAAAAAAGCACTAAGCGATTTAG
*Dd*ZC3HC1_for346	GAAAAGGATAAAAAATCAAGTGTATATTGTTCATATTG
*Dd*ZC3HC1_for486	AGTTTATTTTCAATAGTTGGTAATGGATTCTCTAAAG
*Dd*ZC3HC1_rev271	TGAAATTGAATTAAAATCCCAACCACATAATGC
*Dd*ZC3HC1_rev426	TGTTCGGGCAAATGATTGATTTAAAACTTTTTC
*Dd*ZC3HC1_rev635	TTTCCTATAATGATGGATTGAAGTTGTTAATGAGTTTAC

*Dd*TPR_for1	ATGACATCTGTTAGTGATTCAAATAATC
*Dd*TPR_for282	GCATCACTTTACCAAGAGAGATCAGAGGAA
*Dd*TPR_for660	GGTATGATGACATTATCAGATTTATC
*Dd*TPR_for921	GAAACCTCAATAGCAATGACTCATCAAATC
*Dd*TPR_for1219	CTCTCAAGAATTGGAACAAGCCAAAC
*Dd*TPR_for1351	ATGCGTACTCTTACCGTTAG
*Dd*TPR_for1630	ACCACTCCAACTGTTGTTTCAACTCCAACT
*Dd*TPR_rev659	ACCACTACTGCTATTATTGTTG
*Dd*TPR_rev1350	ATTCTCTTGTTCTTCTTGAAGTTTC
*Dd*TPR_rev2052	TTATTCTTGCGATGGTTGATTATC

Supplemental List of Sequences for ZC3HC1 Homologues

Representative sequences for Figure 3A:

>NP_057562.3[*Homo_sapiens*]
MAAPCEGQAFAVGVEKNWGAVVRSPEGTPQKIRQLIDEGIAPEEGGVDAKDTSATSQSVNGSPQAEQPSLESTSKEAFFSRVETFSSLKWAGKP
FELSPLVCAKYGWVTVECDMLKCSSCQAFLCASLQPAFDFDRYKQRCAELKKALCTAHEKFCFWPDSPSPDRFGMLPLDEPAILVSEFLDRFQS
LCHLDLQLPSLRPEDLKTMCLTEDKISLLLHLLEDELDHRTDERKTTIKLGSDIQVHVTACILSVCGWACSSSLESMQLSLITCSQCMRKVGLW
GFQQIESSMTDLDASFGLTSSPIPGLEGRPERLPLVPESPRRMMTRSQDATFSPGSEQAEKSPGPIVSRTRSWDSSSPVDRPEPEAASPTTRTR
PVTRSMGTGDTPGLEVPSSPLRKAKRARLCSSSSSDTSSRSFFDPTSQHRDWCPWVNITLGKESRENGGTEPDASAPAEPGWKAVLTILLAHKQ
SSQPAETDSMSLSEKSRKVFRIFRQWESLCSC
>XP_041459241.1[*Lytechinus_variegatus*]
MAASNFETSKPRRIKALLSSFLKGISREEKKESETKQVIFESLDTEGFADGFVVVDEVSSEQTSTVQPLNQELFFNRVETFSISSWFAKPDEVC
PLRCAQYGWENIDVDSLKCVSCKEVLYGGLPPKWETDLYENACKKLVDSLKTGHSKICPWQSNPSPASFLEVNLVSSQNAVNDFLHRVASIRCF
GTSVPAVDLSCLQQVDENEDALSRIVSGVLGEEPTCDYKERIESVCFMAACGWSRSSPEGSQSPTMSCQYCRRNVGLWNFTPYEQNAKTVTEDD
SEPTAKRLKVDKGLFNPIEEHRSWCPWIKPTSSTQKVKSLPQDKNQDDERPVRPAWHELLVLLHQRSSPDKQGLLTNKQVTPPSQAWKAVRRIT
NFWQSRNAVNKT
>Own_assembly[*Saccoglossus_kowalevskii*]
MVSDKMAEKSSVLVTPKRVHDLLSSFIHKEETGVDERSDEPNQENIAQSSRQFLPRNREAFFARLETFSAFTWFAKPIELSPLKCAQYGWENTD
NDIVKCVSCKEIVCASLPKTWDPDLYAKRCEELRAALVKSHSNICPWRDSPSPDIFLSIPLLNQSEVQGDVLSRCTSLEKLGRKLPVIETCDIE
SQITAEALSGVVTRQINLLEDIRNDDDSSAINTVCVLSLCGWSTSSCETSQYPTVSCQYCRRQAGLWNFTPVVEPEPDKMTSEEQPTVDSSVES
SDADSAQEPSMKKRKISESKKSAFNPITEHRAWCPWVISYVMQQSDDHKSSPVPTYNNIPGWQAVFTLLAPKTSPLKENIQRLTDKDQTPPNQV
WKAVRKILSFW
>XP_005104988.1[*Aplysia_californica*]
MAATSTTNDTQTHTPEKVKNLLSSFLASSEQTRTEAITRGNASVQGEKTFPSDGTAYDLRPRLACSTSVLRSYDSYLQRLDTFSSLTWFNKPAE
LNPLICARYGWENIDTDMLQCVGCKAFLCGQLPVKTNPEVYEESLSKLKKNLLAAHDKFCALAVNPCPESFCRVPLHDPTNLTAEYTERASKLS
QIQERLPVIDYTRLHELEYDEGQGAAYCKKHLMPDSDVSPQAVTLAFTGWTTSSQNVLVCCMCRRQVGLWNYAQESSRGLAPDSTTKESSDEDE
ESKESGEPEAKKRKMKVSIKQKFDPIEEHWHWCPWVTETEVPCSSPPSGQQAAPAQRQKSLAFITAIKVTAPGLMDNNTGLAHAMKTSPMVEGL
RCFRRVMKSWSSPKLLSAGNSPT
>XP_013395661.2[*Lingula_anatina*]
MQAGFAQRVRTILSSFLHNETDDKKKELKNGHAVEEGDQSPAPSSSPCEAGVTARSGEVQLPTHARDRTAYFHRVETYSAVSWFAKPPSLCPLQ
CARYGWQNVDTDMLRCVSCKAVLCASLPKTYDHDVYDESCKKIAESLVSSHRKICPWPSNPSPVHFMSILYSGRDEALDDLLSRHQNLKQLGSQ
LPKLDIQADHELSGPSVQNLFKIVKQQGSSGGFNLDSALTDQVSCVLALCGWDISSLKKTDILICHFCRRQIGLWNFLSHSSLEQETDQSSQSV
IENGSHSKKEGSASPSPKKRKFLNDSIAKTSFNPIGEHRSWCPWITSTQQDKSNSQKSDQREVVSSYVGDEDSRPGWKRLLDWLVPNSASTDKL
TPKFVRNVKTTPPSEGLKNIRKVLHDWSSPTIGKL
> Own_assembly[*Capitella_teleta*]
MDERIKSALKTLSDTAALTKSGDGPNNSLDEADAPSSIHEDRAAFFDRLQSFSFANWFAKPLWLSPIACARYGWKNVDKDLLECVGCKKPMAGK
LPQSADPIISAKCHERLYQALTSAHHNSCAWKFHPTPVRVFAVPHHNHANATDQFVSRGSSFLALASRLPQIDPSVMESFGISLPVLETLYHVT
ATDGAYLLHDGNWQLLTEKASCDEDLATIPNLLQSACLLSITGWMLHSSKPGNEQIRCSLCQRLIRLAEVQNFTEKHPEMEAESSADHFLESII
ALDAVMKMQRTERSETDQQMAPQTPTVKSTEVVESIMNELLTAVCARNEEQREEPMEIDFRDAISKAKRSAAKKAKLDSKPTLNLLTEHRNWCP
WVSDGSCAHLDKDFKESSSDDFVPGWKTLLHILLPKESANQLNQSVEGLKKIRRSLHQGI
>PAA86276.1[*Macrostomum_lignano*]
MSQSEVESAIALFKTTVDDFDDSDNELHLLVSTQPLTSTEGIIKKRTLAGLLARLKTFSSLSWSVKPIELSPLVCAQYGWIGKKPNLLVCVTCK
NNLCIKLPSDSKLYNHCLKEAIEKLSSNHDNLCPWKLFPAIDAEPVLKFTNPAQDFEILNSIADSLSCLANEIDDSLQFSIGVDADTAEDFLNC
IAGAAATSSEVGSDEQLQIRRRQRCFQLAITGWSRPSPDSDELLKHFKSSQCPSILSCQFCLRRLGVWNLVRLANRQERQQHGEESTESEVNLS
TGNLFNNDSNSHIGDQLEGGVEQSRDDADNSDDAVVSQSSEQPASKRARLSEAPATAAAKLELLSLHWLWCPWSSGQVTKAWCDSVLLASPKRR
RRKPAIPTTTDQQQISTVAADGCAKVMQLLRSIV
>NP_501317.1[*Caenorhabditis_elegans*]
MEVDTASSRHSTVLKRKATDSINEILNYGQSSTSPQKRCKKAASLHKYRDMETYHKIIKTYKAPTWYGCAVSPRDLADYGWACVKKDCVKCIEC
EQYLSTVLPNICKVSFNVYNSSLQDIHEKMTTAHRTTCKLRCGAPPFRIVEPTAKEVMDGIQRRLSDSKKIIDEDLKADIPSDVNLPKIEGVPE
QLIYVAALGWHVSMPKRGSLLFGCDNCARELAIRCGNKFDPIHNHERWCPRIEMDDHGEPSWQSDLNTVLNTKNHVTNRYTGSSIFKEAYAARR
LLDSSLSTIITPNYI
>XP_046451818.1[*Daphnia_pulex*]
MATLNRKRKLDQTLIQKLYHDVPSKDPTRESFLKRLKTYDVFNWSGKPVDPPLCALHGWEIAEKDVLKCVMCHQFMSVTLPSPTKDAPYKHACS
KLKSRLASAHSKFCLYSTNQVPDSVLEIEHVSNMELQDTIQQQLLAFKNIEALCKVSELQDEIKEIFDWFLETTAIPDVHLSSFTFVLTGWKFL
QDDMLLKCDYCNRKWSIEPYLSQKNLTEKNDSVRTTVDPVAQHQRWCAWRAPTRGWKSRLLQLQQLKESRCREKRSRLSSDSCDSLTDRMRTVR
KLLNGTL
>XP_002154618.3[*Hydra_vulgaris*]
MSSANTKNKITDILSSLVSTTPEKSSSHVTCNPQSKDLFLQRVKTFTSSNWVAKPVGLSPLHCAQYGWCTEYLDQLRCVTCNATLDAGLPDEWD
EAAYNEICNKVQNKLQIGHEKLCPWPDNPCPPSFLSLPSYTSEQWCAEMKLSFESLMTLRGNLPELNEDEIASLGVLDNSSIETMLNQVFKWSS
ENDDDALQAKVASILAICGWSVCQPVVEDPSIICTICGMEAGLWNYKSLSSRINHQKRFKTSLEYTNSQQSLTELQENMSTDVSVKSEKSETEK
SDNSGQGSMLNELSRLATSSDSLAQSDLLRAAESQESLLNLRVSDSKVMATDGLEHHIETTHEDFNQLKNQFSEPRLPQATHPELMKELLLSRA

PGSRTRSRYSDSIFSEVGSECFEKRLEETCEKDIEHERAITDNPPPNHPNSSQQQWMKELLFITADACHSEPTESVISEIGSVAFDRRIEDNSS
LNSPRLLTPVHHGMHDYDEDSEPSRIKKMRFQVPDISMFSVIGEHRFWCPWVCSTERFTDHETSLSDSTAFISCKKIPGWKYVLYQLLPYNRPS
PCSTQRHEAWRYVRSTLTECISNKIT

>Own_assembly[*Trichoplax_adhaerens*]

MAEISLVPRKFLSLLDSFIFDKPACPENECKQDKVAEDYFERVETYSAYTWLAKPPALSPLQCARYGWKNVDIDRLKCVTCSATLTVSLPLPST
RSQPYEEAVRTFTDALISRHNPLCPWKDAPVREELIRLPNTYAKCVPILRQRLKSYSSAPHLLPRLELNSTLNTLLSCKEAVETLKDILDCQVI
LTDVDEEAQMVACILAFCGWVLKPSDKLKSSLLICSICRRRAGIWNYIMAISDSSTDSLELSSESIEEQSSSSPSKRRKIEKKKFNPIEEHRYW
CPYFIVDDNNAESREDVERSLGNVHQDNNNDTAGLKSMLSYLFPKRHSRTTDPNLNSCSAKSLRISTIPHQDLCSRSYIIMSLEEEV

>NP_013600.2[*Saccharomyces_cerevisiae*_S288C]

MEKDALEVRLKSIRHSLDKNTKLLPGKYRNTLGERLITKWRYKKKSHNGSSMLPEKCKSHVQLYDDLVQESSKHFVGFRLHDLRALLKRICSIQ
NYTRHVLIEWDVRWVNPLTLASKGWEPYQSASQSQVPFKCCCCHAIMTIPLLKNGDDVADYTMKLNEKIWNSNIIGNHLQKCPWRENQVDLNKE
YYLSSQNLIREIERIHTEIDRIVSGSNEFSLKRNSSRIFHYLSEKEIQKLAFFFDCKDYSLVGLLLLGYTKFQKDDLVQCTACFHRASLKKLEY
TEFNGHALWCRYYNKELLPTMLLELIGKEDKLITKLGVGERLNKLEAVLQTL

>XP_024513553.1[*Cryptococcus_neoformans_var._neoformans*_JEC21]

MELSSNTDDDLRDVFKLLYADDDWALTSDSELDDSEQLGNADGSEIDVADDEEQHTIRIYSGRITKKRLFSALDSLLSPGYETDTKRQRIYNPP
APSIPSLILSTQPMPALPLSKVYAPFSALSLLSRLMTFQPYTYSPQHPLTLSPVRAAMKGWVNEGREGLKCDVCGARWGLGGLEKVRDEAMKSN
LGERLAKGFEERHEKNCAWRICASPGNLYEQLRHLVHPPITSSLAPLASHLLLECLALPSLRLLSPLNPLQVERLVSLFKPSSTFSIPSPATDV
ASQLALFGWFPYHPNYPTIQISLNTPSSRTEIVCCRICHRRIGLWNFSNEKDGVKRFDVLNEHLVWCPVRIQDGEKEWWSESGLLDGQSTQAKR
IGEGGIKGLVKVSEKMEKRSWRRS

>ON368701[*Dictyostelium_discoideum*_AX4]

MDERIKKALSDLDNATVLNQLPILSNDLTTTCGSSSGSSSNDNNNNNNKNNNQYSTLNLIDESNNSTSNSTTSPSLLITSYRPWSNTDYYNRVR
TYTISNWFAKPCEIDPLQCSRFGWINCEADMLECETCKKRLYYKVPSTFSQSLVNKRINDFSISLQSTGHRDNCPWKDNGCPSFFSRLLDIPFQ
TQLEAYIKRSQNIYNNLTTLPMLSSDFYQQWVNKQNLMEPPITSRTNNILNIIVKIAKLPTDEVKSKVSCLLALCGWDFNSISNSNNNNNNNNN
NNNNNNNNNNNNNNNNNNNNNNNNNNNNNNNNNNNNNNNNNNNNDDDDKNEKDKNKNKIKENEKEKDKKSSVYCSYCQRLCGVWNFNKIKPNSTS
PFNEENINTTNNKGFNNSNIGSKRKREEDIEEEKRNIQFEKVLNQSFARTNNNNNNNNNNNNNNNNNNNNNNNNNNNNNNNNNNNNNKKLNS
NSNSNNNSNNNSNNNSLFSIVGNGFSKVTSNSQSTGWDWGNSFSNRISDFKAALEIANATEKKKEFSPINEHRWFCPWMIVVDSNRLIIDNNDI
LGENSQDNNNNSGSSNNSSNSNSSISGWENLLKLLLNQSTFDSKDFIDLKNDKKFHSIVNSLTTSIHHYRK

>NP_175325.2[*Arabidopsis_thaliana*]

MAQDSEKRFHQIMDKLFTPSKSQLPSSSTSSSVEQQSRGKKRQNPSSALALVEPKIVLATIDRSSALKVPAGTSPSGLCRPWDRGDLMRRLATF
KSMTWFAKPQVISAVNCARRGWVNDDADSIACESCGAHLYFSAPSSWSKQQVEKAASVFSLKLESGHKLLCPWIENSCEETLSEFPLMAPQDLV
DRHEERSEALLQLLALPVISPSAIEYMRSSDLEEFLKRPIAPACSDTAAESSQTESLTNHVGASPAQLFYQAQKLISLCGWEPRALPYIVDCKD
KLSETARGTETIDLLPETATRELLSISESTPIPNGISGNNENPTLPDTLNSDPSSVVLDCKLCGACVGLWVFSTVPRPLELCRVTGDTEINIEK
HPKGGTLQHQPSSLKFTIAGGPPATKQNFKATISLPIIGRNLRSRFASYSRDHDHGDVSSIQDQQSRTAENNGDVTQNSNQVMNDIGEKADGGR
NSTDVESDIALQNKDKQMMVVRSNLPENNKPRDSTAEKSATSNKQMEFDPIKQHRHFCPWIWSTGRRGPGWRQTLSALQRHKGSCQTPPSSSSL
FKVDDPLTSVRNLFKSPSPKKRKLNGGSSS

>NP_173164.1[*Arabidopsis_thaliana*]

MKEEDVSSQNVNPRSNRNSVASASASASATPVDRFRRRARSPSPPQTAAASSAGASSPAVLVNAGSVDWTGHGLALSVRSCRTWDRGDLLRRLA
TFKPSNWLGKPKTASSLACAQKGWVSVDLDKLQCEYCGSILQYSPPQDSLNPPEADTTGEKFSKQLDDAHESSCPWVGKSCSESLVQFPPTPPS
ALIGGYKDRCDGLLQFYSLPIVSPSAIDQMRASRRPQIDRLLAHANDDLSFRMDNISAAETYKEEAFSNYSRAQKLISLCGWEPRWLPNIQDCE
EHSAQSARNGCPSGPARNQSRLQDPGPSRKQFSASSRKASGNYEVLGPEYKSESRLPLLDCSLCGVTVRICDFMTTSRPVPFAAINANLPETSK
KMGVTRGTSATSGINGWFANEGMGQQQNEDVDEAETSVKRRLVSNVGLSFYQNAAGASSSAQLNMSVTRDNYQFSDRGKEVLWRQPSGSEVGDR
AASYESRGPSTRKRSLDDGGSTVDRPYLRIQRADSVEGTVVDRDGDEVNDDSAGPSKRTRGSDAHEAYPFLYGRDLSVGGPSHSLDAENEREVN
RSDPFSEGNEQVMAFPGARDSTRASSVIAMDTICHSANDDSMESVENHPGDFDDINYPSVATAQSADFNDPSELNFSNQAQQSACFQPAPVRFN
AEQGISSINDGEEVLNTETVTAQGRDGPSLGVSGGSVGMGASHEAEIHGADVSVHRGDSVVGDMEPVAEVIENLGQSGEFAPDQGLTDDFVPAE
MDREGRLGDSQDRVSQSVVRADSGSKIVDSLKAESVESGEKMSNINVLINDDSVHPSLSCNAIVCSGYEASKEEVTQTWESPLNAGFALPGSSY
TANDQGPQNGDSNDDIVEFDPIKYHNCYCPWVNENVAAAGCSSNSSGSSGFAEAVCGWQLTLDALDSFQSLENPQNQTMESESAASLCKDDHRT
PSQKLLKRHSFISSHGKK

>XP_042921239.1[*Chlamydomonas_reinhardtii*]

MSSVYERITSALSSLGKRRERDSSAHEGDGAGASAAGGGPTSPGGRSAAARTPKRFRPWEQADLHKRLETYKPLTWFGKPASVGPVPCALKGWV
NDGSDCLTCEYCGSKLVYPPHVAYDQRQAAADMFSPSLTTKHTATCPWRQTACQPKLLAYVPSTTPEQLCSLFYSLADKLMRVDVLPDMDTLAI
QTLRSTAMPYGSYDDFITAAAPGGGAVVGGGGAAGYSHDLAPRRRQMPSATIRELDQNGDEVMTPSGSAAGAAAAMAPAAAAGGGGDAAAVLQA
LVAAGDAGEGQAVLVQTSKLAPAQKARLLALLGWDVDVLQPDSASGMAVAPFAAGGSYSLSHLGVKPKAAAAAAAAGAGAGGAAVPGTPGGAGGK
GGKGSSKVPSSQVVLKCPICNSRMGLWNYSGVRPVPVGRLTAPPPPAAGGAAALMLSPRPAAASSGGGAAAAAAPAVPATIGSDPLSCTIAGGQ
YGQFGFGGAASAAKPFGSAAAAAPFRFGSAASTAPVFGLAAMDVDAQRAASAASGPFGSAAAAAAATPSMPAPSGSATPAPAGRKRKAEAPEPM
ALDAQHTPSAGMATPVAAPDGKRQRMAATPLWGGAGFGAVGGPAASPSGLGLGGASALAAASAAGQPRELDPVAQHRSWCPWVYTGSGDEKHMS
GWQHMLSALSQHQQHQQQQANVAATPGAAAASPADARQLRDNALEAIRKL

Representative sequences for Figure 3B1:

>NP_057562.3[*Homo_sapiens*]

MAAPCEGQAFAVGVEKNWGAVVRSPEGTPQKIRQLIDEGIAPEEGGVDAKDTSATSQSVNGSPQAEQPSLESTSKEAFFSRVETFSSLKWAGKP
FELSPLVCAKYGWVTVECDMLKCSSCQAFLCASLQPAFDFDRYKQRCAELKKALCTAHEKFCFWPDSPSPDRFGMLPLDEPAILVSEFLDRFQS
LCHLDLQLPSLRPEDLKTMCLTEDKISLLLHLLEDELDHRTDERKTTIKLGSDIQVHVTACILSVCGWACSSSLESMQLSLITCSQCMRKVGLW
GFQQIESSMTDLDASFGLTSSPIPGLEGRPERLPLVPESPRRMMTRSQDATFSPGSEQAEKSPGPIVSRTRSWDSSSPVDRPEPEAASPTTRTR
PVTRSMGTGDTPGLEVPSSPLRKAKRARLCSSSSSDTSSRSFFDPTSQHRDWCPWVNITLGKESRENGGTEPDASAPAEPGWKAVLTILLAHKQ
SSQPAETDSMSLSEKSRKVFRIFRQWESLCSC

>NP_001186366.2[*Gallus_gallus*]

MAAPSAEEAGGGRSRPPAVTPQQIRDLIDGGIASEGSGPEGKGTSDWSESANGSLQIDALSSESTSKEAYFSRVETFTPLKWAGKPHELSPLVC
AKYGWTNVECDMLKCSSCQAFLCVSLQLTFDFNKYKERCVELKKSLCTAHEKFCFWPDSPCPDRFALLLVDEPRALLQDFLERFQNLCQLELQL
PSLRAEDMKNMSLTEEKISLLLQLIKEELEHRTEGEKPPMKFASESLQVHIPACVLALCGWTCSAVSGSVLSVITCSRCMRKVGLWGFHQLESA
GLELDSWSPSTASTASGERGPPVPTSPRRMLTRSQDTNSPGSEQEKSPSPSISRLKGSDPPSSPVERGGELEATSPTQRNRPITRSMGQGDNVE
VPSSPLRRAKRPRLCSSSSSDTSPRSFFDPSSQHRDWCPWVNAVEGGETPEDPEKEPAKGEPGWQVVLSTLLASRKCDRVPETEPVSLSVKSCK
VFRIFRQWESINPS

>XP_003228779.1[*Anolis_carolinensis*]

MAAPSPAAVSSALPSEAEESKGKPASVTPQKIRELIDGGIAPEETSLEGKDLSALYEVANGSPKTEELPFEATSKEAYFNRVETFTSLKWAGKP
HELSPLICAKYGWTNTECDMLKCASCQAYLCASLQLAFDFSKYKERCLELKKALSTAHEKFCFWPDNPCPDRFSVLLVDEPLALLSDFLERFHS

LCRLELQLPSLKPEDLKSMSLTEEKISQLLQLIEEEADCKAEGEKTPSRKPLDLLQIHITACVLALCGWTSSPSSGSIQLPLISCCRCLRKAGL
WGFHQIESAPPETEVSPGLATPDGRPSSSSDKAGPTVPTSPRRMMTRSRDTTLPPGSEQQEKSPSPVISRMRSWDSTSSGERGEPESASPVPSP
RSRPVTRSMGQGDISGLGAEVPSSPLRKAKRARLCSSSSTDSCARSVFDPASQHRDWCPWVNAVKERPALEAEAGNQVEEGKAALGWQAVLKAL
LATKQSEGPADAESENLSAKSRKVFRIFRQWEAACSS

>NP_001011259.1[*Xenopus_tropicalis*]

MATSCEDVSPVKSPAVTPLKIRELINEGIVTGERSSIGRKETAVVPEENNGFEDPLSNSSYESTSKDAFFGRVESFSSLKWAGKPSELCPLICA
KYGWSNIECDMLKCSSCNAYLCASLQPVLDFSKYKQRCVELQEALRKAHEKFCFWPDSPCPDYFWALMVTEPSSVLSDFVGRFDNLCHLEIQLP
SIKHEDLKNMDITEETVSHLLRLIEDELKSKDGREDNSRLASDSLQVHISACILALCGWSTSYTSGSLCIINCPRCMRKVGLWAFQQLEAVELD
NSLSAPNTPVSPAEGHERSPFGIMSPNRRVTRSRDAEQSPALAYGRTRSSDLLSPADSEAVRSRPVTRSMGQGESSGLSNELHSSPLRRSKRPR
LCSSSSSDTSPRGCFDPLSQHRSWCPWVNVCQASETSTLGSEIQEEASRKEYGWKEVLNVLLAEENSRTLSDPDTSSVPEKSHKVFRIFRQWQM
AASASENP

>NP_001070846.1[*Danio_rerio*]

MAALGSRANRPENGEKQTKSPLVSPLKVRELLNEGVASEDSVLNCSQQDPNTASPNGLGKAPCEAANKEAFFNRVESYSCLKWAGKPSVLSPLR
CARYGWINVDCDMLKCCSCQAFLCASIQATLDFQKYKGRISEVRQQLQTQHEKFCSWPDFPCPDRFWMVPINEPTVLLAAFLERYKSACLLEQQ
LPAMKPEQLKAMTLTEDIISVLLQLIEDEQAKQGSSPSKVSSDPLSVQVAACILALCGWAASPSLHALNLPILACSYCMRKVGMWNFYQMDTAL
EAENPPQSPASSTSVTSTQGMSGDKGTPTSPSQSPTPCRMKLRSQDSTRSEQAESTPLRTRSRDSPTPHDEHPSPLSRGKRPMTRSRGQGEGQG
TDVPSSPQRKTKRPRLSSASGPEGPLHRNMFDPVAQHRDWCPWVSVEKEEDNQDASDFVGCEAELPQPGWKAVLALFLSMKQSLNPVGASPSQG
PHDKSKRVFSIFRQWQVSSPSQ

>XP_042191218.1[*Callorhinchus_milii*]

MATEGGEENAETKSGKDAARTPQKVRELLSDSVAPTDQTNSISESPNASLEESIPPCDSANKEAFFLRVETFTSLKWAGMSFEFSPLYCAKYGW
VNVDCDMLKCSSCQALLCLSLQPTQDSTKYKERVTELHKALKTAHEKFCYWPDSPCPGRFWALPFKEPSVLLSGLTERFRGLCQLEFQLPTLKH
DDLKDMTLTEDTISFLLQLIEDEVKGSAANESSGLKNTTDILSTHVAACILALAGWAAGPSDSLQLPIIMCSYCMRKVGLWSFQQIETLGGGSE
IDLPISLCNTPISPQENKAGRSTPTSLTISPHRMVTRSQDAAQSLPGEQQELSSSPITPRTRSRDTHSPTPVDRSESDSVSPGLRGKRPATRSK
GQGEVPSSPQRKPKRLRLSSSTSSDSPKSYFDPVFQHRDWCPWITRDGEPDRSEDPEQGEVGAVPDTLERRELGWRTVLQVLLSLQPSRSPDEE
SDSFSLSEKSRKVFRIFRQWQVTCSS

>XP_032822323.1[*Petromyzon_marinus*]

MWKSVSGWVPIPPPFTTMDASQTPSSPERATPEKIRQLLSTFISPEKSPDVGQKSPETRVILSRNRERFLKRVETFTPSAWAAKPSCLSPLCCA
ALGWECVARDVLCCCSCRTAQCIVLPPIWETARYDEKLKEVTESLKTSHAKYCTWPDDPCPDWLFLLPLHDPAQLLSSFCSRFQQLHALPSLSP
AALHDVGISEDTMKLLLQALAPAKRAEHGGDAETDGKNVCGREGSNGKNDSLEGATKGEVEIAGATSAMDNGEGKVSGGRGTNGTGGHDASASG
KDDGKEVLSETEGGEGETNGRSGKGEGTPSNVDADSGVQGKDVEGEAAVVQKEAAPGASSEVGEKVDDGVKVDDVSNVDGGATVDDGAKVDTGA
KVDEGAKVDDGAKVDTGAKVDEGEKVDDGAKVDDGAKVDDGAKVDDGAKVDDGAKVDDGAKVDDGAKVDDGAKVDDGAKVDDGAKVDDGAKVDD
GAKVDDGAKVDDGAKVDEVTVDMEPGAVAACVLALCGWDASPNVKSIVSCTICCRRIGLWNFKTQDADSERSCDTMTVGNVTPCGRPSPASAAV
ISPASQQNLVSPPKQQVSPGPRVAVGTKRPIVEDASGGHGGRRDDCASPAKRGRTDVDNITFHPISEHRHWCPWVCPVTVPGPSEADEGASQDK
VPGWRAALNTMLPMIVGEGTVSTLEPTDVWKKVHRSIMSWQVSGSG

>XP_002128832.1[*Ciona_intestinalis*]

MELTSENSSENIPPAIRPCKTVVDQVKNTLSFLLTSAVNSIKKADSEKNEIPVEKSSSVDNPQILARKNKNLGDSPKVVSRSEKLRSKEAFQKR
VKSFTLQNWCGKPLLLNPMLYAQYGWRCSGEDMVCCSSCGAVQCVQLPWPNATNYEEQCLKTRSKIVSGHMKVCSWSSSYCNDSFIIPFHPRYS
NTQQQTCMLEEFQARAKKLLHLKNDLPLITDDVKEEMELSEKILVQLCAAADFNDNDDIENLMVVSSIILALSGWDTKSDGDSSNPGIFCNESS
RLVGLWNFYSVGYLPNETDAPVAKKQKKDEDFTAIEKSYFHPLKQHHVWSPWVVTIKPMSADELSDERTSATYTDDDVLPGWKMLKNLICSDGL
TTSKPTMKTPPRAAVKQARRILSEWSSPM

>CAG5088580.1[*Oikopleura_dioica*]

MSAADIIKETETALKNFLNKLPDPKNEEVRIFDPSAIILLRTFPRYQQRLGTFDVTKWSGKPACFSPTFCAIYGWSCKEKDVLKCPDCGEVLLA
ELPPRNNDYFPKKVDHLLTMLQSGHADYCEFANSHEPFEFLKKNDSPYLFKKRLQTFPGTLDFLPKVTSGISEEDLDFLSRYFSYCVKNKKLQR
EILNLAVNGWSFHHEDETDYLLCEDDVRQIPER

>XP_041459241.1[*Lytechinus_variegatus*]

MAASNFETSKPRRIKALLSSFLKGISREEKKESETKQVIFESLDTEGFADGFVVVDEVSSEQTSTVQPLNQELFFNRVETFSISSWFAKPDEVC
PLRCAQYGWENIDVDSLKCVSCKEVLYGGLPPKWETDLYENACKKLVDSLKTGHSKICPWQSNPSPASFLEVNLVSSQNAVNDFLHRVASIRCF
GTSVPAVDLSCLQQVDENEDALSRIVSGVLGEEPTCDYKERIESVCFMAACGWSRSSPEGSQSPTMSCQYCRRNVGLWNFTPYEQNAKTVTEDD
SEPTAKRLKVDKGLFNPIEEHRSWCPWIKPTSSTQKVKSLPQDKNQDDERPVRPAWHELLVLLHQRSSPDKQGLLTNKQVTPPSQAWKAVRRIT
NFWQSRNAVNKT

>Own_assembly[*Saccoglossus_kowalevskii*]

MVSDKMAEKSSVLVTPKRVHDLLSSFIHKEETGVDERSDEPNQENIAQSSRQFLPRNREAFFARLETFSAFTWFAKPIELSPLKCAQYGWENTD
NDIVKCVSCKEIVCASLPKTWDPDLYAKRCEELRAALVKSHSNICPWRDSPSPDIFLSIPLLNQSEVQGDVLSRCTSLEKLGRKLPVIETCDIE
SQITAEALSGVVTRQINLLEDIRNDDDSSAINTVCVLSLCGWSTSSCETSQYPTVSCQYCRRQAGLWNFTPVVEPEPDKMTSEEQPTVDSSVES
SDADSAQEPSMKKRKISESKKSAFNPITEHRAWCPWVISYVMQQSDDHKSSPVPTYNNIPGWQAVFTLLAPKTSPLKENIQRLTDKDQTPPNQV
WKAVRKILSFW

Representative sequences for Figure 3B2:

>XP_046992160.1[*Schistocerca_americana*]

MVLGKVSMMADDGYEKVRKIKSLLAECMVPPRESQFLNLDRYIEENSEVSFIPDPPSWCNISFRGFQERVLTYRPQHWGADPNAVLWFSKYGWR
CTEKFVIKCDICSSTVECSSLIQKPDLWGDIAHKAHDNLCYWSFCPCPDRFIQIITHPKILCKNICHSWKKIIMYESELPKIQQVVLDKMGLSR
DILEHLFKIIETNCSEEGISALVLVICGWLKSSEDNTLECAYCERHLALRHFFSIADSSKINDSVPVQDDVRPGDEATKMDISETNAGKSLSSE
TNRDNSVADSGCKIESVHTLHPMKRIRRGQPAVHTGIARHRARALSCVTKQKFPSFCNMLHLRYGVKLPKHRGSRKNKKYLGRKYSGSDIIVED
EITTNGNESASEKPTQELYYIDKTDGEDSGPPNGKNGIKRKFPDNEDTENIEICQIDKQQKVAADVSKIEDNNSNMHKVDIDTVSNVKCSTEDS
VKPESDSEMITRNLISENVEISRNMTESNLPVSEQLVSPHELEGKEASSSSNCVQNTLRNKSDDVPPAEEEYRGDSNFEKKQNEIAKIAAISAS
EEIGPNVGKRQLICDDDQQTEGPNKRLNISSENSPLRKKNLNPVVEHRFWCIWRIKTVDRLLGSPKEGWRQILDLLKFGVSPQNSEAEEEAGDM
FEEVKKIHYMMSGW

>CAD7459619.1[*Timema_tahoe*]

MEFEDRIKRYKKLPFETLNGLESSDVSDDIKTAVNQDFDKFVERVATFGVLKWGAYPQLVLQLAQFGWQSEMKDYMIYCTSCSTRLSFSAYLKE
PDDWTDKIKSSHYKFCRWISLGHAYPEEFVKVPSDLKLIRDRVITRTKALLELGTSLPKMIALEHGALQLIVKNILKVPLTEESLSALILSLCG
WGPTTSHNVLSCDFCKRQVGLWNFITIQDEPTLADDYLCILNSPGSCTDEPLSILESSPIQDVDMQLTDPQTTEGSELHEDATEKEESSFIDDQ
YDYGHYDENQDSCDDENEGSVEQYTIENNDEENLDSDQRESAMKGYQDPNLMIDNINLVPDNFSEQDCEDFPGIEPEDGTTSVDTKVSTKPNLL
EGENGGVEILELTSGSEESDGSLEDEEDEEDYPSDDEEAEDEEMYMEEGNIRFMTDEKGLIQKYRKDEESFEDEEEDIEEHCDEKDDPEGEEEE
EATEEEDDPEGEEEEEATEEEDDKEEGTEEEDDDDDDDDDMSDGERVEQVGGNGSPSNGVVDEQSNPQTFEMYDSERDGQNSSVIRAKGENETT
TNVVGSTMLVYSENKVKGENVIEQILVETQNVQAVVNKPIKLMIEEMEIAVTPNTEVAMNHTSHVDKAENKREVKEINNKSDKACILDETMVSS

KDIESESEMLVKSTKETFHYLTNDLLNNDKKTKVFDGPKTLTQQIRREDVEAKPGTAFEKEDSSETTKNLINVKHTNVRPGTSVESQEDLDNQT
RSGLELESGKVEQEPGPPIEIETKTCENVPAEQTISNESDGPECMEAESRTEMISKNSTSELEPCLVSERANSEPMEIDKVETACTGKRLINVE
EEMEVKTENQNVGDDSRQDVKGDINLKDSQSQAWEDEINLKEGNGQEMKEDINLKDSQSQDVGGSKDIQEQDVSTLPSDGSDCVTKEKEHSVSE
ESVEKLLVVSGEVDCQHVLDETEDKTETTYSTCNGPVVDMDITGLGTSVDIGANQDAEDRVHAAGQSRKRRRVSTPLPEIDAKRWRMESVKLDF
DPVQEHRYWCIWGLPVDRGQEDSLIGWQRVLADLVRYTLQKSTIVSEEETTAEEKNIFEELVKYRDVLSTLVLKRGCSLQWEGGVNKHCLPWLI
TPWWSQASQAEGLFIESERVEKGEIAGTLTIVLELPLLYKEPFESEVFHLEVLMSLRTATSTQPYSRSALEFPCDQDRVLVTNLLVEHS
>Own_assembly[*Catajapyx_aquilonaris*]
MNSHSASTTILCLFRSELVRPRCIFKLSKRCAPTAKPWSHHDFVGRLKTFSPINWPYKRVSPIECAMRGWVIYGMNRITCITCKGRIYGGIMDT
KYTDLYEQWVQKLRSNLQERHELCCPWRVNPTRLEFEYIFDPGKVPQLGFIRRLKKFSQVNMLPELSEEFLESISEDTETINSISSRLESVPEE
RVALILALCGWEVKSADVLCCGICLRDVFIRTFGQTVSRASTPSQSGADDSYQNNLTDSDLATDISTSVLEPNTSVNEESVGDVGERNGDCDIG
HLVAQLELNGKVAGDTEKISEEIVVNSDTAEMEVQSESNEDNLGAKTVDTIEMKDSLACSEKDSPSAGVVREDLKIDPKSEERDEAADVMDTDM
TEENTCKQADSDSNATDLEQKLRPEVGEGTKIKSDAMDAVSNEEVNSPSNKKGHQGEDKDISVEPDKNGISLDKNDENVTAEGDSTSDIPSEEV
KKNEIPAEGDEKNAIPAEDDDKKGISIDEGLPAEEKSLPNSNCKNEAVQLEVDANVNTTTSELGEEKCSETGISEAEPSEEAPKNEKNDDTIFV
APKIECHESDVHSEADTVENTFLADDMEAETSSVVAPSTEPNSPNTSFLIPPDPNAASKKRRRSTSIIQMKKFRPSSFHPLNSHRFWCPWAAPN
DIVKHMSNTKLPGWKLYMSNINNNLIRSPDTIRLCHSSTYVSMEHINVRVVANINFFLVDSGRRTAKDTPRPWKVPLAVYRNNSPTKAYFYVYK
IRNFF
>CAG7825680.1[*Allacma_fusca*]
MLLKRKRSLDPGSERGIKLVRESLEAGVSDGKDLNRRRSLESASKADIETFINGIRKPSVDSGLPVSFDEFEASKFVAKENLVRDSQQTALSIE
DFKARLATFDMRRWSRKPDCIASFHCARFGWKLCEKGDALICVTCKQLIPVSGDGNAFAASSSGLKCGTQLRQAIEGNCHANSCPWKKYFSPVT
ILCLPQGFDMFYFLREGVASFQRTFTLPTLHSHYGHIMDNLDLTWMECIAGLKTLGVNIKSEDSENEKILHQQTRLICFLVLSGWSMKATNVED
GIGCYLCLREIPLWLCKSTADANSVCSLSTPVGSLKLGGRKYCSELDPINNHWWWCPWRRFLEFSDAATIVSSNVRKDLKDADFFEQRFEDSLC
LKPHADKEDYLRLKVLIEQECSQAASISEVKVISPQVVSTVGSIMDAFLSPSRCSTLTSLADESLLLPCDFSMKSEGTEAKPVQFKSNSNSMQE
>CAG7712993.1[*Allacma_fusca*]
MISESEMDDDEQEGPSSSKIRRVEKEDHLIIERRVDVYRKSNLGKSLAGALQELLNLKKIEAGLAEVVLQQFDRSVGRNLPHTRNHLVFSAERV
NRYRLIADNWKVTLQNVTFSTPYSELVIYYWRTQDLKPDMLPTSVVGNNRTFNSKSSFILQIKYYLKCAGFNLLIMAEQEVDILEKVRIALDSG
IVNLAKPAPDAGGDPDQNGASCGTTTKQPPGDYIDIDEYCKMLQDFRDDGIGPMDSRNLIGKQQTKLDSQQTSHSVADLHDRVSSFDILKWSQK
PDCISSFQCARFGWKLTEWGFLACVTCKNILPVPSQIPKINGDWANRLRQGIESSGHLPTCPWVRMPSAEDILAVPKGSDLFKFLCESVGSFKM
MKTVPTLENHYKMVSVDLSLKWLCELTSATLPDVAEEKEKGVTPEMVRNMALFLVLNGWSMSEVEDIMTCQLCLREVPLWLCQPTPPQHEILDL
LSPPASPVLNKSFSYKEFNPVSNHWSWCPWRKRLLTNVDESLMSMTPTKDSQQEFIRIKNQPSVDDYEKLLEDFKKECASITLNYDKETSNVRL
IDSVTSLFDNFIGSSVQPLSDGIEDSNDTNGGVDGNGLSKNHDNSEKECNSEKATEEDPADVVTPPKKRIRRELFEAGADI
>XP_046451818.1[*Daphnia_pulex*]
MATLNRKRKLDQTLIQKLYHDVPSKDPTRESFLKRLKTYDVFNWSGKPVDPPLCALHGWEIAEKDVLKCVMCHQFMSVTLPSPTKDAPYKHACS
KLKSRLASAHSKFCLYSTNQVPDSVLEIEHVSNMELQDTIQQQLLAFKNIEALCKVSELQDEIKEIFDWFLETTAIPDVHLSSFTFVLTGWKFL
QDDMLLKCDYCNRKWSIEPYLSQKNLTEKNDSVRTTVDPVAQHQRWCAWRAPTRGWKSRLLQLQQLKESRCREKRSRLSSDSCDSLTDRMRTVR
KLLNGTL
>tr|T1J7V6|T1J7V6_STRMM[*Strigamia_maritima*]
MASVSHSEISVHQLLQAFLVDSSDKASKEDFLKRLATFSISLRCARYGWYNKDADFLKCVSCDSVLCGKLPKRFQFELHKKSLNKLRNQLADAH
HKHCPWRNNPSPEPYYNISRWSKEEVTNEFLSNLNRLKSLEGVLPVLQDSCVNAIEDSLETLQKISDDPKLTLPVAQLAIRGWTCDLNSDANCS
TLYCAYCVRRVGLWNYKSNEEDSCDNPNKKQKFNGDTVEKKAFDPILEHQIWCPWVSTSQENDKLGWKVFLHVLTNKSSKLDHDSSELSSKQHL
GQIRKWLRGLMADSNCGKKFAGNISPTLRRPGCRNPEFLVTFTLRPRSPPKALVVELPGPHSLWGRPTLIERPPIVPSSLTKEDELEKLLEEKS
PVPVIGPTIYTLPKGRTNPKGWWSLYEPQILNLDFVTSNSEYSRYPPNPYTMPISYSVKDRSFTNVSI
>XP_029831140.3[*Ixodes_scapularis*]
MTAFVDAECSQLMDSLTTFSLPGISAKDYADFKSRIETFFDDYGTLSRWPCKPPELSPPQCARFGWTCANESLLVCAACKEYLDCEVSSSLGRK
LHKECLSRLVSLLEGAHKPCCPWKTAPCPKSYTVMQPVLRKDALSQLRERLETLRPILSTLPVLNTDKILSLLSPEDILRIGKLVDKDRGTETQ
RADLLLAITGWQAGAGSGKMKLVTCEYCSRKVATFFYKSAPISESRDEVTTSQDKGACSPGHGTKRKREEDELDPVHEHRPWCIWVLNDDSGKP
GWLVFSECLLRNVDSSHDDSRLSTSSVDAFKHDVEKIISSWREVVKHPTIQKTTTS

Representative sequences for Figure 3C:

>XP_004235730.1[*Solanum_lycopersicum*]
MAEESQKRFQDAMDKIFRTPPKSKLNSSASGVQLSRDKERLDMSSIGKAVSKYNLLATKGSGEAPPCRPWDRDDLFTRMSTFKSMTWFAKPQAI
SAVNCARRGWINVDMDTIACEACGSRMLFTTPPSWAQQQVDKAALVFSLKLDSGHKLLCPWIDNVCDEKLADFPPTATVMLVDQYKIRHSVLSQ
LAALPVISPKAIDFLRNPQLEQFLRESLTVEHDESMHTPQEETRNAPTSVSSLTYYQVQKLISLCGWELRRLPYMVDPKDQLNQSSKDANLSEK
SILSRKSEIITVYGSCTDKTSESKTDDDNRASEEAIINPNSVVLDCKLCGACIGLWDFSMVSRPLEFLRVSGYTQVNNDHINHTHGDKNHFSGN
SGRDKSRECTGQVTTSANTMLDRRPPNFNLTIAGGPPPVTHDYRAKISLPIIGRNLRAWFIAESELKDDLVTKSSSGVSKNPEFLAGENTEEGS
SLSTSEVSTEAQLENNQAAAQVSGNTTEMADNTESMNKVDPAVTDPCKDKVGNDFGSSSRGKELPILSLDKALEFDPFKLHRYFCPWIASNGVS
PSGWEQTLSALERHEESSSPLSNHAPSSLIKVDDPVASVQKLFTSPQAKRRKLVRPS
>XP_010323636.1[*Solanum_lycopersicum*]
MKEEAISSSHDPQLPPKSSSPPPIPTPAASSVGASSPAVPTNAGGTDWFAQAQGSKAASLSRIGSQPMWTSVSNSAGGSALGSSQPSCRPWERG
DLLRRLSTFQPTNWFGKPKASSSLACARRGWVNVDADTIECEACGANLRFVSSATWTSGEADIAGEEFAKKLDEGHKATCPWRGNSCAESLVQF
PPTPPSALIGGYKDRCDGLLQFPSLPIVAASAIEHIKVSRSPEIDRLLAQSQAFGGMEPIFRLEIMSGTETNTEDVFLVYSRANKLISLCGWEP
RWLPNVQDCEEHSAQSARSGYSIGPTKYHTSLQDFGHGENVLPSSKKKVHSKNEAVGPRSKGESRSPLLDCSLCGATVRIWDFLTVVRPACFAP
NSNDIPETSKKMALTRGASAASGISGWVAADGVEKEQTEDLDEAATNDVGRSLSNIGVDLNLTMAGGLSSSQVNMDAKPEQFEDGHKRRYPVTG
QPSSSEVGGQAASYESRGPSSRKRNLEEGGSTVDRPQLPLQPADSVEGTVIDRDGDEVNDGSQYSAGPSKRPCQSDAFGTHHTSYGKDSSGAGP
SLSLGFEIGTSAPRDDTFGRRHEQLTGVPSTRDSTHVSSVIAMDTVHGTDDSMESVENLPGDFDDVHFPSTSMLRSADPVETSELNYSNQAQQS
TCPAVVRSAGEMGVSSTNDEEVVNADTATANVRDGPSFGISGGSIGMGASHEAEIHGTDASVHRADSVAGEVEAVAEITENQGQTGEFAPDPGL
MGDYVPEEVDRGDPNGDSQDLTSRSVGRADSGSKVVGSAKAESIESGEKNCHVQPMLPNSPHPSLSCNAVVCSAHEASKEEVTQNNAPATDDCG
FVESDYMLANGTGPPIGESNYEEAVEFDPIKHHNFFCPWVNGNVAAAGCSNSGSSSSNSGAIALCGWQLTLDALDSFQSLGHIPVQTVESESAA
SLYKDDHRAPGRKLLARHSFSKHHGHN
>XP_008374705.2[*Malus_domestica*]
MSKDSEKKFHLIMDKLFFAPKSAPSSASSSSGVQTSRGKKRANPSSALALVEPKSRGDRMEVSRHFSAPAVAAHAPLCRPWDRGDLMRRVATFK
SMTWFAKPKVVSALNCARRGWINVDADILACESCGARLFFSTPSSWNQQQVEKAALVFSLKLDNGHKILCPWIDNACVETLAEFPPTPPPVLVD
KFRERCYALLELSVLPVISSSAIEYMKSPQLEQFLGQSSMFYGNGSGDISRTEHSDNEGNADSAKLYYQAQKLISLCGWEPRLLPYVVDSGNRL
NHSATNRQNPSISVHSASNDEHKNASACTNIQAEHDSVVLDCKLCGASVGLWAFSTVPRPVECFRLVGYAEVNSESHSGTHDSNAESHCDSRID
VLNAGVDGATLSKDRFANLKLTIAGGPPPTNQNFKAIISIPVIGRNLRARISYDSELRDCLSVGQEGMQSDTQMEKEENHYQENAENGGLENSE

VCGPGTPDANATHLNGEMDKSDPLVMVSSKGDLLHSGTIVEHSEEHESTSVPSSFEANADLNSSRTDPEPTSNQEASEDTVQIPANGELVACSS
GKDLKHVVPGSMMEFDPIRQHRYFCPWIASTGNGAPGWKQTLSALQRQEGGSPSSASIIKVDDPITSIRNLFTSPSPKRTKPTVLTTRTSEQ
>XP_028947922.1[*Malus_domestica*]
MSKDSEKKFHSIMDKLFFAPKSAPSSDSSSSGVQTSRGKKRANPSSALALVEPKSRGDRMGVSRHFSAPAVAAHAPLCRPWDRGDLMRRVATFK
SMTWFAKPKVVSALNCARRGWINVDADILVCESCGARLLFSTPSSWNQQQVEKAALVFSLRLDNGHKILCPWIDNACDETLAEFPPMPPPVLVD
KFRERCYALLELSVLPVISSSAIEYMKSPQLEQFLGQSSMFYGNGSGDISRTEHSVNEDSADSAKLYYQAQKLISLCGWEPRLLPYVVDSENRQ
NYSATNRQNLGINVHSASNDELMKSHNTSIQSEHNSVVLDCKLCGASVGLWAFSTVPRPVECFRLVGFAEVNSESRSGTHDSNTESHCDSRIDI
LNAGVDGATLSKDRFSNLNLTIAGGPPPTNQNFKAKILLPVIGRNLRARISYDTELRDCLSVGQEGMQSDSQMEKEEDHYRENAGHGGLENSEV
SGPGTPDADITHLNGEIDKSDSLVMVSSKGDLLHSGTIVEHSEEHESPSVPSSFEANADLSSSRNDPQPTSNQEASEGIVQIPANNELVACSSG
KDLKHVVPDGRMEFDPIRQHRYFCPWIASTVNGAPGWKQTLSALQRQEGGSPSSTSIIKVDDPITSIRNLFMSPSPKRMKPTVLTTRSSDQ
>XP_008371629.2[*Malus_domestica*]
MREEVISSGGNIDPAPAASSAGASSPTVPANVGSVDGSIHGQGSKGASISCVGSQPPVTSLSTSAGGGGGGDSSVFGSSRLSCRPWERGDLLRR
LATFKPSNWFSKPKVISSLACARRGWVNVDVDKIACESCGASLGFALLPSWTPDEVQNAGDAFVKQLDSGHKAACPWRGNSCPESLVQFPPTPQ
SALIGGYKDRCDGLLQFHSLPNVAASAIEQMLVSRGPQVDRFLMAGEVDFKPESIPEQESSRDGSICLYSRAQKLISLCGWEPRWLLNAQDCEE
HSAQSARNGYSLGPTYAQVHLSQEPGPSKKAVSASARKDAGKSKMLVKESRRDPRSPLLDCSLCGATVRILDFLTIPRPVRFTPNNIDIPDTSK
KLGLIRGASAASGISGWVATDDAEKEQTEDRDEVATTTEGSLFPKTDVDLNLTMGGGFTFNRFGRPEMSENIQDADMGRDLMIGQPAGSEVGDR
AASYESRGPSSRKRSLEKGGSSVDRPHLRTQHADSFEGTVIDRDGDEVTDGGQYSAGPSKRARDSDMFDTYCSSGAGPSHSMGLDIYADANRVA
SFPQGSDQFGIHSNMDSARASSVIAMDTIGHGTDDDSMESVENYPGDVDDVHFPTSSTYGNLDMNDTSELNYSNQAQQSVGFQPVADVVIGEIG
VSSTNDGEEIFNTETVTAQARDGISFGISVGSVGMCASHEAEIHGADVSVHRADSVVGDVEPRTEDAENQGQTGESAPDPGLMDEIVPDEINRE
DPHGDSQEMISRSIGRADSGSKIDGSTKAESVESGEKISQGFKFENSARPSLSCNANVFSNYRTTKEVKSAGKSSFTNNCVYQESEYAVANGLG
PPKGESNYEEPMEFDPIGHHNQFCPWVNGNVAAAGSSSCGHGSSVAAVALCGWQLTLDALDALRSLGQDAIQTLQSESAASLYKDDHQTPSQKL
LQNHSISRSQGQY
>XP_003609078.2[*Medicago_truncatula*]
MSQDSEKRFRSIMDKLFHSSKSSSNNPDKSSSGVQLSSSRGKKRGFQSIVDRRGDEQYLSATAVSESQGHLCRPWDRADFMRRLATFKSISWFA
KPKKVSAVNCARRGWINVDVDTIACEECGARLLFSTPASWNHHQVEKAALVFSLKLDNGHKLLCPWIDNACSETLARFPPTSPPVLVDNFRERC
SALLELSTLPRIASSALDHMQSPYMDDFLGQSLMQECGNGSAENFGIEDVSSQEELKLYYQAQRLISLCGWELRYLPYAVDCRDVSDQSHKNST
IVYSPRVVSDARNNNLTVYSADNNESSKMDENSKHSIGEQMDPNSAVLDCSLCGATVGLWAFCTVPRPVESIRLVGYAEVNVDNDLESRQGVNN
ALSDIANSSKDTSLGLNMTIAGGPPPTKQNFKAIISLPIIGQNLRARLSYDYDIRDHFFVDRGGSQSDSQEIKIQEKTDNTVDASIGQLVPVSS
EIREISNCETGSQQASICDSVLDNDLEGTSSAGQPSGFKEKMPVQAETGGLKNSSAEDPSSSQTDMAEDEALSHKTKEGSHVETSGVKERAENP
INREDVHNSIGKFKNPSLPGKAMEFDPIRQHRHFCPWIASEDGVEPGWKQTLSALYRPKEHLRHSSNTSPSSMSIMKVDDPVGSIRKLFMSPPT
SRRKLTHISSQNAEHR
>XP_024629233.1[*Medicago_truncatula*]
MREEVISSGGTVDPTTAASSSAGASSPTVPMNVGSIDGSSHGQGSKAASLSCVGSQPPWTSISTSVGGSAFGSSRSSCRPWERGDLLKRLATFA
PLNWSGKPQVIDSLACAQKGWMNIGEDKIACESCGACLSFTSLLSWTVAEAQDASESFARQLDSGHKANCPWKGNSCPESLVQFPPTSQSALIG
GYKDRCDGLLQFHYLPVVAISAIELMRVSRGPQIERFLSQSQNFMSGTDFKPENISELESSQDEAYCSFTRAQKLISLCGWEPRWLLNVQDCEE
HSAQSERNGYSFGPSKTQLRLAQDPGPKAVSASTKMDPRKGKEPFKESSLEYRSPMLDCSLCGATVRILDFLTVPRPSRFAPNNIDNPDTSKKI
GLTRGGSAASGINGWIAADDAEKDQTEDRDEVATTNEGKSLANTDLDLNLTMAGGFRCTPFGRTATSENMHDVDMGRDLMIGQPSGSEIGGRAA
SYESRGPSSRKRNLEKGGSSDDRLVLRSQQQADSVEGTVIDRDGDEVTDGGQYSAGPSKRVRDSDIFDTYCSPLQRDSSGAGPSNSLGFEGYVT
GNRVSSFHQGSDGLIGIQSARDSARASSVIAMDTICHSVNDDSMESVENYPGDLEEVHLPSSSTYGNVDMNETSELNNSNAAQQSTCLQTAPEV
VRGEVGVSSTNYGEENFNAETVTAQARDGFSLGISGGSVGMCASHEAEIHGADVSVHRTNSVVGDMEHRVEDAENQGQTGESVPDPGLMDEIIP
DDINREYPVGDSQEMMSHSAGRADSGSKIGCSTKAESVESGEKISQNCKLPPANNSHPSQSCNANIYSDCGTTKEEIMKDGKSSFTNNCALVGS
DFATANRIGPPKGDNNYEEAVEFDPIVYHNQYCPWVNGNVAAAGCPSSFPGTGSDAIALCGWQLTLDALQSLGNAIPTVQSESAASLYKQNDPQ
APRKKLLHNHSMSRSHGQL
>XP_024632064.2[*Medicago_truncatula*]
MKEDDVVTSSKKKNHKPHSAASSAGASSPPYDTTGEASRRDKSSADSYMLIASALHGASNPSCRPWERCDLLRRLSTFKIAGKLPKVGGPLACA
KRGWVNVDVSKIECELCGVQLDYALPSASSAEEADASSEELSKQLDRGHKINCPWRGNSCPESLVQFPPTSHSALIGGFKDRCDGLLQFYSLPI
VSSSAVEQMRVTHGPQIDRFIAQLQIQTAGELGYRAETSLTGEQAPHSYSHAQKLISLCGWEPRWLPNVLDCGEQSAESAKNGYNSDPAKGSAP
GPAPSKEFSNSSRKDTGDNDVLGSEFNCESRSPLLDCSLCGATVRIWDFLTAPRPVHLTPCGTDTPQTSKKIASMRGISAASGINEWAAADGVE
KERTGDRDEATTSGKRKLVSNKGLDLNLKMASGPRRSLINVTSTLDHVQYAGEGSNLRNRGPSGSDVGGPAASYESQGPNVRKRRLDDGATRAD
RPPLSMQQADSADRTVVNHDNNEISGGQQYSAGPSKRARDANHLETLQFSLRNTSGAVPSYSANIQSEAEENTVNQLNAEKDHVTSMPFTREST
HASSVIAMNGRYHSSDDESMESVENSPADFNEVNFPSVDLNETSELNSSYQAQQSACNQPPLERTGGEAGLSSSNVCGEVLNTEILTAQARDGP
SFGISGGSVGMGASHEAEIHGTDVSVHRVDSLGDAEQIAEVIENHGHVSEFTPYHGHNGDFVPEEMSREDPQGDSQAVVSQSTARVDSGSKTIA
STKVESVESGEKTSCSMETPGLENSAHPSLSCNAVVCSAYEVSKEEVAQTGKPSYIDDGAHPSLSCNAVVCSAYEVSKEEVAQTGKPSYIDDGA
HPSLSCNAVVCSAYEVSKEEVTQTGKPSYIDDGAHPSLSCNAVVCSAYEVSKEEVTQTGKESYIDVSTYHESGNLDADVVGTPYRDNSSGRVEF
DPIKLHNDYCPWVNGVVAAAGSDSPCSTSDVGPAARCGWQLTLEALDSFQLLGHLPVQTLESESAASMCKGDRFTSSQKLLARNSFVRHQGKN
>XP_021625743.1[*Manihot_esculenta*]
MADDPEKRFHSIMDKLFHAPKSLSNPSSSSGVELSRGKKRPNPESALALVEPRTRGDVVGSSQRSLAPADAPLCRPWDRGDLMRRMATFKSMTW
FAKPKVVSAVNCARRGWINLDMDIIGCEACGARLLFSTPSSWTQQQVEKAAMVFSLKLDNGHKLLCPWIDNACDERLAEFPPTPPPVLVDKFRE
RSSALLQLLGLPMISSSALEYMKSSQLEEFLRQAPTLDCGNGSIKISQVEYPGNESEAYSANLYYQAQKLISLCGWEPRLLPYVVDCKAKPKKR
IKDANTLNSSHIFTNGQNTSIGFYSATTNENAEATEDFNAPGGLQADPHSIVLDCKLCGASVGLWTFSTVPRPVELFRLVGYTEVNSRKNYGQD
SENESQVNDRQVINSSSNGVLSSIDRPSTLNFTIAGGPPPTKQNFKATISLPVIGRNLRARFSHDSGFRDHTFNDLEPQSRPDKYLCMEESSIT
ENFGEQVSLPESVGMLKSKTTDQGQCSSASGDQSSCLNIENGKKGSDLRKDSDSNRECTTESTADAAQGFDQSNRLPENALNVGSLDSPAGSLG
SSQIIVSSMSGPGATVTAGNGNSTRDSLALVTSEGGNQQQVPGADVLCGKDVNLKIDLTKGKELKEISDEGMEFDPIRQHRHFCPWIVSTESWA
AGWKQTLSALFRLKDLSSPSTKSPSSTSTVKVDDPITSVRKLFMSPSAKKMKPTRGSS
>XP_021598693.1[*Manihot_esculenta*]
MREEVISSGGTMDPTPAARYQITRLPSFLPRSAGASSPAVPANTHASKAASLSGVGSQLPWTSLSTSAGGSVLGSSRPSCRPWERGDLLRRLAT
FKPSNWFGKPKIASSLACAQRGWMNIEIDKIVCESCGACLSFVLLPSWTPTEVESAGEVFARQLDDGHKTSCPWKGNSCPESLVQFPPTPQSAL
IGGYKDRCDGLMQFQFLPIVAASAVEQMRVSWGPVVDRFLSYSQNFTFGEGDFKPEGIQELENSRDGASYLYSRAQKLISLCGWEPRWLLNVQD
CEEHSAQSARNGCSFGPAQAQVHLSHDPGPSKRAHSASATKNTGKNRLVAESRCDSRSPLLDCSLCGATVRILDFLTVPRPACFAPNNIDIPDA
SKKMALTRGVSAASGISGWVAVDDTEKEPTEDRDEVATTDKGKLLQNTEVDLNLTMAGSLPFYLPDKAAIPESVRHLEMGRDLIIGQPSGSEVG
DRAASYESRGPTRKRSLEIGGSSDNRPHLMMQPVDSVEGTVIDRDGDEVTDGGQFSAGPSKRARDSDFDTHCSPCQRDSCGAGPSHSVGMEIYA
DGNMVNLFRQGSDQVVGIPSARDSTRASSVIAMDTVCHSTDDSMESVENYPGDIDDVHFPSSSTHGNLDMNETSELNYSNQAQQSISVKYAAEV
AHGEMGVSSTNDGEEIFNAETVTVQARDGPSFGISGGSVGMCDSHEAEIRGVDVSVHRTDSVVGDVEPRVEDVENQGQTGESAPGPGLMDEVVP
DEINREDPHGGDSQEMFSRSVERADSGSKIDGSAKAESVESGEKASQSCKLALGNNDGPSLSCNANMYSGYQTTKKGVGKAGKSSSTNNGIGPP
KGESNYEEAIEFDPIIHHNQFCPWVNGNVAAAGCSSRSSGNNADADALCGWQLTLEALDALQSLGHIPIQTVQSESAASLYKDDHQTPGQLLRR
HSMNRSHGQH
>XP_043807289.1[*Manihot_esculenta*]

MREEVISSGGTMDPTPAASSAGASSPAVPGNICGMERSSHAHTSKAASVSGVGSQLPRASLSTSAGGSVLGSSRPSCRPWERGDLLRRLATFKP
SNWFGKPKMANSLACAQRGWMNVDVDKIVCESCGACLSFVLLASWTPAEVESSGEAFAKQLDDGHKASCPWRGNSCPESLVQFPPTPQSALIGG
YKDRCDGLLQFLFLPVVAASAVEQMRVSRGPVVDRFLSQSHNFTSGEGDFKSEGMPEFETSRDGASCLYSRAQKLISLCGWEPRWLLNVQDCEE
HSAQSARNGCSFGPAQAQVHLSHDPGPGKKAHSASAKKDTEKNKLLAESRCDSRSPLLDCSLCGATVRILDFLTVPRPARFAPNNIDIPDASKK
MVLTRGVSAASGISGWVAADDTDKEHTEDRDEVATTDKGKLLQNTEVDLNLTMAGALPFTQADRLAITDNVHDVEMGRDLMIGQPSGSEVGDRA
ASYESRGPSSRKRSLEIGGSSDDRPNLTQPADSVEGTVIDRDGDEVTDSRQFSAGPSKRTRDSDFFDTHCSPYKRDSCGAGPSHSVGMEMYAEG
NRVNLFHQGSDQVVGITSVRDSTRASSVIAMDTVCHSADDDSMESVENYPGDIDVHFPSSSTYGNLDMNETSELNYSNQAQQSICFRHTAEVAP
GEMGVSSTNDGEEIFNAETATAHARDGPSFGISGGSVGMCASHEAEIHGADVSVHRTESVVGDVEPRIEDVENQGQTGESAPDPGLMDEVVPDE
INREDPHGDSQEMLSRSMERADSGSKVDGSTKAESVESGEKEASQSFKLALDSNAHPSLSCNANMYSGYQTNKKGVSKAGKSSSTNNFPCLESD
YTIANGIGPPKGESNYEEAIEFDPIIHHNQFCPWVNGNVAAAGCSSHDSGNNADADALCGWQLTLDALDALRSLGNVPIQTVQSESAASLYKDD
HQTPGQKLLRRHSMSRSHGQY

>NP_175325.2[*Arabidopsis_thaliana*]

MAQDSEKRFHQIMDKLFTPSKSQLPSSSTSSSVEQQSRGKKRQNPSSALALVEPKIVLATIDRSSALKVPAGTSPSGLCRPWDRGDLMRRLATF
KSMTWFAKPQVISAVNCARRGWVNDDADSIACESCGAHLYFSAPSSWSKQQVEKAASVFSLKLESGHKLLCPWIENSCEETLSEFPLMAPQDLV
DRHEERSEALLQLLALPVISPSAIEYMRSSDLEEFLKRPIAPACSDTAAESSQTESLTNHVGASPAQLFYQAQKLISLCGWEPRALPYIVDCKD
KLSETARGTETIDLLPETATRELLSISESTPIPNGISGNNENPTLPDTLNSDPSSVVLDCKLCGACVGLWVFSTVPRPLELCRVTGDTEINIEK
HPKGGTLQHQPSSLKFTIAGGPPATKQNFKATISLPIIGRNLRSRFASYSRDHDHGDVSSIQDQQSRTAENNGDVTQNSNQVMNDIGEKADGGR
NSTDVESDIALQNKDKQMMVVRSNLPENNKPRDSTAEKSATSNKQMEFDPIKQHRHFCPWIWSTGRRGPGWRQTLSALQRHKGSCQTPPSSSSL
FKVDDPLTSVRNLFKSPSPKKRKLNGGSSS

>NP_173164.1[*Arabidopsis_thaliana*]

MKEEDVSSQNVNPRSNRNSVASASASASATPVDRFRRRARSPSPPQTAAASSAGASSPAVLVNAGSVDWTGHGLALSVRSCRTWDRGDLLRRLA
TFKPSNWLGKPKTASSLACAQKGWVSVDLDKLQCEYCGSILQYSPPQDSLNPPEADTTGEKFSKQLDDAHESSCPWVGKSCSESLVQFPPTPPS
ALIGGYKDRCDGLLQFYSLPIVSPSAIDQMRASRRPQIDRLLAHANDDLSFRMDNISAAETYKEEAFSNYSRAQKLISLCGWEPRWLPNIQDCE
EHSAQSARNGCPSGPARNQSRLQDPGPSRKQFSASSRKASGNYEVLGPEYKSESRLPLLDCSLCGVTVRICDFMTTSRPVPFAAINANLPETSK
KMGVTRGTSATSGINGWFANEGMGQQQNEDVDEAETSVKRRLVSNVGLSFYQNAAGASSSAQLNMSVTRDNYQFSDRGKEVLWRQPSGSEVGDR
AASYESRGPSTRKRSLDDGGSTVDRPYLRIQRADSVEGTVVDRDGDEVNDDSAGPSKRTRGSDAHEAYPFLYGRDLSVGGPSHSLDAENEREVN
RSDPFSEGNEQVMAFPGARDSTRASSVIAMDTICHSANDDSMESVENHPGDFDDINYPSVATAQSADFNDPSELNFSNQAQQSACFQPAPVRFN
AEQGISSINDGEEVLNTETVTAQGRDGPSLGVSGGSVGMGASHEAEIHGADVSVHRGDSVVGDMEPVAEVIENLGQSGEFAPDQGLTDDFVPAE
MDREGRLGDSQDRVSQSVVRADSGSKIVDSLKAESVESGEKMSNINVLINDDSVHPSLSCNAIVCSGYEASKEEVTQTWESPLNAGFALPGSSY
TANDQGPQNGDSNDDIVEFDPIKYHNCYCPWVNENVAAAGCSSNSSGSSGFAEAVCGWQLTLDALDSFQSLENPQNQTMESESAASLCKDDHRT
PSQKLLKRHSFISSHGKK

>XP_009107327.1[*Brassica_rapa*]

MAQDSEKRFHQIMDKLFTPSKSPLPSSPSSTSSPVEQQSRGKKRPNPSSALALVEPKTALATTIDRSLKVPATGTSQSGLCRPWDRGDLMRRLA
SFKSMTWFAKPQVISALNCARRGWVNDDTDTISCESCGAHLYFSAPASWSKQQVEKAASVFSLKLDNGHKLLCPWIENSCEETLSEFPSMTPQD
LVDRHEERSEALLQLLALPVISPSAIDYMKSSDLEEYLRRHIASGDTTAECSQTESLINHVGASPAQLFYQAQKLISLCGWEPRALPYIVDCKD
KSGEAAKGTDTIDLLPETATRELLSSSSSTSNPNGVSENSENPVVPDTLNSDPSSVVLDCKLCGACVGLWVFSTVPRPLELCRVTGDTEVNTEK
NSRDDTLQRQTSSLQFTIAGGPPATKQNFKATISLPIVGRNLRSRFASYSRDRDHGTDNSIQDQQCRTPERNGGGMENSDQDMIDVGEKADGGR
NASDLVSNTTPQTKDKQLMVVTSSLPENYKPKDSTGDTGISNKQMEFDPINQHRHFCPWIWSTGRRGPGWRQTLSALQRQKGSCQTPPAPSSIF
KVDDPLTSVRNLFKSPSPKKARLNRGSSS

>XP_033132690.1[*Brassica_rapa*]

MKEEGESSQNVKPRSKRNSVASASASASATPVNRFRHRSARSPSPPLTAAASSMFNSSVGASSYAVPVNAGSVDWTGQGMGSSGRPCRPWDRGD
LLRRLATFKPSNWLAKPKTASSLVCAQKGWVGVDLDKIQCEFCGSSLHYSPPQNSLKRPEADSNGEEFSKQLDVAHESSCPWVGNCCPESLVQF
PPTPPSALIGGFKDRCDGLLQFYSLPIVSVSAIDQMRASRGPQIDRLLALPQVYSNDDPSFRMGNISATETSKEEALSNYARAQKLISLCGWEP
RWLPNIQDCEEHSAQSTRNGCPSGTARNQSRLQDPGPSMKQFSASSRKASGNYEVLGPEYKSESRSPLLDCSLCGVTIRIWDFLTTSRPVPLAP
INANLPETSKKMGVTRGTSETSGINGWFANGGMAQQQNEEVDEAETSGKRKLVSNTGTSFYQTAAGASSSAQLNMSVTRDNYQFSDRGKEVMRR
QPSGSETGDRAASYESRGPSTRKRNLEDGGSTADRPPYLRIQHADSVEGSVVDRDGDEVNDDSAGPSKRTRGSEVQDTCLPFYGRDLSVGGPSH
SVDAENEREVNRSEGNEQALAFRGARDSARASSVIAMDTICHSANDDSMESVENRPGDFDDVNYPSVATAQSADLNDPSEFNLSNQAQQSACFQ
PAPVRSNAEQGISSINDGDEVLNTETVTAQGRDGPSLGVSGGSVGMGASHEAEIHGADVSVHRGDSVVGSMEPVAEVIENLGEFAPDQGVTDDF
VPEEMDREDRLGDSQDRVSQSVAKADSGSKIVDSSKAESVESGEKMSNMNVYDSVHPSLSCNAIVCSGFEASKDEVTQTWNESPLNAGFALPGS
SYTANGQGPPNGDSNDEIVEFDPIKYHNCYCPWVNENVTAAGCSSNSSSSSSVAEALCGWQLTLDALDSFQSLENAQIQPMESESAASLCKDDH
RAPSQKLLKRSFISSHGKK

>XP_009149168.2[*Brassica_rapa*]

MKEDDVSSRNVNPRSNRNSVASASASASAAPVDSLRRRARSPSPPQTAAASSVGASSPAVPVNAGSVDWTGHGLGSSGRSCRPWDRGDLLRRLA
TFKPCNWLGKPKTASSLACAQKGWVSIDLDKIQCEYCGSSLHYSPPQHQLNHPQADSSREEFSKKLDDAHEGSCPWIGNCCPESLVQFPPTPPS
ALIGGYKDRCDGLLQFYSLPIVSVSAIDQMRASRRLQIDRLLAQPQVYAHDDPSLRMDNTLAAETSKQEALSNYSRAQKLISLCGWEARWLPNI
QDCEEHSAQSARNGCPSGPSRNQSRFQDPGPSRKQLSASSRKASGNYEVLGPEYKSESRSPLLDCSLCGVTIRIWDFLTTSRPVPLAPINANLP
ETSKKTALTRGNSATSGINGWFANEGMEQQQNEDVDEAETSVKRRLASNAGISFYQTAAGASSSAQLNMSVTRDNYQFSDRGKEILLRQPSGSE
VGDRAASYESRGPSTHKRNLEDGGSTADRPYLRVQHTDSVEGTVVDRDGDEVNDDSAGPSKRSRGSEVHETYLPSYGRELSVGGPSHSVDAENE
REVNRSDPFSEGNEQAMAFPGARDSARASSVIAMDTICHSANDDSMESVENQPGDFDDVNYPPAATGQSADPSELNFSNQAQQSACFQPAPVRS
NAEAGISSINDGEEVMNTETVTAQGRDGPSIGVSGGSVGMGASHEAEIHGADLSVHRGDSVVGDMEPVAEVIENLGQSGEFAPDQGVTDDFVPE
EMDREGRVGDIQDRVSQSVARADSGSKIVDSLKAESVESGEKMSNVNALMNEDSVHPSLSCNAIVCSGFEASKEEVTQTWNESPLNAGFALPGS
SYTANDQGPPNGDSNDEIMEFDPIKYHNCYCPWVNKNVAAAGCSSNSSSSSSIAEALCGWQLTIDALDSFQSLENAQIQPMESESAASLCKDDH
RTPSQKLLKRHSFISRHGKK

>XP_012466404.1[*Gossypium_raimondii*]

MADDPEKRFYSIMDKLFHSSKSTTPFSSSPPAPGTGGQRQLLRAKKRPVPSYTTAVEKPQHCLAASEAPLCRPWDRGDLLRRLSTFKSMTWFAK
PKVVNAVNCARRGWVNVDMDIIACESCGARLLFSTPSSWKRQQVEKAALVFSLKLDSEHKLLCPWIDNTCDERLAEFPPSVPADLVDKFRERSD
SLFQLIALPVISSLAIEFMRSPQLEQFLRQPLMLDCLKGNAEFSHLERIEDGSAVDSAILYYQAQKLLSLCGWEPRSLPYVVDCKDGQNQFVKD
ADILSSSQGVGYGLNLHLSFRPTDENENLEANKGFENSFGLQYDPKSVVLDCRLCGASVGLWAFSTVQRPVELFRLFGCEEVNPGVHDSGHESD
VCEVPFNSGSSSMEQSSNSKLTIAGGPPPTRQNFKARIYVPVIGESLRARLLYHPEIRDQIYSNPKNTLVESNCNRILGEIDCFNNSVNQLGVP
LADLRTLNGKKDGQVNCNSKSSDQSPCSNYDVCSGDDTFRNVTPLEGTDFTAKENSPYTGIDDSNIGGQIESSQNLVLDSCQSNNFPEKVDNDR
TCNLAVKNSDAMLVGESSVMTQGANVSPRNEGAEANDSSVMVTSEKYYPEQNAEPDKVCDKKNCFSNRDSTCVASCLEADVNVDGTNKMNSRED
KTCSNSEEGVIAEVQAVQNNKVLSCPKGKDLKRLHMDKISEFDPIRQHRHFCPWIAPMSGGAPGWQQTLSALLYGKDFPHSSPVCSTSTVSMIK
VDDPIASVRKLFMSPTAKRTKITRE

>XP_012449448.1[*Gossypium_raimondii*]

MREEVISSGGTMDPTPAASSAGASSPAVPTNVGSVDWSGHGQNSKAASQSCVGSQAQWISLYSTAGGSALGSSRTSCRPWERGDLLRRLATFKP
VNWFGKPKVASSLSCARRGWINIDVDKIACETCGACLNFASSPSWATSEAEDAGQAFSKQLDVGHKVACPWRGNSCPESLVQFPPTPQSALIAG
YKDRCDGLMQFQSLPVVAASAVEHMRVSRGPQLDRLLYQLQNHMAEFESRSESILEADSARDGAFCLYSRSQKLISLCGWEPRWLLNVQDCEEH

SAQSARNGCSFGPNTTKVHRSQDPGPSKNALIASGKDIGKNKLIVVEARSEYRSPLLDCSLCGATVRILDFLTVPRPARVAPNIDIPDTSKKMG
LTRGVSAASGISGWVAIDDPEKEPTEDRDEVGTTDERNLMQKTDVELNLTMAGSLSFSQLGRAATSRNMNDADMGRDLMIGQPSDSEVGDRAAS
YESRGPSSRKRSLEIGASSEDRPQLRPQQADSVEGTVIDRDGDEVTNARQYSAGPSKRARDSDIFDTYCSPYPRDSSDAGPSHAMGCETSVDGN
KVALFRQGSSHVIGIPSARDSTRASSVIAMDTVCHSADDDSMESVENYRGDVDDIHFPSSSIYGHLDVNDTSELNYSNQAQQSICFQQTAEAVP
GEVGISSTNDGDEIFNAETVTAHARDGLSFGISGGSVGMCASHEADIHGADVSVHRTDSVVGDIEPRIEDAENQGQTGESAPDPGLMDEVVPDE
IDREDPLGDCREMLSRSLGRDDSGSKVDGSAKAESIESGEKISQSCKVIPDNNALPSLSCNANVYSGNETTKEIKNAGKSSSINNCTYPDPDSD
LAVATGIGPPKGESNYEEAIEFDPIIHHNQFCPWVNGNVAAAGCSGYSSSSSCSNADVVALCGWQLTLDALDALRSLGHIPVQTVQSESAASLH
KDDQQTPGKRLLQRHSVNKSHGQH
>XP_012453776.1[*Gossypium_raimondii*]
MREEVISSGGTIDPTPAASSAGASSPAVPTNVGSVDWSGHGQNSKAASQSCVGSQAPRISFSTSAGGSALGSSRTSCRPWERGDLLRRLATFKP
MNWFGKPKVASSLACAQRGWVNIDVDKIVCETCGACLHFASSPSWATSEVEDAGEAFSKQLDIGHKVSCPWRGNSCPESLVQFPPTPQSALIAG
YKDRCDGLVQFQSLPIIATSAMEHMRVSRGPQVDRLLSLLQNYVSEFESRSESVPELDVTRDGAFCLYSRSQKLISLCGWEPRWLLNVQDCEEH
SAQSARNGCSFGPNRAQVHLSQDPGPSKNALAPSAKDTGKNKVLVMESRSEFRVPLLDCSLCGATVRILDFLIVPRPARVAPNNIDIPDTSKKM
GLTRGLSAASGISGWVAADDPEKELTEDRDEVGTTDERKLVPKTDVDLNLTMAGGLSFYKLGRATSSRNMNDADMGRDLMIGQPSGSEVGDRAA
SYESRGPSPRKRSLEIGASSDDRPQLCTQQADSVEETVIDRDGDKFNDCRQYSAGPSKRARDSDFFDTYCSPYPRDSSEAGPSHSVGFETHGDG
GNRVALFRQGSNQVIEIPSVRDSMRASSVIAMDTLCHSAGGDSMESVENYRGDVDDIHFPSSSTYGHLDMNETSELNYSNQAQQSICFQPAAEE
VPGEMGISSTNDGEEIFNAEPETVTAQARDGLSFGISGGSVGMCASHEAEIHGADVSVHRTDSVVGDVEPRIEDVENQGQTGESAPDPGLMDEV
VPGEINREDPHGDSQEMLSRSLGRADSGSKVDGSVKAESVESGEKISQSCKLAPDNGAHPSLSCNANMYSGNETPKKEEKDAGKSSSINNCPEP
ESDFAVANGIGPPKGESNYEEAVEFDPVIHHNQFCPWVNGTVAAAGCNGSSADVVALCGWQLTLDALDALRSQGHIPVQTVQSESAASLYRDDH
QTPGKKLHRRRPMNKNHGQ
>XP_015622239.1[*Oryza_sativa*_Japonica_Group]
MATGGGGGGDIGADSERRLKKAMDKLYHFPKPKAGTGPGSSKPSSASTSSALSIGRAGKAAGAGGRRFGMVRGSRLPSQLAAMSAISPPPPCRP
WDRADLMRRLATFKAMTWFAKPKVISPVNCARRGWINIEPDVITCEACEARLLFSTPSSWAPQQVEKAAAVFSLKLDNGHKLLCPWIDNICDES
LALFPPTPPPVLVENYHEGFSSLLRLSALPRISCSSLESMKKRSPQLEQFLLKPFSSSVVLKGGFILTEDSTIKDLDHTFQDADTYYQALKIIS
LCGWEPRLLPYAVDCGTKSHSDANSSSTLTQPGLINNSMEDRVVVYAPNEVDGSTVIADARQAYQHYDPLSVVLDCQFCGACVALWPFSLVERP
LQLFKLISDSSRQDEQTEGHAGRVSGAGPSKTANIGFNFTIAGGPPPTRQNFRPRVSLPVVSRHLKADLSSHGHFISSGSDNHMVPVTLHASGL
TKHKRSMDESHMLEGNNTISTDAGTTTNGADHQRENSVNGTSNLVANPEHQQGGSHSDTSRVTSTGEVSNEESETGHAAIKSHTSTDELGQHGS
DPKSLPVEDSSNAHDLAKTCTNNSRPVQAATLTKSSNDGEKGASQPSGSQGLYDKLNEFDPMKQHRTFCPWICPDGGETLPGWRLTLPALLSQD
KRIDEDSQVEPQISLLSEEDDPVTSVRKLFMTPPSKKLRIHRAEKG
>NP_001389926.1[*Oryza_sativa*_Japonica_Group]
MREEVRSSSAAPPDPPPRSASPPATPVASSAGASSPPAQTNAASIDWLGGEPISKVESSSQIAPHAPRPSLSTNAAGAAVDFSQPSCRPWERGD
LLRRLATFKSSTWASKPKAASSLACARRGWVNIEMDKIACESCGAHLIFTALTSWSPAEVANAGEAFAEQLDASHLGDCPWRGNSCADSLVQFH
LTPSALVGGFKDRCDGLLQFISLPVIAKSAIESMKLTRSPQIDRVLSQAITILSGELGYKTDSTTGIDINHQDESCSYSQAQKLISLCGWEPRW
LPNVQDWEENSTRSAKHTASADPDQIHSRLPEHKQNSYSASVKKDKGKGKIHVKDSGCSMRSPLLDCSLCGATVRIWDFRSVPRPSHLSINNID
APDMRKGVLTRGISATSGINGWVAEGTERENVEGRGEAGTDEGKSLSNAQVDLNLTMAGGLPSTHSVMPSMHDHFNDGGMGRDLMIGQPTGSEL
GGFAASFESRGPSSRKRNLEEGGSTADKPLNRLHPADSIEGTVIDRDGDEVDDGAQDSDIRSNKRPRGFNLFDVNQPSSSGAGPSRNLSFDLDI
DVNKFDTYKAEGPSALHNPSASMRASSVIAMDTVHSAEENSTESVEYHPCDVDDVHKPSSAVRSGGMSEALDLNYSNQAPQSSFVQPAAESNAR
EIGGSSMNGGEEVLNAETAPAFARDQLSLGVSGGSVGMGASHEAEIHGVDVSEHKTDSVVGDVEPAPELTENMGNTGESAPGPGMMDEFVPEDV
GREEPQGDSQDVASRLVGRADSGSKICGSTKADSVESGEKMSHGIGHESNLQHSLSRNARVYSGIDLSKDEVTQIAKLPANDDYDPGDDLAANG
GNDYEAGLPEFDPISHHNNYCPWVNGHVAAACCINTGSSTSTGLSGWQLTVDALETIQSLAQAQNQIMPSDSAASLYKDDHVAPSRKLLKRASH
SKC
>XP_015630572.1[*Oryza_sativa*_Japonica_Group]
MREEVRSSSGAAAEPPPTPVASSAGPSSPAMQANVASIDWSGSRQASRVDSSSHVAPHAHQPSHSFDATGTALDSAPSCRPWERGDLLRRLATY
KPTTWASRPKAASSLACARRGWVNVDMDKIECESCGAHLIFSTLTSWSPAEVSNAGEAFAEQLDASHHNSCPWRGNSCADSLVQLHLTQSALIG
GFKDRCDGLLQFTSLPVIASSAIEHMRLTRSSQIDRLLSQSITFLSGELSYKAESTTGIDIQQDSSCSYSKARKLISLCGWEPRWLPNVQDCEE
NSTHSAKNADSVEPFFPRFAEHQKNSFSGSAKKDKGKGKRPLKDSGCSMRSPLLDCSFCGSTVKIWDFRSVSRPCRFSPNNIDAPETGKKLALT
RGISAASGINEWVTDGMERDPAEGRDEEATNEGKSLSNAGVDLNLTMAGGLPSIQSSIPIASERFNGGLGRDLMIGQPTGSEVGDHATSYESRG
PSSRKRNHEEGGSTVDKPQDRLQHADSIEGSVIDRDGEEVDDAAQDSDIPNKRSRGFDLFGSYLPSSSGAGPSRNFCFDPDADAGKFSHARAAG
LAAVDRDSMRESSVAAMDTVHSADEDSMESVEYYPGDGNDIDMPSSSAHRNIEMDDVLGLNYSNQAQQSACVQPASGSDGREIGGSSTNEGEEV
LDAVTAPAFARDQLSVGISGGSVGMGASHEAEIHGIDVSLQRAESVVGDAEPNTELTETMGHTGESVPGPGLMDEFVPDEVDRQEPHGDSQDMV
SQSVGQADSGSKIYGSTKADSVESGEKIGGHAVGHASRMHPSLSCNAGMQTGLDVSKEEVTQAGKLLIAGDVPMGLDYDPQNGLGATNGENDFE
SGLPEFDPVKHHNSYCPWVNGTVAAACCSNTESSSSSSPLSGWQLTVDALDTFQSLGQAQNHAMRSDSAASLYMDDHVTPNHKLARRASVSRSH
GKC
>XP_039810120.1[*Panicum_virgatum*]
MAAGGGGGGDIGADSERRLKKAMDKLYHFPKPKPSGPGGSKPSSSSAPAPSSGRPVGKAAAEAARRFGLVRGSRLPPQVTAMSAISPPPPCRPW
DRADLMRRLGSFKAMTWFAKPKVISPVNCARRGWINIEPDVITCEACGARLLFSTPSSWTTQQVEKAAAVFSLKLDTGHKLLCPWIDNICDESL
ALFPPTPPPVLVENYYECFSSLLRLVALPRISCSSLEIMKKRSPQLEQFLSEPFSSSVVLKGRFVLTEDSTIKDLDDAFQDADTYYQALKIISL
CGWEPRLLPYAIDCGTESHSDASSSPKLAQPQQISKTMEDRIILYSPNDANGARASADANREDQHYDPLSVVLDCQFCGACVALWPFSLVERPL
QLFKLVSDSNGQDDKDNGHANVVCGVGHSKDANIGFNFTIAGGPPPTRQSFRPKVSFPVVSRHLKADLNSRGNSLSSGSDGHMVPVASKALGSM
KRKRSTDQPDLLEGDTDDVDTSPIGAKSHQPGDNSEKSMPNPEVMNEQEQGGSHSDTDKYINMDGASNEKQPESSSPSRKSITSTDAALDQHGS
EPRFPSVQGTNEEPSNGVTLAETHANNSRPTELSTVTKSLVNKEKGAYGPSEKQGLYDRMNEFDPIKQHRTFCPWVSPDISESLPGWRLTLTAL
LAQDKRYDGDSRGEVQIGLLDEEDDPLTSVRKLFMTPPPKRRRIQQSEKS
>XP_039848146.1[*Panicum_virgatum*]
MPNGRQQLPAAAACKRITTPSPSLPPPIPHPAPATSMAAGGGGGGDIGADSERRLKKAMDKLYHFPKPKPSGSKPSSSSAPAPSSGRPVGKAAA
EAARRFGVVRGSRLPPQMAAMSAISPPPPCRPWDRADLMRRLGSFKAMTWFAKPKVISPVNCARRGWTNIEPDVITCEACGARLLFSTPSSWTT
QQVEKAAAVFSLKLDTGHKLLCPWIDNICDESLALFPPTPPPVLVENYYECFSSLLRLLALPRISCSSLEMMKKRSPQLEQFLSEPSSSSVVLK
GRFVLTEDSTIKDLDDAFQDADTYYQQALKIISLCGWEPRLLPYAIDCGTESHSDASSTPKLAQPHQISKTMEDRVILYSPNDANGARASADAN
QEDQHYDPLSAVLDCQFCGACVALWPFYLVERPLQLFKLVSDSNGQDDKDNGHANVVSGVGLSKDANIGFNFTIAGGPPPTRQSFRPKVSFPVV
SRHLKADLNYRGNLLSSGSDSHMVPVASETSGSMKRKRSTDQPDLLEGDTDDVDTSPIGAKPHQPGDNSEKSIPNSEVGNGQEQGGSHSDTDKN
INMDGASNEKQPESSSPSRKSITSTDAALDQHGSEPRFPSVQGTNEEPSNGATLAETHANNSRPTELSTVTKSLANKEKGAYGPSEKQGLYDRM
NEFDPIKQHRTFCPWVSPDDSKSLPGWRLTLAALLTQDKRSDGDSRGEVQIGLLDEEDDPLTSVRKLFMTPPPKRRRIQPSEKS
>XP_039827893.1[*Panicum_virgatum*]
MREEVRSSSGAAAEPPLAVARSSSPPHTPVASSAGASSPALQTNIGRQASRVDSSSQVAAHAYHPSHSFDAAGTAMDSAPSCRPWERGDLLRRL
ATFKPSTWASKPKAASSLACAQRGWVNIDLDKIECESCGAHLIFNALMSWSPVEVASAGEAFAEQLDAAHQNSCPWRGNSCADSLVQLPLTQSA
LIGGFKDRCDGLLQFTSLPVIASSAIENMRTTRSAQIDRLLSQSITFLSGVLGCKAESAAGVEIQQDSSCSYSQAQKLIGLCGWEPRWLPNVQD
CEENSTHSAKNAPSVGPDEPFYPHFVDHIKNSFSASAKKDKGKGKLPLRDSGCSMRSPLLDCSLCGATVRMWDFRPVLRPSRLSPNNIDVPETG
RKLTLICGISAASGINEWLTDGVERGQEEGRDEAATNEGKSPLIIGVDLNLTMAGGLPSPRSATPAASERFNNGGMGRDLMIGQPTGSEVGDCE

TSYESRGPSSRKRNLEEGGSTADNPQDRLHHADSIEGNFIDHDGEEVDDAAQDSDVPNKKSRGFDLFDAYRPSSGAGPSRNLSFDPDVGAGMFS
SSRSIDLAVERPAARDSLRASSVIAMDTVRTSEEDSMESVEYYPGDGNDIDMPSSSAHRNIEMNDVLDLNYSNQVQQSANAHAAAGSDAREIGG
SSINEGEEVINAETAPAFGRDQLSIGISGGSVGMGASHEAEIHGNAASLHRAESVVGDAEPIAELTETMGQTGESGPGPGLMDEFVPEEVNREE
PHGDSQDMVSRSVGQADSGSKIYGSTKADSVESREKIGHATGIESSMRPSLSCNAGMCAGFDPAKDDVTQSGRIILTTDDTLMGLDYDPGNGLG
ATNGENDYEAGLLEFDPVKHHNSYCPWVNGIVAAACCNNIGSSSSSSALSGWQLTIDALDTFHSLGQAQNQIMQSDSAASLYMDDQNQITNNRR
LGRRPSVSRSYGKC

>XP_039782290.1[*Panicum_virgatum*]

MREEVRSSSGAAAEPPLAVARSSSPLHTPVASSAGASSPAMQANIGRQASRVDSSSQVAAHVYHPSHSFDAAGTAMDSAPSCRPWERGDLLRRL
ATFKPSTWASKPKAASSLACAQRGWVNIDLDKIECESCGAHLIFNALMSWSPVEVASAGEAFAEQLDAAHQNSCPWRGNSCADSLVQLPLTQSA
LIGGFKDRCDGLLQFTSLPVIASSAIENMRMARSAQIDRLLSQSITFLSGVLGCKAECTAGVEIHQDASCDYSQAQKLIGLCGWEPRWLPNVQD
CEENSTHSAKNAPSVGPDEPFYPHFVDHIKNSFSASAKRDKGKGKLPLRDSGCSMRSPLLDCSLCGATVRMWDFKPVLRPSRLSPNNIDVPETG
RKLTLTRGISAASGINEWVADGVERGQDEGRDEAATNEGKSPSIIGVDLNLTMAGGLPSPRSATPAASERFNNGGMGRDLMIGQPTGSEVGDCE
ISYESCGPSSRKRNLEEGGSTADNPQDRLQHADSIEGNFIDHDGEEVDDAAQDSDVPNKKSRGLDLFDAYRPSSGAGPSRNLSFDPDVGAGMLS
PSRTIDLAVERPAARDSLRASSVIAMDTVRTSEEDSMESVEYYPGDGNDTDMPSSSAHRNIEMNDVLDLNYSNHAQQSANAHAAAGSDAREIGG
SSINEGEEVINAETAPAFGRDQLSIGISGGSVGMGASHEAEIHGNAASLHRVESVVGDAEPIAELTETMGQTGESGPGPGLMDEFVPEEVNREE
PHGDSQDMVSRSVGQADSGSKIYGSTKADSVESREKIGHATGIESSMRPSLSCNAGMCAGFDPAKDDVTQSGRKILTTDDALMGLDYDPGNGLG
ATNGENDYEAGLLEFDPVKHHNSYCPWVNGIVAAACCNNFGSSSSSSALSGWQLTIDALDTFHSLGQAQNQIMQSDSAASLYMGDQITNNRRLG
RRPSVSRSYGKC

>XP_039793133.1[*Panicum_virgatum*]

MSVSVGKTRVGRYELGRTLGEGTFAKVKFARNVETGENVAIKILDKEKVLKHKMIAQIKREISTMKLIRHPNVIRMYEVMASKTKIYIVMELVT
GGELFDKIASRGRLKENDAKKYFQQVINAVDYCHSRGVYHRDLKPENLLLDASGTLKVSDFGLSALSQQVREDGLLHTTCGTPNYVAPEVINNK
GYDGAKADLWSCGVILFVLMAGYLPFEDSNLMSLYKKIFKADFSCPSWFSTSAKKLIKKILDPNPNTRITIAELINNEWFKKGYQPPRFETVDV
NLDDVNSIFDESGDPAQLVVERREERPSVMNAFELISTSQGLNLGTLFEKQTGSVKKETRFASRLPANEILSKIEAAAGPMGFNVQKRNYKLKL
QGENPGRKGQLAIATEVFEVTPSLYMVELRKSNGDTLEFHKFYHNISNGLKDVMWKPDGSIVEGDEARHRRTATSKKKNSSHTPRARPASSAPP
PDPTRRGLLPRRPRERASAAAMREEVRSSSAAPPDPPPARSASPPPTPVASSAGASSPPAQAIVASIDWLGSDQVSKAGSSHVAPPASQPALST
NADGAAADFFQSSCRPWERGDLLRRLAMFKHSTWASKPKAASSLACAQRGWVNIDVDKIECESCGAHLIFTALTSWSPAEVANAGEAFAEQLDA
SHQNDCPWRGNSCADSLVQFHLTPSALVGGFKDRCDGLLQFVSLPVIASSAIESMKLTRSFQIDRILSQSVTILSGELGYRTDITTGIDINQQD
ETCCYSQAQKLISVCGWEPRWLPNVQDWEENSTRSARNAGSAEPDGQFHSQFAEHRQSSYSASVKKEKGKGKMRVKDSGCSMRSPLLDCSLCGA
TVRIWDFKSVPRPSHFSLNNIDMPDTGRKPVLTRGISATSGINGLVAEGAEKENVEGRDEGGTDEQKSVSNAQVDLNLTMAGGLPSNYSALPPM
PGHFNYGGMGRDLIIGQPTGSELGGHAASFESRGPSSRKRNLEEGGSTADKPINRLQPADSIEGTVIDRDGDEVDDAAHDSGARNKRPRGFNLF
DINRPSSSGAGPSRNLSFDLDIDVNRFDTSNAEGPSALHNTFPKDSMRESSVIAMDTVHSAEENSMESVEYHPCDGDDVNKPSSALRSGGMSEA
LDLNYSNQAQQSSFVQPAPETESNAREIGGSSMNGGEEVLNAETTPASARDQFSLGVSGGSVGMGASHEAEIHGTDVSEHKTGSVVGDADPVPE
LIETMGHTGESAPGPTLMDEFAPEEVGREDPHGDSQDMASRLAVRADSGSKVCGSTKADSVESGEKMSHAVGPENSAHPSLSCNARVFSGVDAS
KEEVTGIMLTNDDYDPGNGLGATNGENDYETDLPDFDPIKHHNNYCPWVNGNVAAACCISTGSSTALSGWQLTVDAIETLQSVGQAQNQTRQSD
SAASLYKDDHAPPRRKLLKRANHSRS

>XP_039834233.1[*Panicum_virgatum*]

MSVSVGKTRVGRYELGRTLGEGTFAKVKFARNVETGENVAIKILDKEKVLKHKMIAQIKREISTMKLIRHPNVIRMYEVMASKTKIYIVMELVT
GGELFDKIASRGRLKEDDARKYFQQVINAVDYCHSRGVYHRDLKPENLLLDASGTLKVSDFGLSALSQQVREDGLLHTTCGTPNYVAPEVINNK
GYDGAKADLWSCGVILFVLMAGYLPFEDSNLMSLYKKIFKADFSCPSWFSTSAKKLIKKILDPNPNTRITIAELINNEWFKKGYQPPRFETVDV
NLDDVNSIFDESGDPAQLVVERREERPSVMNAFELISTSQGLNLGTLFEKQTGSVKKETRFASRLPANEILSKIEAAAGPMGFNVQKRNYKLKL
QGENPGRKGQLAIATEVFEVTPSLYMVELRKSNGDTLEFHKFYRNISNGLKDVMWKPDGSIVEGNEARHRRTPRRFHQTKSMDNVNEGMCRVSI
GLSKHRRGPAGDLDVLRRSCILSVADPDAVVAQFSCACLTGPSTPALAAATTPTAVGGNGLSSDNDEQEGEDLALVRIIRKNLHRVNKASPASS
LPPGDAPGGGDTSSPRSILFGGSIAETTQPRQEEEPKAQGRSITAQSASAELNGASPRSFAHAALALPADLLCSARPDPTRPPPPTTLPQSERP
EAAMREEVRSSSAAPPDPPPARSASPPPTPVASSAGASSPPAQGSDQVSKAGSSHVVPPASQPALSTNADGAAADFFQSSCRPWERGDLLRRLA
TFKHSTWASKPKAASSLACAQRGWVNIDVDKIECESCGAHLIFTALTSWSPAEVANAGEAFAEQLDASHQNDCPWRGNSCADSLVQFHLTPSAL
VGGFKDRCDGLLQFASLPVIASSAIESMKLTRSVQIDRILSQSVTILSGELGYRTDSTTGIDISQQNESCCYSQAQKLISVCGWEPRWLPNVQD
WEENSTRSDRNAGSAEPDGQFHSRFAENRQSSYSASVKKEKGKGKMRVKDSGCSMRSPLLDCSLCGATVRIWDFKSVPRPSHFSLNNIDMPDTG
RKPVLIRGISATSGINGLVAEGGEKENVEGRDEAGTDECKSVSTAQVDLNLTMAGGLPSSHSALPPMHGHFNYGGMGRDLIIGQPTGSELGGHA
ASFESRGPSSRKRNLEEGGSTADKPINRLQPADSIEGTVIDRDGDEVDDAAHDSGDRSKRPRGFNLFDINRPSSSGAGPSRNLSFDLDIDVNRF
DTSNAEGPSALHNPFPKDSMRESSVIAMDTVHSAEENSMESVEYHPCDGDDVNKPSSALRSGGMSEALDLNYSNQAQQSSFVQPAAETESNARE
IGGSSMNGGEEVLNVETTPASARDQFSLGVSGGSVGMGASHEAEIHGTDISEHKTGSVVGDADPVPELVETMGHTGESTPGPMLMDEFAPEEVT
REDPRGDSQDMASRLAVRADSGSKVCGSTKADSVESGEKMSHAVGPENSAHPSLSCNARVFSGIDASKEEVTGIMLTNDDYDPGNGLGATNGEN
DYETDLPDFDPIKQHNNYCPWVNGNVAAACCINTGSSTALSGWQLTVDAIETLQSAGQAQNQTMQSDSAASLYKDDHAPPRRKLLKRANHSRS

>XP_002963700.1[*Selaginella_moellendorffii*]

MTSGDKDDDAEQRIQRAMDRIFSSPIQAASSCSSSPPTKSILERRVVTPLALERSPGEKNAGEKNAGEIASSSTPSCRPWDREDLLRRLGTFKS
VSWFGKPSAAGPVACAQRGWINVDMDLLCCEVCGSRLSFSFPATWSKKEVETAGLEFSRKLHDGHKTSCPWKGNGCGEDLAAFPPTPAPVLVQA
YEARLQSVALLSDLPVISSSTVERMKISRGDQVASLLALPSNDAAVRELEAAQGEAVQKLRQTYEAFLQAQKLISLCGWEVRLLPYAVDSHDSN
VDSHELRVSLATGSDPCSAVLECRLCKASVGLWRFRTLSRSSLSITAILSTIEASAKKNVEVLPAGDVNAHVDDNAAENIDTVNAEATISEDND
AAAVDDSKKNPGLDLTLTIAGGPRPTRLSAPSPASIPIPGLNSQRHDDFQPRKSTLEQEPAEKTTVQDRSSSKRKRDSESAHRKKLKAVDGLPG
SSSVNAVETSYNHNRHENSAESVECSPQGSDEEQDTVLSREKAASQDVAKEAAIFSGSPSEFDPVHHHRYFCPWISSNAADQSGKCGWQMTIDA
IFSCAATNAKSGVVSDRDKAAAVNKMDPLVSVRRMLGGKGKGVAVNGGAISMSRAGT

>XP_002981891.1[*Selaginella_moellendorffii*]

MAEDAAERRMERPLFGVSPPTPTASSAGPTLAVQGNYASIDWHGLAQKRPAISGTSAGPPRPAVSTSTAAVSGSSSHRHLCRPWDCGDLLRRLS
TFRTSNWNAQVIGPAVCARKGWVNVDVDMIACEGCDTHLSFALPLQTEVEAASESFRKQLETSHQRSCPWKGNACSESLAQFPSSAMALIGGYN
DRCDALLQLPSLPVVSTFAVDQMRLSRGPQIERLLSLPAMHFPERNGAGPLTDDFVKAQRIISFCGWEARLLPHAGDLEDYSAHSSRKPNKASA
SLKRAKRTMPRSDKEGDSRGARQTASTLLECVYCGASVPILRFQTVARPGGGSTGSEYPSSDNKSLPLVRGASAASSIDIHKRRQRLEGGEAGE
ATEQKPPSLTITAARASPTNLNVTPVARPEQQPEGSEMGDCGVASYESRGPRDDHQGTAAQGDSSTYVPQLRAESAGGTNGDFDNEDEGKNAAE
SSKRKRVPESLAADQHSLGMAVSGNAATCEQEGETEDRKNKKVCIGPATAIERTVSLEVPDNTYNRSARSLPVRQENLRRRVTREYPCSSSVNA
IDTCFQNKMEDSMDSVEFAPQDDAQQHTAASGYTENEWLFDEPNSTVQGQQSNSYAPAAIQEQATGETNAAVISTGTATGCGGSVGMAGIRLGS
QRVQSNEADIQGAELSELQTESVAGEPADAVVDAVVDQGDPGLVCDSTPLTAAQDCAGGGDESGESGSKASLRPRNGFSEERTIDTTNAVVTGC
SIGTIAKEMTEGSVEVAAVGDNVRAVNVNSAPTVKEAEDTLFDPIRCHRSFCPWVNGLVLSAANGTFGPGPVYCGWQLTVDALDAFHQQENASA
GVTESESTASMCKDDGRGRIFAQGSSSQPCNGSSRLEPN

>XP_024380728.1[*Physcomitrium_patens*]

MEVTEVSEKRFERAMERLFSGSSTPAASSARVPSPVKEKKEDEENTSGRVFQTAGVATPLSGSHGCRPWDRGDLLRRLATYKSISWFGKPQVAG
PVACARRGWVNVDIDLLACEICGSRLSFPVSSSWSRHQVEQAALVFAEKLDTAHKGLCAWKNNPCAETLAHFPPTPVSVLRGAYTDRCEALLQL
SALPVISDAAKSLMKLSRGPQVDQLLSELNPPSPGFLVGNGASSSSTENEIFANSKAYYEAQRMIAVCGWEPRLLPYTVDCEDRSGAQSIHEQI
GTSHGPGPSVTVHMQGGQQSKVAQGQIQSTGTDVSDPASAVLDCNLCGASVGLWNFATLNRPAPLLNSGLEELFSSKNRSSGSNPVRDDAAGAV

GGPLLASPEAAEMVDAKPPEVVPVNVLERAAPPKGVLDLKLTIAGGPPPTRLIAPASVPPSFGIPGLPHTVMQPRKIEAITYAAASYESRRPAH
QGRGHNDTGTPTYHVEGEVIQNREMKDAEESKDAEYFSKRKREKGNDESEGVFSPNTKRKREVGSQWPGFTVKLPARDLPHASSVNAIDTCYPP
KQENSMESVDNLPLGSDGQGANTAEYHVNGPESRVQAEHSMSRQDGIDAGKSICGGRVEEGVQNNVVVICPGAGISGSHETEIQGVEANLERSE
SVAEFATDVIELMEEHVSGRGLMDEFIPEDTLKAIVTDDHEGSRQAMLGISHTFVKDTSSAGVSERYQRNVAQRDADEDANAGSTLETTNAIIQ
GVDMVANIQVKEVTAGRTVGESPSERNEEVQSHPSFPPGLLLDDVKKLEIQTGEFDPIRQHRHFCPWVNAHVAAATSGTGSSKFCGWQIVLDAL
QPQPPSPHQQHQHQQGSVESEFTGSKYKDDPILSVRKLLGSVSSNYLPSS

>XP_042921239.1[*Chlamydomonas_reinhardtii*]

MSSVYERITSALSSLGKRRERDSSAHEGDGAGASAAGGGPTSPGGRSAAARTPKRFRPWEQADLHKRLETYKPLTWFGKPASVGPVPCALKGWV
NDGSDCLTCEYCGSKLVYPPHVAYDQRQAAADMFSPSLTTKHTATCPWRQTACQPKLLAYVPSTTPEQLCSLFYSLADKLMRVDVLPDMDTLAI
QTLRSTAMPYGSYDDFITAAAPGGGAVVGGGGAAGYSHDLAPRRRQMPSATIRELDQNGDEVMTPSGSAAGAAAAMAPAAAAGGGGDAAAVLQA
LVAAGDAGEGQAVLVQTSKLAPAQKARLLALLGWDVDVLQPDSASGMAVAPFAAGGSYSLSHLGVKPKAAAAAAAGAGAGGAAVPGTPGGAGGK
GGKGSSKVPSSQVVLKCPICNSRMGLWNYSGVRPVPVGRLTAPPPPAAGGAAALMLSPRPAAASSGGGAAAAAAPAVPATIGSDPLSCTIAGGQ
YGQFGFGGAASAAKPFGSAAAAAPFRFGSAASTAPVFGLAAMDVDAQRAASAASGPFGSAAAAAAATPSMPAPSGSATPAPAGRKRKAEAPEPM
ALDAQHTPSAGMATPVAAPDGKRQRMAATPLWGGAGFGAVGGPAASPSGLGLGGASALAAASAAGQPRELDPVAQHRSWCPWVYTGSGDEKHMS
GWQHMLSALSQHQQHQQQQANVAATPGAAAASPADARQLRDNALEAIRKL

Representative sequences for Figure 3D:

>OTA34089.1[*Hortaea_werneckii*]

MAEAIATKKRNFYKSLDAFNNPNPSSTSVATEPATKRPRRNLSAASAASRLTTATANHPATPAKPNQSPKPPPAFSPWSQDTFLARLRTFSRVS
LWHPKPQSISEVKWAKRGWSCVDVNTVACKGCCGKRVVVSLDFAKTESVNRGEDVEGDGDNGEAQENSEQDEDELEAALALKYQALIVDGHSDS
CPWRRTGCPDDIYRLQVIRAASWQLELRRRYQSLHQISDAIREVTLRGSSQDKQSLIPIDQLLADLPADVLGPPGEEQPAPEDSLKALEIAMHG
WKGSEDSGNELLHCDACFQRVGLWMYQPGYKPARSSSDDEDQTAIVDLVELHREHCPWRNPDNQCALGTLKGLNACQVLQTCVSAFVKDERRRD
ERQRKSVHQPETTEDEQEAESSPPSPAPSRDEIEKQDKERESRLKRLKSLFTIKRKSTVVAPPNPKPSIVGKRPATRG

>OTA24219.1[*Hortaea_werneckii*]

MAEAIATKKRNFYKSLDAFNNPNASSTSVATEPAAKRPRRKLSTASVASRHTTATANNPATPVKPNQSPKPPPAFSPWSQDTFLARLRTFSRVS
LWHPKPQSISEVKWAKRGWSCVDVNTVACKGCCGKRVVVSLDFAKAEGVNRGEGVKSDDDDAQGDTEQDEDELETALASKYQALIVDGHSDSC
PWRRTGCPDDIYRLQVIRAASWQPELRRRYQSLHQISDAIRDVTLRGLPQDKQSLVPTDQLLADLPADVLGPPGEEQPAPEDSLKALEIAMHGW
TGSEDSGNELLHCDACFQRIGLWMYQPGYKPARYSSDDDDQTAAVVDLVELHREHCPWRNPDSQCALGTLKGLNACQVLQTCVSAFVKDERRRE
ERQRRGVQQPDTNGDEEGHESAPPSPAPSRDEIEKQDKERESRLKRLKSLFTIKRKSTAVAPPKPKPSLVGRRPATRG

>KKK13521.1[*Aspergillus_rambellii*]

MSYALETKKRKFHRVLESLTRPLNGESSPKLTSASSAPSLEHAPSAKRARLSGLGDGDFPSVRKKTFQPARPSSSNSSSSFSPRPSFVPWDRDR
FLERLETFRRVDRWSPKPSAINEVEWAKRGWVCSDVSRVTCAGGCGGSVVVKLPDELDELDGYDSEKIQERKEVRTKLVNEYANLVIQGHGENC
PWRNKGCDATIHRLPLANPDTAISGLQTRYSHLLKMADKLPSLVDLQLPEHWDLQAIISVLPLEGFQGLESQVETTDTQPPAGGDESQQRELQT
STHPEPAVNESAFVLAFFGWDSVADGAVGLAGCGACFRRLGLWMYKPRQEGKSSAHDPLDVVNEHMEYCPWINGKTQSGTGKPSEKMEGLRSGW
ELLAQGLKVKHLRYIRSTEPIGSRAGSEAPSVGDSVAEETSDDTKKAKDREWWAKIRRMRQVLNVKSPKPKT

>XP_037155881.1[*Letharia_lupina*]

MPTGTALSTTKRKFHKILDSISNASSTSLATKSNHDNYNASTTTLPTTMDPPAKKPRIVRPASAYVPPSTRILTSQSPNLRAAAATAKQPSPIV
TMNEERKTPNFAPWDRGQFLERLKTYRHVDKWMGKPERINEVQWAKRGWSCVGKERVECVGGCGKEVVITLESSREEKHDNGETQDTEKRPSDE
EEDEDEWREKAQEQLVEKYAEMVVTSHDGGCLWRRRGCDDTIQRLPLAHHKTATDELRQRYTSLVAVASELPPDPSTPEGFDLSSLSQKLAPLL
HPPSPDPPSPTPSSPPNPPPNTTTSLPPINNSALALALFGWRAEEGHVVGLATCTACFRRLGLWLFKPASESPSHSSMDRLDVVGEHRDYCPWI
SPLSQNGATSRRTSLDGLAGWEALLRAVNASAIHKRHGDEDTTPVTARAADGLGSEVASLAHSSATREELGVRDERDKERWAKLKRLKQAFHVK
RRKGKDNGETKGGNGKV

>XP_957690.1[*Neurospora_crassa*]

MNATVKRKFNSLLQGIGNRPTNPDSPSSTRDNDSLSSTPASSSSSRFTNMANDSLDYLSKKRRVGGLPSTPSAITLTTPTKGQTTISNVTLRKW
NSHGGPGSSPAPGAGGGSSNAKGDSPVTKLQPPKYCPGDRNQLVRRLATFQELTDWTPKPDRVNEIEWAKRGWVCQGKERVKCTLCNNELAVKL
NRKEVDGKEIPVLIAADIAESVVDQYVELIITSHREDCLWRKKGCDDSLLRLPLPNPKLALETLRQRYDELCQRKDFLPYEFNLRLPKGLDIDI
ILSYLPSNFFAEPPASSTVDSSVASQPASPNPSTSQQPQAVNRTALALALLGWQGLTNPRLGTAVPNSASCHTCLRRLGLWMFKSKQVDPETNT
ILVPAPMDHLDPLREHRFFCPWKNPQAQRNPGAKPLARGETNKAAWEVLVEGLKNESRLREKARDLMHGRSKSSSSGFGFGLGGKKGTPHRATG
STSGFLGVPTTPDGRGVTGQQPNSAPGGLQVGGQEGGGQEEEGFEEEDDDESEEARKKKDQAMMSRLKRVKTLFNTKGSKLKKSGASPSPSAVN
IPDSPRPGSSHSTRTTGTPGTAATTGISTNAPAE

>PUU81978.1[*Tuber_borchii*]

MLYSTKRKLHNLINGPPAPSTSISAPSTPAKQPTDLPTTTTAAFDDNDVVLIAPAVADAAKKRRLGGLGNRSRPSVRAVSPTGSIRSTVSTTSS
QQMPTYSPWDRAAFLERLRTYRFVDKWSAKPVDVNEVEWARRGWSCIDKNRVRCGVCKREVVVKVELDEEQDSDITKAVVEKYKEMIVTEHEDR
CLWKKRGCDDTIYRLQLANPSVSRPSFVSRYSSLLRIRPEIPPSLSYPTADFPEHILETIHENTLLLEEQHSGALVLALFGWQNEDPGIPSLVT
CSACFRRLGLWLFRKKVVSIFDSVDEQEEASVCRLDVIGEHRDYCPWINATNQGTEPGWQIMLRILQQPNKGPALGSYTERDAEDQSKLKRLRK
LGAMYLGATKKTKGKGKESKERPKTPKTPKTPTKEAPPPKTPKTPKTPSKDASKTPKTPSRDPPKTPKTPSREAQKTPGRSEE

>NP_013600.2[*Saccharomyces_cerevisiae*_S288C]

MEKDALEVRLKSIRHSLDKNTKLLPGKYRNTLGERLITKWRYKKKSHNGSSMLPEKCKSHVQLYDDLVQESSKHFVGFRLHDLRALLKRICSIQ
NYTRHVLIEWDVRWVNPLTLASKGWEPYQSASQSQVPFKCCCCHAIMTIPLLKNGDDVADYTMKLNEKIWNSNIIGNHLQKCPWRENQVDLNKE
YYLSSQNLIREIERIHTEIDRIVSGSNEFSLKRNSSRIFHYLSEKEIQKLAFFFDCKDYSLVGLLLLGYTKFQKDDLVQCTACFHRASLKKLEY
TEFNGHALWCRYYNKELLPTMLLELIGKEDKLITKLGVGERLNKLEAVLQTL

>NP_588231.1[*Schizosaccharomyces_pombe*]

MSFPTDMETNEILDQLDKIDERNEDILLKSLKASKCTYKPWSREEFLRRLLTYRSRWAYVNDPQIGEINCCLNGWLCESNNILVCDVCRNKINL
TALQQVDAENDSLNELPEKTKERLEVSLKEEHQDNCLWRLHKFPPDIYHLSVSAELVQVGRRFNSLSTRLVSTHLPEEMTLKRLEKVANKIRVD
WEKEDAAVLLGIALTGWSEQVPGRLYVCNYCHRRLGVWNLQSEGQDFDVLEEHKKSCPWVIPQPFTDLLGWQQIFELLCKESIFQSTTKTMDVS
QYTDYTFSLLQGLR

>XP_024513553.1[*Cryptococcus_neoformans_var._neoformans_JEC21*]

MELSSNTDDDLRDVFKLLYADDDWALTSDSELDDSEQLGNADGSEIDVADDEEQHTIRIYSGRITKKRLFSALDSLLSPGYETDTKRQRIYNPP
APSIPSLILSTQPMPALPLSKVYAPFSALSLLSRLMTFQPYTYSPQHPLTLSPVRAAMKGWVNEGREGLKCDVCGARWGLGGLEKVRDEAMKSN
LGERLAKGFEERHEKNCAWRICASPGNLYEQLRHLVHPPITSSLAPLASHLLLECLALPSLRLLSPLNPLQVERLVSLFKPSSTFSIPSPATDV
ASQLALFGWFPYHPNYPTIQISLNTPSSRTEIVCCRICHRRIGLWNFSNEKDGVKRFDVLNEHLVWCPVRIQDGEKEWWSESGLLDGQSTQAKR
IGEGGIKGLVKVSEKMEKRSWRRS

Additional sequences:

>NP_001298015.1[*Mus_musculus*]
MAATSEGPLFAASIEKTWGSVVRSPEGTPQKVRELIDEGIVPEEGGTEPKDTAATFQSVDGSPQAEQSPLESTSKEAFFHRVETFSSLKWAGKP
PELSPLICAKYGWVTVECDMLKCSSCQAFLCASLQPTFDFGRYKERCAELKKSLCSAHEKFCFWPDSPSPDRFGMLPLGEPAVLISEFLDRFQS
LCHLDLQLPSLRPEDLKTMCLTEDAVSALLHLLEDELDFHADDRKTTSKLGSDVQVQATACVLSLCGWACSSLEPTQLSLITCYQCMRKVGLWG
FQQIESSMTDLEASFGLTSSPIPGVEGRPEHFPLVPESPRRMMTRSQDATVSPGSEQSEKSPGPIVSRTRSWESSSPVDRPELEAASPTTRSRP
VTRSMGTGDSAGVEVPSSPLRRTKRARLCSSSSSDTSPRSFFDPTSQHRDWCPWVNITLVKETKENGETEVDACTPAEPGWKAVLTILLAHKRS
NQPAETDSMSLSEKSRKVFRIFRQWESSSSS
>CAB55333.1[*Yarrowia_lipolytica*]
MHNTSTYHHTMPTEEQLHGIMESLREVTRKSGSAPTTPTKHSPRNSTLKTATPNRFTTASSTSGKISKRPSLMERIRQVKEKDYRRTTKEITEL
APTTTATSTPATYTPWSKEDFLDRVSTYTYQKYPIETSLYPKLSPYNVARYGWKCTSSKMLQCVSCGSYLAVVCGEEDDEATIKVVQDKYLGLI
TRNHSTRCLWKNKPCSESLGSIMGNIGRLRKDLGGKIAIPEGVEVTVDGQSVEDFFKKLLLEVDGEVNKEIDENRGLDLKEEVKENGSGSNKDS
NDLTQSAELGSDSKLIPEEVSRITLAAGWRESHNMFKCHVCSRIVKPSETFDVVQEHRDWCPYVVEKEGDKPAWWQVLTKPSKESSKKRLSNIR
EVYFGV
>XP_002634353.1[*Caenorhabditis_briggsae*]
MEVDSANNRHAAVLKRKATDSINEVLSFGQSSSSPQKRTKKTPLHKIRDVEAYKKIIKTYKAPTWFGCAVSPRDLADYGWECVKKDCVKCVECE
ELLCTSLPNICKVSFNVYNSRLQEIHDQLSSAHRTTCKLRTGAPPIRFTEPTSKEIMSGIQSRLSDSKSIEDDDFVVHIPSDVNLPKLEGISDR
LMYVAALGWHVTKPRRGTLMFGCDYCARELAIRCGNGFDPIHNHERWCPRIDMDEHGEPSWQSDISIVLNTKNRVSHRYSGSSIFKEAYAARRL
IDSSLSTIISPNLL
>KAF4260764.1[*Aspergillus_fumigatus*]
MSYAVETKKRKFHRMLESLTKPSTVEPAAKKIPASPSPARERLPADLSIKKVRLSDKDESNFAAVGRSILKARASSKGSTISSATRPSFVPWDR
ERFLERLETFRRVDRWSPKPAVISEVEWAKRGWICTDVSRVSCVGGCGGSVVVKLPDELDELDGYALDKVQERKEVRDKLVEEYASLLVKGHGE
HCPWRNKGCDATIHRLPLTNTDTAIASLQKRYSNISKIADKLPAEDIIRTPESFNLDDVLKIWPRESFETGDGLRSTESQREQQDQSQDQESSE
EIRGESSQVAPAPSKPIDRAAFALAFFGWDAVSNETAGLVGCSACFRRLGLWMYKPKDNGDATVYDALDVANEHMEYCPWISGKAQSGTGRATE
KQAELRSGWELLVQALKVKHRRQVRSSTSMDTLRAVSETPSGDFPVVDEVSEEQKKASDREWWAKLRRMRQVLNVKSPHAKKSVVP
>XP_006958443.1[*Wallemia_mellicola*]
MNKRKIEDALTRLDKAFQSEDSVKAESSKRTKKPKIPAELEERLRWFTMTHNLQSRRSKSTDLLKKKEQSDLFSFHNFILRLQSFSLRTYTSKP
IELSPPAVALRGWQHDEAHRNRILCSRCKVGFIVDLSGSQANSYQKLIDTYVEAIESKHTSHCPWKYQQCASSTYRIHELSLPPNLAANVIAER
ARKIDSNLNFSIRVKHPLSNEQVQSLFNAMPEPKPSEDATILAIYGWEYKSTISSSSYLLTSELDVANVSVKPEKVFDVVREHRFYAPQLMPAN
EGSKNTGVEALLALITRRGRKKEIQESMIVNSVSVGSNTATVSLLI
>XP_037145256.1[*Zygotorulaspora_mrakii*]
MDSLSHGRLQSLFGMMLRDSEGDKGRNLRMILGTPETRRIIKKWKYRTKNCERATSRNAFLPEKLQKLQPLYYNVSEIVGKEYKGLQLYSLEQA
LERLNSIVVGTNCVLLSWDDKWINELSLASKGWKFHSLAGETPNTLVLLCSCGRCDTKIYLDLHSTENHNNDNVQNLINERYWEDIVTKSRPSQ
CPWVSNQFDLSDYHLKEANLIHDITRMQGHETVHFGTSGEITHNSTPLFSQEQLFSLSEFFKCADKRKLELMLRGFIPVEGCNDAVICVRCFRK
AFIGSITGSDYLNPHAPWCRYHDETKLPTMITSQLLSAKKTDDIKKRLSDLENYFESV
>KAF2227358.1[*Elsinoe_ampelina*]
MPEATATRKRRFYGLLDKLTQSSGPASKPSKTSAPTSRPTTSGGVTSNPRPSTPSSHPSISSPRPSTSSQRPSISAPRPIRPDRPTTLATPGAP
PPIPRIPHFTPWSHEDFLERLKTFAPVTSWFPKPEGVGEVEWAKRGWECVGNETVGCKGCKRRVVVDFTINGIGGDDEQAEDNVDESEEEAEFE
NTFEKALAEKYAEEIIKGHSESCPWRKTGCKDDIYRLPVVRTAWWQDTVRTSFTSVLEIKEDIENLRIHPISASPPADKLLLHIPPIFFNPNAT
PRNNSVLSNGSVDDPSVPSDEIMARALMIALTGWHATCESRTNLLVCDACFQRIGLWMYQSKPSTSPTTIPAGTSPLPTTPSTQSTSLTPAIKS
VSFGPSPPSSPSPTSSHPPLDLLASHREHCPYRSPSSQAATGDYVGFPAWRILWTTAARYADEQRRRSVAAKPGLGMGGLPGLGLGMKEGLSRE
EVARLDKERVNKLRRLKSALGIKLGVPRRGGGGREGEGSWV
>Mext011234[*Medauroidea_extradentata*]
MGVAVLLEGKVWTAEGRPVSRGAFVPIPSERKVWSQPYMGVEARKFNKTIVVTGPCLSVEKDDVLKKVEQNTSNPMSFRGFVKRMQTYNIVCWY
VHRRLALQLARRGWENVKDYVVKCCFCTAEVDLRNHISSQEEELLQLLYKRHASFCRWLTITSPEFFACVPHVQSSQGLKNTVATTATQLLELG
QELPKIPEVVLHKMKLEHETLELLISGLLKDVSVSEISISAVALTLCGWSPASTKGILCCCYCDRRLALRHWMSIQEFDEQRRLVLSDSNMKIC
SASYMQSSYADGAEEEDDDSQSPLSDQSIITDCSDEEEEVDEEEEENEEEFEEENEEGNEEMEVEEYELYEKHAEQDNECGNNEISDDGEEQSS
QTRNCQNEDNIENKYEDFQCRDEEMDENYDEINARALEENNFDDDDDEETEDEMPPNENGPSDEEVEEAEVSDESIMSDNEFKNENPKIFRGPN
KHTRYQSYVKRNKDSSNDLQAQYDSCGNEEDVESSEDDLLVENEVEDGDEEEEENEQNEGEEIGEEEDDEDDDDDDEEEEEDDEEEDDDKDDE
DDEELPDDSKYHENNSDKVIELLSDSDEEIEQQPIEKIQSDSDEEIESQPVEQVQSVSSPTSAVVLETQTVVKENNVSNENKQSHCEKLCVEPK
TETENNDVDVREIIEKEIECDSDIALRSECENQEVKSLSLAEAIIMDDSKVRESQYDGNNSTQQEKVTLKRKRDCDEVETEQSLSIKRQQISLH
ESDKPLRVNENDMVITGGNPDCDKNNIEVEENTCSEGNDKNAEMVNSKALNENDCKTSAACERSVVVELVEHSKSQKECKLNGTLSLSKEKCEL
SVNSCEDSASAAVEGTNNLEQTCIENIEESVSSTAEMQTGVSETPAHSQNVVQKPLPKSEINSEVTVLKIETVCSIDTTQVIQKQKSRGKFVEN
NCTNVPLLLPEMPSENGLVIVQEEVCNVENTSSNIPLLLLENRSSDDDAGQEKGVICDKGGEPEVLATVQAVQDNSGEVEQAQILGEKAENKDA
QLEVPPLPGVQNGGGEVVENNSARGEETTKEDSVLSEVSCSLKGTSLPTEKGSENELSLQAGEDVKDTTVTNEAEDRTVGETTSLNNGNTSEEV
VQEYKSSEGNECSEELNPEECVHNNEESSTCDKSEADKKGEEGVTEMCESEALSVCAEKDGVMLEAMEVCEAGEQSSSRGVKRNRESDLEHSSP
EAKRPHQSTEVRRQPSLLDPLAEHRFWCLWAPSRGSASFGQSGFEIVFKEILDKILLQRREQDEMDIIGKLRSTQEQIMPL

Supplemental References

Adl SM, Simpson AGB, Lane CE, Lukeš J, Bass D, Bowser SS, Brown MW, Burki F, Dunthorn M, Hampl V, *et al* (2012) The revised classification of eukaryotes. *Journal of Eukaryotic Microbiology* 59: 429–493

Aherrahrou R, Reinberger T, Werner J, Otto M, Al-Hasani J, Munoz-Venegas ML, Civelek M, Schunkert H, Kessler T, Erdmann J, *et al* (2021) Deficiency of ZC3HC1 increases vascular smooth muscle cell migration, proliferation and neointima formation following injury. *bioRxiv*: 2021.09.29.462212

Aitchison JD, Rout MP, Marelli M, Blobel G & Wozniak RW (1995) Two novel related yeast nucleoporins Nup170p and Nup157p: complementation with the vertebrate homologue Nup155p and functional interactions with the yeast nuclear pore-membrane protein Pom152p. *J Cell Biol* 131: 1133–1148

Akashi H, Osada N & Ohta T (2012) Weak selection and protein evolution. *Genetics* 192: 15–31

Albalat R & Cañestro C (2016) Evolution by gene loss. *Nat Rev Genet* 17: 379–391

Altschul SF, Gish W, Miller W, Myers EW & Lipman DJ (1990) Basic local alignment search tool. *J Mol Biol* 215: 403–410

Altschul SF, Madden TL, Schäffer AA, Zhang J, Zhang Z, Miller W & Lipman DJ (1997) Gapped BLAST and PSI-BLAST: a new generation of protein database search programs. *Nucleic Acids Res* 25: 3389–402

Anderson JT, Lee C-R, Rushworth CA, Colautti RI & Mitchell-Olds T (2013) Genetic trade-offs and conditional neutrality contribute to local adaptation. *Mol Ecol* 22: 699–708

Anderson JT, Willis JH & Mitchell-Olds T (2011) Evolutionary genetics of plant adaptation. *Trends in Genetics* 27: 258–266

Austad SN & Hoffman JM (2018) Is antagonistic pleiotropy ubiquitous in aging biology? *Evol Med Public Health* 2018: 287–294

Bairoch A & Apweiler R (1997) The SWISS-PROT protein sequence data bank and its supplement TrEMBL. *Nucleic Acids Res* 26: 38–42

Bargiello T & Grossfield J (1979) Biochemical Polymorphisms: the unit of selection and hypothesis of conditional neutrality. *Biosystems* 11: 183–192

Bassermann F, von Klitzing C, Illert AL, Münch S, Morris SW, Pagano M, Peschel C, Duyster J, Klitzing C von, Illert AL, *et al* (2007) Multisite phosphorylation of nuclear interaction partner of ALK (NIPA) at G2/M involves cyclin B1/Cdk1. *J Biol Chem* 282: 15965–15972

Bassermann F, von Klitzing C, Münch S, Bai R-Y, Kawaguchi H, Morris SW, Peschel C, Duyster J, Klitzing C von, Münch S, *et al* (2005a) NIPA defines an SCF-type mammalian E3 ligase that regulates mitotic entry. *Cell* 122: 45–57

Bassermann F, Peschel C & Duyster J (2005b) Mitotic entry: a matter of oscillating destruction. *Cell Cycle* 4: 1515–1517

Beck M, Förster F, Ecke M, Plitzko JM, Melchior F, Gerisch G, Baumeister W & Medalia O (2004) Nuclear pore complex structure and dynamics revealed by cryoelectron tomography. *Science* 306: 1387–1390

Bekker-Jensen DB, Kelstrup CD, Batth TS, Larsen SC, Haldrup C, Bramsen JB, Sørensen KD, Høyer S, Ørntoft TF, Andersen CL, *et al* (2017) An optimized shotgun strategy for the rapid generation of comprehensive human proteomes. *Cell Syst* 4: 587-599.e4

Bensidoun P, Reiter T, Montpetit B, Zenklusen D & Oeffinger M (2021) Nuclear mRNA metabolism drives selective basket assembly on a subset of nuclear pores in budding yeast. *bioRxiv*: 2021.11.07.467636

Berthelet J & Dubrez L (2013) Regulation of Apoptosis by Inhibitors of Apoptosis (IAPs). *Cells* 2: 163–187

Birnbaum MJ, Clem RJ & Miller LK (1994) An apoptosis-inhibiting gene from a nuclear polyhedrosis virus encoding a polypeptide with Cys/His sequence motifs. *J Virol* 68: 2521–2528

Blanc G & Wolfe KH (2004) Functional divergence of duplicated genes formed by polyploidy during Arabidopsis evolution. *Plant Cell* 16: 1679–1691

Blethrow JD, Glavy JS, Morgan DO & Shokat KM (2008) Covalent capture of kinase-specific phosphopeptides reveals Cdk1-cyclin B substrates. *Proc Natl Acad Sci U S A* 105: 1442–1447

Boratyn GM, Schäffer AA, Agarwala R, Altschul SF, Lipman DJ & Madden TL (2012) Domain enhanced lookup time accelerated BLAST. *Biol Direct* 7: 12

Bowman S, Churcher C, Badcock K, Brown D, Chillingworth T, Connor R, Dedman K, Devlin K, Gentles S, Hamlin N, *et al* (1997) The nucleotide sequence of Saccharomyces cerevisiae chromosome XIII. *Nature* 387: 90–93

Brayer KJ & Segal DJ (2008) Keep your fingers off my DNA: protein-protein interactions mediated by C2H2 zinc finger domains. *Cell Biochem Biophys* 50: 111–131

Brennan MB & Struhl K (1980) Mechanisms of increasing expression of a yeast gene in Escherichia coli. *J Mol Biol* 136: 333–338

Breslow DK, Cameron DM, Collins SR, Schuldiner M, Stewart-Ornstein J, Newman HW, Braun S, Madhani HD, Krogan NJ & Weissman JS (2008) A comprehensive strategy enabling high-resolution functional analysis of the yeast genome. *Nat Methods* 5: 711–718

Bretes H, Rouviere JO, Leger T, Oeffinger M, Devaux F, Doye V & Palancade B (2014) Sumoylation of the THO complex regulates the biogenesis of a subset of mRNPs. *Nucleic Acids Res* 42: 5043–5058

Brown JAM, Sherlock G, Myers CL, Burrows NM, Deng C, Wu HI, McCann KE, Troyanskaya OG & Brown JAM (2006) Global analysis of gene function in yeast by quantitative phenotypic profiling. *Mol Syst Biol* 2: 2006.0001

Burki F (2014) The eukaryotic tree of life from a global phylogenomic perspective. *Cold Spring Harb Perspect Biol* 6: a016147

Cao L, Wang Z, Yang X, Xie L & Yu L (2008) The evolution of BIR domain and its containing proteins. *FEBS Lett* 582: 3817–3822

Capili AD, Schultz DC, RauscherIII FJ & Borden KL (2001) Solution structure of the PHD domain from the KAP-1 corepressor: structural determinants for PHD, RING and LIM zinc-binding domains. *EMBO J* 20: 165–177

Carter AJR & Nguyen AQ (2011) Antagonistic pleiotropy as a widespread mechanism for the maintenance of polymorphic disease alleles. *BMC Med Genet* 12: 160

de Castro E, Sigrist CJA, Gattiker A, Bulliard V, Langendijk-Genevaux PS, Gasteiger E, Bairoch A & Hulo N (2006) ScanProsite: detection of PROSITE signature matches and ProRule-associated functional and structural residues in proteins. *Nucleic Acids Res* 34: W362-5

Chai J, Shiozaki E, Srinivasula SM, Wu Q, Datta P, Alnemri ES, Shi Y & Dataa P (2001) Structural basis of caspase-7 inhibition by XIAP. *Cell* 104: 769–780

Chi Y, Welcker M, Hizli AA, Posakony JJ, Aebersold R & Clurman BE (2008) Identification of CDK2 substrates in human cell lysates. *Genome Biol* 9: R149

Christensen GL, Kelstrup CD, Lyngsø C, Sarwar U, Bøgebo R, Sheikh SP, Gammeltoft S, Olsen J v & Hansen JL (2010) Quantitative phosphoproteomics dissection of seven-transmembrane receptor signaling using full and biased agonists. *Molecular & cellular proteomics* 9: 1540–1553

Cordes VC, Reidenbach S, Rackwitz HR & Franke WW (1997) Identification of protein p270/TPR as a constitutive component of the nuclear pore complex-attached intranuclear filaments. *J Cell Biol* 136: 515–529

Corti A, Milani M, Lecis D, Seneci P, de Rosa M, Mastrangelo E & Cossu F (2018) Structure-based design and molecular profiling of Smac-mimetics selective for cellular IAPs. *FEBS J* 285: 3286–3298

Cossu F, Milani M, Mastrangelo E & Lecis D (2019) Targeting the BIR Domains of Inhibitor of Apoptosis (IAP) Proteins in Cancer Treatment. *Comput Struct Biotechnol J* 17: 142–150

Cronshaw JM, Krutchinsky AN, Zhang W, Chait BT & Matunis MJ (2002) Proteomic analysis of the mammalian nuclear pore complex. *J Cell Biol* 158: 915–927

Crooks GE, Hon G, Chandonia J-M & Brenner SE (2004) WebLogo: a sequence logo generator. *Genome Res* 14: 1188–90

Damgaard RB & Gyrd-Hansen M (2011) Inhibitor of apoptosis (IAP) proteins in regulation of inflammation and innate immunity. *Discov Med* 11: 221–231

Dephoure N, Zhou C, Villén J, Beausoleil SA, Bakalarski CE, Elledge SJ & Gygi SP (2008) A quantitative atlas of mitotic phosphorylation. *Proc Natl Acad Sci U S A* 105: 10762–10767

Deshaies RJ & Joazeiro CAP (2009) RING domain E3 ubiquitin ligases. *Annu Rev Biochem* 78: 399–434

Deveraux QL & Reed JC (1999) IAP family proteins - Suppressors of apoptosis. *Genes Dev* 13: 239–252

Dubrez-Daloz L, Dupoux A & Cartier J (2008) IAPs: More than just inhibitors of apoptosis proteins. *Cell Cycle* 7: 1036–1046

Duckett CS, Nava VE, Gedrich RW, Clem RJ, van Dongen JL, Gilfillan MC, Shiels H, Hardwick JM & Thompson CB (1996) A conserved family of cellular genes related to the baculovirus iap gene and encoding apoptosis inhibitors. *EMBO J* 15: 2685–94

Dultz E, Wojtynek M, Medalia O & Onischenko E (2022) The Nuclear Pore Complex: Birth, Life, and Death of a Cellular Behemoth. *Cells* 11: 1–28

Durfee T, Becherer K, Chen PL, Yeh SH, Yang Y, Kilburn AE, Lee WH & Elledge SJ (1993) The retinoblastoma protein associates with the protein phosphatase type 1 catalytic subunit. *Genes Dev* 7: 555–569

Eddy SR (2011) Accelerated Profile HMM Searches. *PLoS Comput Biol* 7: e1002195

Elena SF & Lenski RE (2003) Evolution experiments with microorganisms: the dynamics and genetic bases of adaptation. *Nat Rev Genet* 4: 457–469

Fernandez-Martinez J & Rout MP (2021) One Ring to Rule them All? Structural and Functional Diversity in the Nuclear Pore Complex. *Trends Biochem Sci* 46: 595–607

Feuerbach F, Galy V, Trelles-Sticken E, Fromont-Racine M, Jacquier A, Gilson E, Olivo-Marin J-C, Scherthan H & Nehrbass U (2002) Nuclear architecture and spatial positioning help establish transcriptional states of telomeres in yeast. *Nat Cell Biol* 4: 214–221

Fields S & Song O (1989) A novel genetic system to detect protein-protein interactions. *Nature* 340: 245–246

Finn RD, Clements J & Eddy SR (2011) HMMER web server: interactive sequence similarity searching. *Nucleic Acids Res* 39: W29-37

Finn RD, Mistry J, Tate J, Coggill P, Heger A, Pollington JE, Gavin OL, Gunasekaran P, Ceric G, Forslund K, *et al* (2010) The Pfam protein families database. *Nucleic Acids Res* 38: D211-22

Finn RD, Tate J, Mistry J, Coggill PC, Sammut SJ, Hotz H-R, Ceric G, Forslund K, Eddy SR, Sonnhammer ELL, *et al* (2008) The Pfam protein families database. *Nucleic Acids Res* 36: D281--288

Finn RD, Mistry J, Schuster-Böckler B, Griffiths-Jones S, Hollich V, Lassmann T, Moxon S, Marshall M, Khanna A, Durbin R, *et al* (2006) Pfam: clans, web tools and services. *Nucleic Acids Res* 34: 247–251

Floch AG, Palancade B & Doye V (2014) Fifty years of nuclear pores and nucleocytoplasmic transport studies: multiple tools revealing complex rules. *Methods Cell Biol* 122: 1–40

Freudenreich CH & Su XA (2016) Relocalization of DNA lesions to the nuclear pore complex. *FEMS Yeast Res* 16: 1–9

Galtier N (2016) Adaptive Protein Evolution in Animals and the Effective Population Size Hypothesis. *PLoS Genet* 12: e1005774

Gamsjaeger R, Liew CK, Loughlin FE, Crossley M & Mackay JP (2007) Sticky fingers: zinc-fingers as protein-recognition motifs. *Trends Biochem Sci* 32: 63–70

Garcia-Bonete MJ & Katona G (2019) Bayesian machine learning improves single-wavelength anomalous diffraction phasing. *Acta Crystallogr A Found Adv* 75: 851–860

Gavrilov LA & Gavrilova NS (2002) Evolutionary theories of aging and longevity. *ScientificWorldJournal* 2: 339–56

Gomes CM & Wittung-Stafshede P (2010) Chapter Metal Ions, Protein Folding, and Conformational States: An Introduction. In *Protein Folding and Metal Ions*, Gomes CM & Wittung-Stafshede P (eds) CRC Press

Görlich D & Kutay U (1999) Transport between the cell nucleus and the cytoplasm. *Annu Rev Cell Dev Biol* 15: 607–660

Görlich D, Vogel F, Mills AD, Hartmann E & Laskey RA (1995) Distinct functions for the two importin subunits in nuclear protein import. *Nature* 377: 246–248

Göttfert F, Wurm CA, Mueller V, Berning S, Cordes VC, Honigmann A & Hell SW (2013) Coaligned dual-channel STED nanoscopy and molecular diffusion analysis at 20 nm resolution. *Biophys J* 105: L01-3

Green LM & Berg JM (1989) A retroviral Cys-Xaa2-Cys-Xaa4-His-Xaa4-Cys peptide binds metal ions: spectroscopic studies and a proposed three-dimensional structure. *Proc Natl Acad Sci U S A* 86: 4047–4051

Grossman E, Medalia O & Zwerger M (2012) Functional architecture of the nuclear pore complex. *Annu Rev Biophys* 41: 557–584

Gunkel P & Cordes VC (2022) ZC3HC1 is a structural element of the nuclear basket effecting interlinkage of TPR polypeptides. *Mol Biol Cell*: mbcE22020037

Gunkel P, Iino H, Krull S & Cordes VC (2021) ZC3HC1 Is a Novel Inherent Component of the Nuclear Basket, Resident in a State of Reciprocal Dependence with TPR. *Cells* 10: 1937

Güttler T & Görlich D (2011) Ran-dependent nuclear export mediators: a structural perspective. *EMBO J* 30: 3457–3474

Gyrd-Hansen M & Meier P (2010) IAPs: from caspase inhibitors to modulators of NF-kappaB, inflammation and cancer. *Nat Rev Cancer* 10: 561–574

Hart T, Chandrashekhar M, Aregger M, Steinhart Z, Brown KR, MacLeod G, Mis M, Zimmermann M, Fradet-Turcotte A, Sun S, *et al* (2015) High-resolution CRISPR screens reveal fitness genes and genotype-specific cancer liabilities. *Cell* 163: 1515–1526

Hase ME & Cordes VC (2003) Direct interaction with NUP153 mediates binding of TPR to the periphery of the nuclear pore complex. *Mol Biol Cell* 14: 1923–1940

Hase ME, Kuznetsov N v & Cordes VC (2001) Amino acid substitutions of coiled-coil protein TPR abrogate anchorage to the nuclear pore complex but not parallel, in-register homodimerization. *Mol Biol Cell* 12: 2433–2452

Hashimoto H, Ramirez DH, Lautier O, Pawlak N, Blobel G, Palancade B & Debler EW (2022) Structure of the pre-mRNA leakage 39-kDa protein reveals a single domain of integrated zf-C3HC and Rsm1 modules. *bioRxiv*: 2022.08.11.503642

He F, Umehara T, Tsuda K, Inoue M, Kigawa T, Matsuda T, Yabuki T, Aoki M, Seki E, Terada T, *et al* (2007) Solution structure of the zinc finger HIT domain in protein FON. *Protein Science* 16: 1577–1587

Higashi K, Takasawa R, Yoshimori A, Goh T, Tanuma S & Kuchitsu K (2005) Identification of a novel gene family, paralogs of inhibitor of apoptosis proteins present in plants, fungi, and animals. *Apoptosis* 10: 471–480

Hillenmeyer ME, Fung E, Wildenhain J, Pierce SE, Hoon S, Lee W, Proctor M, St.Onge RP, Tyers M, Koller D, *et al* (2008) The Chemical Genomic Portrait of Yeast: Uncovering a Phenotype for All Genes. *Science* 320: 362–365

Houben K, Wasielewski E, Dominguez C, Kellenberger E, Atkinson RA, Timmers HTM, Kieffer B & Boelens R (2005) Dynamics and metal exchange properties of C4C4 RING domains from CNOT4 and the p44 subunit of TFIIH. *J Mol Biol* 349: 621–637

Huang Y, Park YC, Rich RL, Segal D, Myszka DG & Wu H (2001) Structural basis of caspase inhibition by XIAP: differential roles of the linker versus the BIR domain. *Cell* 104: 781–790

Hu C-W, Hsu C-L, Wang Y-C, Ishihama Y, Ku W-C, Huang H-C & Juan H-F (2015) Temporal phosphoproteome dynamics induced by an ATP synthase inhibitor citreoviridin. *Molecular & cellular proteomics* 14: 3284–3298

Illert AL, Kawaguchi H, Antinozzi C, Bassermann F, Quintanilla-Martinez L, Klitzing C von, Hiwatari M, Peschel C, de Rooij DG, Morris SW, *et al* (2012) Targeted inactivation of nuclear interaction partner of ALK disrupts meiotic prophase. *Development* 139: 2523–2534

Janke C, Magiera MM, Rathfelder N, Taxis C, Reber S, Maekawa H, Moreno-Borchart A, Doenges G, Schwob E, Schiebel E, *et al* (2004) A versatile toolbox for PCR-based tagging of yeast genes: new fluorescent proteins, more markers and promoter substitution cassettes. *Yeast* 21: 947–962

Jarnik M & Aebi U (1991) Toward a more complete 3-D structure of the nuclear pore complex. *J Struct Biol* 107: 291–308

Johnson LS, Eddy SR & Portugaly E (2010) Hidden Markov model speed heuristic and iterative HMM search procedure. *BMC Bioinformatics* 11: 431

Jumper J, Evans R, Pritzel A, Green T, Figurnov M, Ronneberger O, Tunyasuvunakool K, Bates R, Žídek A, Potapenko A, *et al* (2021) Highly accurate protein structure prediction with AlphaFold. *Nature* 596: 583–589

Kandias NG, Chasapis CT, Bentrop D, Episkopou V & Spyroulias GA (2009) High yield expression and NMR characterization of Arkadia E3 ubiquitin ligase RING-H2 finger domain. *Biochem Biophys Res Commun* 378: 498–502

van Kempen M, Kim SS, Tumescheit C, Mirdita M, Söding J & Steinegger M (2022) Foldseek: fast and accurate protein structure search. *bioRxiv*: 2022.02.07.479398

Kim JG & Hudson LD (1992) Novel member of the zinc finger superfamily: A C2-HC finger that recognizes a glia-specific gene. *Mol Cell Biol* 12: 5632–5639

Kim SJ, Fernandez-Martinez J, Nudelman I, Shi Y, Zhang W, Raveh B, Herricks T, Slaughter BD, Hogan JA, Upla P, *et al* (2018) Integrative structure and functional anatomy of a nuclear pore complex. *Nature* 555: 475–482

Kirkwood TBL (2002) Evolution of ageing. *Mech Ageing Dev* 123: 737–745

Kırlı K, Karaca S, Dehne HJ, Samwer M, Pan KT, Lenz C, Urlaub H & Görlich D (2015) A deep proteomics perspective on CRM1-mediated nuclear export and nucleocytoplasmic partitioning. *Elife* 4: e11466

Kiseleva E, Goldberg MW, Allen TD & Akey CW (1998) Active nuclear pore complexes in Chironomus: visualization of transporter configurations related to mRNP export. *J Cell Sci* 111 (Pt 2): 223–236

Kiseleva E, Goldberg MW, Daneholt B & Allen TD (1996) RNP export is mediated by structural reorganization of the nuclear pore basket. *J Mol Biol* 260: 304–311

Klitzing C von, Huss R, Illert AL, Fröschl A, Wötzel S, Peschel C, Bassermann F, Duyster J, von Klitzing C, Huss R, *et al* (2011) APC/C(Cdh1)-mediated degradation of the F-box protein NIPA is regulated by its association with SKP1. *PLoS One* 6: e28998

Köhler A & Hurt E (2007) Exporting RNA from the nucleus to the cytoplasm. *Nat Rev Mol Cell Biol* 8: 761–773

Köhler A & Hurt E (2010) Gene regulation by nucleoporins and links to cancer. *Mol Cell* 38: 6–15

Kokoszynska K, Rychlewski L & Wyrwicz LS (2008) The mitotic entry regulator NIPA is a prototypic BIR domain protein. *Cell cycle* 7: 2073–2075

Kreutmair S, Erlacher M, Andrieux G, Istvanffy R, Mueller-Rudorf A, Zwick M, Rückert T, Pantic M, Poggio T, Shoumariyeh K, *et al* (2020) Loss of the Fanconi anemia–associated protein NIPA causes bone marrow failure. *Journal of Clinical Investigation* 130(6): 2827–2844

Krull S, Thyberg J, Björkroth B, Rackwitz H-R & Cordes VC (2004) Nucleoporins as components of the nuclear pore complex core structure and TPR as the architectural element of the nuclear basket. *Mol Biol Cell* 15: 4261–4277

Kuznetsov N v, Sandblad L, Hase ME, Hunziker A, Hergt M & Cordes VC (2002) The evolutionarily conserved single-copy gene for murine TPR encodes one prevalent isoform in somatic cells and lacks paralogs in higher eukaryotes. *Chromosoma* 111: 236–255

Laitaoja M, Valjakka J & Jänis J (2013) Zinc coordination spheres in protein structures. *Inorg Chem* 52: 10983–10991

Lalaoui N & Vaux DL (2018) Recent advances in understanding inhibitor of apoptosis proteins. *F1000Res* 7: 1–15

Lamm N, Rogers S & Cesare AJ (2021) Chromatin mobility and relocation in DNA repair. *Trends Cell Biol* 31: 843–855

Legge GB, Martinez-Yamout MA, Hambly DM, Trinh T, Lee BM, Dyson HJ & Wright PE (2004) ZZ domain of CBP: an unusual zinc finger fold in a protein interaction module. *J Mol Biol* 343: 1081–1093

Lin DH & Hoelz A (2019) The Structure of the Nuclear Pore Complex (An Update). *Annu Rev Biochem* 88: 725–783

Lin S-C, Huang Y, Lo Y-C, Lu M & Wu H (2007) Crystal structure of the BIR1 domain of XIAP in two crystal forms. *J Mol Biol* 372: 847–854

Li Z, Tiley GP, Galuska SR, Reardon CR, Kidder TI, Rundell RJ & Barker MS (2018) Multiple large-scale gene and genome duplications during the evolution of hexapods. *Proc Natl Acad Sci U S A* 115: 4713–4718

Lu Y, Dai J, Yang L, La Y, Zhou S, Qiang S, Wang Q, Tan F, Wu Y, Kong W, *et al* (2020) Involvement of MEM1 in DNA demethylation in Arabidopsis. *Plant Mol Biol* 102: 307–322

Lu M, Lin S-C, Huang Y, Kang YJ, Rich R, Lo Y-C, Myszka D, Han J & Wu H (2007) XIAP induces NF-kappaB activation via the BIR1/TAB1 interaction and BIR1 dimerization. *Mol Cell* 26: 689–702

Mace PD, Shirley S & Day CL (2010a) Assembling the building blocks: Structure and function of inhibitor of apoptosis proteins. *Cell Death Differ* 17: 46–53

Mace PD, Smits C, Vaux DL, Silke J & Day CL (2010b) Asymmetric recruitment of cIAPs by TRAF2. *J Mol Biol* 400: 8–15

Maret W & Li Y (2009) Coordination dynamics of zinc in proteins. *Chem Rev* 109: 4682–707

Massiah MA, Matts JAB, Short KM, Simmons BN, Singireddy S, Yi Z & Cox TC (2007) Solution structure of the MID1 B-box2 CHC(D/C)C(2)H(2) zinc-binding domain: insights into an evolutionarily conserved RING fold. *J Mol Biol* 369: 1–10

Massiah MA, Simmons BN, Short KM & Cox TC (2006) Solution structure of the RBCC/TRIM B-box1 domain of human MID1: B-box with a RING. *J Mol Biol* 358: 532–545

Mastrangelo E, Cossu F, Milani M, Sorrentino G, Lecis D, Delia D, Manzoni L, Drago C, Seneci P, Scolastico C, *et al* (2008) Targeting the X-linked inhibitor of apoptosis protein through 4-substituted azabicyclo[5.3.0]alkane smac mimetics. Structure, activity, and recognition principles. *J Mol Biol* 384: 673–689

McCormick MA, Delaney JR, Tsuchiya M, Tsuchiyama S, Shemorry A, Sim S, Chou AC-Z, Ahmed U, Carr D, Murakami CJ, *et al* (2015) A Comprehensive Analysis of Replicative Lifespan in 4,698 Single-Gene Deletion Strains Uncovers Conserved Mechanisms of Aging. *Cell Metab* 22: 895–906

Mirdita M, Schütze K, Moriwaki Y, Heo L, Ovchinnikov S & Steinegger M (2021) ColabFold - Making protein folding accessible to all. *bioRxiv*: 2021.08.15.456425

Mirdita M, Schütze K, Moriwaki Y, Heo L, Ovchinnikov S & Steinegger M (2022) ColabFold: making protein folding accessible to all. *Nat Methods* 19: 679–682

Mitchell-Olds T, Willis JH & Goldstein DB (2007) Which evolutionary processes influence natural genetic variation for phenotypic traits? *Nat Rev Genet* 8: 845–856

Mitic K, Grafe M, Batsios P & Meyer I (2022) Partial Disassembly of the Nuclear Pore Complex Proteins during Semi-Closed Mitosis in Dictyostelium discoideum. *Cells* 11

Montano M & Long K (2011) RNA surveillance-an emerging role for RNA regulatory networks in aging. *Ageing Res Rev* 10: 216–224

Moritz A, Li Y, Guo A, Villén J, Wang Y, MacNeill J, Kornhauser J, Sprott K, Zhou J, Possemato A, *et al* (2010) Akt-RSK-S6 kinase signaling networks activated by oncogenic receptor tyrosine kinases. *Sci Signal* 3: ra64

Niepel M, Molloy KR, Williams R, Farr JC, Meinema AC, Vecchietti N, Cristea IM, Chait BT, Rout MP & Strambio-De-Castillia C (2013) The nuclear basket proteins Mlp1p and Mlp2p are part of a dynamic interactome including Esc1p and the proteasome. *Mol Biol Cell* 24: 3920–3938

Niepel M, Strambio-de-Castillia C, Fasolo J, Chait BT & Rout MP (2005) The nuclear pore complex-associated protein, Mlp2p, binds to the yeast spindle pole body and promotes its efficient assembly. *J Cell Biol* 170: 225–235

Obado SO, Brillantes M, Uryu K, Zhang W, Ketaren NE, Chait BT, Field MC & Rout MP (2016) Interactome Mapping Reveals the Evolutionary History of the Nuclear Pore Complex. *PLoS Biol* 14: e1002365

Oberoi-Khanuja TK, Murali A & Rajalingam K (2013) IAPs on the move: role of inhibitors of apoptosis proteins in cell migration. *Cell Death Dis* 4: e784

Orme M & Meier P (2009) Inhibitor of apoptosis proteins in Drosophila: gatekeepers of death. *Apoptosis* 14: 950–960

Ouyang T, Bai R-Y, Bassermann F, von Klitzing C, Klumpen S, Miething C, Morris SW, Peschel C, Duyster J, Klitzing C von, *et al* (2003) Identification and characterization of a nuclear interacting partner of anaplastic lymphoma kinase (NIPA). *J Biol Chem* 278: 30028–30036

Padjasek M, Kocyła A, Kluska K, Kerber O, Tran JB & Krężel A (2020) Structural zinc binding sites shaped for greater works: Structure-function relations in classical zinc finger, hook and clasp domains. *J Inorg Biochem* 204: 110955

Palancade B, Zuccolo M, Loeillet S, Nicolas A & Doye V (2005) Pml39, a novel protein of the nuclear periphery required for nuclear retention of improper messenger ribonucleoparticles. *Mol Biol Cell* 16: 5258–5268

Pawlowski J (2013) The new micro-kingdoms of eukaryotes. *BMC Biol* 11: 40

Potter SC, Luciani A, Eddy SR, Park Y, Lopez R & Finn RD (2018) HMMER web server: 2018 update. *Nucleic Acids Res* 46: W200–W204

Ptak C, Aitchison JD & Wozniak RW (2014) The multifunctional nuclear pore complex: a platform for controlling gene expression. *Curr Opin Cell Biol* 28: 46–53

Qian W, Ma D, Xiao C, Wang Z & Zhang J (2012) The genomic landscape and evolutionary resolution of antagonistic pleiotropy in yeast. *Cell Rep* 2: 1399–1410

Qiao X, Li Q, Yin H, Qi K, Li L, Wang R, Zhang S & Paterson AH (2019) Gene duplication and evolution in recurring polyploidization-diploidization cycles in plants. *Genome Biol* 20: 1–23

Remmert M, Biegert A, Hauser A & Söding J (2011) HHblits: lightning-fast iterative protein sequence searching by HMM-HMM alignment. *Nat Methods* 9: 173–5

Richter BW, Mir SS, Eiben LJ, Lewis J, Reffey SB, Frattini A, Tian L, Frank S, Youle RJ, Nelson DL, *et al* (2001) Molecular cloning of ILP-2, a novel member of the inhibitor of apoptosis protein family. *Mol Cell Biol* 21: 4292–301

Riedl SJ, Fuentes-Prior P, Renatus M, Kairies N, Krapp S, Huber R, Salvesen GS & Bode W (2001) Structural basis for the activation of human procaspase-7. *Proc Natl Acad Sci U S A* 98: 14790–14795

Ris H (1991) The three-dimensional structure of the nuclear pore complex as seen by high voltage electron microscopy and high resolution low voltage scanning electron microscopy. *EMSA Bulletin* 21(1): 54–56

Ris H (1997) High-resolution field-emission scanning electron microscopy of nuclear pore complex. *Scanning* 19: 368–375

Robitaille AM, Christen S, Shimobayashi M, Cornu M, Fava LL, Moes S, Prescianotto-Baschong C, Sauer U, Jenoe P & Hall MN (2013) Quantitative phosphoproteomics reveal mTORC1 activates de novo pyrimidine synthesis. *Science* 339: 1320–1323

Roff DA & Fairbairn DJ (2007) The evolution of trade-offs: where are we? *J Evol Biol* 20: 433–47

Rothe M, Pan MG, Henzel WJ, Ayres TM & Goeddel D v (1995) The TNFR2-TRAF signaling complex contains two novel proteins related to baculoviral inhibitor of apoptosis proteins. *Cell* 83: 1243–1252

Rout MP, Aitchison JD, Suprapto A, Hjertaas K, Zhao Y & Chait BT (2000) The yeast nuclear pore complex: composition, architecture, and transport mechanism. *J Cell Biol* 148: 635–651

Roy N, Deveraux QL, Takahashi R, Salvesen GS & Reed JC (1997) The c-IAP-1 and c-IAP-2 proteins are direct inhibitors of specific caspases. *EMBO J* 16: 6914–25

Rual J-F, Ceron J, Koreth J, Hao T, Nicot A, Hirozane-Kishikawa T, Vandenhaute J, Orkin SH, Hill DE, van den Heuvel S, *et al* (2004) Toward improving Caenorhabditis elegans phenome mapping with an ORFeome-based RNAi library. *Genome Res* 14: 2162–2168

Samuel T, Welsh K, Lober T, Togo SH, Zapata JM & Reed JC (2006) Distinct BIR domains of cIAP1 mediate binding to and ubiquitination of tumor necrosis factor receptor-associated factor 2 and second mitochondrial activator of caspases. *Journal of Biological Chemistry* 281: 1080–1090

Saroufim M-A, Bensidoun P, Raymond P, Rahman S, Krause MR, Oeffinger M & Zenklusen D (2015) The nuclear basket mediates perinuclear mRNA scanning in budding yeast. *J Cell Biol* 211: 1131–1140

Schunkert H, König IR, Kathiresan S, Reilly MP, Assimes TL, Holm H, Preuss M, Stewart AFR, Barbalic M, Gieger C, *et al* (2011) Large-scale association analysis identifies 13 new susceptibility loci for coronary artery disease. *Nat Genet* 43: 333–338

Sharma S, Kaufmann T & Biswas S (2017) Impact of inhibitor of apoptosis proteins on immune modulation and inflammation. *Immunol Cell Biol* 95: 236–243

Sharma K, D'Souza RCJ, Tyanova S, Schaab C, Wiśniewski JR, Cox J & Mann M (2014) Ultradeep human phosphoproteome reveals a distinct regulatory nature of Tyr and Ser/Thr-based signaling. *Cell Rep* 8: 1583–1594

Silke J & Vaux DL (2015) IAP gene deletion and conditional knockout models. *Semin Cell Dev Biol* 39: 97–105

Silke J & Vucic D (2014) IAP family of cell death and signaling regulators. *Methods Enzymol* 545: 35–65

Sinha S, Flibotte S, Neira M, Formby S, Plemenitaš A, Cimerman NG, Lenassi M, Gostinčar C, Stajich JE & Nislow C (2017) Insight into the Recent Genome Duplication of the Halophilic Yeast Hortaea werneckii: Combining an Improved Genome with Gene Expression and Chromatin Structure. *G3 (Bethesda)* 7: 2015–2022

Söding J (2005) Protein homology detection by HMM-HMM comparison. *Bioinformatics* 21: 951–60

Sönnichsen B, Koski LB, Walsh A, Marschall P, Neumann B, Brehm M, Alleaume A-M, Artelt J, Bettencourt P, Cassin E, *et al* (2005) Full-genome RNAi profiling of early embryogenesis in Caenorhabditis elegans. *Nature* 434: 462–469

Soop T, Ivarsson B, Björkroth B, Fomproix N, Masich S, Cordes VC & Daneholt B (2005) NUP153 affects entry of messenger and ribosomal ribonucleoproteins into the nuclear basket during export. *Mol Biol Cell* 16: 5610–5620

Sos ML, Levin RS, Gordan JD, Oses-Prieto JA, Webber JT, Salt M, Hann B, Burlingame AL, McCormick F, Bandyopadhyay S, *et al* (2014) Oncogene mimicry as a mechanism of primary resistance to BRAF inhibitors. *Cell Rep* 8: 1037–1048

Steinegger M, Meier M, Mirdita M, Vöhringer H, Haunsberger SJ & Söding J (2019) HH-suite3 for fast remote homology detection and deep protein annotation. *BMC Bioinformatics* 20: 473

Steinegger M & Söding J (2017) MMseqs2 enables sensitive protein sequence searching for the analysis of massive data sets. *Nat Biotechnol* 35: 1026–1028

Takahashi R, Deveraux Q, Tamm I, Welsh K, Assa-Munt N, Salvesen GS & Reed JC (1998) A single BIR domain of XIAP sufficient for inhibiting caspases. *Journal of Biological Chemistry* 273: 7787–7790

Thomas JA, Trueman JWH, Rambaut A & Welch JJ (2013) Relaxed phylogenetics and the palaeoptera problem: resolving deep ancestral splits in the insect phylogeny. *Syst Biol* 62: 285–97

Tunyasuvunakool K, Adler J, Wu Z, Green T, Zielinski M, Žídek A, Bridgland A, Cowie A, Meyer C, Laydon A, *et al* (2021) Highly accurate protein structure prediction for the human proteome. *Nature* 596: 590–596

Vandenberg CJ, Gergely F, Ong CY, Pace P, Mallery DL, Hiom K & Patel KJ (2003) BRCA1-independent ubiquitination of FANCD2. *Mol Cell* 12: 247–254

Veitia RA (2005) Gene dosage balance: deletions, duplications and dominance. *Trends in Genetics* 21: 33–35

Verdecia MA, Huang H, Dutil E, Kaiser DA, Hunter T & Noel JP (2000) Structure of the human anti-apoptotic protein survivin reveals a dimeric arrangement. *Nat Struct Biol* 7: 602–608

Verhagen AM, Coulson EJ & Vaux DL (2001) Inhibitor of apoptosis proteins and their relatives: IAPs and other BIRPs. *Genome Biol* 2: reviews3009.1--3009.10

Wang Q, La Y, Xia H, Zhou S, Zhai Z & La H (2022) Roles of MEM1 in safeguarding Arabidopsis genome against DNA damage, inhibiting ATM/SOG1-mediated DNA damage response, and antagonizing global DNA hypermethylation. *J Integr Plant Biol* 64: 87–104

Wei D & Sun Y (2010) Small RING Finger Proteins RBX1 and RBX2 of SCF E3 Ubiquitin Ligases: The Role in Cancer and as Cancer Targets. *Genes Cancer* 1: 700–7

Weintz G, Olsen J v, Frühauf K, Niedzielska M, Amit I, Jantsch J, Mages J, Frech C, Dölken L, Mann M, *et al* (2010) The phosphoproteome of toll-like receptor-activated macrophages. *Mol Syst Biol* 6: 371

Whalen JM & Freudenreich CH (2020) Location, Location, Location: The Role of Nuclear Positioning in the Repair of Collapsed Forks and Protection of Genome Stability. *Genes (Basel)* 11

Wheeler TJ, Clements J & Finn RD (2014) Skylign: a tool for creating informative, interactive logos representing sequence alignments and profile hidden Markov models. *BMC Bioinformatics* 15: 7

Wigington CP, Roy J, Damle NP, Yadav VK, Blikstad C, Resch E, Wong CJ, Mackay DR, Wang JT, Krystkowiak I, *et al* (2020) Systematic discovery of short linear motifs decodes calcineurin phosphatase signaling. *Mol Cell* 79: 342-358.e12

Williams GC (1957) Pleiotropy, Natural Selection, and the Evolution of Senescence. *Evolution (N Y)* 11: 398

Winzeler EA, Shoemaker DD, Astromoff A, Liang H, Anderson K, Andre B, Bangham R, Benito R, Boeke JD, Bussey H, *et al* (1999) Functional characterization of the S. cerevisiae genome by gene deletion and parallel analysis. *Science* 285: 901–906

Wu G, Chai J, Suber TL, Wu JW, Du C, Wang X & Shi Y (2000) Structural basis of IAP recognition by Smac/DIABLO. *Nature* 408: 1008–1012

Yadav L, Tamene F, Göös H, van Drogen A, Katainen R, Aebersold R, Gstaiger M & Varjosalo M (2017) Systematic analysis of human protein phosphatase interactions and dynamics. *Cell Syst* 4: 430-444.e5

Yoon JH (2004) Schizosaccharomyces pombe rsm1 genetically interacts with spmex67, which is involved in mRNA export. *J Microbiol* 42: 32–36

Yu Y, Yoon S-O, Poulogiannis G, Yang Q, Ma XM, Villén J, Kubica N, Hoffman GR, Cantley LC, Gygi SP, *et al* (2011) Phosphoproteomic analysis identifies Grb10 as an mTORC1 substrate that negatively regulates insulin signaling. *Science* 332: 1322–1326

Zhang Z, Schäffer AA, Miller W, Madden TL, Lipman DJ, Koonin E v & Altschul SF (1998) Protein sequence similarity searches using patterns as seeds. *Nucleic Acids Res* 26: 3986–3990

Zhou H, di Palma S, Preisinger C, Peng M, Polat AN, Heck AJR & Mohammed S (2013) Toward a comprehensive characterization of a human cancer cell phosphoproteome. *J Proteome Res* 12: 260–271

Zimmermann L, Stephens A, Nam S-Z, Rau D, Kübler J, Lozajic M, Gabler F, Söding J, Lupas AN & Alva V (2018) A completely reimplemented MPI bioinformatics toolkit with a new HHpred server at its core. *J Mol Biol* 430: 2237–2243